UNIVERSITAT POLITÈCNICA DE CATALUNYA
BARCELONATECH
Escola d'Enginyeria de Barcelona Est

MASTER FINAL PROJECT

Master in Science and Engineering of Materials

INTRODUCTION TO THE BINDER JET TECHNOLOGY IN ADDITIVE MANUFACTURING OF METALS

Memory and Annexes

Author: María del Mar Blanes Martinez
Director: Emilio Jiménez
Co-Director: Jéssica Calvo

Announcement: June 2020

Abstract

Metal additive manufacturing is poised to be a manufacturing technology that positively affects all of the world's major industries as it has seen very rapid growth in recent years thanks to technological developments and research investments.

Among the different additive manufacturing methods, there is the technique of Binder Jetting, which is based on the manufacture of piece layer by layer by the selective deposition of fluid binder on a bed of metallic powder. After the printing process, the pieces obtained must undergo curing and subsequent densification. This is the only manufacturing process for powder bed additives that is not based on melting, so the manufactured parts have isotropic properties and are free of residual stresses since the thermal gradients during the process are eliminated. Along with this, the fact that it does not require a camera under specific conditions makes this technique potentially more scalable than other additive manufacturing techniques. Additionally, these processes allow the ability to produce various metal parts, of different sizes, functional and complex geometries for various applications at a lower cost and a shorter delivery time than other technologies.

The American company *HP Inc* has adopted this technology to manufacture metal 3D printers. Being a recent technology, its research focuses on the most used metals, such as 316L stainless steel due to its wide range of applications, such as biomaterials, automobile parts, nuclear reactors, and any application that requires resistance to corrosion.

This work collects the information necessary to understand this technique, in addition to being a guide on the selection of the raw material and the optimization of the process parameters. The characteristics of the powder, the properties of the binder, and the parameters of the printing process that most influence the properties of the final pieces are reviewed. Therefore, what this is about is that this work is a prelude to future projects in collaboration with *HP* where the metallic powder is studied and its influence on the selection of some process parameters.

Resumen

La fabricación aditiva (en inglés *additive manufacturing*) de metal está preparada para ser una tecnología de fabricación que afecta positivamente a todas las principales industrias del mundo ya que, en los últimos años, ha experimentado un crecimiento muy rápido gracias a los desarrollos tecnológicos y a las inversiones en investigación.

Entre los diferentes métodos de fabricación aditiva existe la técnica de inyección de aglomerante o *binder jetting* en inglés, el cual se basa en la fabricación de una pieza capa por capa mediante la deposición selectiva de aglutinante fluido sobre un lecho de polvo metálico. Tras el proceso de impresión, las piezas obtenidas deben de someterse a un curado y a una densificación posterior. Este es el único proceso de fabricación aditiva de lecho de polvo que no está basado en fusión, por lo que las piezas fabricadas poseen propiedades isotrópicas y están libres de tensiones residuales ya que los gradientes térmicos durante el proceso son eliminados. Junto a esto, el hecho de que no requiera una cámara bajo condiciones específicas, hace que esta técnica sea potencialmente más escalable que otras técnicas de fabricación aditiva. A todo esto, se le suma la capacidad de producir varias piezas metálicas, de diferente tamaño, funcionales y de geometrías complejas para diversas aplicaciones a un costo menor y un tiempo de entrega más corto que otras tecnologías.

Esta tecnología ha sido la adoptada por la empresa estadounidense *HP Inc*. para la fabricación de impresoras 3D de metales. Al ser una tecnología reciente, sus investigaciones se centran en los metales más utilizados, como es el caso del acero inoxidable 316L debido a su amplio abanico de aplicaciones, como por ejemplo en biomateriales, piezas de automóviles, reactores nucleares y cualquier aplicación que requiera resistencia a la corrosión.

En este trabajo se recopila información necesaria para poder comprender dicha técnica, además de ser una guía sobre la selección de la materia prima y la optimización de los parámetros del proceso. Se revisan las características del polvo, las propiedades del aglutinante y los parámetros del proceso de impresión que más influyen en las propiedades de las piezas finales. Por lo tanto, lo que se trata es de que este trabajo sea como una antesala a futuros proyectos en colaboración con HP donde se proceda a estudiar el polvo metálico y su influencia en la selección de algunos parámetros de del proceso.

Resum

La fabricació additiva de metall està preparada per ser una tecnologia de fabricació que afecta positivament a totes les principals indústries del món ja que en els últims anys, ha experimentat un creixement molt ràpid gràcies als desenvolupaments tecnològics i a les inversions en recerca.

Entre els diferents mètodes de fabricació additiva hi està la tècnica d'injecció d'aglomerant, la qual es basa en la fabricació d'una peça capa per capa mitjançant la deposició selectiva d'aglutinant fluid sobre un llit de pols metàl·lic. Després del procés d'impressió, les peces obtingudes s'han de sotmetre a un curat i a una densificació posterior. Aquest és l'únic procés de fabricació additiva de llit de pols que no està basada en la fusió, de manera que les peces fabricades posseeixen propietats isotròpiques i estan lliures de tensions residuals ja que els gradients tèrmics durant el procés són eliminats. A més a més, el fet que no requereixi una càmera sota condicions específiques, fa que aquesta tècnica sigui potencialment més escalable que altres tècniques de fabricació additiva. A tot això se li suma la capacitat de produir diverses peces metàl·liques, de diferent grandària, funcionals i de geometries complexes per a diverses aplicacions a un cost menor i un temps de lliurament més curt que les altres tecnologies.

Aquesta tecnologia ha segut l'adoptada per l'empresa nord-americana *HP Inc* per a la fabricació d'impressores 3D de metalls. Al ser una tecnologia recent, les seves investigacions se centren en els metalls més utilitzats, com és el cas de l'acer inoxidable 316L a causa del seu ampli ventall d'aplicacions, com per exemple en biomaterials, peces d'automòbils, reactors nuclears i qualsevol aplicació que requereixi resistència a la corrosió.

En aquest treball es recopila informació necessària per poder comprendre aquesta tècnica, a més de ser una guia sobre la selecció de la matèria primera i l'optimització dels paràmetres del procés. Es revisen les característiques de la pols, les propietats de l'aglutinant i els paràmetres del procés d'impressió que més influeixen en les propietats de les peces finals. Per tant, el que es tracta és que aquest treball sigui com una avantsala a futurs projectes en col·laboració amb HP on es procedeixi a estudiar la pols metàl·lic i la seva influència en la selecció d'alguns paràmetres de de el procés.

Acknowledgment

En esta sección, permítanme que exprese mis agradecimientos en mi lengua materna.

En primer lugar, me gustaría expresar mi sincero agradecimiento a mi supervisor y tutor de tesis, el Dr. Emilio Jiménez Piqué y a la cotutora, la Dra. Jéssica Calvo, por sus directrices, su disposición a adaptarse y su apoyo moral tras la situación vivida a causa del COVID19. También agradecerles el tiempo invertido en este proyecto puesto que no es fácil adaptarse a esta nueva situación y tener que conciliar la vida laboral con el ambiente del hogar. Del mismo modo, quisiera expresar mi agradecimiento a todo el personal de la Universitat Politècnica de Catalunya (UPC), por su prestarme su ayuda en todas las dificultades que enfrenté durante mi trabajo a nivel de gestión.

Quiero agradecer especialmente a todos mis antiguos compañeros y manager de HP, Aleix Oriol. Gracias a ellos, he podido conocer de primera mano el funcionamiento completo de las impresoras 3D HP. Reconocimiento especial a Rocío Muñoz Moreno, quien estuvo a cargo de detallar el primer proyecto junto con Emilio y Lluis Miguel Llanes, haciéndome participe en todo momento de las decisiones tomadas. Otros compañeros que me han brindado su desinteresada ayuda han sido Sergi Bafaluy Ojea y David Barreda, dispuestos en todo momento a solventar las diferentes dudas surgidas relacionadas con la impresión de metales.

Además, agradezco a los compañeros del master, que me han aconsejado en todo momento, no solo en el período que duró este proyecto, sino también en los dos años que ha durado el master. Dos años llenos de risas, horas de estudio, esfuerzo y compañerismo.

Finalmente, pero no por esto menos importante, gracias a mi familia y amigos por mostrarme su apoyo y compresión durante estos meses de trabajo constante en los que he elaborado este proyecto.

En este apartado me gustaría también hacer una mención especial a un profesor del máster que ha fallecido a causa del COVID19, Jesus Jorcano Molins. Le agradezco su gran pasión por la docencia, demostrando un empeño excepcional en todas sus clases.

Glossary of terms

.stl	*Standard Tessellation/Triangle Language*
3D	*Three -Dimensional*
AAS	*Atomic Absortion Spectroscopy with flame atomizer*
ACI	*Alloy Casting Institute*
ACT	*Additive Technology Center*
AD	*Accumulating Direction*
AES	*Auger Electron Spectroscopy*
AFM	*Atomic Force Microscopy*
AFNOR	*French Association for Standardization*
AISI:	*American Iron and Steel Institute*
AM:	*Additive Manufacturing*
ANSI:	*American National Standards Institute*
AOR	*Angle of Repose*
ASME	*American Society of Mechanical Engineers*
ASTM	*American Society for Testing and Materials*
AWS	*American Elding Society*
BCC	*Body-Centred-Cubic*
BET	*Brunauer-Emmett-Teller Technique*
BFE	*Basic Flow Energy*
BJ	*Binder Jet*
BJH	*Barrett-Joyner-Halena*
BSE	*Backward Scattered Electron*
CAD	*Computer-Aided Design*
CAGR	*Compound Annual Growth Rate*
CBD	*Bulk Density*
CI	*Carr Index*
CJ	*Continuous jet print head*
CNC	*Computer Numerical Control*
CR	*Counter-Roll*
CT/XCT	*Computed Tomography by X-Ray*
D	*penetration depth of the binder*
DED	*Direct energy deposition*
DLS	*Dynamic Light Scattering*
DMD	*Direct Metal Deposition*
DMLS	*Direct metal laser sintering*
DoD	*Drop-on demand print head*
DS	*Double Smoothing*
DSC	*Differential Scanning Calorimetry*
DTA	*Differential Thermal Analysis*
EBAM	*Electron Beam Additive Manufacturing*
EB-PBF	*Electron beam melting*

EDM	*Wire Electroerosion*
EDX/EDAX	*Energy Dispersive X-Ray Spectroscopy*
EEBE	*Escola d'Enginyeria Barcelona Est*
EELS	*Electron Energy Loss Spectroscopy*
EI	*Empirical Explosive Index*
EPMA	*Electronic probe X-Ray Microanalysis*
FCC	*Face-Centred-Cubic*
FDM	*Fused Deposition Modelling*
FESEM	*Field Emission Scanning Electron Microscope*
FIB	*Focused Ion Beam*
GDP	*Gross Domestic Product*
GE	*General Electric*
GS-AAS	*Atomic Absortion Spectroscopy with graphite furnace*
HIP	*Hot Isostatic Pressing*
HP	*HP Printing and Computing Solution S.L.*
HR	*Hausner Ratio*
HRTEM	*High Resolution Electron Transmission Microscope*
ICP-OES	*Optical Emission Spectroscopy with Inductively Coupled Plasma source*
ICT	*Information and communications technology*
IMF	*International Monetary Fund*
IPC-MS	*Mass Spectroscopy with Inductively Coupled Plasma source*
IR	*Infrared Absortion*
ISO	*International Organization for Standardization*
LB-PBF	*Selective Laser Powder Bed Melting*
LD	*Laser Diffraction*
LENS	*Laser Designed Network Shaping*
LOM	*Laminated Object Manufacturing*
ME	*Metal Extrusion*
MIM	*Metal Injection Molding*
MIT	*Massachusetts Institute of Technology*
MJ	*Material jet*
MPIF	*Federation of Metal Powder Industries*
NIST	*National Institute of Standards and Technology*
NPJ	*NanoParticle Jetting*
Oh	*Ohnesorge number*
OM	*Optical Microscopy*
PBF	*Powder bed fusion*
PM	*Powder Metallurgy*
PREP	*Plasma Rotating Electrode Process*
PSD	*Particle Size Distribution*
R&D	*Research and Development*
RBS	*Rutherford Backscatter Spectroscopy*

RD	*Rolling Direction*
Re	*Reynolds number*
REP	*Rotating Electrode Process*
RH	*Relative humidity*
RP	*Rapid prototyping*
RPA	*Revolution Powder Analyser*
SAE	*Society of Automotive Engineers*
SE	*Specific Energy*
SE detector	*Secondary Electron Detector*
SEM	*Scanning Electron Microscope*
SGC	*Solid Ground Curing*
SH	*Spherical Harmonic Analysis*
SI	*Stability Index*
SL	*Sheet Lamination*
SLA /SL	*Stereolithography*
SLM	*Selective Laser Fusion/Melting*
SLS	*Selective Laser Sintering*
SPM	*Scanning Probe Microscopy*
TC	*Thermal Conductivity*
TEM	*Transmission Electron Microscope*
TFM	*Trabajo Final de Máster*
TGA	*Thermogravimetic Analysis*
TMA	*Thermomagnetic Analysis*
TPA	*Thermoparticles Analysis*
UC/USL/UAM	*Ultrasonic Consolidation Sheet Lamination*
UNS	*Unifred Numbering System*
UPC	*Universitat Politècnica de Catalunya*
USA	*Unated State*
VD	*Vibrating Direction*
W	*Extension of the binder*
WD	*Working Distance*
We	*Weber number*
WEDM	*Electric Wire Discharge Machining*
XPS	*X-Ray Photoelectron Spectroscopy*
XRD	*X-Ray Diffraction*

Index

Index of Figures

Index of Tables

Preface

Origin of the Project

Initially, this work was to be part of an ongoing research collaboration between *HP Printing and Computing Solution S.L* (HP) and the *Department of Materials Science and Metallurgy* of the *Universitat Politècnica de Catalunya* (UPC-EEBE). This research would have been to characterize a series of dust samples that HP uses for 3D metal printing. This powder is 316L stainless steel. The supposed objectives were to quantify the parameters that affected the process in order to establish quality criteria and check if the powder underwent any changes after printing to ensure that it can effectively be recycled. In other words, it would be a matter of analyzing stainless steel metal powder to better understand its behavior and thus optimize the printing process.

The problem arose when, due to the coronavirus pandemic, the state of alarm was declared on 14th of March of 2020 in Spain, and all kinds of activities were prohibited. As a consequence, it was decided to adapt this project to a possible end-of-Master's project that did not require experimental work. This is how this bibliographic work emerged, where different studies related to metal 3D printing are compiled, focusing on the technology used in HP and 316L stainless steel. Therefore, this work could be the prelude to a future project for the characterization of metallic dust used in HP.

Motivation

3D printing is the technology that is revolutionizing traditional manufacturing systems. Layered manufacturing methodology represents a disruptive change in the industry that requires careful analysis for optimal exploitation. The evolution that this technology is experiencing is dizzying and it is very important to be updated on the new processes, materials and solutions that are appearing.

From the point of view of an engineer, the possibilities presented by this technique are very interesting since it presents substantial improvements in the production processes in terms of efficiency and flexibility.

As we have been able to observe these two months of health crisis where many of the population has suffered from a severe acute respiratory syndrome caused by the coronavirus (*SARS-CoV-2*), it has been possible to manufacture in record time, unimaginable if the old manufacturing techniques had been used, parts for medical respirators and other useful utensils for health workers. Some of the companies that have made this possible have been both large companies such as *HP* and *Materialize*, as well as small

shops or technology centers such as the *Leitat Technological Center*. It is true that most of these parts have been manufactured using polymeric materials such as polyamide 12. This is because additive manufacturing on an industrial scale is more evolved with these materials.

During my internship at HP, I was very interested in its 3D printing technology, since its focus is industrial production, and has become a competitor of traditional technologies. For this reason, I wanted to carry out a project with this company, to be able to take advantage of this opportunity and learn more about the materials and the process. After having several meetings with different departments of the university and commenting on their respective proposals, the decision was made, opting for this project.

Prerequisites

The objective of this master's thesis is to understand the behaviour of metallic powder used during the HP printing process. To give an overview of the organization of this work, the first part of the master's thesis focuses on a short introduction and presentation of additive manufacturing (AM) and then, in the second chapter, expand on its development, commenting on the different AM technologies or do a little analysis of the current situation. This part is where the Binder Jet technology of metal AM will be presented. After this section, we will proceed to discuss how metallic powders are made and the different properties to take into account in their characterization. The last chapter is a compilation of the results of different studies, where the suitable properties and parameters of the process are specified to optimize 3D metal printing using Binder Jet technology.

Two aspects to consider in future dust characterization projects used by HP 316L stainless steel are also set out in the annexes. Annex A will be a summary of stainless steel, their composition, and their different types. Annex B details the advanced techniques that could be successful in the characterization of metallic powder, possible techniques to take into account in a future characterization of the powder.

.

Objectives

The main objective of this research work is to carry out a general review of the additive manufacturing technology known as Binder Jetting, in order to know its operation and thus be able to better understand the technique in future studies. Therefore, it is contributing to the development of additive manufacturing technologies for obtaining metal parts.

For this, we will proceed to:

- Get an overview of 3D printing technologies for metallic materials.
- Know the possible manufacturing processes of metallic powder and the advantages of these, to be able to select the appropriate raw material and estimate its cost.
- Know how to characterize metallic powders and the analytical techniques used to obtain or measure this property.
- Understand the relationship between the physical properties of metallic powders and their printing capacity using Binder Jetting technology.
- Provide a comprehensive guide to select the optimal parameters of the BJ printing process. These optimal conditions will lead to achieving the total density and desired properties of parts manufactured by BJ.

1. Industry 4.0 and Additive Manufacturing.

1.1. Digital economy and Industry 4.0.

In the last decades, there has been a transition towards the new digital paradigm established in the globalized world. The term "digital economy" refers to the increase in technical and technological applications from the computer and telecommunications sector (ICT), which have caused a change at the social, cultural and economic level. This term was first defined in 1998 in the report of the United States Department of Commerce "*The emerging digital economy*"[1]. Don Tapscott's book *" Digital Economy: Promise and Peril in the Age of networked Intelligence*" talks about new interesting business possibilities for the industry [2]. In this new environment of an interconnected system, the economy involved a modification of the production models in aspects such as location, production size, and business relationships between suppliers, customers and competitors. In addition, thanks to ICTs, there was growth in the global market as we know it today [3].

The introduction of new digital technologies in the industry allows a connection between the technologies that emerged in The Third Industrial Revolution, such as process automation, and digital technologies focused on data storage, processing and transmission. The collaboration between the physical world (devices, installations and machinery) and the digital world (systems) created the intelligent industry, which is known as Industry 4.0. This new trend has allowed the interconnection of value chains and business models. In other words, business models have emerged in which value chains are integrated and digitized, where individualized management of the product-customer binomial is made thanks to the development of personalized products and real-time connections.[4]

In summary, the digital transformation emerged as a response to the new needs of the productive processes such as the reduction of the consumption of material resources and time, the maximization of efficiency, flexibility and productivity. Nowadays it is not just about generating a competitive advantage but it is already a matter of survival for companies.

The Figure 1 shows a way to group the new technologies that emerged in the new panorama.

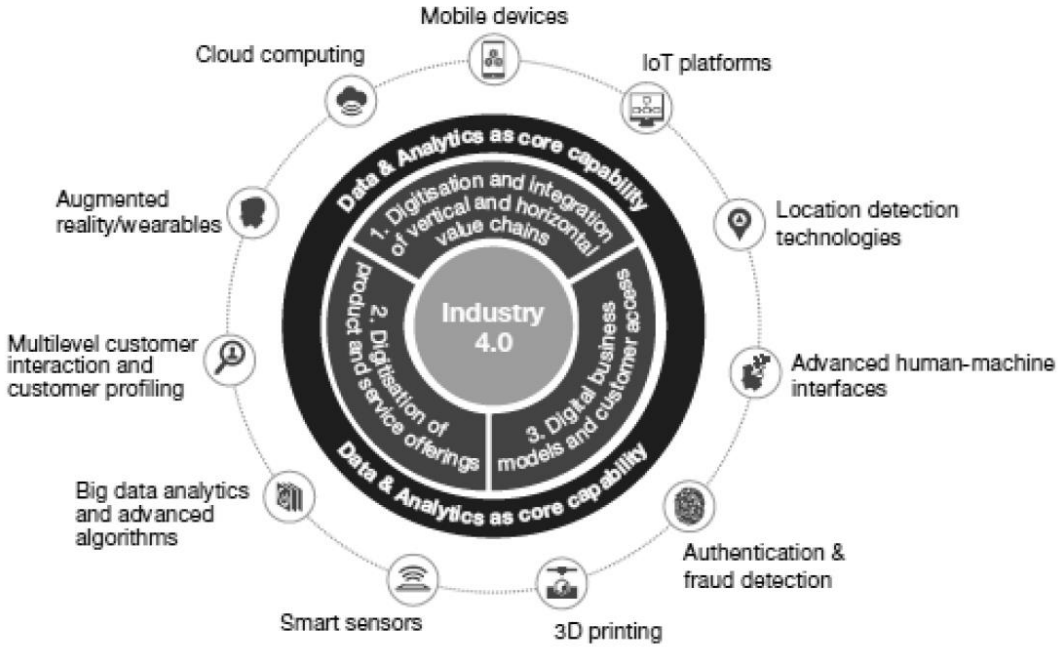

Figure 1. Technologies that are part of the Industry 4.0 .[5]

The eight techniques are additive manufacturing (AM), collaborative robotics, cyber-physical systems, cloud computing, big data, augmented reality, artificial vision or virtual reality, and cybersecurity. All these techniques have allowed huge amounts of data to be processed at high speed and mechanical systems to be operated, exceeding the limits of reliability and precision. However, manufacturing processes are still largely traditional. The physical limitations of these traditional methods make it difficult to develop new products with high additive value or with new functionalities.

1.2. Additive manufacturing techniques

Additive manufacturing (AM) techniques allow to overcome these barriers, reducing the distance between the conceivable and the achievable, giving designers great freedom, thus opening a new field of exploitation of the individuality of consumers, that is, to personalization. It also allows you to go from a digital object to a real one more easily. Therefore, it has the potential to outline a future where productive centers exist; delocalized, working in a network, and collaboratively multiplying my means and resources, reducing displacement, delays and waste. [6, 7]

The limitations of AM, which are currently conditioned by the current state of the art, do not lie in the process, but in the materials, its cost and productivity. During these last years, AM has been a focus of

attention throughout Europe. The main European R&D financing programs have different open calls for this type of technology, thus demonstrating the great potential and interest it arouses.

At the beginning, AM techniques came up with the name of rapid prototyping (RP) since they were originally conceived for this purpose. The first RP-reproduced object occurred on March 9, 1983 by Charles W. Hull (USA), who obtained one object by consolidating multiple layers of an acrylic-based photopolymeric material. Later the patent was obtained in 1986, coining the term stereolithography (SLA) and it was from the North American company *3D Systems*. This technique arrived in Europe in 1990 and later new AM techniques emerged and with them applications [8]. The following AM technologies emerged in 1991 and were the Fused Deposition Modelling (FDM) of the American company *Stratasys*, Solid Ground Curing (SGC), from the Israeli *Cubital* and Laminated Object Manufacturing (LOM), from the American *Helisus*. In 1992, the sintering system known under the name of Selective Laser Sintering (SLS) was born from the hand of American company *DTM*. From this moment on, new technologies were continuously developed in search of new applications such as the Polyjet technique. However, it was not until the open-source movement of Dr. Adrian Bowyer's RepRap project appeared in 2005 when the barriers of 3D printing started to slowly fall until today. [9]

The basic operation of AM is to selectively build the final piece layer by layer from three-dimensional (3D) models. Various materials can be used as a raw feedstock, including metals, ceramics, polymers, sand and glass.[6, 10-19]. The increasing attention in AM techniques is due to the ability to produce complex parts in a simple way, directly from a computer-aided design (CAD), assuming a minimization of cost, consumption of energy and raw material, amount of waste produced, steps of production and therefore time spent and human resources used. [6, 16, 20-26]. Another reason for the current interest in metal AM is that the final products, which were the result of the assembly and the union of different parts using the previous techniques, are produced as a monolithic piece or reduce the number of subcomponents. This can be critical on parts designed to handle air and liquids, because gaskets and sealing surfaces are points where mechanical failures and leaks occur. [7]

In addition, life cycle studies have been carried out, comparing AM and conventional manufacturing. All studies concluded that the energy consumption of AM dominates environmental impacts.[27-29]

Although there are a wide variety of different AM processes, they all have a series of steps or phases in common, specifically in three general phases. The first phase is the conception or conceptualization of the object and subsequent digitization, obtaining the CAD model in three dimensions. Reverse engineering can also be applied and the CAD model can be obtained from a physical object by means of three-dimensional scanning of that object. After obtaining the CAD model, the geometry is discretized through a mesh of interconnected triangles. This new format is the well-known stereolithography and its corresponding extension is *".stl"* (Standard Tessellation Language or Standard Triangle Language). As the

Figure 2 shows, the level of precision with which the geometry is defined depends on the size or number of the triangles in the mesh.

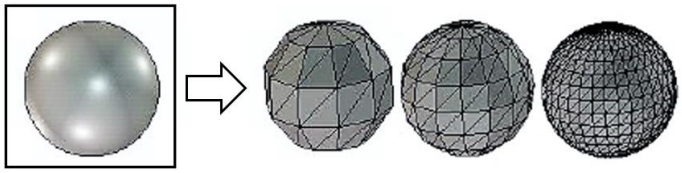

Figure 2. Discretization of a sphere using different mesh. [W1]

The last software used in this stage is specialized software for the reproductive equipment. This defines the location of the object on the construction platform, the orientation of the pieces, their labeling if necessary, and the definition of supports or container-boxes. Some software allow you to define some of the physical properties of the object such as the infill of the part. Some of the software that currently exist in the market are *MAGICS* by *Materialize*, *CURA*, *slic3r* (open source created by David Braam and Alessandro Ranellucci respectively), *Creative Workshop* created by Steve Hernández and Shai Segar or Netfabb acquired by *Autodesk*. These allow going from a digital file in STL format that defines the geometry, to a new format readable by the AM machine that defines the sequence of instructions necessary for it to proceed. Once defined how the pieces will be reproduced, these software are responsible for discretizing the file in layers. The number of layers is defined by the thickness of the layers. Slicing causes the simplification of a 3D geometry into a set of two-dimensional (2D) elements. Therefore, the thickness of the layer influences manufacturing time, productivity, the smoothness of the curves and thus the quality of the final part. This is how the way in which objects are reproduced becomes important, because it is not the same to print vertically than horizontally, since the number of layers, the mechanical properties of the object or the "aesthetic" quality of the piece will change.

The next stage is manufacturing where the necessary human resources are few or none. This is one of the advantages of AM techniques since it allows the delocalization of the manufacturing. The last stage would be the one known as post-processing or finishing. This is made up of all the processes that intervene in the finalization of the piece, such as, for example, the removal of the supports or excess dust, the curing to increase hardening, heat treatments or surface finishing processes.

2. Metal Additive Manufacturing's technology

Following commercialisation in the 1990s, today metal 3D printing is advancing rapidly, becoming more advanced, increasing print speeds and having greater range of industrial materials. 3D metal printing is targeted to compete with traditional methods. These traditional manufacturing methods for shaping metal material components range from metal forming (for example rolling, extrusion, injection moulding, forging, drawing), metal bonding (for example welding, brazing), machining, casting, and powder metallurgy (press and sinter processes).

Because of this, there is currently wide variety of technologies available and integrating them into existing workflows can be challenging for many companies. In competing with traditional manufacturing methods, several factors influence AM implementation in the industry, such as technological factors, organizational factors, strategic factors, operational factors, and supply chain.[30]

The interest arising from this form of manufacturing is due to the potential it presents compared to traditional manufacturing processes [31]. The key potential benefits of 3D metal printing are[32]:

- Time saving and cost reduction: AM tools such as moulds are eliminated, which reduces costs and accelerates the transition from design to production and therefore the time used. It also avoids further assembly or assembly processes which also significantly reduces time and labour.
- Less waste production: since it is not a subtractive manufacturing method, it generates less waste. In many cases, non-sintered metal powders can even be reused, greatly increasing the efficiency of the process.
- Higher level of complexity and innovation in design. Lightweight metal parts with improved functionality and complex mechanical properties or geometries can be produced more cost-effectively using design tools such as topology optimization and generative design.
- Cost-Effectiveness of Low-Volume Production and Customization: Because no tools are required, the production of custom parts is cost-effective whether it is a single part or a small batch. This also creates an on-demand demand market. In other words, companies can offer a printing service that reduces the need to store parts in a physical inventory and thus simplify logistics and the supply chain.

Therefore, it follows that AM technologies reduce production costs. Gebler et al. demonstrated by calculations made using their model, that 3D printing contains the potential to reduce costs by 150–535 billion of €, total primary energy supply by 2.54–9.30 EJ, and CO_2 emissions by 130.5 –525.5 Mt by 2025.[33]

The benefits of metal 3D printing are clear, but such a manufacturing method faces challenges such as high prices. Admittedly, the price of 3D printers has dropped significantly in the past decade; the cost of

AM metal systems remains one of the top challenges for companies looking to invest in technology. Nevertheless, it is not just the price of the machine, the current metal materials available on the market are generally quite limited, and the costs are significantly higher than those of the metals used in traditional metal fabrication. Other challenges are the multiple control parameters make it a complex process, and the control of the variables is important to allow high quality and repeatable metal parts. Knowledge of the relationship between printing processes and the properties of the resulting material is not yet accurate, so confidence in these parts for structural applications is low. [34]

Printer manufactures, material suppliers and all the companies that have their niche in metal 3D printing are prepared to cover the expected demand that is worth 17B € in 2029. This growth was analysed in the latest market intelligence report from *IDTechEx Research*, *3D Printing Metals 2018-2028: Technology and Market Analysis* [35]. Exponential growth rates will continue as new technologies at lower price hit the market. Exponential growth rates will continue as the new lower-priced technologies hit the market. The Compound Annual Growth Rate (CAGR) will continue to be a high value, of 23% between 2018 and 2028. Long-term materials revenue will grow at faster rate than for printers. [W2]

2.1. Common materials used

The metallic materials used are generally high-quality powder and must meet certain characteristics, such as the shape and size of the particles, and the density of the powder. It is true that the range of metals for 3D printing is limited due to the time required to adapt and produce these metals for the printing process. This does not happen in all techniques, as there are some that can use metals used in traditional processes. The most commonly used materials today are light metals such as aluminium, titanium and stainless steel. Refractory metals and cobalt chromium alloys are also being used, due to their interest in the aviation and oil-gas sectors. The table below (Table 1) shows the most used metals and their applications, along with the characteristics that make them optimal for these applications [36-38].

Table 1. The most used metals in 3D metal printing industries. [W3]

Material	Applications	Characteristics
Aluminium and alloys *AlSi10Mg*	Lightweight or/and geometrically complex parts. In electronic, automotive and aerospace industries	• High corrosion resistance • Easy post-processing • High strength to weight ratio • If it is alloyed with silicon, its resistance is greater. • High temperature resistance and thermal and electrical conductivity.
Titanium and alloys *Ti6Al4V*	Motorsport, aviation, aerospace and medical/dental industries	• Excellent biocompatibility • Good strength and toughness • High corrosion resistance • High density but lightweight • High cost.
Stainless steel *316L*	Aerospace, oil & gas, food processing and medical industries. In consumer products such as cutlery.	• High hardness and toughness • Biocompatible • High resistance to corrosion • Good weldability • High ductility • Lower cost than titanium or nickel
Cobalt chromium alloy *CoCrMo*	Medical and dental devices, gas and wind turbines, engine components.	• Excellent strength • High corrosion resistance • Temperature resistance • Non-magnetic • Biocompatible
Nickel alloys *Inconel 625 and 718*	High-temperature applications. Aerospace, chemical process and power industries.	• High corrosion resistance • Great strength and toughness at high temperature • Excellent weldability
Copper alloys	Tool inserts electrical engineering and thermal management applications.	• Good rigidity • Excellent thermal and electrical conduction
Refractory metals *(tantalum, niobium and tungsten)*	High-stress applications (missile and rocket thruster nozzles; valves and manifolds; implants)	• High hardness • Heat and wear resistant • High corrosion resistance • Chemical inert • High thermal stability • High biocompatibility and low toxicity (tantalum)
Precious Metals *(silver, gold, platinum, brass and bronze)*	jewellery, accessories, and decorative objects	• Printing precious metals directly is very limited.
Maraging steel *(iron alloy exposed to high temperatures)*	Production of moulds and tools for injection moulding Components requiring high strength.	• High strength, hardness and malleability. • Easily machined and welded.

2.2. Metal Additive Manufacturing's techniques

With the development of laser-based powder bed fusion, the first technology for metal Additive Manufacturing was established. Today we know more than 18 different metal 3D printing processes, adding new ones almost every day. Many of these processes have their origins in long-established technologies such as build-up welding and metal injection moulding. Others are completely new technologies.[W4] While each has its benefits and limitations, all are united by the fundamental 3D printing principle of creating metal parts layer by layer [39]. An outline of the classification, based on the ASTM / ISO 52900 standards, of the different technologies for the manufacture of metallic additives are shown in Figure 3. Although it is true that these new technologies have emerged, that are not classified by these standards or there are methods that are the combination of two others and, therefore, are not easily classifiable.

In general, AM techniques fall into two categories that include (1) methods based on metal fusion, such as direct energy deposition (DED), laser powder bed fusion (LB-PBF), fusion of electron beam (EB-PBF); and (2) non-fusion based methods such as extrusion, binder jet (BJ), material jet (MJ), and sheet lamination (SL). Each process has its own nuances with respect to the processable materials and the properties of the final pieces built.[13, 40, 41]

Another way to classify the different metal printing technologies is according to the state of the raw material used. One of these types are AM metal processes that use a powder bed. Using a powder bed is a common method of producing parts through AM. The raw material of the final piece comes in the form of a powder, which spreads on the bed in a thin layer. The particles of one layer are joined forming a 2D figure and after this, the platform is lowered to proceed to the distribution of the next layer of powder and repeat the process layer by layer [42, 43]. After printing, the powder bed must be cooled to remove the non-fused powder from the container and clean the printed part. Within this group, there are techniques that, as mentioned above, are based on the selective fusion of the powder bed and other techniques in which the particles adhere by another agent. [W5,W6]

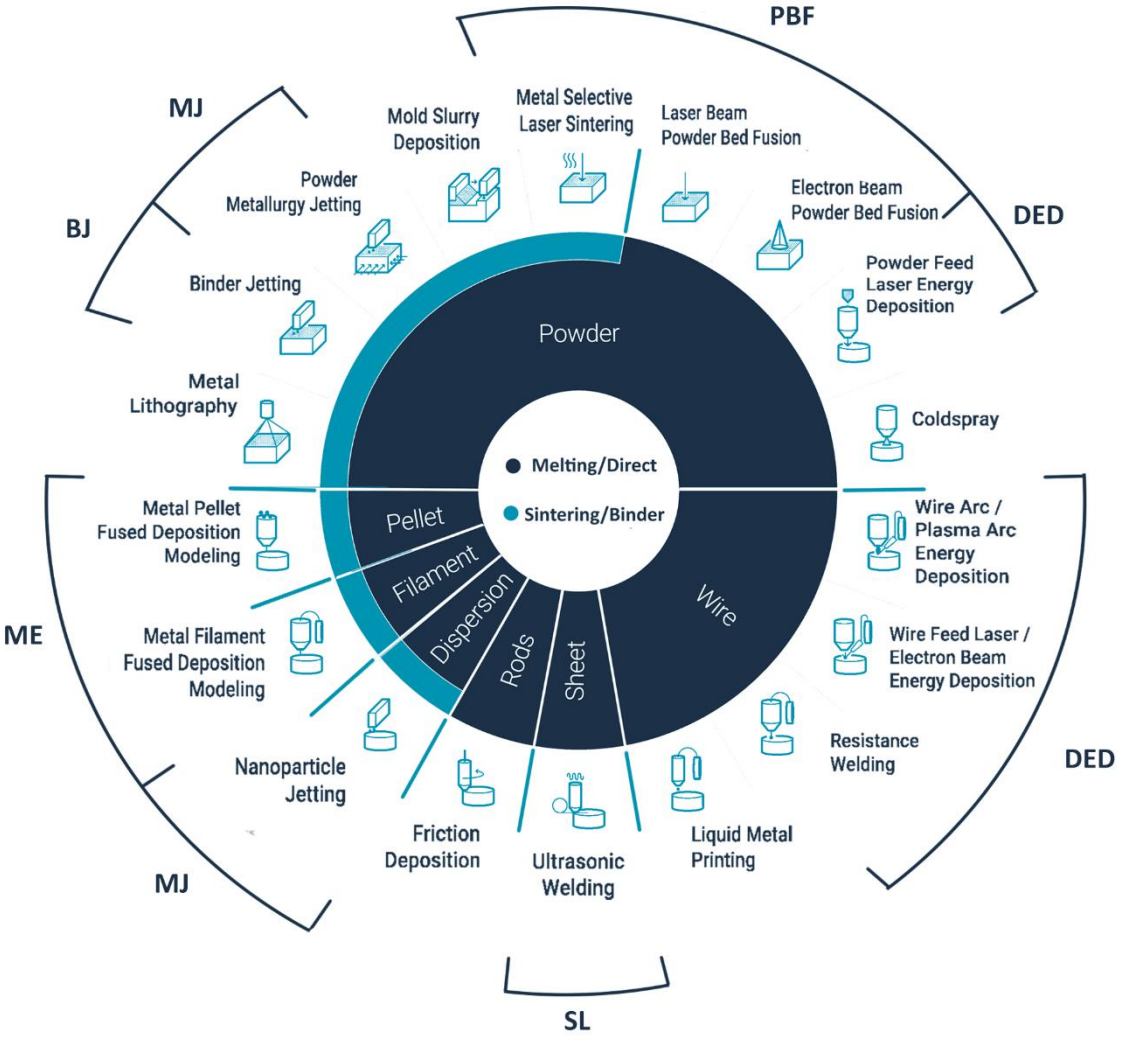

Figure 3. Actual metal AM techniques [W4].

As seen in the previous graph (Figure 3), eighteen different operating principles are currently known with more than 190 machines on the market, as will be detailed later (Figure 18). To successfully work with metal AM, you need to understand the printing process and its properties. In addition, design, process chain, and cost structure must be considered.

It is true that it is difficult to find a unique way of encompassing and naming each technique. This is because new techniques are emerging each time that are based on new operating principles or a combination of two existing ones. In addition, some identical operating techniques with different names are presented. In this section an effort has been made to try to detail the main techniques of metal AM, taking into account the standard issued by ASTM Committee F42 on AM terminology[44].

- Powder bed fusion (PBF)
    - Selective laser melting (LB-PBF)
    - Electron beam melting (EB-PBF)
- Direct energy deposition (DED)
- Sheet lamination (SL):
    - Ultrasonic additive manufacturing (USL) Figure 3.
    - Object Lamination Manufacturing Technology (LOM)
- Metal Extrusion (ME)
- Material Jetting (MJ)
- Binder Jetting (BJ)

2.2.1. Powder Bed Fusion (PBF)

Metal Powder Bed Fusion (PBF) is perhaps the most established Metal AM. With this technique, the powder metal layers are distributed on the platform of a machine and selectively fused by an energy source such as a laser or electron beam. There are two categories: Laser Powder Bed Fusion (LB-PBF) and Electron Beam Fusion (EB-PBF). The first is also known under the following names: Selective Laser Fusion (SLM) or Direct Metal Laser Sintering (DMLS).

As a curiosity, in the 90s, several companies were studying powder bed fusion technology using a laser. In 1994, the *EOS Company* patented its process called Direct Metal Laser Sintering (DMLS); while in 1995, the *Fraunhofer Institute* introduced the term SLM to define the Selective Laser Fusion process. It is worth noting that SLM is currently also the name of a manufacturer of industrial 3D printers. Both processes are based on powder bed laser melting, although the term DMLS uses the word sintering. It should be understood that this is a mistake. The difference between sintering and fusion is quite simple: fusion involves a change of physical state through energy, going from a solid phase to a liquid phase; instead, sintering does not allow the metal to melt because the temperature used is not high enough. As a result, the metal particles clump together [W5]. This is why in this project it has been decided to name this technique as PBF.

Many scientific papers study PBF because they are the most dominant technologies. According to the report by IDTechEx Research, LB-PBF has the largest installed base in the world. Specifically, according to the report made by *IDTechEx Research*, LB-PBF have the largest installed base worldwide. Specifically, LB-PBF had 84% market share in 2016 and the remainder of the market is fragmented across the other four major technology types.[35, 45].These data may currently differ since in 2016 metal 3D printing technologies such as liquid metal deposition, polymer metal filament extrusion and electroplating were not commercially available. Currently, the new techniques mentioned above probably have a significant

market share, as they compete with the established 3D printing technologies in terms of process and specifications.

The operation of both techniques is based on the fusion of metal particles applying a powerful laser selectively and linearly layer by layer. The main differences between LB-PBF and EB-PBF reside in the heat source used and the working conditions.[32]

LB-PBF generally operates under an argon or nitrogen atmosphere at ambient temperature and pressure. This is to prevent uncontrolled oxygen corrosion of the metal powder and to maintain the proper temperature during the printing process. The heat source comes from a laser beam that is manipulated by a series of moving mirrors. The laser used is usually an optic laser fiber (200/400 W) [W5]. An important parameter is the intensity of the laser beam [46]. Due to the operation at room temperature, the thermal gradients are usually high and, therefore, the pieces must be subjected to a subsequent heat treatment to relieve stresses [47]. Below is the schematic diagram of the operation of the LB-PBF process and the components that make up the printing machine. (Figure 4)

Generally, in this technique, the piece is usually attached to the tray using printed supports. These supports are not necessary since, like all powder bed techniques, the unused powder itself supports the parts. However, this technique is recommended to reduce the deformation and distortion phenomena observed at high processing temperatures. One way to remove such supports is by cutting or machining methods or wire electroerosion (EDM). [W5]

This method has the advantage of lower porosity of the final parts with better mechanical properties, complex shape manufacturing capacity and excellent scanning efficiency. Furthermore, the parts can be easily processed in a short period of time, it is a flexible and precise process. The main challenge of this method is that the process is difficult to control due to the large number of parameters involved.

The most widely used material in selective laser fusion has been stainless steel [48], mainly with austenitic grade 316L stainless steels and precipitation hardened stainless steels [49, 50]. Other suitable materials are aluminium alloys, titanium alloys, nickel-based alloys, cobalt and precious metals such as platinum or gold. Magnesium and carbides are not currently commercially available, although in the case of magnesium it is being processed in R&D environments.

Selective laser fusion has wide application in the field of aerospace, medical, and automotive engineering due to the ability to control component stiffness in a desired model [51].

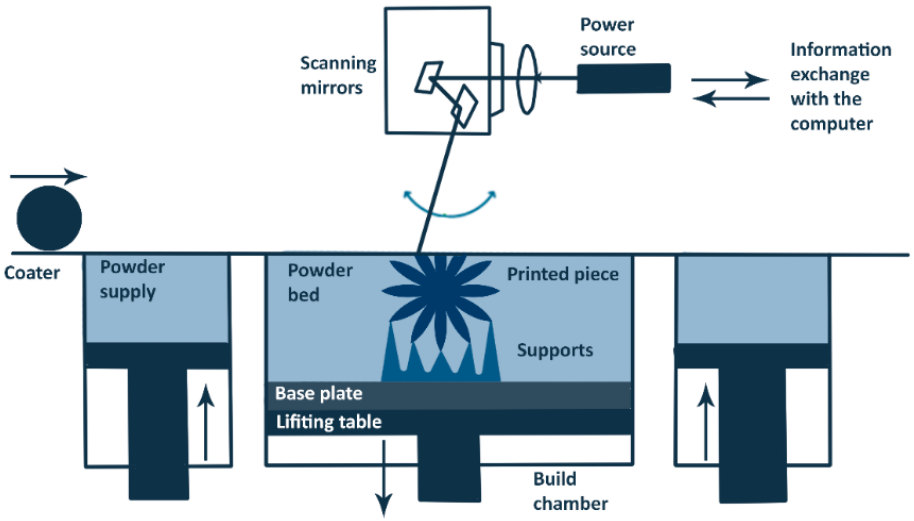

Figure 4. Schematic diagram of Power Bed Fusion process (PBF) [43, 52].

On the other hand, EB-PBF relies on a high-powered electron beam to heat first and then melt the powder bed. The electrons are removed from a tungsten filament under vacuum and then accelerated and projected onto the layer of metallic powder deposited on the platform plate. The other difference is that you must work in a vacuum environment.

In EB-PBF, since almost the entire powder layer is partially sintered before the part geometry melts, the construction temperature is close to the melting temperature of the material and results in on-site stress relief during the construction itself. The powder bed is generally heated to a temperature equal to the melting temperature of the material multiplied by a value factor 0.8. It is worth mentioning that the thermal gradients in the EB-PBF system can be manipulated to influence the texture of the material [53]. A drawback to this technique is that by using electrons, you are limited to using conductive materials. Without this, interaction between the electron beam and dust cannot occur. Even so, if the proper parameters are not used, the construction may fail due to the accumulation effect of electrostatic charge [54].

Today, EB-PBF technology mainly uses titanium and cobalt chromium alloys. The main manufacturer, *Arcam*, has restricted the range of materials and if the user wishes to use other materials, this company must first authorize said material. In terms of applications, EB-PBF technology is mainly used in the aeronautical and medical sectors, particularly to design implants. This is why the most widely used metals are titanium and cobalt-chromium alloy, due to their biocompatibility. [W7]

Some of the differences between EB-PBF and LB-PBF is precision, EB-PBF technology is less compared to LB-PBF. This is because the layer thickness in SLM/LB-PBF is thinner (between 20 and 100 microns) than in EB-PBF (between 50 and 200 microns) [55] In contrast, EB-PBF exhibits higher deposition rates, due to the fast speeds at which the electron beam can be manipulated [56]. An electron beam is very powerful, more than a laser. Therefore, EB-PBF is often used with high temperature metal super alloys to create part for highly demanding applications such as jet engines, gas turbines for the aerospace industry. Something to keep in mind when investing in EB-PBF is its high cost.

In the table shown below (Table 2) the advantages of both technologies will be summarized, making a comparison between the LB-PBF and EB-PBF techniques.

Table 2. Advantages of the respective PBF technologies

LB-PBF	EB-PBF
• Higher dust level precision since the laser is narrower than the electron beam. • Greater manufacturing volume (at least double that of EB-PBF) and therefore the size of the pieces may be greater.	• Preheating the powder before melting limits deformation, therefore reduces the need for reinforcements, and supports during manufacturing. • Higher manufacturing speed because the electron beam can be separated to heat the powder in several places simultaneously. Rather, a laser must scan the surface point by point.

Columnar grain formation is common to PBF techniques in many materials due to the layered solidification of each part as it is built. This leads to the end piece having anisotropic properties, such as different tensile strength and fatigue depending on the printing direction. This is why many of the powder bed fusion techniques need post-processing to improve mechanical, dimensional, and aesthetic properties.[57]

2.2.2. Direct Energy Deposition (DED)

Direct Energy Deposition (DED) is a more complex 3D printing process, which is generally used to repair or add additional material to existing parts, although it is entirely possible to make models from scratch using this technology.

Like SLM technology, this technology can often be called by different names, depending on its manufacturer, application, or specific method. One of these is the Electron Beam Additive Manufacturing (EBAM) method, created by the American company Sciaky. Other names by which they are known are Laser Designed Network Shaping (LENS) or Direct Metal Deposition (DMD). [W7, W8]

The DED operation is based on melting the metal using a focused energy source (a laser, electron beam electric current or plasma arc) and at the same time depositing it through a nozzle on the platform. The nozzle is mounted on a multi-axis arm, usually four or five as it improves its stability and handling. The

metallic material that is fed to the nozzle is provided in the form of powder or wire. [58-61] You could say that, in a way, technology is on the border between extrusion of material and fusion of powder bed.

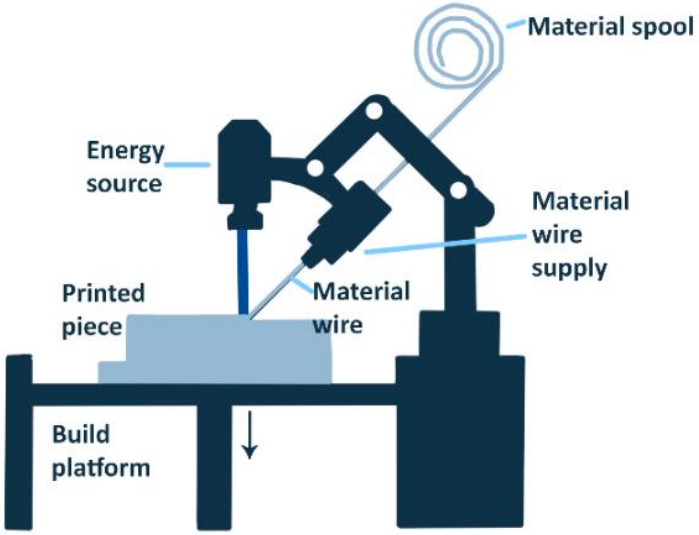

Figure 5. Schematic diagram of Direct Energy Deposition.

In the case of electron beam-based systems, the process must be performed in a vacuum to prevent electrons from interacting or being deflected by air molecules. Laser based systems require an inert gas atmosphere if working with reactive metals. You can also work with an air chamber but with controlled oxygen levels. In the same way, the solidification and cooling process occurs in a closed chamber in an argon atmosphere to prevent oxidation of the melt bath. [W7]

This process allows the use of a wide variety of metals and alloys, almost any metal that is wieldable can be 3D printed with DED. For example, stainless steel, mostly of austenitic grades, and other metals such as titanium and its alloys, composite materials and materials with functional classification [62-65]. Much research related to DED technology has been carried out using stainless steel and / or stainless steel composite material, making a great effort to improve wear resistance and resistance property. It is true that there are still materials that are being developed such as aluminium alloys, steel maraging, copper and bronze. On the contrary, there are materials that cannot be used, such as carbides, since they are non-wieldable materials.

It is worth mentioning that it is possible to use DED with ceramic and polymeric materials. Although this is not relevant to this project, the AREVO Company uses polymer DED with a carbon fiber filament to make lightweight composite parts for end use applications. [W9]

The wire used generally varies from 1-3 mm in diameter and the powder particle sizes are similar to those used in powder metallurgy processes, between 50 and 150 µm. [W8]

The advantages of this AM technique compared to others will be explained below.

- Production of large parts with minimal tooling requirement and relatively little post-processing. According to ASTM International, it has the capacity to produce parts with a construction volume greater than 1000 mm^3. Another example is Sciaky's EBAM technology, which can produce parts over six meters in length. [W10]
- Manufacture components with composition gradients, or hybrid structures consisting of multiple materials of different compositions and structures.
- The cost of the materials used in DED is significantly less than that of the metal powders used in the AM metal powder bed.
- In general, DED machines have high material deposition rates and therefore a high printing speed. For example, some DED processes can reach a speed of up to 11 kg of metal per hour.
- Less waste of material than with the SLM and EB-PBF processes, because with DED only the necessary amount of material is deposited, and therefore there is no waste to recycle. In contrast to techniques using a powder bed, the powder is spread on the build deck and then, even though the unused powder is recycled, a large amount of dust is wasted. This results in efficient use of the material and cost savings.
- Production of high-quality parts, dense and with mechanical properties as good as or better than those of compact or forged materials.
- Hybrid manufacturing capabilities. This means that it is suitable for producing very complex metal parts faster and with greater flexibility because the deposition nozzle can be integrated into a multi-axis machining system.
- Serial production capacity and existence of a dedicated periphery.
- Reproducibility is very good. The process is well controlled and only occasional defects occur.
- The process can be controlled by sensors allowing a good quality control in process.

Although a number of advantages have been previously exposed, this technique also has limitations that sometimes do not make it suitable for use. The main one is its high cost (over 500,000€), being little competitive with traditional methods. In relation to the obtained parts, these tend to have low resolution and a poor surface finish, so they require secondary machining that will add time and cost to the overall process. Furthermore, the pieces do not have supports and the technology does not lend itself to creating support structures, which limits the production of parts with certain geometries, for example, cantilevers. [W7]

DED has been successfully applied in various industries, including aerospace, oil and gas, defence, marine, and architecture. Aerospace manufacturers will increasingly use the technology to produce structural parts for satellites and military aircraft. *Lockheed Martin Space*, for example, recently rated *Sciaky's* EBAM process for building titanium fuel tank domes for satellites. Using technology, the company was able to reduce component production time by 87% and reduce delivery time from two years to three months. Another example is aircraft titanium parts for the *Boeing 787 Dreamliner*, manufactured by *Norsk Titanium* using its proprietary Rapid Plasma Deposition technology. [W7]

Also included in this DED category are Joule Printing (Resistance Welding) technology, patented by *Digital Alloys*, that uses metal wire, which is placed into a moving feed system. Subsequently, the electric current circulates through the cable and subsequently to the printing bed together with the piece. The electric current melts the metal wire as the power system moves, and drops of molten metal form the part. It is a system similar to the electrospinning process. In this technique, it is important that the material is conductive. As it is a relatively new technology, it is not going to be detailed.

2.2.3. Sheet Lamination (SL)

Sheet lamination is an additive manufacturing (AM) methodology where thin sheets of material (usually supplied through a feed roll system) are joined layer by layer to form a 3D part. The bonding of the layers can be by adhesion or metallurgical bonding by brazing, diffusion bonding, [66] laser welding, [67] resistance welding [68] or ultrasonic consolidation. Due to all the joining possibilities, there are different LS technologies. Some examples are Laminate Object Manufacturing (LOM) and Ultrasonic Consolidation (UC / USL / UAM). [W11]

Object Lamination Manufacturing Technology (LOM) is an additive manufacturing process developed by Cubic Technologies. This is a little used technique in metallic laminates because the layers of the metallic material must be covered with a special adhesive. A heat roller passes over the sheet of material on the build deck to fuse the applied adhesive and press the sheets onto the deck. Subsequently, a computer-controlled laser or knife cut the material into the desired shape. [W11]

In 2003, *White* developed an innovative foil lamination process in which the foils were joined by ultrasonic vibrations under pressure, also known as ultrasonic welding (USL) [69]. Despite the above, the date or the creator of this technology are not entirely true, since in 1999 a proposal of this technology emerged by the North American company *Solidica*. What is true is that currently, the USL process is one of the most widely used technologies in metal SL. Therefore, next, we will proceed to detail this technology.

This technique works using ultrasonic vibrations (typically 20,000 Hz) that are applied to sheets of metallic materials, bonded under pressure, to create a solid-state weld because it works at low temperatures.

[W12]. A computer numerical control (CNC) milling machine outlines to create the necessary shape for each layer and thus remove any excess material.[67] (Figure 6)

Metallurgical bonding is achieved due to these two events: on the one hand, adiabatic heating due to the high deformation rate, and, on the other hand, the movement of the grain boundary at the original interface during recrystallization [W12]. The study to achieve a good union has been carried out by Schick et al. [70], Dehoff and Babu [71] and Fujii et al.[72]. Demonstrating that the interfaces with a recrystallization grain texture presented a better metallurgical union.

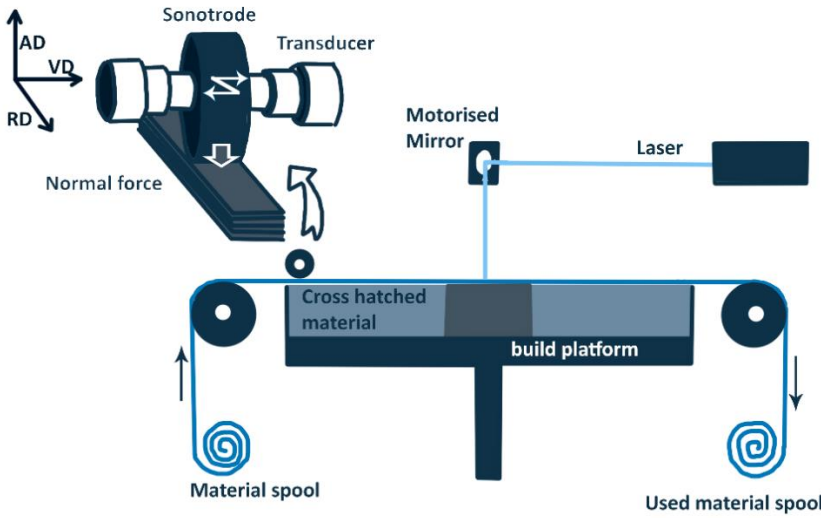

Figure 6 Schematic diagram of Ultrasonic Sheet Lamination (AD: accumulating direction; VD: vibrating direction; RD: rolling direction) [73]

USL can use a variety of materials such as paper, polymer, and metal, but each requires a different method of bonding the sheets of material. Because it allows the exchange of materials in the printing medium and that it works at low temperatures, it is possible to work with different metals with different melting temperatures, since the temperature is not a limiting parameter of the process and, therefore, allows the manufacture of composite materials. Working at low temperatures also allows you to create parts with cables or electronic components inside the part without damaging them.[74]

It is said to work at low temperatures because the overall temperature rise throughout the construction is very low and the process temperature remains around room temperature [75]. Although, it is true that the process introduces a high temperature into the localized region of the interface (being able to reach up to 380 ° C during consolidation) [76].

In summary, the key advantages of this technique are its low cost, its fast printing speeds, and the possibility of creating inaccessible internal geometries and/or manufacturing large parts, the material does

not present microstructural alteration during the process and is a flexible process. Another great advantage, which has already been mentioned, is the ability to print on different materials, such as aluminium and copper, two metals with different melting temperatures that are difficult to combine in the same piece with other technologies.[47] USL is one of the least accurate AM methods with a poor surface finish. Geometric precision in the Z direction is difficult to obtain due to the swelling effects.[77] The anisotropic properties prevail in SL constructions due to the type of bonding processes. Finally, it is worth mentioning that it is one of the few AM methods that produces a considerable waste of material. Another drawback is that the process cannot manufacture complex overhangs as no support material is deposited to provide mechanical support.

Manufacturers use it as a fast, low-cost way to 3D print non-functional prototypes, casting moulds, and other simple designs with easy-to-handle materials for applications in the aerospace and tool design industries.[78, 79]

2.2.4. Metal Extrusion-based additive manufacturing (ME)

Extrusion-based metal 3D printing works similarly to fused deposition modelling (FDM). Pellets or a thermoplastic filament are heated and extruded through a nozzle, layer by layer creating a piece in a "green state". This green body must be further processed: deburring to carbonize and remove the binder polymer and subsequent sintering to obtain a metallic solid body with certain mechanical properties. (Figure 7)

The feedstocks are mixtures of a polymeric binder (40% to 60% by volume) and a solid fine-grained metal powder. In the case of pellets, the metallic powder is enclosed or covered by the polymeric material.

Like the operation of an extruder, the material is pushed into a hot nozzle by one of the following possible mechanisms: the controlled axial movement of a piston inside a heated barrel, or the controlled axial rotation of a worm screw inside a barrel heated, or controlled rotation of two feed endless rollers. If you work with a filament, it can be heated by a laser, very similar to the DED technique. [80]

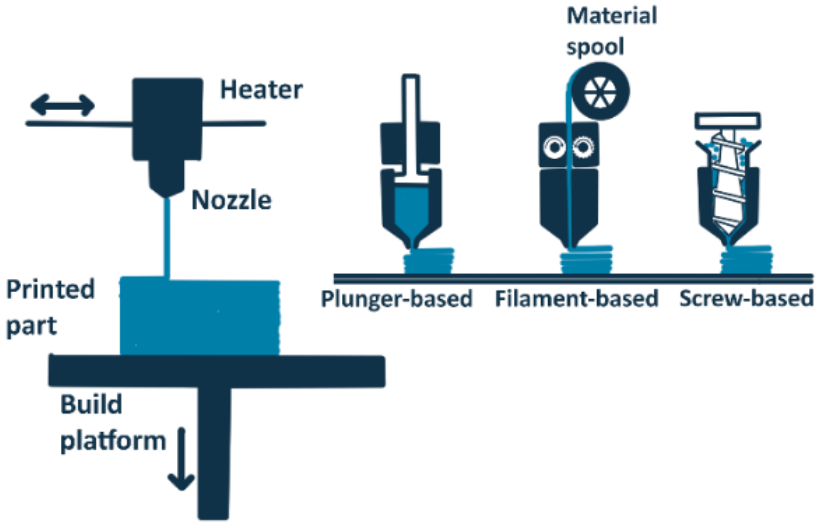

Figure 7. Schematic diagram of Metal Extrusion-based technique.

With this method, complex 3D parts with certain mechanical properties can be manufactured simply and accurately. In addition, it can be considered that it is an affordable technique because it uses the same materials that they use in metal injection moulding (MIM). As this is an advanced and highly studied technique, the materials are significantly less expensive than the metallic powders used in powder bed processes. The drawbacks of this additive manufacturing technology include poor surface finish, time-consuming and high porosity of the manufactured parts.

It was in 1995 when the *Fraunhofer IFAM* designed a rapid prototyping system, from a mixture of powdered binder that is extracted through a computer-controlled nozzle [81]. Then in 2015, the *Politecnico di Milano* developed a 3D printing machine for MIM metals and CIM ceramics, based on the extrusion of pellets with a stationary piston-based extruder on an inverted *Delta Robot table* [82]. After this event, some of the current commercial providers of this technology for metallic applications emerged, such as *ExAM* by *AIM3d*, *Metal X* by *Markforged*, and *Studio System* by *Desktop Metal*. These last two companies are the most prominent in the manufacture of parts by extrusion of metal filaments.

2.2.5. Material Jetting (MJ)

Material Jetting is a process that is based on inkjet, which is made up of metallic particles suspended in a photoreactive fluid material. This technique has been used in polymers, receiving the name of stereolithography. It was the first commercial AM method used to create a layer of solidified material using ultraviolet radiation to selectively polymerize a curable resin [83].

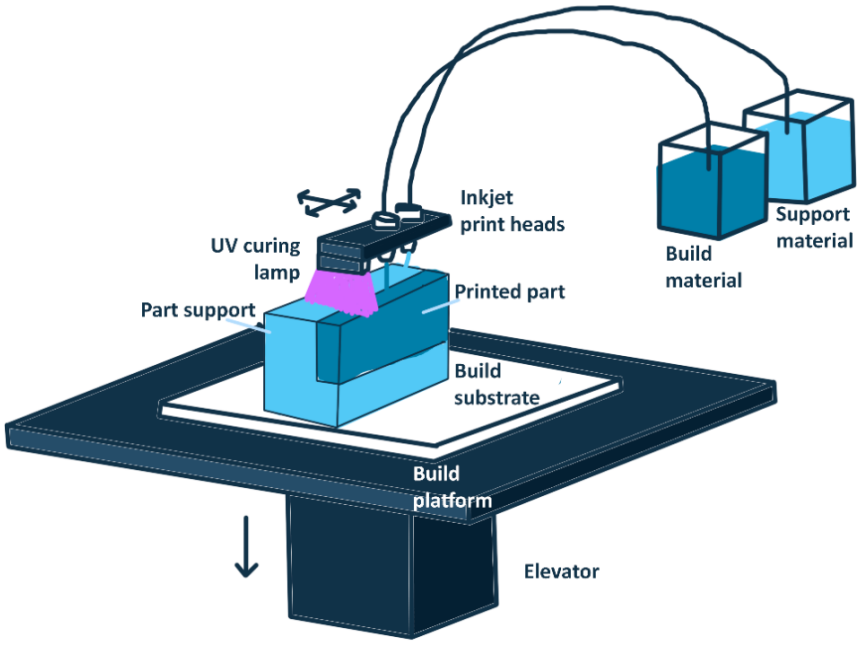

Figure 8. Schematic diagram of Metal Jetting process.

Currently, the Israeli company, *XJet*, has developed a new metallic inkjet technique that can achieve a high level of detail and finish, known as the *NanoParticle Jetting* ™ (NPJ). As the ink is deposited, the heated chamber causes evaporation of the liquid phase of the ink to leave only the metallic particles. The particles have a small layer of bonding agent, allowing them to bond with each other. Once printing is complete, a subsequent sintering process is required.[84]

Its advantages include high construction speed and flexibility. The main disadvantages are the high cost of materials and process errors due to over-curing.

This technology can be used for both functional prototyping and on-demand fabrication of small and medium metal components.

2.2.6. Binder Jetting (BJ)

The additive manufacturing technique by binder injection (BJ) is defined by ASTM F2792 as, *"An additive manufacturing process in which a liquid bonding agent is selectively deposited to bond powder materials."* Originally, BJ was known as "*3D printing*" or "*ProMetal*" technology [85-87]; however, in 2013, the ASTM committee established the terminology for AM technologies and changed the name of the technology to "binder injection" [44].

Over the decades, many studies have been conducted on fusion-based AM (for example fusion and solidification) in structural materials [13], ceramics [88], polymers [7, 89], biomaterials [90-93], functional materials [94] and microfabrication [95], however, in comparison, there have been a limited number of published works with reference to BJ, and most of the published works have mainly presented studies of microstructure and density of pieces[96]. However, when compared to other methods of AM, BJ is developing rapidly, allowing reaching a state of maturity (in reference to knowledge) very soon. This rapid advance is due to the vast history of research and knowledge of the process that has been carried out and developed in traditional manufacturing through powder metallurgy (PM) and the sintering process that can be directly used in the consolidation of materials in powder formed with BJ. However, much work is still needed.

As a curiosity, it will proceed to narrate a series of events related to BJ arranged chronologically. BJ's technology was initially developed at the *Massachusetts Institute of Technology* (MIT) and was patented in 1993 by Emanuel Sachs, who developed the process using ceramic powder and a glycerine binder deposited through thermo-bubble inkjet heads [97]. The technology was marketed by *Z Corporation*, who dubbed it as the "3D Printing" and developed the ability to print in full colour [98]. They also introduced the use of metal powders [99]. In 1996, *Extrude Hone* was authorized to start producing metal parts with BJ technology. In 2005, the *ExOne Company* split with *Extrude Hone*, focusing on the use of bronze-infiltrated stainless steel [100].

As this project focuses on this type of AM technology, a more detailed description of the AM process, of the materials used, and their machine manufacturers, among other aspects, will be made.

2.2.6.1. Printing process

BJ technology can be said to be similar to printing on paper because it involves the use of one or more print heads. The print heads move on the build platform, dropping droplets of the binding agent onto a bed of metal powder, leaving the particles adhered creating the part. After deposition of the binder, external heat is applied to the entire surface area of the printed layer to partially cure the binder and to ensure adequate mechanical strength for subsequent printing steps. This process is repeated for each layer until the printed part, called the "green body", is obtained. These green bodies possess limited strength and require further processing such as sintering and, optionally, infiltration of a second metal to achieve the desired mechanical performance. [101]

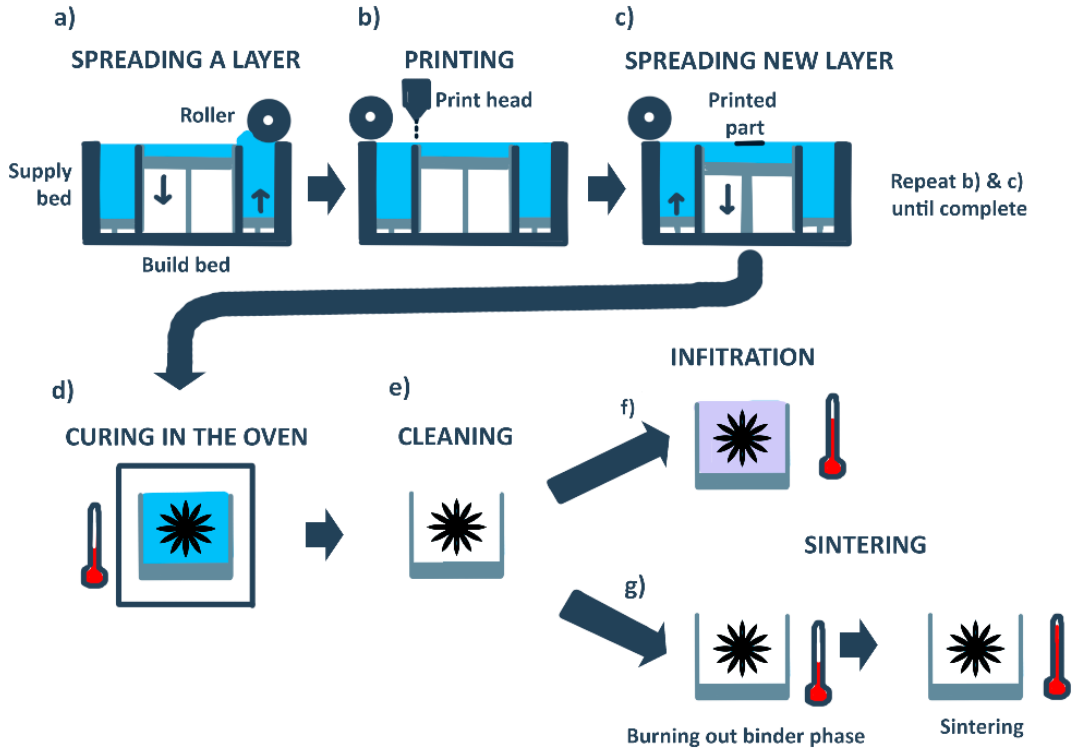

Figure 9. Schematic diagram of the Binder Jetting process [23]. (a) Distribution of the powder layer, (b, c) printing of the binder on the powder bed and then spreading a new layer of powder, (d) oven-cured; (e) cleaning of the pieces and lastly (f) infiltration or (g) stripping and sintering in a controlled atmosphere.

As mentioned, the process can be divided into the following stages: printing, curing, sintering or infiltration and final finishing (Figure 9). Each of these stages consists of a series of considerations, which will be discussed below.

2.2.6.1.1 The printing process.

The following steps must be followed in order to manufacture the green part[102]:

First, a thin layer of metal powder, supplied previously, is spread over the build platform, constituting the printing area known as the bed. The way of supplying and spreading the powder differs according to the manufacturer. A lifting platform or a gravity-fed hopper tank can be used as the delivery system [103]. Likewise, a dispersion system, named coater, is used to slightly spread and compact the powder layer. For example in Powder Bed Fusion (PBF), a blade is used, but a comb or counter-rotating roller can be used.

The latter promotes the fluidity of the powder. [104]. It is important that this system produce an even, smooth and aligned layer, in addition to not compacting the powder excessively.

Then a liquid binder (usually a dissolved thermoset polymer or aqueous solution) is injected from the print head onto the powder layer [105]. The binder saturation is calculated based on the estimated density of the powder bed and is used as input by the user. The injection techniques used are those that can be found in a common printer.

After depositing the binder, an electric heater passes over the powder bed. This process is called partial curing of the binder. In addition to curing the thermoset, it also serves to dry the powder bed and prepare it to spread the following layer. Curing time after the printing of each layer is an important factor in that sufficient drying time is required to allow the binder to fully bond with the powder to prevent cracking of the powder bed or agglomeration and adhesion of dust on the roller surface during printing. A much-used heater are infrared ray lamps.

After drying, the build platform piston drops, reducing build-up at the height of a layer, which generally ranges from 50-200 µm. Following this, the coater again spreads a new layer of powder over the bed from the powder supply site.[105]

2.2.6.1.2 Printed parts curing

After printing, post-curing is required to dry the binder and give the printed powder its "green" strength. To do this, the “build box” containing the powder bed and the printed parts are moved to an oven to cure by heating at 180–200 ° C for a concreted number of hours (usually taking 6 to 12 hours) depending on the volume of the construction box and the characteristics of the binder [106]. For example, Watters et al. proposed a specific cure protocol that includes vacuum, heat, visible light and pressure to improve the resistance of the pieces [106]. After curing, the green parts have enough strength to be handled and transferred to the densification oven. In this step, loose dust in the build box is removed by vacuuming and careful manual brushing by an operator. Sometimes a low-pressure air gun is used for parts with a lot of detail. Admittedly, curing requires little operator involvement, but it is still an additional step in the process that manufacturers are working to avoid in the future. Cleaning must be done carefully to avoid breaking the pieces.

In a process derived from BJ, the curing step is omitted since the entire bed is cured simultaneously and the green part is machined in the initial drying and curing stage.

After curing, densification is carried out by sintering or infiltration with another material to achieve full density and desirable mechanical properties. Nevertheless, before densification, the printed parts will be removed from the powder bed and cleaned. Cleaning unused dust adhering to the part is generally the most stressful step for the operator, as a potentially heavy dust bed must be lifted, brushing the surface a

little bit aggressively to remove highly adhered dust, but with extreme caution not to interfere with the quality of the piece in green.

2.2.6.1.3 Sintering and/or infiltration:

The density of the green part after curing is typically in the range of 50-60%. If viewed under a microscope, the individual dust particles are bonded with the polymer at the contact points with other particles. These pieces do not have the desired mechanical properties, which is why they must be densified. Densification can be achieved from various methods, such as infiltration [107] or sintering [105, 108]. Regardless of the densification method chosen, an exhaustion step at ~ 600–700 ° C is required to fully pyrolyze the binder before proceeding with sintering or infiltration.

The appropriate part densification process must be defined taking into account a series of factors. For example, in sintering different factors such as material composition, powder size, sintering atmosphere, temperature, and retention time should be considered [109]. Since each material has specific sintering characteristics, to facilitate and obtain good results, it is advisable to use mixed powder with various sizes of powder and/or coated particles [110, 111]. A possible process for the sintering of some base metals is usually∼1100 ° C for 24–36 hours, reaching a final density between 60 and 70%. [W13]

On the other hand, infiltration is usually used with ceramic powder, using metal as the infiltrated material. This is because ceramics have significantly higher sintering temperatures and a lower densification potential compared to metallic powders, and therefore infiltration is the most optimal strategy. [112, 113]. Infiltration occurs when the partially sintered material is contacted with a molten bath of a second material with a lower melting temperature than that of the sintered material. This allows the liquid metal to infiltrate the structure provided by capillary action to form a denser part. Bronze infiltration of stainless steel can achieve a final density of 95%.[W13] Infiltration is not unique to Binder Jetting but is a common method for commercial production.

Some of the factors to take into account when choosing one of the densification processes are the design factors. If the part is required to meet certain tolerances and precise dimensions, the technique to be used is infiltration. Infiltration generally produces highly accurate dimensions, while the sintering of simple alloys results in highly deformed geometries. However, there are alternatives such as consolidation. Consolidation is an alternative process for infiltration. The process works by distorting the design of the part geometry to accommodate uniform shrinkage during sintering. This designed distortion is not entirely controlled and therefore the result may not be as expected.

2.2.6.1.4 The finishing process:

After sintering, a series of processes must be carried out to achieve the desired standards. For example, the average roughness of parts obtained using BJ is traditionally around 6 µm (Ra) after sintering, and therefore post-processing to improve surface finish is a very common practice [17]. The most common techniques to improve surface finish are shot blasting and drum polishing; however, plating, machining [114], extrusion polishing [115], surface infiltration [116] and manual polishing are also used. Shot blasting can reduce surface roughness to a maximum of 7.4 µm, while tumbling polishing can result in an average roughness of 1.25 µm[41].

2.2.6.2. Materials employed

Compared to other melting metal AM methods, the BJ technique has received less attention in the research community and industry. Since the 1990s, various companies and institutions have worked and collaborated to develop and improve the metal BJ process. Much of the research focuses on material development: high utility alloys such as Inconel, stainless steel, and tool steel. In general, although the selection of BJ material is currently limited in terms of commercial availability, there is increasing use of parts made by BJ.

2.2.6.3. Advantages and disadvantages

The important characteristics to optimize in AM processes are the maximum size and complexity of the parts produced the production times, and the qualities of the parts, such as dimensional precision and defects in the final product.

The advantages that make this technique attractive at an industrial level are presented below. On the contrary, the known weak points of this technique and how a solution or improvement is being sought will also be exposed.

A study has shown the advantage of binder injection over its PBF counterparts in terms of performance and operator load [117]. Overall, the study showed that the batch processing strategy made employed in BJ is better than in PBF technologies. Furthermore, by avoiding the use of expensive vacuum or inerting-sealed chambers, the construction volume of BJ machines is currently one of the largest (up to 2200 x 1200 x 600 mm). The ability to produce large volumes of parts more cost-effectively than other AM methods and faster print speed are the reasons why the BJ has high production rates.

In relation to temperature, the BJ technique has different advantages over other AM technologies. For example, since the shaping process occurs under atmospheric conditions (ambient temperature) and without the use of an aggressive external heat source, problems related to oxidation, residual stress, elemental segregation, and phase changes are avoided [118], making unused dust around the printed part

being highly recyclable. Another advantage is that a relatively uniform thermal profile is induced throughout the printing part, which lends itself to produce materials with equiaxial grains. This results in the printed parts having isotropic materials properties. This ability to produce similar microstructures is one of the main motivations for advancing and researching BJ as a candidate for mass adoption in conventional manufacturing.

Some other advantages of the binder jet are:

High resolution on printed parts, the same as inkjet on paper. BJ enables complex objects to be manufactured with less waste, less delivery time, and more variety. This is corroborated by *ExOne*, which manufactures high-volume custom metal geometries for *Shapeways* and other customers. [W14-W15] Furthermore, compared to fusion-based AM, various densities with controlled porosity in terms of shape and size can be achieved by modifying the inkjet parameters and sintering time. The possibility of manufacturing parts with a controlled internal porosity gradient is due to, as reported by many researchers; a greater contraction was detected in the z direction, which could have had more porosity between the layers than within the same layer. Thanks to this, parts with custom heat transfer properties or fluid permeability can be manufactured along the same part. However, the surface finish is in line with many PBF processes. The surface finish of the parts after annealing is indicated at 15 µm [Ra], and further processing is reduced to reduce the roughness to 1.25 µm [Ra] .[W13]

In some AM processes based on the fusion of the material, support is required to stabilize the part and adhere it to a building plate and, therefore, requires more time and material. On the contrary, in the BJ process the part is supported by loose powder in the work box, thus not requiring a support structure for any part geometry during printing.

Unlike PBF technologies, BJ is compatible with virtually any powder material and therefore offers one of the widest material ranges of all AM processes [85]. Although it is true that many of these materials are still under development.

Last but not least, it is worth noting the lower price of the machines since, as mentioned, they work in atmospheric conditions and do not require the use of a highly powerful heat source.

On the other hand, a drawback is the limitation of the mechanical properties due to the porosity of the final pieces. Porosity is an important concern with BJ parts since BJ is essentially a powder metallurgy (PM) process and in addition, by pyrolyzing the binder, trapped gas can remain. That is why the final sintering process is so important since it will serve to weld the dust particles and promote the diffusion of the alloying elements, using a solid-state diffusion mechanism.

The main drawbacks of binder injection include:

- BJ is a multi-step process that requires post-processing steps (curing and densification). Post processing strategy development is still necessary for most materials, making the BJ process more expensive.
- Printed parts show a lower relative density (~ 50-60%) compared to PBF processes, and the densification of this state generally produces a significant distortion of geometry.
- Unfortunately, the most significant aspect of the BJ process that currently limits this potential is the inability to predict a large amount of distortion that occurs when sintering individual alloys at full density, which reduces the overall precision of the process [119]. However, computational tools are currently being developed to address this problem [120].

2.2.6.4. Applications

Despite the drawbacks of the process, the excitement of using BJ in structural materials, biocompatible materials, composites, and functional materials is not only not moderating but is increasing with each passing day.

As technology improves, their interest in various applications across different industries grows. Recently, BJ has been used for different applications (using different materials such as polymers, metals or ceramics), such as electrochemical energy storage [121-123], electronic devices [124, 125], food technology [126-128], solid oxide fuel cell [129], moulds for sand casting [130-140], waveguide circuits and antennas[137, 141, 142], concrete construction [143-148], bio-based renewable materials [149], ceramic scaffolding [150-154], biopolymers [155-160], sandstone production [161-163], and biomedical applications and drug administration [164-171]

It should be noted that some of its applications are due to the ability to produce porous parts, such as parts for energy management, light structures, biomaterials, etc. Binder injection has been used to develop a wide variety of different biomaterials (stainless steels and titanium) as a feasible solution for the development of porosity components and controlled bone tissue. Ziaee et al. [172].

2.2.6.5. Machinery manufacturers.

The main companies that produce commercial binder injection 3DP machines are:

ExOne Company (Irwin, PA), which is currently the leading manufacturer of BJ 3D printers for applications with different build volume and speed of 160 × 65 × 65 mm3 and 120 layers per hour (I*nnoven*t printer) at 1800 × 1000 × 700 mm^3 and 60–85 layers per hour (*S-Max* printer) [W16]. The BJ Printer I*nconel 625* has been recently developed for the manufacture of metal parts. In addition, it offers the widest range of materials from all equipment manufacturers, including 316, 420, and 17-4PH stainless steel, 625 and 718

nickel super alloy, iron, iron-chrome-aluminium, chromite, cobalt-chrome, zircon, bonded tungsten, tungsten carbide, ceramic beads, and silica sand. This wide range of printers demonstrates that BJ is a scalable technology that does not require a closed chamber and high-performance characteristics thanks to inkjet printing technology [173]. Specifications for some of these machines can be found in Gibson et al. publication [174].

HP Printing and Computing Solutions (Palo Alto, USA) is a company that, using BJ technology, is working to overcome the current limitations of 3D printing in the serial production industry, competing with common manufacturing techniques. For more than 30 years, *HP* inkjet technologies have been leaders in the printing market. It was not until 2014 when *HP* started working with the revolutionary 3D printing technology they had created. Initially they began to develop a polymer 3D printer, the technology was known as *HP Multi Jet Fusion*. Because *HP* is an ink expert, this technology relied on the printing of droplets of functional liquid agents on a bed of polymer powder. This is how *HP* took advantage of extensive experience in printing and imaging to enter the 3D world, manufacturing highly functional parts with high benefit. [W17]

It was not until 2018 when HP created its first BJ machine for metals, Metal Jet. HP digital printing technology for metals offers the ability to quickly and cheaply produce high-value, industrial large-scale runs. The printing process (Figure 10) is the same as that explained in the previous section. The differences with other commercialized MBJ machines are that it uses a patented binder developed with the help of HP Latex ink technology; the binder removal process is done inside the printer; and it has a large number of print heads (HP Thermal Inkjet). Additionally, Metal Jet uses metal injection moulding (MIM) powders and is capable of producing isotropic parts that have ASTM issues. All this allows the process to be faster, cheaper and much easier. [W17]

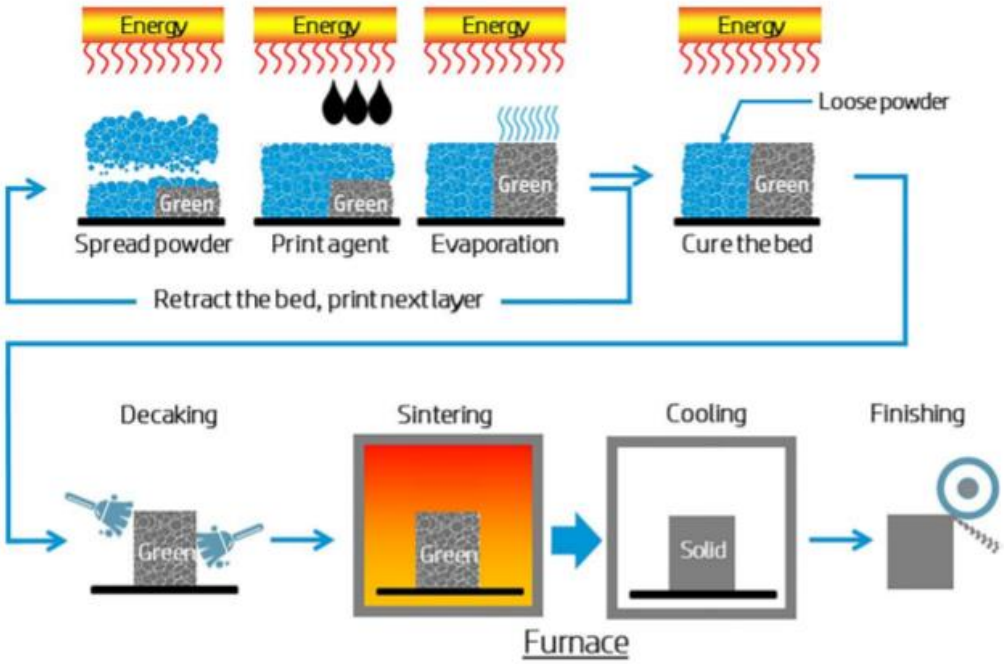

Figure 10. Schematic diagram of HP Metal Jet printing process [W18].

Other advantages of HP 3D Metal Jet are [W18]:

- Multiple pieces produced at the same time, or large pieces, in a powder bed with a print volume of 430 x 320 x 200 mm (16.9 x 12.6 x 7.9 in).
- Parts can be freely placed on multiple levels in the powder bed to optimize packing density, productivity and cost.
- No build plate required, compared to Selective Laser Fusion (SLM).
- Low-cost, high-quality end pieces are obtained for mass production of up to 100,000 pieces. This technology enables 50 times more mass production in terms of productivity and a cost reduction of 50% compared to selective laser fusion (SLM) and other competing BJ machines.
- 1,200 x 1,200 dpi (dots per inch) addressing capability in a 50-100 µm thick layer.
- Finished parts with isotropic properties that meet or exceed ASTM and MPIF standards.
- High reuse of materials can reduce cost and material waste without compromising part quality. Compared to SLM and based on internal testing of HP Metal Jet technology.
- Density after sintering greater than 93%, similar to MIM.
- The HP Metal Jet machine sells for less than $ 399,000 USD. With this price, the American manufacturer positions itself in the niche of industrial machines such as 3D Systems, EOS or Arcam. However, it is true that at a price level, this is far from being Desktop Metal and Markforged, which offer very low-cost equipment.

Figure 11. Photo of the HP 3D Metal Jet printer. Image shown may differ from actual product [W18].

Voxeljet Technology (Augsburg, Germany) has a sand base system for metal casting and a PMMA based system for plastic parts. *Z Corporation* (Burlington, MA, known as *3D Systems* since 2012), *Digital Metal* (Bruksgatan, Sweden), *Desktop Metal, General Electric* (GE), and *3DEO* have proposed other systems.

2.3. Parts finishing processes

The metallic pieces obtained using the AM techniques require to be post-processed to improve the quality of the metallic piece: the mechanical properties, the dimensional precision or / and the aesthetics.[13]

Below we will talk about some techniques or processes carried out to achieve the desired specifications after printing the pieces.

One of the first processes to perform after printing is to remove the part from the build deck. To remove excess material, it is carried out by means of electric wire discharge machining (WEDM). WEDM involves creating electrical arresters, releasing sparks that quickly cut through the material. Although the process is relatively slow and is used only with electrically conductive metals, it leaves a clean and smooth surface. Admittedly, there is another, faster method, bandsaw machining, but it is less accurate.

All powder bed processes need post-processing to remove dust that is both adhered to the surface of the printed parts and dust trapped inside the parts if necessary. In the first case, dust can be removed manually or with automated equipment. In the second case, you must design a way to escape the dust, either in the part design step, take this into account and draw two holes through which to evacuate the internal dust.

If the AM technique needs to add supports in the part design, once the printing process is finished, it will be necessary to remove the added supports. The most common way to remove supports is by CNC machining. Powder bed fusion technologies such as SLM and DMLS are the ones that require supports as the parts need to be anchored to the motherboard. In addition, the supports will serve to mitigate the effects caused by residual stresses and minimize defects such as deformations or cracks resulting from high processing temperatures.

A problem with most of the parts manufactured by AM's techniques is that, due to the high temperatures and the speed and little control of the cooling, the parts have residual stresses. For this reason, it will be necessary to subject the pieces, the pieces produced from a powder bed, to a post-processing to alleviate the residual stresses of the pieces and thus avoid possible deformations. The number of stress relief cycles depends on the metal or alloy used to produce a part. One of the drawbacks or possible problems that can arise in this process is oxidation, therefore the heat treatment should be carried out using an inert gas atmosphere, typically argon is used. In the thermal cycle, the entire platform is placed in an oven, where the part is heated to a temperature range between 550-675 ° C, depending on the metal, for 1 to 2 hours and then slowly cooled. Stress corrosion cracking can also be reduced through this stress relief process.

Another possible post-treatment is the heat treatment known as hot isostatic pressing (HIP), which helps to obtain the optimum microstructure and mechanical properties, and can be compared with cast and forged alloys. It is about applying high temperatures (up to 2,200ºC) and isostatic inert gas pressure (from 100 to 3,100 bar) to the pieces to achieve the highest possible density, reduce porosity and eliminate internal voids. This process can consist of natural cooling that takes between 8 and 12 hours or rapid and uniform cooling, which allows parts to cool from 1,260 to 300 ° C in less than 30 minutes. Another way to increase the density is to infiltrate the voids in the part with a molten bronze bath. This process significantly improves the mechanical properties of the metal part. For example, bronze infiltration of stainless steel can reach a final density of 95%. [W17]

Surface finishing is a very common operation performed after printing. With this process, you want to obtain a surface with specific characteristics, for example a smooth finish. There are several common surface finishing techniques, including machining, sandblasting, media blasting, and polishing. Polishing is used to achieve a 'mirror' finish, which is required for other surface treatments, to avoid corrosion and improve the appearance of the part. Abrasive blasting (sandblasting, bead blasting and media blasting) is used to achieve a smooth surface.

2.4. Industrial applications

Metal AM technology was originally considered a process for rapid prototyping. Today this technology has extended in many other areas. From prototyping to manufacturing of industrial parts of small batch or

large-scale manufacturing. Admittedly, this technology is not yet ready for mass production of identical parts today. However, it is not ruled out that such a goal will be achieved in the future.

Typical applications of metal AM can be grouped into the following groups:

- Production of prototypes or products that are in the development phase.
- Production in short series, being a substitute for expensive traditional procedures.
- Production of pieces of high geometric complexity.
- Serial production of parts in the medical, automotive, and aerospace industries. [24].

Some current examples where metal AM technology has been used with great results are shown below.

The aerospace industry has pioneered the use of metal 3D printing. It has been used for different reasons such as obtaining functional prototypes, the manufacture of tools, spare parts, aircraft structural components or to obtain lighter parts with specific geometries. [W19] An example of a company in the aeronautical sector that makes use of 3D metal printing to manufacture its products or part of them is General Electric (GE). More specifically, GE Aviation produces fuel nozzles for the LEAP family of jet engines using Electron Beam Melting (EB-PBF) technology. In 2018, they printed 30,000 nozzle, which consists of a single unit, 25% lighter and 15% more efficient than those produced using traditional techniques. [W20] The same company has also tested 3D printing over a third of a new advanced turboprop engine. All parts were printed at GE Aviation's Additive Technology Center (ACT) in Cincinnati, which is one of the largest and most advanced additive manufacturing factories in the world completely amazed. [W21]

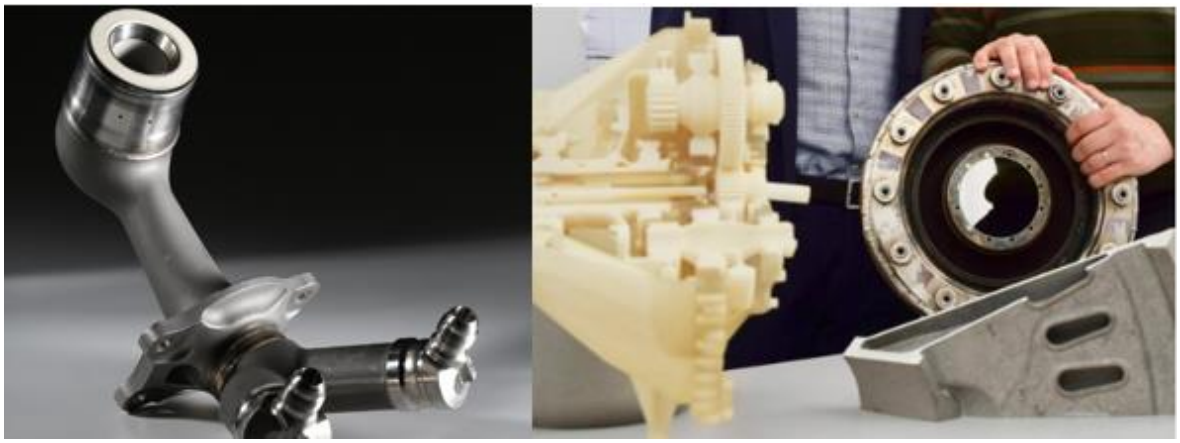

Figure 12. Parts manufactured by the company GE using metal 3D printing technology.

Another of the industries is automotive, where we find well-known automobile manufacturers such as Ford Motor Company. Automotive companies can use 3D metal printing to create lightweight metal parts, improving vehicle performance and reducing fuel consumption. Another area of interest to the industry is also using 3D printing to produce replacement parts that are normally produced in low volumes. Below

are some examples of these companies and some of their applications. For example, the company BMW is making use of 3D printing for the serial production of a component of its 2018 BMW i8 Roadster vehicle. Specifically, it is an accessory for the folding / unfolding mechanism of the soft top of the vehicle and has been manufactured using aluminium alloy powder ($AlSi_{10}Mg$). The company has verified that the requirements for extreme strength, stiffness and temperature are met. Audi presents a different business case for 3D metal printing. In this case, the German automaker is using the technology to produce smaller, more complex, low-demand replacement components. A good example is the Audi W12 engine water adapters. [W22]

3D printing is also being widely used in the medical field, since it allows the customization of materials, such as orthopedic implants or dental implants [175-178]. For example, implants can be designed with better porosity and surface texture, facilitating tissue growth around the implant. SmarTech Publishing predicts that more than 2 million implants will be 3D printed on metal by 2025. [W23]

Lima Corporate uses Electron Beam Melting (EB-PBF) technology to manufacture biocompatible titanium hip implants in solid cellular structures that resemble natural bone. These structures are used to cover an implant, allowing it to better integrate with human tissue. [W24]

But there are not only applications in these areas, also in the manufacture of equipment or tools, such as the manufacture of moulds. The technology enables rapid design iterations, allowing changes to be made with relative ease. Another advantage is the possibility of a more complex design, being able to improve the shaped cooling channels.[179, 180] GW Plastics 3D prints injection moulds with conformal cooling using hybrid metal. The company itself says that 3D printed moulds can save up to 30% of cycle time by reducing cooling time [W25, W26].

2.5. The current market for metal 3D printing machines.

Currently there is a great interest focused on 3D printing technologies, and because of this, you can find numerous annual reports of market research, the scope or predictions related to this technology. Some examples are reports made by SmartTech Analysis or Wohlers. [W27-W30]. These additive manufacturing market analysis reports conclude that the global additive manufacturing market is growing, reaching a value of over $ 10 billion in 2009. Many of these global estimates exclude money spent on AM development from big companies like Airbus, Adidas, Ford, Toyota, and hundreds of others. They also exclude more than $ 1 billion in venture capital and other private investments in AM-related companies. Therefore, the above estimate of global revenue only includes the purchase of industrial systems, desktop 3D printers, materials and parts from service providers.

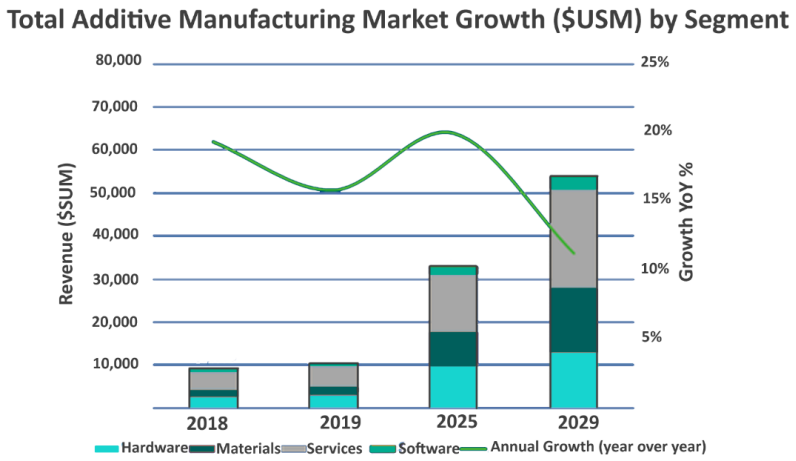

Figure 13 Global Additive Manufacturing Market Outlook (millions $) by *SmartTech Analysis* [W27]

"*2020 Additive Manufacturing Market Outlook and Summary of Opportunities*" [W27] report provides information on AM's market size, trends, growth, cost structure, capacity, revenue, and forecast for 2029. The report provides for international markets, as well as development trends, competitive landscape analysis, and the state of development of key regions. Development policies and plans are discussed, as well as manufacturing processes and cost structures. This report is a comprehensive quantitative analysis of the AM industry and provides data to develop strategies to increase the growth and effectiveness of the AM market.

Several factors are driving the growth of the industry, making it difficult to keep track of the companies and trends driving 3D printing.

The company *AMFG Autonomous Manufacturing*, has launched a second time a technical infographic that offers a clear understanding of the current AM ecosystem and key trends. According to this AMFG study, this year there are 238 companies within the AM panorama (Figure 18).

As in the Smart Tech report, the landscape is divided into different segments (Figure 18):

- Software providers (Design and simulation, Slicer and data preparation, Workflow and MES, Security).
- Post processing system manufacturers.
- Research institutions.
- Material suppliers (polymers and compounds, metals).
- Hardware manufacturers (polymers, desktop, metals, composites, ceramics, electronics).

This last segment represents more than half of the AM market, hoping that it will increase in future years due to the great interest in the development of new systems. According to a Forbes magazine article, the

AM industry in 2019 received 77 early-stage investments valued at $ 1.1 billion, most of which went towards hardware development.

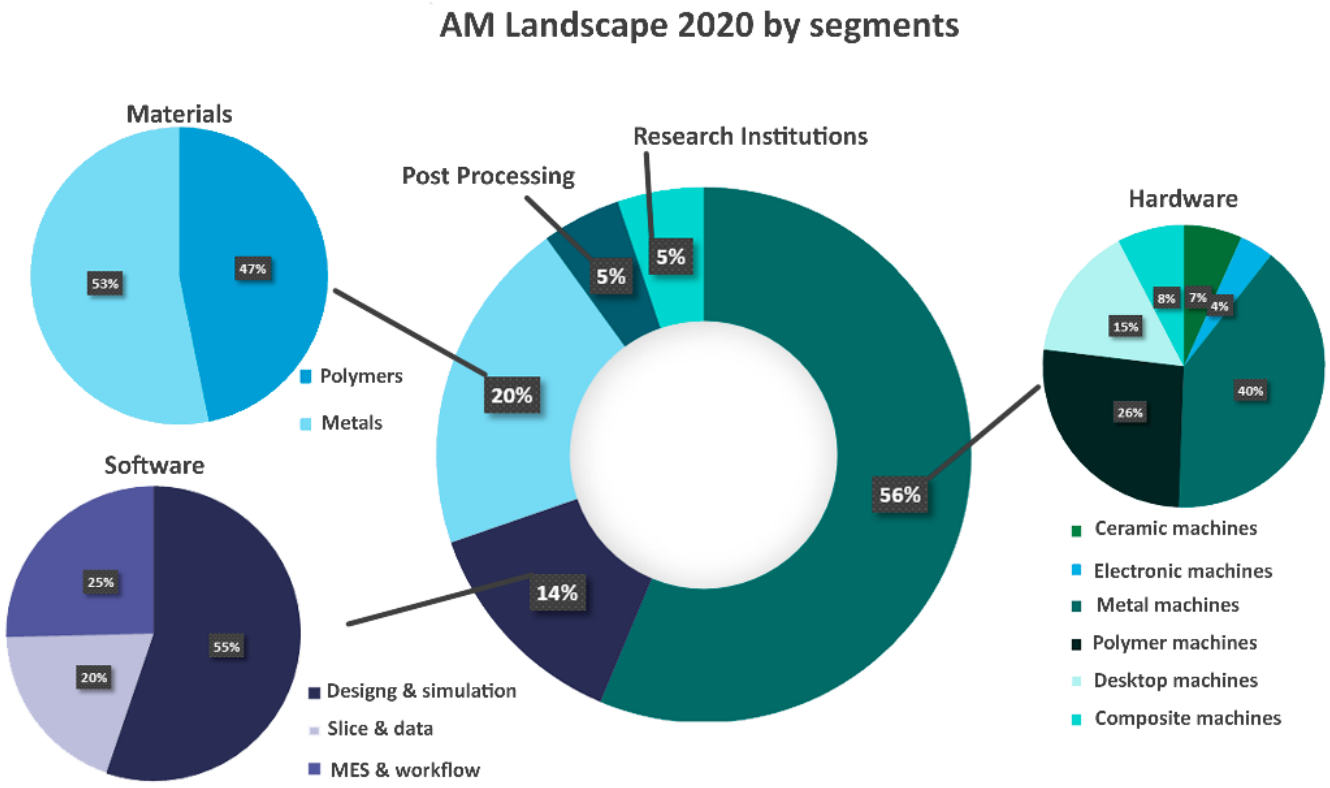

Figure 14. A breakdown of the AM landscape, featuring the hardware, software, materials, post-processing system, QA and process inspection categories. AMFG Report Updated 05/27/2020[W31].

If the topic focuses on metal AM technology, it is discovered that of all the segments, the manufacture of metal printers represents 22.5% of the general panorama, being the largest segment. It is true that some experts point out a slight decrease in sales of metal 3D printers in 2019, however, as Figure 13 shows, this segment is expected to recover in the long term. [W32, W33]

The metal 3D printer market is largely dominated by powder bed fusion AM methods (Figure 15), corresponding to the overall AM hardware manufacturing landscape (Figure 19). This image shows the different producers of AM machines classified according to the AM technology categories according to the AMST standard.

Although the metal fusion technique is still the most widely used, it is worth noting the strong drive towards the development of machines that use binder jetting. These are usually cheaper, faster machines

and have a wider range of materials. One of the leading providers of binder injection printers for metal 3D printing is *ExOne*, although it is accompanied by *Digital Metal*, *GE*, *Desktop Metal*, and *HP*. These last two in particular have a strategy to make this technology compete with traditional metal fabrication, such as forging or casting.

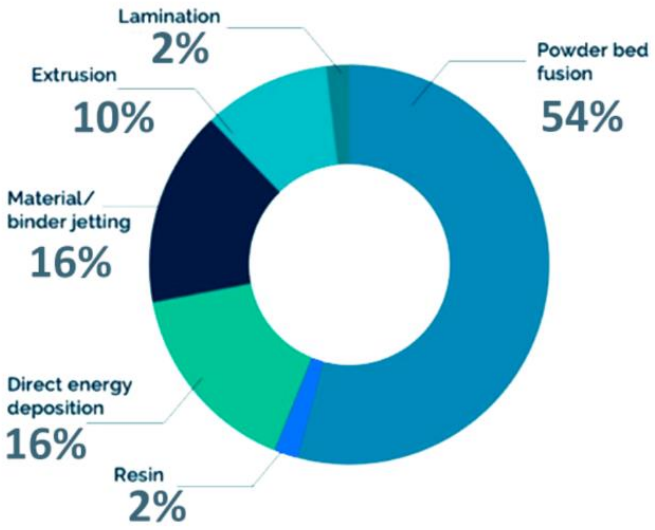

Figure 15. The number of 3D printer models per technology market in 2019 [W34]

Knowing all these facts, it will not be surprising if, in the future, this technology came to dominate the AM machine market. It is true that for this to happen, the technology must reach an adequate maturity index. Figure 16 shows how the different AM technologies are found with respect to this maturity index.

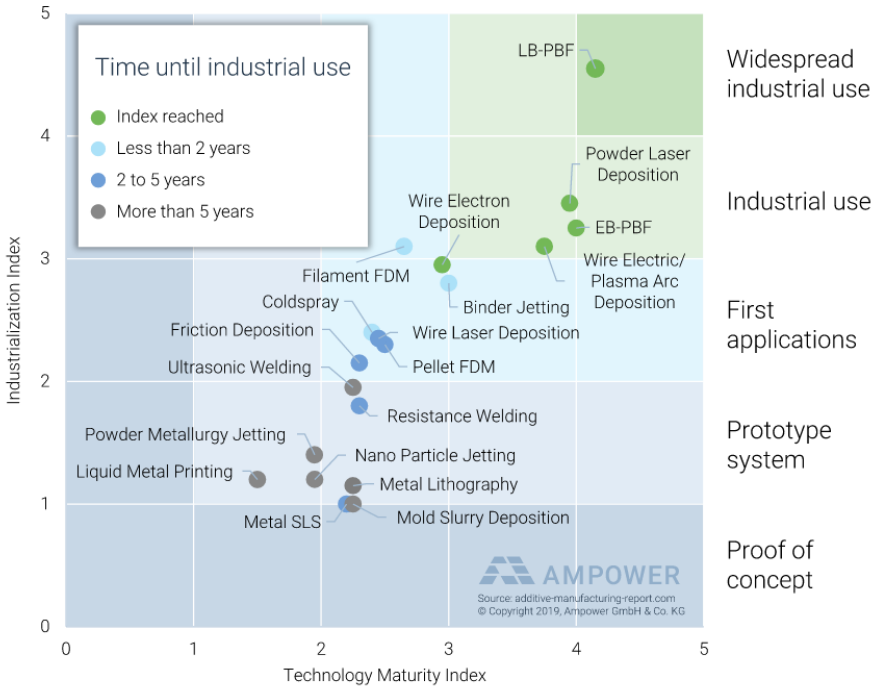

Figure 16. AM Maturity Index 2020. AMPOWER [W35]

In reference to the range of 3D printing materials, according to the Senvol database [W36], the number of AM materials is increasing, although the cost of these continues to be a key barrier to the widespread adoption of AM techniques. Although in the manufacture of machines the segment related to materials is the largest, in terms of materials, it happens the opposite. Polymers are the most popular materials and this is due to the lower cost of production. Even so, in 2019, the market for metallic materials for AM (powder and wire) reached a sales number of 5,227 tons. According to the AMPOWER report, it is expected that this will continue to grow with an annual increase of 29.3%. (Figure 13). The most widely used metallic material is Ti-6Al-4V titanium alloy because this alloy is used in biomedical and aeronautical applications. These companies make most use of AM technologies.

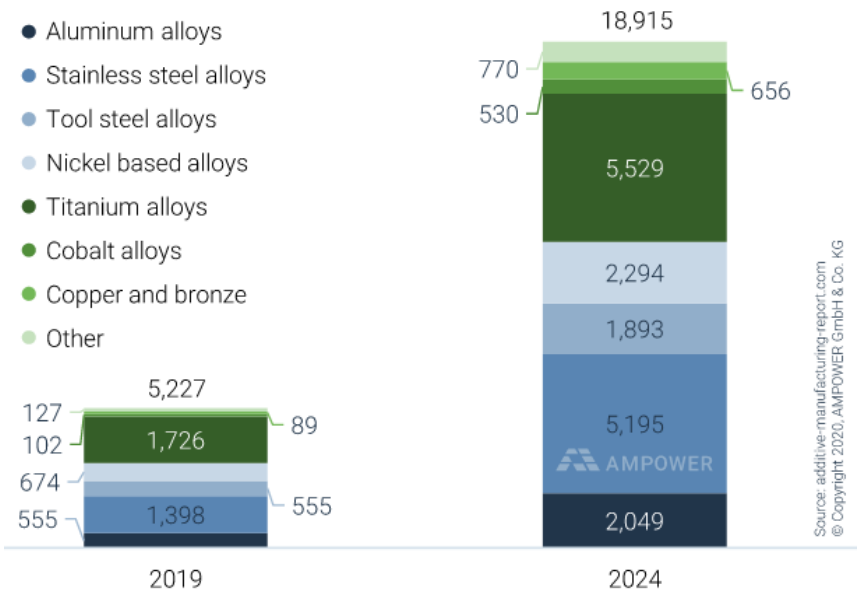

Figure 17. Material consumption 2019 and forecast 2024 [tons] [W35]

Figure 18. Additive Manufacturing Landscape 2020 (AMFG Report Updated 05/27/2020) [W32]

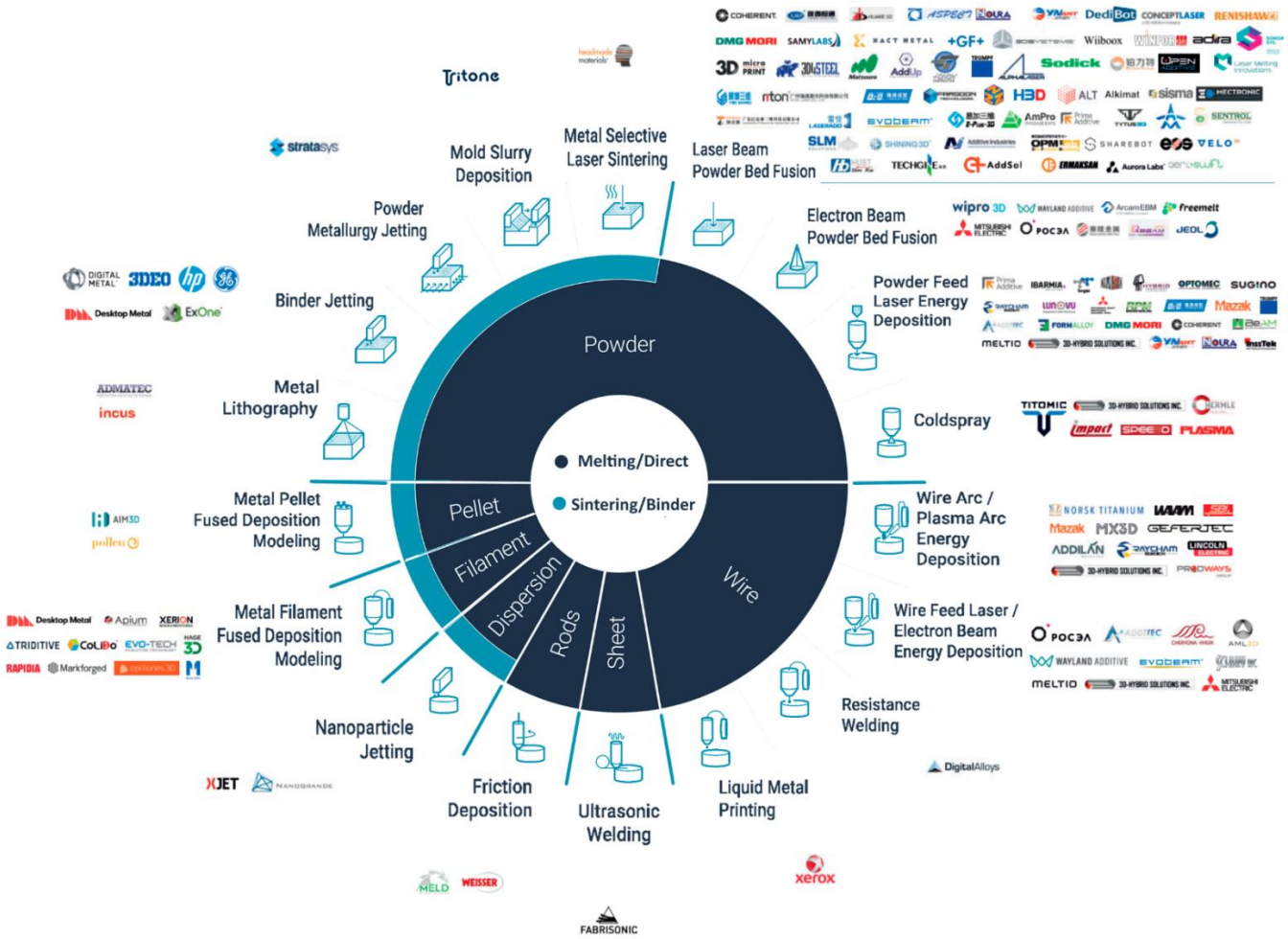

Figure 19. Metal AM techniques and their manufacturers in actual market. [W4]

2.5.1. The impact of the COVID-19 pandemic to the Metal Additive Manufacturing market.

At the end of 2019 and the beginning of this year 2020, the disease known as COVID-19 was discovered, becoming a global pandemic. This global outbreak of the coronavirus virus led to the total or partial blockade of industrialized countries and a ban on travel between them. In the last days, there are many analysts who study current and future situations. In relation to the development of the metal AM market, these reports ensure that, in 2020 and the following years, the development of AM will be directly affected.

During the days of the health crisis, quick, unconventional, and solidary help was obtained from many users and R&D departments to manufacture face shields, breath masks, or respirator parts. This demonstrated the enormous potential of AM, allowing for flexible and fast production. The reasons that most of these applications were printed with polymer AM technologies are the high requirements and necessary certifications. The metal AM industry was unable to cope with reaction times as fast as times used by polymers technologies. This is why in this crisis it has been shown that standardization and certification are currently a major challenge for 3D printing.

These extraordinary times have exposed some advantages over the 3D printing industry, making even the most sceptical people about the use of such technology give it the value it deserves.

For example, one of the key things that the current crisis has shown is that these technologies can be used for volume manufacturing. As supply chain disruption has had to be addressed, 3D printing has become an invaluable resource to supplant this resource shortage. Some companies have started using these technologies to produce in volume. An example is the Formlabs Company, which has produced 1,500,000 COVID-19 test swabs. Here you can also see another of the advantages they have revealed. Switching to an AM production is not a panacea, quite the opposite, as it fits perfectly into the established production line due to its high flexibility.

AMPOWER has carried out a survey of various companies that work in AM to write the *AMPOWER 2020 Report* (May 2020), where it analyses the impact of COVID-19, posing different possible scenarios on the future of metal AM technologies. [W4]

Subsequently, in this section, the information from the said report will be compiled and will be presented in summary form.

The report highlights the effects of the current situation on the activities of users of these technologies. The industries using AM will be affected due to the blockade, the travel ban and the general recession

caused by the COVID-19 pandemic. Most industrial sectors are in a moment of uncertainty as they do not yet know if there will be a long-term recovery. A prominent example is the aviation industry, which, due to current restrictions on international travel, airlines and aircraft manufacturers, such as the *Boeing* and *Airbus* companies, have been affected. It will be very difficult for these companies to invest capital in the development of AM processes since it will be economically favourable to use technologies and products already known. Other companies facing challenges similar to those of civil aviation are the oil and gas industry.

Attention should be paid to the automotive industry, which is the company with the highest investment in R&D efforts in metal AM. According to the report, a decrease in investment is predicted in the short term to reduce costs. But in the long term, it is not yet known for sure, since it is possible that users of AM techniques consider them an enabling alternative. In other words, due to the advantage of on-site production of spare parts and the reduction of storage needs, they could generate greater investment in AM to improve flexibility and reaction to the future economic crisis. This will occur in many other industries such as mechanical engineering or tools. It is true that the interruption of the international raw material supply chain has been or may be another incentive to increase activities using AM metal in the short term.

There are also exceptions such as defence and space applications, that are not affected at all. Especially, the defence sector is continuously growing due to international tensions and increasing military budgets. Another sector that relies on AM as one of its main technologies is that of medical applications.

The report also talks about the short-term effects on companies supplying AM systems. These are facing both low budgets for R&D activities and to different operational challenges that have arisen after the blockade. The general travel ban makes it difficult to perform services such as the installation or maintenance of machinery. Not only these departments have been affected, but many others as well. For example, the activity of the marketing and sales departments has also been affected due to the interruption of exhibitions and conferences. That is why companies have had to change their conventional methods, transferring their activities to online channels and remote maintenance tools.

Added to all these challenges is the unexpected increase in demand for the service. Usuary companies explore their local production and fast delivery options, as well as converting to AM parts. However, the number of sustainable start-ups from the current increase is difficult to predict in the long term.

However, some companies have decided to launch new systems on the market. As stated by Rainer Grünauer, Head of Additive Manufacturing Sales at *Trumpf*, the coronavirus crisis is a great technological opportunity for metal MA. In the interview, he mentions that it is a good time to strengthen cooperation

between partners. This is why this company has just released two new systems: the *TruPrint 2000*, which is ideal for medical technology, and the *TruPrint 5000* with many new automation functions.

This report also highlights the differentiation between AM technologies already established in the market and those that emerged relatively recently. The least established technologies are Binder Jetting (BJ) or Material Jetting (MJ). The R&D departments of the user companies will find it difficult to invest in these technologies because they would have to make a high investment acquiring the machines without knowing if the serial production capacities will be necessary to benefit.

Successful companies will focus their activities on cash flow and revenue-related operations, while less successful companies will be forced to join forces with their competitors or disappear from the market. For example, less mature technologies will see less R&D investment by large OEMs, which is their main sales driver at the current stage of the system and market maturity. That is why they will focus their efforts on accelerating the consolidation of the supply chain.

Regarding the collaboration agreements between different types of companies related to AM, it can be said that it is a good time to establish a symbiotic relationship. Many additive manufacturing providers are new or small companies. They have the advantage that they are innovative and can react quickly and flexibly to new requirements. However, they often lack the financial scope to launch new products. Large companies, on the other hand, have more staying power in times of crisis. Cooperations could benefit everyone involved.

Not only does he talk about the difference between metal AM techniques, but it also says that their applications are also changing. The demand for custom or fast delivery products is increasing exponentially. An example of a possible application is protective equipment. In contrast, prototyping is declining. This is because companies that used prototyping, such as the automotive one, are experiencing a decrease in demand.

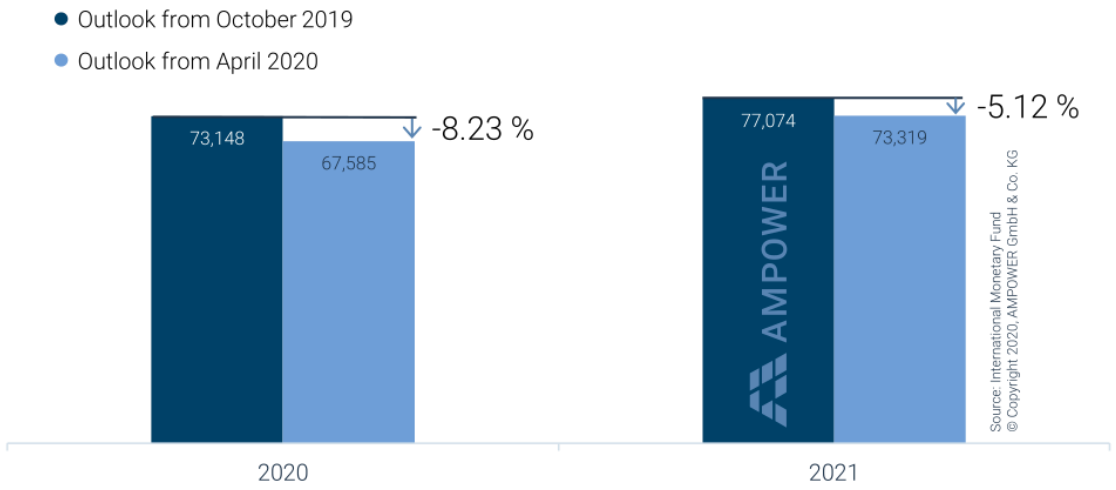

Figure 20. GDP Outlook for G7+China by IMF for 2020 and 2021 before (October 2019) and after (April 2020) COVID-19 outbreak [In $ million]. [W4]

The *AMPOWER 2020 Report* (May 2020) also includes the economic perspectives published in the monthly reports of the International Monetary Fund (IMF). The last correction of the IMF collected by the Report is in April 2020. This is expected a global recession followed by a slow increase in gross domestic product (GDP) in 2021 (Figure 20). It is true that not all countries will be equally affected for this crisis. For example, for the G7 countries, which represent the majority of the AM metals market, the IMF analysis expects that GDP in 2021 will be at the same level as in 2019, therefore 2020 will be a lost year in terms of growth. For China, a small GDP growth is expected in 2021 compared to 2019. This scenario is consistent with AMPOWER's interviews with representatives of the metal additive manufacturing industry.

As mentioned at the beginning of this section, the forecast made in this report contemplates different scenarios, specifically, two scenarios for the impact of the COVID-19 pandemic on the metal additive manufacturing industry. An optimistic scenario is shown with reduced growth and a pessimistic one considering the lost year. It should be mentioned that this forecast was made basing on the IMF forecast and the market forecast made through the statements obtained in a survey conducted before the severity of the pandemic was obvious. The following figure (Figure 21) shows a description of the two possible scenarios.

1

Scenario 1 - Reduced Growth

In the first scenario this forecast is reduced by the percentual shrinkage of G7 and China's GDP, predicted by the IMF in April 2020. Including the IMF economy shrinkage of 8.23 %, the corrected forecast is a market volume of EUR 2.4 billion in 2020. For 2021, the reduction is expected to be at 5.12 % leading to a total metal Additive Manufacturing market volume of EUR 3.1 billion. This scenario assumes that the current lockdown will be gradually released leading to an increase in market activities by late summer 2020.

2

Scenario 2 - Regaining 2019 level in 2021

In the second scenario the absolute GDP values are considered. This leads to the assumption, that the economy will regain the level of 2019 in the year 2021. The impact of this scenario is more severe. The projections arrive at a metal AM market volume of EUR 1.6 billion in 2020 and EUR 2.02 billion in 2021, which is identical to the market volume of 2019.

Figure 21. Description of the two possible scenarios raised in the *AMPOWER 2020 Report* (May 2020). [W4]

As seen in the graph in the Figure 22, the metal AM market was originally expected to reach a volume of 2.58 billion euros in 2020. Although, if the scenarios are true, this economic performance will never be reached.

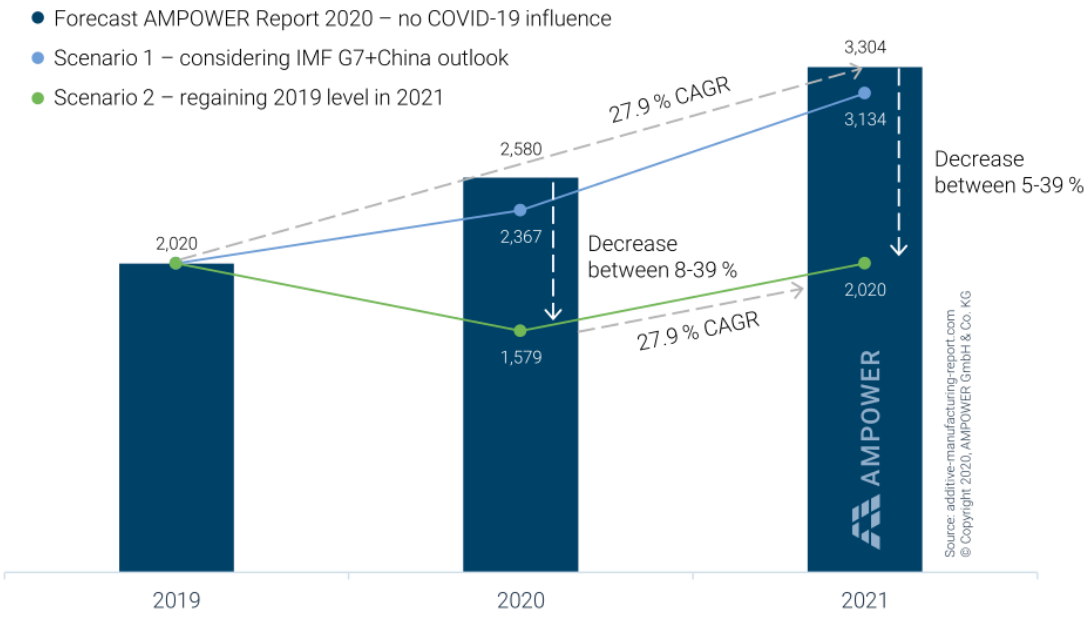

Figure 22. Metal AM market 2019 and supplier forecast 2020, 2021 considering COVID-19 scenarios [€ million] [W4]

In short, the future of AM technologies is very uncertain. Many producers are suspicious and fear that, due to the overcapacity in the market created in the last 3 years and the associated very low market prices, many companies in the AM area will not be able to generate profits and will therefore disappear from the market. However, these facts do not discourage all producers as they consider that good management

and planning can lead the AM industry to obtain benefits from the crisis. Ludovico Camarda, *Coherent* General Manager, makes a series of recommendations that he says will ensure the success of his company.

3. Metal Powder

More than half of all metal AM technologies use dust as raw material. Specifically, taking into account the installed base of AM systems, more than 80% of all operating systems work with metal dust. This is why many of the powder suppliers, which originally produced the powder for other technologies such as powder metallurgy, have had to adapt to this demand by adding powder suitable for AM to their product portfolio.

In recent years, powder metallurgy has experienced significant growth due to the development of AM processes. Processes using powder have advantages that cannot be achieved with traditional methods. Dust particles are characterized by having a high ratio between the surface area / volume that increases the reactivity of the material, in addition, they flow due to the effect of gravity.

The physical properties of the powder must meet the strict metallurgical requirements of the AM process to be used, varying according to the technology used. Some factors to take into account are the purity, the morphology and the size of the particles, since they influence the behaviour that the powders will have.

According to the Wohlers Report 2017, powder costs are the second or third largest cost associated with the production of additively manufactured (AM) parts. That is why the procedure for producing metal powder is important for the growth of the AM metals market.[181]

3.1. Metal powder production

In this chapter, the main processes for the production of metal powders will be exposed. Significant manufacturing methods are classified as follows:

1. Chemical methods
2. Physical methods
3. Mechanical methods.

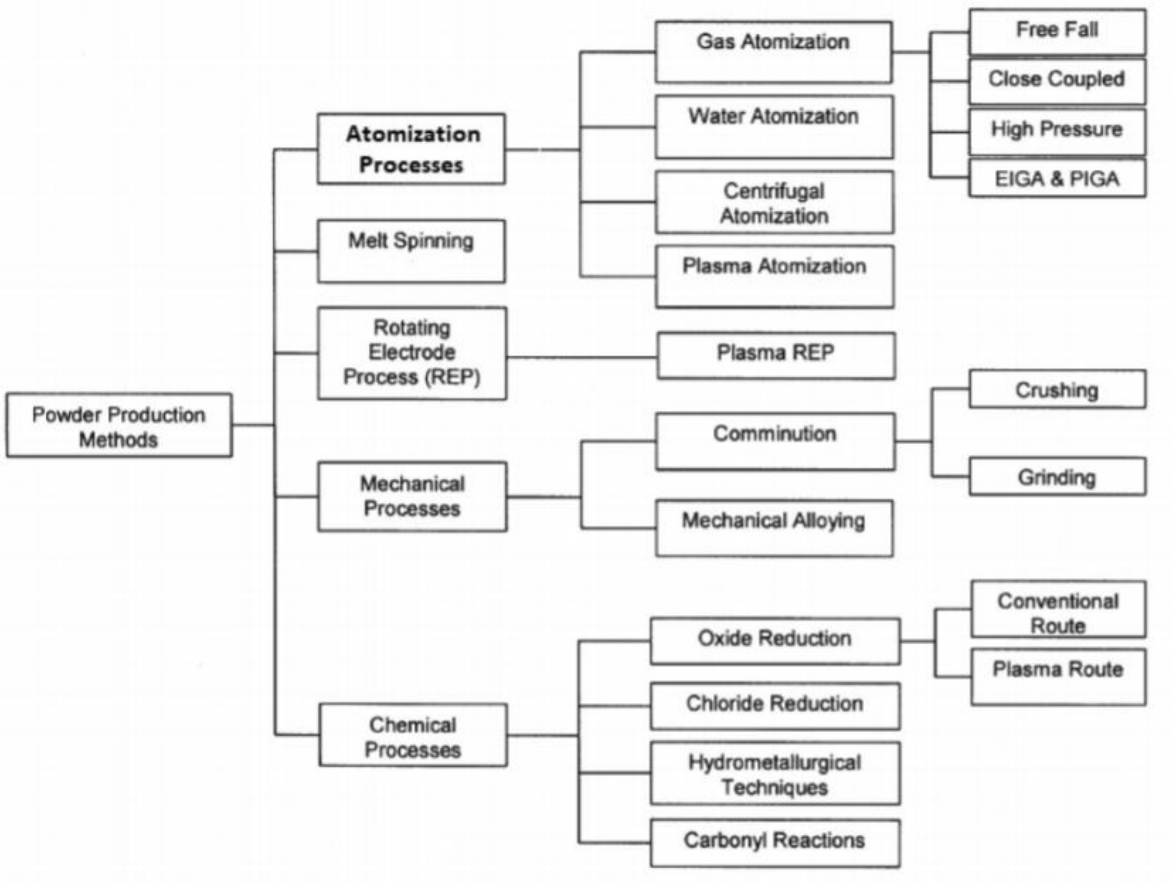

Figure 23. Powder production methods and processes

The choice of method will depend on the type of application and the desired properties and structure of the final product (type of end application) and the raw material used.[182, 183]

3.1.1. Chemical methods

Within this group we find two ways of production: the reduction method and the decomposition method.[184]

3.1.1.1. Chemical reduction

Normally, it starts with a chemical compound that can gain electrons, that is, is able to reduce its oxidation level chemically. The most common are oxides, halides, or metal salts.

The most common ways are:

In solid state. An example is the Höganäs process used to produce fluffy iron powder. In this process the magnetite mineral (Fe_3O_4) with high purity is used and it is reduced with a carbonaceous material. This is

a static operation since the material does not move during the entire reduction process. The process begins with grinding the ore until the desired particle size is reached. The powder is introduced into silicon carbide containers, known as "saggers", together with a concentric layer to this of a mixture of coke and limestone. These are introduced into an oven and that is when carbon monoxide, produced from coke, reduces iron ore. The total reduction time is of the order of 24 hours at a reduction temperature of 1200ºC. Limestone is used to prevent contamination of iron with possible traces of sulphur. Once the spongy iron is obtained, it is mechanically removed from the "saggers" and ground again. A purification process must be carried out using a magnetic separate. The final stage would be a final annealing, the powder is transported through a continuous furnace in a hydrogen atmosphere on a stainless steel belt. There are other metal powders that use this method. For example the production method of "Pyron iron powder", which deals with a reduction using hydrogen. In this process, the metal Fe_3O_4 is annealed first in an air atmosphere, thus obtaining Fe_2O_3. This oxide is then reduced in a hydrogen atmosphere. The annealing step is carried out since the reduction kinetics with hydrogen is faster. Another example is reduction is tungsten, in which WO_3 is reduced to tungsten powder with hydrogen. This process is more complex.[185]

In gaseous state: For example, the Kroll process, a vapour reduction of titanium tetrachloride with molten magnesium.

In aqueous solution: As are the methods used to obtain precipitated copper powder by leaching a solution of copper sulphate with iron or the Sherrit Gordon process to obtain complex dust cores of Cu Ni and Co. This hydrometallurgical process is a reduction of a solution of ammoniacal nickel salt with hydrogen at a pressure of 1.38MPa and a temperature close to 200ºC. the reaction followed is as follows: $M^{2+} + H_2 \rightarrow M + 2H^+$.One of the advantages of this process is that it allows you to control the size and shape of the nickel powder.[186]

3.1.1.2. Chemical decomposition

Some of the most common ways to obtain dust by chemical decomposition are:

Decomposition of metal hydrides: Used metals must first be hydrided, they must be refractory metals such as Ti, Zr, Hf, V, Th or U. At the same time, they are heated in a hydrogen atmosphere. It is very important that the atmosphere is pure hydrogen, since some traces of other gases such as O_2 and N_2 can lead to other unwanted reactions. Each metal has an opium temperature range to form its hydride. Hydrides are quite fragile and therefore easy to grind. These can be dehydrated by performing the reverse process, heating them in a good vacuum at the same temperature at which the hydride formed.

Decomposition of metal carbonyls: The example we find is the production of iron and nickel powder. The metal is first reacted with carbide monoxide gas under pressure to obtain carbonyls as a product.

Carbonyls are liquid compounds at room temperature and with a low boiling point. Once the carbonyls are obtained, they are gasified at atmospheric pressure. Powder particles must be formed in suspension of the gas to obtain particles as uniform and spherical as possible. The powder obtained is quite pure but contains a considerable amount of carbon and oxygen (fraction of a percentage). In the case of iron, these impurities can be avoided by adding ammonia during the decomposition of the carbonyl and by subsequent annealing treatment. But these would naturally increase the cost.

3.1.2. Physical methods

In this large group are the electrolytic method and atomization.

3.1.2.1. Electrolytic method

It is one of the most widely used methods to obtain copper, beryllium, iron and nickel powders due to its high performance, since the metal obtained is of high purity. In order for electrodeposition of the metal to take place on the cathode in the form of flakes as in the case of copper or forming a sheet like iron, it is necessary to work in the optimal chemical and physical conditions. These flakes are then ground to powder particles. It is true that the cost is higher than other methods, because it requires the control of many process variables. The following actions can be considered to favour deposition: use high current densities; work with weak metal concentrations; add colloids and acids; work at low temperature; have a high viscosity solution and/or do not shake the said solution.

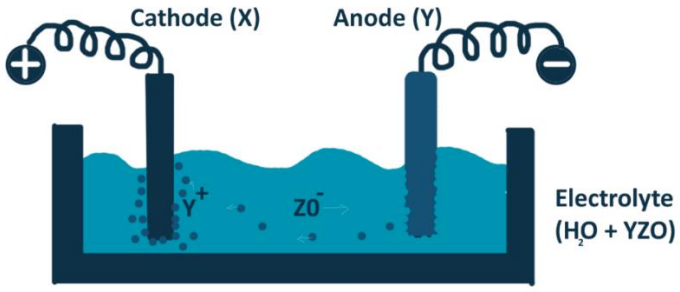

Figure 24. Schema of the powder production process by electrolysis

3.1.2.2. Atomization

The atomization method to obtain powder is being adopted due to its advantages. Melt atomization is a high productivity technique (400 kg / min) that is applied to any metal or alloy that can melt, and can be converted into high purity powder or pre-alloyed by disintegrating the liquid into drops. The size of the

final particles depends on several factors, but the greater the energy supplied to the broth, the smaller the particle size.[187, 188]

It can be classified into different categories according to the medium used. The most commons are gas atomization, water atomization, plasma and centrifugal atomization [183, 189, 190].

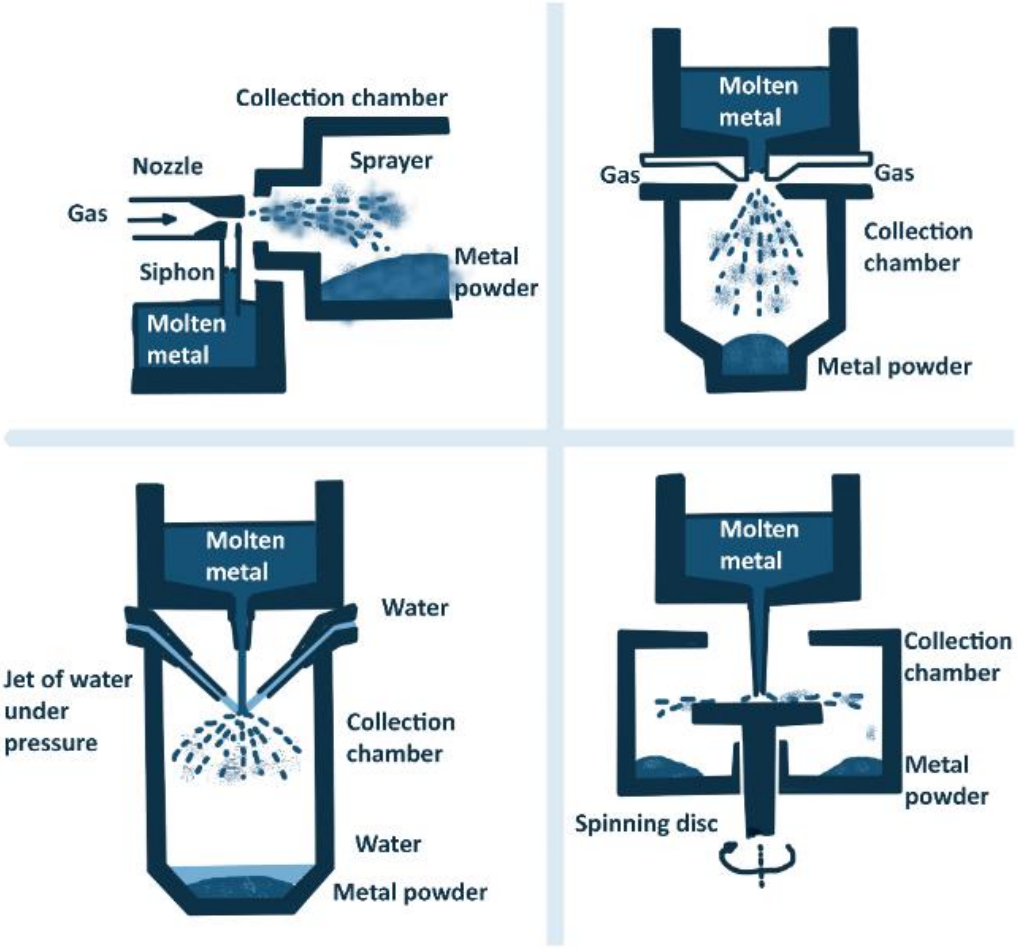

Figure 25. Scheme of different methods of production of metal powders by atomization.

Next, each spraying technique will be explained, but before a summary table of each technique is presented, showing its advantages and disadvantages of them.

Table 3. Metal particle characteristics by manufacturing methods [191-198]

Atomization process	Particle size (µm)	Particle shape	Advantages	Disadvantages	Common material used
Gas atomization	0-500	Spherical shape	Wide range of alloys available Suitable for reactive alloys Only requires feedstock in ingot form High throughput Range of particle sizes Use of EIGA allows for reactive powders to be processed Spherical particles	Satellites present Wide PSD Low yield of powder between 20 and 150 µm	Ni, Co, Fe, Ti (EIGA), Al
Water atomization	0-500	Irregular droplet shape	High throughput Range of particle sizes Only requires feedstock in ingot form	Post processing required to remove water Irregular particle morphology Satellites present Wide PSD Low yield of powder between 20 and 150 µm	Non-reactive
Plasma atomization	0-200	Highly spherical	Extremely spherical particles	Requires feedstock to either be in wire form or powder form High cost	Ti (Ti64 most common)
Centrifugal atomization	0-600	Spherical shape	Wide range of particle sizes with very narrow PSD	Difficult to make extremely fine powder unless very high speed can be achieved	Solder pastes, Zinc of alkaline batteries, Ti and steel shot

Liquid atomization with gas [GA]

The medium used is an inert gas to prevent oxidation; the most common are nitrogen and argon. If oxidation is not a problem, air can be used.

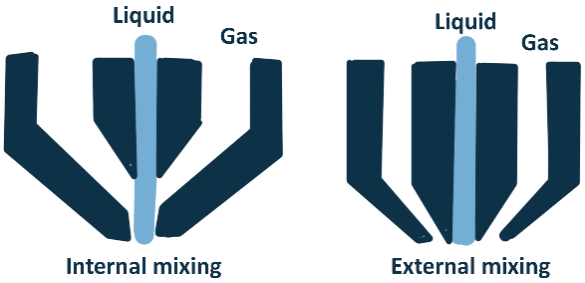

Figure 26 Two fluid atomization design.

There are two possible processes for gas atomization, but only one is interesting in the elaboration of metallic powder. This is known as "external mixing". The broth is melted in an induction oven and poured through a nozzle. The contact between the atomizing medium (gas) and the molten broth is made outside the nozzle. It is necessary for the gas to be extracted to avoid over-pressure in the chamber.

The process is governed by a series of interrelated operating parameters. Controllable variables include the temperature of the molten broth and that of the gas, the viscosity of the fluid, the distance of the jet, the pressure of the jet, the flow rates of the gaseous and molten jet, the type of gas, the geometry of the gas outlet, among others.

The powder obtained is made up of spherical particles, with smooth surfaces of high purity. The solidification speed of the drops is low, causing the metal to undergo an effect similar to that of an effort. Efforts are known as heat treatment of metals, assimilable to long annealing, which aims to produce globular grains and improve their deformability. Particle size can be reduced by increasing pressure, viscosity, temperature, and gas-induced acceleration or by decreasing the jetting distance.

The disadvantages of this method are that it suffers from very low overall energy efficiency (~ 3%) and this is expensive if inert gases other than nitrogen have to be used. Gas atomized powders, on the other hand, have poor green strength.[199]

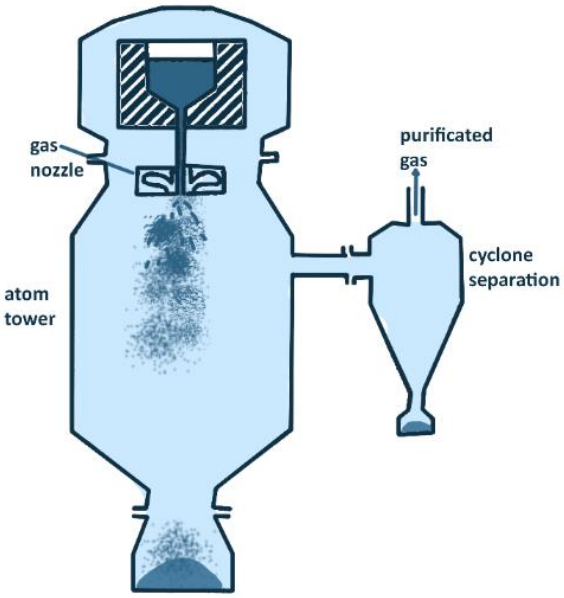

Figure 27 Schema of vertical gas atomisation. [200]

Liquid atomization with water (WA):

Water atomization is the most used technique to produce elemental or pre-alloyed powders with a melting point of less than 1600ºC. It is significant for low and high alloy steels, including stainless steel.[201] On the contrary, for reactive metals, its use is not recommended due to the formation of oxide, as is the case of titanium or super-alloys. The production speed using this method is estimated to be 400kg / min.[202]

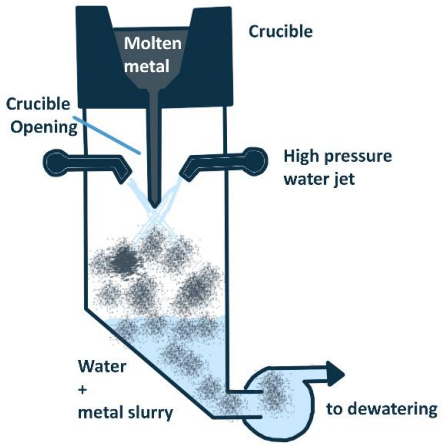

Figure 28 Water atomising unit.[200]

In this process, a high-pressure stream of water is forced through nozzles to form a dispersed phase of droplets that then impact on the metal stream. In this method, large amounts of energy are required to supply the water at high pressure.

The advantages of this technique are:

- Freedom to alloy
- All the particles have the same uniform composition.
- Control of the shape, size, and structure of the particles.
- Lower capital cost.

In general, powders of irregular geometry are obtained, with lower purity and with rough surfaces due to oxidation. A smaller particle size is obtained with low viscosity and low metal surface tension, by overheating the metal and/or using a nozzle with a smaller diameter hole, thus lowering the metal feed rate. You can also increase the pressure, volume, speed, or viscosity of the water or shorten the length of the jet and work with the optimal angle. Figure 29 shows the different variables, which have been discussed previously, that affect the size of the particles.[203]

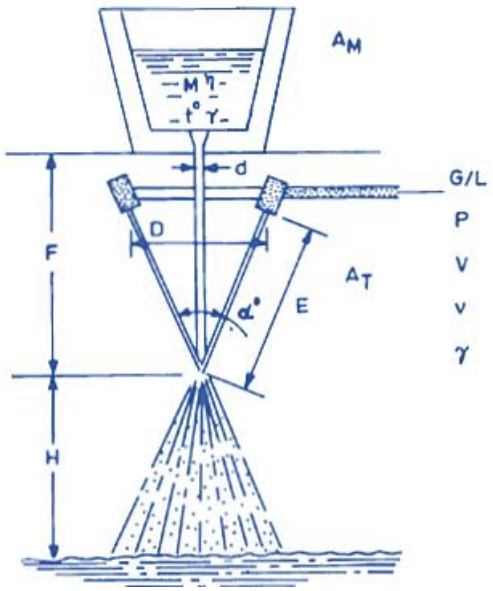

Figure 29 Major variables in the atomizing process.

It is true that an attempt has been made to define the size of the particles by means of a mathematical equation. In the end, Eq. 1 was reached, where d is the diameter of the particle, P the water pressure, v the water velocity, K a constant and α: the angle formed by the water-metal interface (it is indicated in the Figure 29). In this equation only the factors that most influence the size of the particles are considered.[204]

$$d = K\frac{\ln(P)}{v \cdot sen \propto} \qquad \textbf{Eq. 1}$$

Previously it has been commented that irregular particles are obtained, but this is not entirely true. The sphericity of the particles is favoured by:

- High metal surface tension
- Narrow melting range
- High pouring temperature
- Gas atomization, especially inert gas
- Low jet velocity
- Long apex angles in water atomization
- Long flight paths

The factors discussed above will be explained below. The surface tension of liquid metals is high and once a drop forms, it tends to assume the spherical shape. That is why the higher this is, the greater the sphericity of the particles. If the cooling rate is so high that it does not leave enough time for surface tension forces to operate to sphericalize the droplet, and therefore more irregular is the shape of the particle. Similarly, anything that influences by decreasing surface energy will promote irregular particle shapes. This group includes impurities, some alloying elements, or surface reactions such as oxidation. For example, small amounts of phosphorous in copper cause the formation of a surface film of phosphoric oxide (P_2O_5), which increases the energy of the surface and results in the formation of spherical droplets. This does not always happen the same way. For example, the existence of a film of solid oxide like ZnO acts in the opposite way, tending to give less rounded particles. The addition of silicon is a well-known method of influencing the particulate shape of atomized stainless steel powder. A higher pour temperature causes sufficient overheating to allow surface tensions to continue to act, creating more regular spheroids.[203]

Higher pressure or viscosity of the atomizing medium (water) results in greater deformation and therefore more irregular particle shapes. This is due to higher impact forces and higher volumes of water that make cooling faster.

Liquid atomization by centrifugation:

The foundation of centrifugal atomization is the expulsion of molten metal from a rapidly rotating container, plate, or disk.

Within this group is the rotating electrode process (REP) where a metal rod electrode rotates rapidly while melting at one end using an electric arc. The anode of the material to be sprayed rotates at 50,000 rpm. The drops of the molten metal solidified before hitting the walls of the outer container. The entire process is carried out under inert atmosphere conditions. Dimensional precision and alignment of the electrode are essential parameters to obtain good results.

It is mainly used for atomizing titanium and high purity, low oxygen super alloys. It should be noted that both the powders obtained by this procedure and by atomization with gas are not suitable for cold pressing applications and subsequent sintering of the green body. Its consolidation must be achieved by hot isostatic pressing (HIP) or some other high temperature method in which the voids between particles are closed more easily.

The powder obtained is made up of smooth, spherical particles with a size between approximately 50–400 μm (diameter). Precisely controlled rotation is essential to be able to obtain a desired range of particle size distribution. The diameter of the drop depends on some parameters such as the type of material (the surface tension of the liquid metal), the centrifugal forces (related to the speed of rotation) and the dynamics of the drops through the inert gas.

One of the drawbacks is contamination from the stationary REP electrode. It is for this reason that the plasma rotating electrode (PREP) process emerged, in which contamination of the electrode is avoided. Another problem that REPs face is the resonance effect. The REP or PREP kit design includes sufficient damping to resist resonant vibrations of moderate amplitude.[205]

It is not an appropriate method if you want a high production volume, a fine size powder and it is also considered a high cost process.

Other methods of metal disintegration:

Plasma atomization must be highlighted. As its name indicates, it is based on the application of plasma to produce high purity powders. This method is considered relatively novel and its technology is advanced. Specifically, what is done is to pass a metal wire through plasma torches, which transform it into drops that then solidify into powder. During the process, it works in an inert atmosphere together with a high velocity of a hot ionized jet of inert gas that produces adequate atomization. The process can produce powders with highly spherical particles and relatively small size. The powder produced by plasma atomization has a particle size distribution of 0 to 200 μm [206, 207]. Because it is produced under inert atmosphere conditions, the surface structure of the powders has a negligible level of impurities and, therefore, a low oxygen content [208, 209]. This technique has a significant number of disadvantages compared to the advantages it presents. For example, the starting material must be able to be transformed into wire, which means that materials that cannot be in that form are impossible to be

atomized by plasma [210]. This type of powder has its niche in additive manufacturing applications [211], or in the industry in biomedicine and sports articles [212-215]. Some of the companies that use this technology as the main process for powder production are AP&C (ex Raymor), PyroGenesis, and Hydro-Quebec (LTEE).

Another process used is the liquid atomization with cryogenic liquid gas, created by The Krupp Company. In this atomization process, the molten metal is atomized using cryogenic liquid gas (argon or nitrogen) at –200º C. Compression and cooling operations of the liquid gas are carried out simultaneously to prevent this fluid from vaporizing instantly with the opening of the jet. A uniform current is generated, which atomizes the melt in a manner comparable to the atomization of water and which cools rapidly. The advantage of this other method is that, since cryogenic liquid gas is vaporized, gas and dust can be easily separated in the cyclone. The advantage of this other method is that since the cryogenic liquid gas is vaporized, the gas and dust can be easily separated in the cyclone. Using this process, a high purity powder is obtained, highly spherical particles, and with an average size of 6-125 µm, better than in gas atomization.

Another less known method is vacuum atomization or soluble gas patented by Homogeneous Metal, Inc. Its principle is based on vacuum applying a molten metal supersaturated with gas under pressure, the gas expands, leaves the solution, causing the metal liquid is sprayed. This is outlined in Figure 30. Nickel, copper, cobalt, iron and aluminium based alloy powders can be vacuum atomized with hydrogen. Powders are spherical, clean and of high purity compared to powders produced by other processing methods.

In addition, there are also other methods of mechanical atomization, such as roller atomization (Crucible Melt Extraction), vibrating electrode atomization, and ultrasonic atomization. [216, 217]

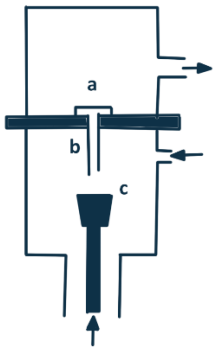

Figure 30 Schematic representation of vacuum atomization. (a) trap door, (b) transfer tube, (c) molten metal.

3.1.3. Mechanical methods

The production of metallic powder by mechanical grinding methods depends on the combination of four types of forces: wear/attrition (generation of particles as a residue of wear generated between particles in low friction), shear (breakage by fragile shear-mat processes), compression and impact.

Mechanical processes are not widely used as primary processes, but are usually secondary processes used to adapt powders already obtained by other methods. In other words, the goals of these methods are:

As a primary process, the production of:

- Mechanical alloys using reactive materials, such as beryllium and metal hydrides.
- Easy to fracture materials and hard materials such as pure antimony and bismuth, metal ceramic alloys.
- Common metals that are required in the form of flakes (avoiding a secondary process), such as aluminium and iron.

As a secondary process:

- Reduction of particle size
- Shape change: Flake metal powders are produced by flattening *equiaxial* particles produced by another method.
- Thickening of size.
- Agglomerate formation.
- Modification, change or alteration of material properties: density, hardness, grain size ...
- Mixing of various materials or mixing of phases.

A common method is the use of a ball mill consisting of a rotating drum with wear-resistant balls, that is, a material with greater hardness than the material to be crushed. The critical factor is the speed of rotation of the drum. The optimal speed is the one that avoids that both the material and the balls are pressed against the drum wall by such high centrifugal forces, or conversely that the movement of the balls is not enough to impact against the dust. Another process is the vortex mill, which, as the name indicates, is made up of propellers that rotate at high speed colliding against the particles, breaking them up.

A disadvantage of the mechanical method for the production of dust is the possible contamination due to the impact against the equipment material, this being able to fracture, detaching polluting particles. In many of these processes, lubricants or coolants are used to decrease wear on the machinery and prevent the particles from welding or agglomerating.

3.2. Important properties in the characterization of metallic powder

The success of any powder metallurgical process depends on the control of metal powders and, therefore, on an adequate characterization. The characterization of the raw material used for printing is necessary to ensure quality and repeatability in order to obtain a printed part with consistent and predictable properties.

Chemistry, particle structure, and particle size distribution are one of the properties that influence the behaviour of the powder during compaction and sintering, and the composition, structure, and properties of the sintered material. For example, metal powders used in AM are assumed to be nominally spherical, and have a particle size distribution that is designed to facilitate good packing behaviour, such that the final manufactured part has good mechanical properties and is fully dense. In the case of using metallic powder, the standardized measurement methods for the properties of the powder are various. The National Institute of Standards and Technology (NIST) has been dedicated to developing measures and standards for the characterization of metal powders suitable for additive manufacturing [218, 219]. Not only NIST, but also national and international standardization activities can be registered. For example, the French Association for Standardization (AFNOR) in France, which approved a standard on dust specifications (XPE 67-010: 2012) , which was replaced in 2014 by NF E67-01.[220] International standards organizations (ASTM and ISO) are also working on developing such standards[221]. In 2014, ASTM F3049 was approved, which is the first specific standard for the characterization of virgin and used metal powders processed in AM systems developed by ASTM F42 [232]. There are already existing standards (ASTM F3049-14) related with this, that may be applicable for. It is true that some authors such as Monzón et al. say that the existing general standards defined for other processes cannot be used when characterizing the powder used in AM, since this technique requires a more extensive characterization [220].

The reasons NIST has focused on defining dust characterization methods are: to ensure that the powder used meets the characteristics necessary to obtain a good final part, to determine the variability of powders from nominally identical batches and to determine the impact of recycling on dust characteristics, since using this type of powder reduces production costs in AM techniques that use powder[219]. Powder properties can be classified in multiple ways. One of the possible classifications would be the following: the physical or chemical properties of the individual particles, the properties of the powder assembly as a whole, and the properties of the powder under specific process conditions. It is true that the closer the characterization method is to the real conditions of the process, the clearer the relationship with the property of the final part will be.

Taking into account only the properties of the bulk powder is not enough to be able to perform a comprehensive classification of the powder. The properties of the bulk powder will serve to define the basic requirements, but in order to obtain a correlation between the powder and its behaviour during the

process, a combination of several characterization methods using specific process parameters will be necessary [222]. However, since these test techniques are not available by default and would not be comparable between them, the goal of many authors has been to find relationships between the different levels of powder properties and correlate them with the performance in the process.

Table 4. Different Powder properties and their recommended analysis techniques. [182]

	Powder characteristic	Analysis technique
individual particle properties	Local chemical composition	XPS, EPMA, EDAX, FIB, AES…
	Microstructure	optical metallography, SEM, EDAX, X-ray diffraction
	Microhardness	Vickers Hardness Test
	Morphology	microscopy (OM, SEM, TEM), shape parameters, morphological analysis, fractals
	Topography and surface area	CTomography, stereology, mercury porosimetry, gas absorption (BET), permeametry SEM, confocal microscopy
	Particle size and size distribution particle density	sieving, microscopy, sedimentation, turbidimetry (light obscuration), light scattering, , elutriation, electronic resistivity, permeability, surface area helium pycnometry, mercury porosimetry
Bulk properties	Bulk chemical composition	EDX/EDS, rudimentary chemical analysis
	Bulk density	Funnel analysis
	flow rate	Flowmeter Funnel, HR, CI, AOR, Revolution Powder Analyser, shear testers, computational methods
	green strength	flexural strength test
	thermal properties	TGA, DSC, DTA, TMA, TPA…

3.2.1. Metallurgical properties

3.2.1.1. Chemical composition and impurities

Chemical analysis of powder is relevant information to determine the type and extent of chemical reactions of the powder during handling. The chemical composition of the powder is an important factor in determining the conditions of the printing and sintering process, determining: the process temperature and the required atmosphere. This influence is due to the fact that the chemistry of the powder indicates how the thermodynamics of the solidus and liquidus curves can change. Solidus temperature is vital in choosing the proper sintering for the process [223-225]. Therefore, the final properties of a sintered material generally depend on the composition of the material.

From a chemical point of view, metallic powders are classified as elemental and prealloyed. Elemental powders, pure metal, are used in applications where high purity is required. The pre-alloyed powders are

obtained directly from an alloy obtained after mixing molten metals. In these powders, each particle must contain the specific composition of the alloy.

Due to the manufacturing processes of the powder or due to subsequent changes in its storage, metallic powders can have metallic or non-metallic impurities. The amounts of impurity elements are important both for processing, due to the change in the properties of the particles (hardness, reactivity ...) and for the properties of the final product.

Just as it is important to know the fractions of these elements (impurities), it is also important to know if these elements are present in their elemental form or if they are part of a chemical compound. Generally, these elements can be found in oxides, inert compounds or ceramics.

Surface films are a problem because of the large area per unit weight of the metal and because it is a powder. The amount of such contamination increases with decreasing particle size and with increasing surface chemical activity. Possible films that can form on the surface of the films include oxides, silicas, adsorbed organic materials, and moisture. Surface oxides are mainly because during dust storage they absorb considerable amounts of water vapour and other gases. Oxides present on surfaces can interfere with compaction and sintering and possibly remain in the sintered material. It is essential to remove such films before beginning the printing and sintering process.

One way to perform a qualitative and quantitative elemental analysis of particles is by using an energy-dispersed spectrometer (EDX-EDS). Often the SEM microscope is equipped with one. This device monitors the X-rays that are simultaneously emitted by the sample when it is bombarded with electrons. It is a simple, fast, direct and easy to interpret technique. Its limitation is that it has a limited spatial resolution and that it is not a technique capable of detecting elements with low atomic numbers. Another possibility is to use a TEM to which a transmission sweep unit (STEM) is coupled and thus obtain a sample composition map.

Along with the increased use of technologies that work with metallic powder, there was also a great interest in determining the elemental composition of particles (type of atoms and their relationship to each other). Some advanced techniques that can be used are Atomic Absorption Spectroscopy (AAS) with flame atomizer, with graphite furnace (GS-AAS), Optical Emission Spectroscopy with an Inductively Coupled Plasma source (ICP-OES), or Mass Spectroscopy with Inductively Coupled Plasma source (ICP-MS). These techniques are widely used in the elemental characterization of nanoparticles, but in the case of AM metallic powder, less analytical precision is required.

If you want to know the surface chemical composition, the most used analytical techniques are X-ray spectroscopy (XPS) and Rutherford backscatter spectroscopy (RBS). These techniques are non-destructive and very useful for detecting the surface composition of dust particles. XPS requires ultra-high vacuum

conditions since the sample is bombarded by a monochromatic high-energy X-ray beam (approximately 1 keV). The energy of the photoelectrons released from the sample is provided by a high-resolution electron analyser. This provides a spectrum where you can see energy peaks corresponding to the characteristic binding energy of each element. That is why it is an elemental characterization technique of the material surface. On the other hand, the RBS technique is highly sensitive and accurately provides the elemental composition through the measurement of the ions dispersed by the sample.

It is true that industry does not usually work with this level of precision and, therefore, less sophisticated equipment is used, much cheaper but that provides the necessary information to be able to carry out a simple analysis of dust quality. Some of the equipment is outlined below.

To verify the evolution of the content of the impurity elements, the chemical elements of C, S, N, and O in raw powders and sintered parts were analysed using a C / S analyser and an N / O analyser. The operation of these teams is based on fusing the metallic sample under a stream of helium gas that flows at ideal temperatures to release oxygen, nitrogen, and hydrogen. Before measurement, these instruments must be calibrated to ensure that the data is reliable to standards. Sample preparation involves placing the powder inside a tin capsule, then placing the powder inside a nickel basket in a graphite crucible before placing it in the instrument.

- The oxygen in the sample, in any form present, combines with the carbon in the crucible to form carbon monoxide and is measured by infrared absorption (IR). To correct the oxygen inside the graphite crucible, the nickel basket and the capsule of tin, the oxygen content of three samples without powder was measured and the average oxygen content of all samples containing powder was subtracted.
- The nitrogen present in the sample is released as molecular nitrogen and is detected and measured by thermal conductivity (TC).
- The hydrogen present is released as hydrogen gas and is also measured by infrared absorption.

Another commonly used way to obtain the level of oxygen impurities is the loss of hydrogen. It is used only in those metallic powders whose oxides are easily reducible by hydrogen, such as iron, tungsten, copper, or nickel. However, this value may not be exact due to the incomplete reduction of oxide. Details of the procedures for determining these parameters can be obtained from the standards of the Federation of Metal Powder Industries (MPIF) and the American Society for Testing and Materials (ASTM).

3.2.1.2. Microstructure

On the other hand, the microstructure of the crystalline powder is significantly influencing the behaviour of the powder in the process, in the sintering and in the properties of the final product. As the grain size is already known, it is a parameter to take into account in metals. In the case of powders, this depends on the particle size and the particular method of powder production. If the particles are rapidly cooled, it would naturally give rise to small particles and also to small grain sizes. An optimal sintering is obtained using powders with fine grain sizes, and therefore, the mechanical properties and the uniformity of dimensional changes of the final pieces.

It is true that if the powder is prealloyed, they can contain various phases. Multiphase microstructures depend on the composition and phase diagram of the alloy, the thermal history, and the method of powder production. In the case of water atomized solid solution type alloys, the microstructure consists of a core structure. It will be of great importance to know all the phases that constitute the microstructure of the powder.

In the same way, it is very important to know the structural defects since they also influence the compaction and sintering response of the powders. For example, a powder made by a cold mechanism exhibits a high displacement density that can be reduced by annealing.

The study of the surface microstructure and the metallographic sections give valuable information regarding the solidification rate of liquid metal droplets, the phase distribution and the phenomena of mass transport at different length scales.

This study could be done using a microscope (optical or scanning electron microscope). X-ray powder diffraction (XRD) technology can also be used for the identification and analysis of qualitative and quantitative phases, the determination of crystalline or amorphous phases, the determination of network parameters, the characterization of thin films and the identification of its phases. Thanks to this technique, foreign substances can also be identified by comparing the diffraction data obtained with the database of the *International Center of Diffraction Data*. Another advanced technology is TEM with an Electron Energy Loss Spectrometry (EELS) unit, which improves the structural information of the sample.

3.2.1.3. Microhardness

Measuring the hardness of the powder should be made with a Vickers Hardness. A square-based pyramid diamond is used in the Vickers hardness. It has an angle of 136 degrees between the opposite faces at the vertex. The tip is pressed into the surface of one of the grain leaving an area imprint.

The Vickers Hardness measurement is calculated by the ratio between the maximum applied load and the area of imprint, as it is defined by the equation:

$$H_v = 1.8544 \frac{P}{d^2} \qquad \text{Eq. 2}$$

Where P is the maximum load applied and d is the average length of the diagonals of the imprint [226]. The microhardness values (Hv) vary with the load used in the test. This is why it is necessary to specify this value P. P loads are generally less than 0.2 Kg. If you want to compare hardness results, you should perform the test applying the same load or, alternatively, use different loads but produce dimensionally equal footprints.

The sample used to analyse the microhardness will be the same as to analyse the microstructure of the powder and is explain in the page 67.

3.2.2. Geometric properties

3.2.2.1. Particle Surface Topography and Surface area

The shape of the particle is not the only important characteristic of the powder, but the nature of the surface of the individual particles is also. A spherical particle can have a smooth or bumpy surface.

The topography of the surface is a property to consider since it directly influences the friction forces between the particles. These are important in the case of the bulk movement of particles, when dust flows, settles, or during compaction. Other parameters that are influenced by roughness is the extent of actual contact between particles during sintering and the chemical reactivity of the powder. A greater roughness, more contact area, and therefore, greater reactivity. This leads to define another important property in the characterization of the powder, the actual amount of surface per unit mass of powder.

The topography of the surface depends on the process of obtaining dust and surface contamination, among other causes. For example, the powder obtained through metal reduction has a highly rough surface and those obtained by spraying have a smoother surface.

The surface area of a powder is measured by the BET method (Brunauer - Emmett - Teller), which is based on the adsorption of a gas to obtain a specific surface value (SW) considering that the surface is completely covered by a layer of monomolecular gas. From the knowledge of the area occupied by a gas molecule and the amount of gas absorbed in the layer, the total area of the dust sample can be obtained. The BET method for determining specific surface area is widely used for catalysts. Its use for metal powder is mainly for very fine and / or porous powders.

An advanced technology that is beginning to be widely used, not only at the research level, is computed tomography by X-ray (CT). In this, X-ray radiographs are taken at different angles with respect to the sample. Mathematical algorithms are responsible for collecting this information and reconstructing a three-dimensional image from hundreds of cross-section images. This information is then processed by software to obtain data on parameters such as porosity, volume, dimensions and the surface area of the sample.

3.2.2.2. External shape of the particle

The particles that form the metallic powder are three-dimensional in nature and can be considered equaxial. This means that they do not have a preferential orientation, but rather a random distribution of orientations. Despite the fact that Figure 31 shows a series of possible shapes that metal powder particles can have, it is true that the ideal and simplest shape is the sphere. As the Figure 31 shows, the particles can be classified by their morphology into: nodular, dendritic, acicular, fibrous, flake, spheroidal, angular, irregular and granular. This classification is defined in the ISO 3252 standard. In general, the shape of the particles is a consequence of the manufacturing process and the treatment of dust.

In some cases, the assumption of that the particles have this geometry is made and this facilitates calculations.

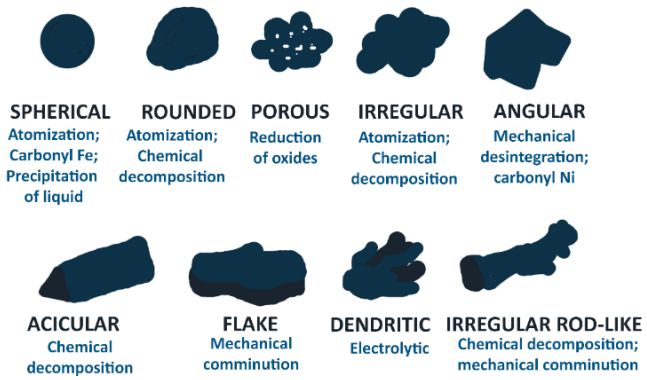

Figure 31. Set of possible particle shapes.

To qualitatively determine the shape of the particles, multiple shape factors have been developed that are a function of the shape parameters of the particles. The most frequent factors are found in Table 5. The stereology technique, three-dimensional interpretation of flat sections of materials, will be used to determine these factors.

Table 5. Form factor and definition [227, 228].

Form factor		Equation		Parameters
Specific volume surface		$S_v = \frac{S}{V}$	**Eq. 3**	**S:** particle surface area **V:** particle volume
Hausner	Elongation quotient	$x = \frac{a}{b}$	**Eq. 4**	**a:** length of smallest area surrounding rectangle. **b**: width of the rectangle **c:** perimeter of projected section **A:** projected area of the particle.
	Volume factor	$y = \frac{A}{A \cdot b}$	**Eq. 5**	
	Surface factor	$z = \frac{c^2}{4\sqrt{A}}$	**Eq. 6**	
Heywood quotients	Elongation quotient	$n = \frac{L_h}{B_h}$	**Eq. 7**	$\mathbf{T_h}$: minimum distance between two parallel planes tangential to the particle, one of them is the plane of maximum stability (thickness) $\mathbf{B_h}$: minimum distance between two parallel planes perpendicular to the Th plane (width) $\mathbf{L_h}$: distance between two parallel planes perpendicular to Bh and Th planes (length)
	Laminar quotient	$m = \frac{B_h}{T_h}$	**Eq. 8**	
Heywood form factor		$\not{f}_h = \frac{f}{k} = \frac{S}{V}$	**Eq. 9**	**S**: particle surface area **V:** particle volume. Only for spheres: n=m=1 , $\not{f}_h = 6$
CAR (Centroid Aspect Ratio)		$CAR = \frac{d_m}{d_p}$	**Eq. 10**	$\mathbf{d_m}$: length of longest chord that passes through the centroid. $\mathbf{d_p}$: length of chord that passes through the centroid and is perpendicular to d_m.

Form factors characterize the shape of particles morphologically and mathematically, quantifying their relative differences (for example sphericity) being defined through dimensionless relationships between different sizes that can be attribute to these. The most used form factors are those of Hausner, whose methodology is based on drawing a rectangle with a minimum area around the cross section of the particle observed under the microscope. Detailed characterization of particle morphology is carried out using a scanning electron microscope (SEM). Specifically, using the SE secondary electron mode. The SEM-SE also allows the observation of the surface state, specifically, roughness and surface porosity.

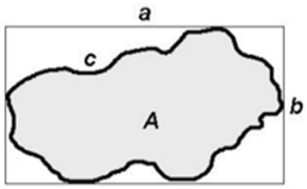

A: projected surface area of the particle.
a: length of the rectangle
b: width of the rectangle
c: circumference of the projected particle.

Figure 32. Parameters of Hausner form factors.[228]

.

3.2.2.3. Particle Size

In any real dust sample, all prepared in the same way, it is impossible for all the particles to be the same size. That is why we must speak of a size distribution (PSD) when accurately describing powders. The PSD curves relate the particle size to the corresponding fraction of the powder at that size. Figure 33 illustrates various size distributions. The size of a particle is not a specific value because, as already mentioned, the shape of said particle can have several dimensional values depending on where it is measured.

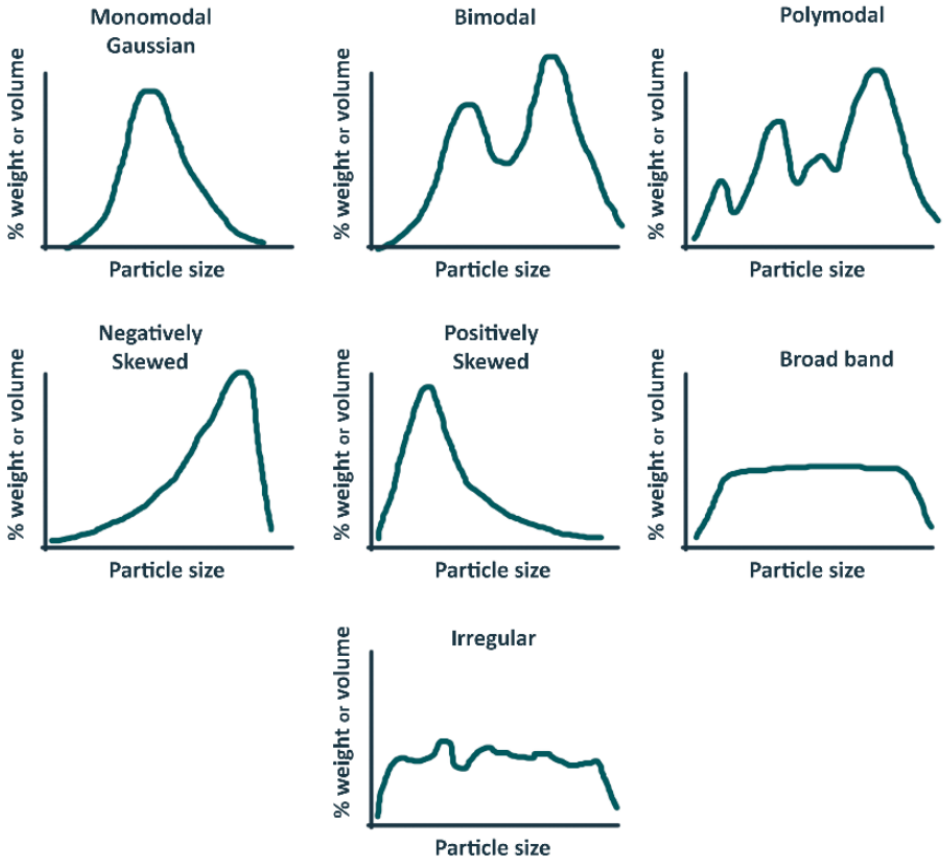

Figure 33. Some realistic particle size distributions.[229]

In the Figure 33, a polymodal distribution is presented, consisting of several narrow bands of particle sizes, with practically no particles between said bands. On the contrary, if there is only a maximum, most of the particles have a critical size and the distribution is called unimodal. Unimodal distributions can take different forms. In the Gaussian distributions (also known as the normal distribution), the mean, mode, and median concur in a single central trend of the curve; however, with the variation in the fraction of coarse and fine dust particles, it is possible to have an asymmetric distribution like the negatively and positively skewed distributions. A uniform concentration of particles with a size in a wide range leads to observing the broadband distribution. Outside this range, practically no particles are observed. As seen in

the last graph of the Figure 33, the irregular distribution represents a continuous and finite variation of particle sizes within a relatively wide range.

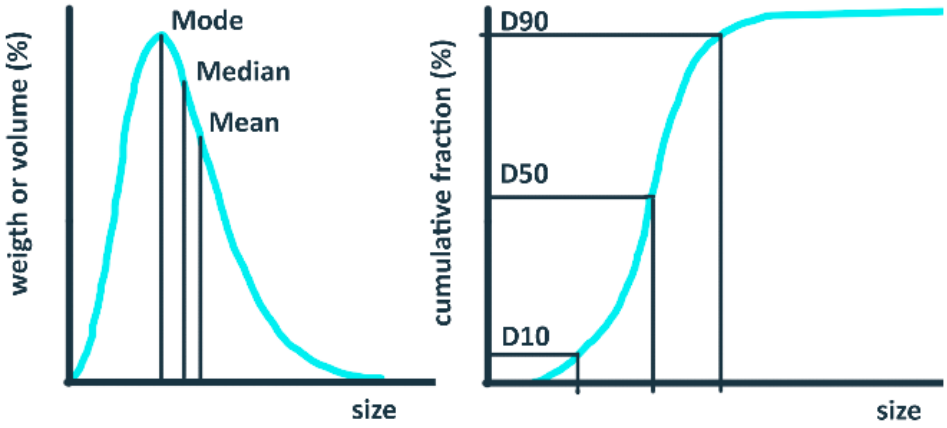

Figure 34. Differential and cumulative size distribution.

This is why it is not only important to know the average or maximum size, but also that the PSD is necessary for a complete characterization. As Figure 34 shows, it is common to present the results of the powder size distribution on a differential curve to better interpret the particle size, and a cumulative graph to identify the counting percentile of the size meters values: D10, D50 and D90. [19, 230, 231].

There are several methods that can be used to obtain the PSD, each with its own limitations such as the estimation of considering the particles as perfect spheres for calculations. Next, in Table 6, some of the possible methods to obtain said distribution and their limitations of applicability are shown, as considered by RM German.[232]

Table 6. Characterization techniques most used to obtain the particle size distribution and their size limit range for their applicability.[232, 233]

Method		Size range (μm)
Sieving	Using mechanical agitation or induced ultrasonic agitation.	44-800
Microscopy	Micromesh screens	5-50
	Visible light	0.2-100
	Electron microscopy	0.001-5
Sedimentation	Gravitational	1-250
	Centrifugal	0.05-60
Turbidimetry	Light intensity attenuation measurements	0.05-500
Elutriation		5-50
Electrolytic resistivity	Coulter counter	0.5-800
Permeability	Fisher sub-sieve sizer	0.2-50
Surface area	Adsorption from gas phase (BET)	0.01-20
	Adsorption from liquid phase	0.01-50

Many of the microscopy techniques used to define the size distribution are subjective because many particles have irregular shapes. The image obtained from a specific particle is treated as an equivalent spherical particle. The most common measurements are:

- Feret Diameter (F): maximum length of a particle measured in a fixed direction.
- Martin diameter (M): length of a horizontal line that divides the image area of the particle into two equal parts, all particles must be measured in the same direction.
- The diameter of the projected area (da): diameter of a circle with the same area as that projected by the particle.
- Largest dimension (Fmax): maximum Feret diameter for each particle, it has no fixed steering system.
- Perimeter diameter (d_p): diameter of a circle that has the same circumference as the perimeter of the particle.

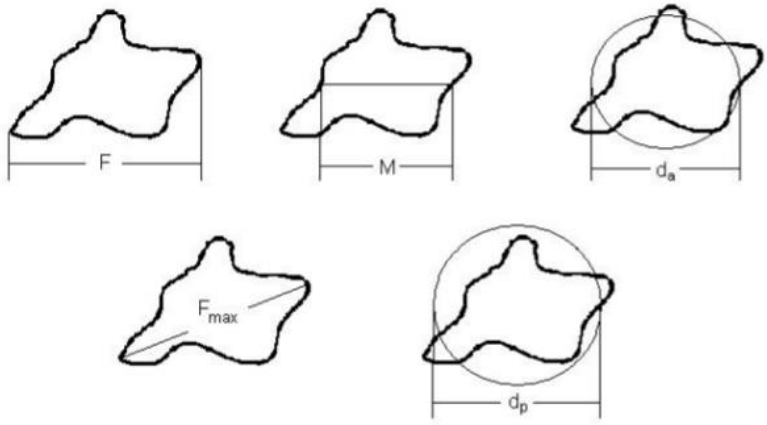

Figure 35. Techniques to measure particle size with irregular shapes.

The geometric properties of dust particles such as size and shape are important characteristics that affect their physical stability and behaviour. Therefore, knowing them is essential to understand their behaviour during the AM process.

Microscopy can be used to observe the morphology of the particles and measure their dimensions [234]. Electron microscopy techniques are very common and reliable. The scanning electron microscope (SEM) analyses the secondary electrons that come from the sample and provide information on the size and shape of the particles. Another device that can be used is the FESEM (Field Emission SEM), which allows obtaining images with higher magnification than traditional SEM and provides information on surface roughness. In the transmission electron microscope (TEM) the images are generated from an electron beam that passes through the sample, obtaining images with higher resolution than in the case of the two previous teams. If an extremely precise measurement of particle size is desired, the HRTEM (High Resolution Electron Transmission Microscope) technique can be used. Furthermore, with HRTEM it is possible to visualize the limits of the crystalline framework and obtain crystallographic information on the crystalline phases and the structural parameters. It is true that these last two technologies are not very common in the characterization of dust used in AM technologies since the size of this powder is large enough to obtain good results using SEM or FESEM.

Another alternative to obtain information on the morphology of the sample is to use scanning probe microscopy (SPM) techniques. This group of techniques includes, for example, atomic force microscopy (AFM). This technique is based on the use of a probe equipped with a tip the size of tenths of nanometers. This probe is guided by the surface of the sample and can perform the analysis in contact or non-contact mode. With this technique, information on surface topography can be obtained.

As can be seen, microscopy techniques are very useful in characterizing dust particles, but in many cases, sample preparation is laborious and affects the original morphology of the particle in some cases. It is for this reason that techniques based on light scattering measurements are used to characterize the morphology of the particles (especially to obtain their size).

DLS (Dynamic Light Scattering) is especially useful for obtaining particle size distributions (PSD) [235]. Its operation is based on measuring fluctuations in the intensity of the scattered light, thus determining the particle's diffusion coefficient that is directly related to the diameter of the particle. DLS is a simple, non-invasive, non-destructive and cheap technique. If the equipment is equipped with a potential measurement unit (Z), the net surface charge of the particles can be determined in addition to their size. Knowing this value is important since the net surface charge conditions the electrostatic interactions of the particles and therefore the tendency of the particles to flow or agglomerate can be predicted.

CT can also be used to obtain dimensional parameters of the particles [236].

3.2.3. Physical properties

3.2.3.1. Particle and bulk density.

Density is another highly important textural property in solid materials. According to the British Standard Institution, there are two types of density for solids depending on the volume being considered: true and apparent [237, 238]. True density is obtained by dividing the mass of a particle by its volume, excluding open and closed pores. On the other hand, the apparent density is the mass of a powder divided by its apparent volume. The apparent density can be obtained under specific conditions, known as tap density.[237] Bulk or apparent density is the packaging configuration that a powder assumes after free fall (ASTM B417-13) and tap density is the powder density that results when subjected to repetitive vertical shock (ASTM B527-15).

To obtain the true density of the dust particles it is necessary to know the real volume. Helium pycnometers are capable to measure the actual volume of solid materials whether they are powders or porous solids. This equipment is based on the gas displacement technique and Boyle's Law. Helium is used since it is an inert gas that also penetrates very fine pores (up to 2 Angstroms), therefore allowing a very precise measurement of the real volume.[218, 239] The drawback of the pycnometer is that if the particles themselves have an internal porosity that is inaccessible from the surface of the particle, this porosity will be taken into account in the determination of the density of the particles, giving the measurement a wrong density value. To avoid such a problem, the CT technique could be used to obtain the actual volume of the powder sample.

Apparent density is a critical characteristic of a powder as it influences the transport of the powder, the behaviour of the powder during sintering, and the density of the final solid. Other characteristics that have a direct relationship with apparent density are the size and shape of the particles, the surface area, the topography, and their distribution.[240] The Table 7 shows the apparent density of different metal powders and their dependence on particle size. To determine this density, the ASTM B 212 standard entitled *Test Method for Apparent Density of Free-Flowing Metal Powders* is applied. The Hall flowmeter is used, where a container of known volume (25 ml) is completely filled with a metallic powder that flows through a Hall funnel [241].

Table 7. Effect of particle size on bulk density for different metal powders[227, 242].

Material	Dust production process	Average particle diameter (µm)	Apparent density(g/cm^3)
Aluminium	Atomizes	5.8	0.62
		6.8	0.75
		15.5	0.98
		17.0	1.04
		18.0	1.09
Nickel	Carbonyl	3.2	0.61
		3.8	1.81
		4.1	1.87
	Precipitation	3.5	1.81
		4.4	2.10
		8.0	2.09
Tungsten	Oxide reduction	1.2	2.16
		2.5	2.52
		2.9	3.67
		6.9	4.40
		26.0	10.20
Iron	Carbonyl	7.0	3.40
	Reduction	6.0	0.97
		51.0	2.19
		68.0	3.03
	Electrolytic	53.0	2.05
		63.0	2.56
		78.0	3.32

There are other methods to determine the bulk density of metal powders. For powders that do not flow easily, due to a particle size that forms agglomerates, ASTM B417 and MPIF28 standards apply. This procedure is similar to the Hall apparatus; however, a Carney funnel (5mm) is used. Another very frequent instrument is the Scott volumetric, whose operation is detailed in the ASTM B329 standard. Finally, there is another device called the Arnold meter, the methodology for using it is described in the MPIF48 standard. The figure shows this different equipment used to determine the density of metal powders. It is true that there are other methods to obtain the bulk density of powders. These are described in the

following standards: ISO 3923/2: *Determination of apparent density of metallic powders*, and Standard Test Method ASTM 32990: Apparent Density of Metal Powders and Compounds.

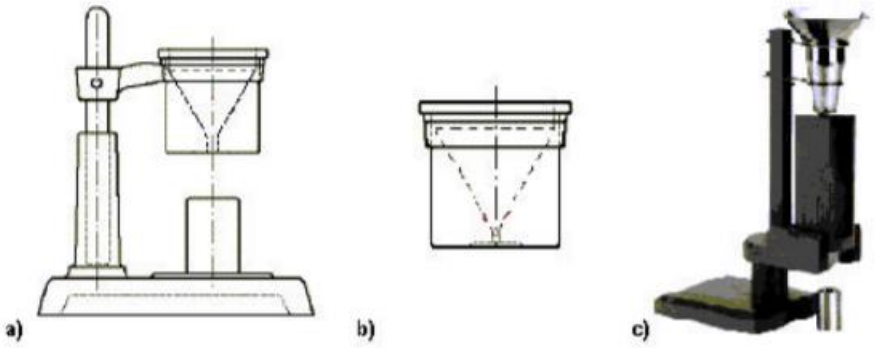

Figure 36. Equipment for determining the apparent density of metallic powders. a) Hall apparatus, b) Carney funnel and c) Scott volumetric.

On the other hand, the degree of compaction is a very important property for storage and handling of powdered materials. In a powdery material, the degree of compaction depends on the actual density of the solid, the particle size, the shape of the particle and the cohesiveness. The process to obtain the value of this type of density (the tap density) consists of measuring, under controlled conditions, the volume occupied by a known quantity of material. The concrete quantity of powder is contained in a test tube and it is struck mechanically successively, without applying external pressure. This measurement method is covered in many international regulations, such as ISO 3953, ISO 787/11, ASTM B527, ASTM D4781 or MPIF46.

The evolution of the apparent density measured as a function of tapping is represented as a non-linear curve, where the positive slope of the curve decreases until the density becomes constant. This reported final value corresponds to the tap density [233]. The amount of increase in density due to knocking depends on the extent of the original friction forces between the particles. The higher the friction conditions in the original powder (small sizes, irregular shapes, and rough surface), the greater the increase in density due to knocking.

3.2.3.2. Flow Rate

The flow factor is defined as the ability of the powder to flow freely depending on its own weight and is influenced by the friction between the particles of the same; therefore, it has a direct influence on the

rearrangement and packaging of the latter. This is why it is said that it is not an integral and inherent property of bulk powder.[243]

This property is influenced by the characteristics of the surface of the particles, such as oxide films or roughness. For example, the presence of an oxide film increases the friction between the particles and therefore tends to increase the flow rate. Other parameters that affect are some pertinent characteristics of the material, such as the theoretical density, the electrostatic interaction forces, among others. The lower the specific weight of a material, the greater the ability to flow. Regarding the morphology of the particles, the spherical particles are those that have the best fluidity. On the contrary, if the particles are too small, they do not flow under their own weight, because the electrostatic forces of attraction induce the formation of agglomerates.

The ability of the powder to flow freely is a very interesting property in AM processes since it will be possible to predict how the powder will behave in its handling during the entire AM printing process. For example, in the distribution of the layer on the impression bed.

There are different methods to determine the flow rate, some of these are compiled in the following ASTM B213, ASTM F3049-14, MPIF 03, or ISO 4490 standards. That is why when a flow value is given it must be specified with respect to the applied test device.

Some of the different techniques used to quantify or determine the flow velocity are explained below.

Some widely used techniques to measure the flow of metal powders are the Hall Funnel and the Carney Funnel (ASTM B213 and ASTM B964, respectively). The operation of both techniques is the same; their only difference is the diameter of the funnel. The hole in the Carney funnel is twice the diameter of the Hall and therefore serves to characterize fine powders since this type of dust does not circulate through the Hall funnel.

These techniques are based on measuring the time (in seconds) for 50 grams of powder to flow through the action of gravity through a container with a standardized shape and bottom hole. Normally a funnel is used, which has an angle of inclination of 60º.

Several authors conclude that the funnel tests are only simple comparative tests that do not allow a quantitative statement of powder flow [244, 245]. On the contrary, other authors consider that these techniques are not the most adequate to characterize the metallic powder used in AM, although they are closer to the AM process than other flow characterization techniques [246]

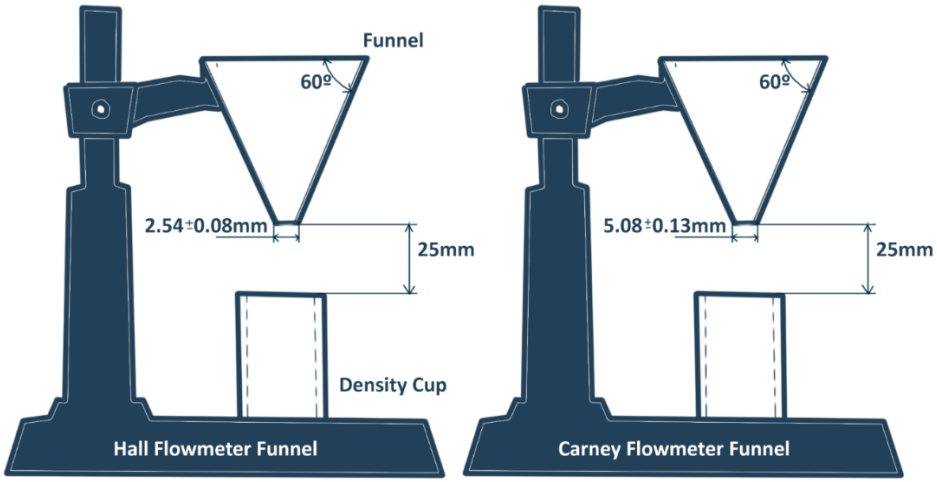

Figure 37. Schematic diagram of a) Hall Flowmeter Funnel and Carney Flowmeter Funnel with their corresponding dimensions. .

The Hausner ratio (HR) is a number that is correlated with the fluidity of the powder. This rudimentary prediction technique takes into account the apparent density and the tap density (Eq. 11). This dimensionless value is not an absolute property of the material, its value may vary depending on the methodology used to determine it.

$$HR = \frac{\rho_{tap}}{\rho_{apparent}} \qquad \textbf{Eq. 11}$$

Since bulk densities and tap density are a function of the internal friction exhibited by powders, the ratio of the two quantities is related to the cohesion of the material, which affects fluidity. As the Hausner ratio increases, the dust becomes less fluid, suggesting an increase in friction between particles. An HR value greater than 1.25 is considered to be an indicator of poor fluidity. [245, 247].

Table 8. Hausner ratio and Carr Index values to measure flowability.

Hausner ratio	Carr Index (%)	Flowability
1.09-1.10	8.26-9.09	Excellent
1.10-1.14	9.09-12.28	Very good
1.14-1.19	12.28-15.97	Good
1.19-1.25	15.97-20	Normal
>1.25	>20	Poor

The Hausner ratio (HR) is related to the Carr index (CI), as described in ASTM D7481-09 (Eq. 13). It is also known as the compressibility index and is another index indicative of fluidity. Indeed, Hausner's is related

to a measure of the friction between particles and the Carr index with the resistance and stability of the bonds between the dust particles [247].

$$\boldsymbol{CI}\ (\%) = \frac{\boldsymbol{\rho_{tap} - \rho_{apparent}}}{\boldsymbol{\rho_{tap}}} \cdot \mathbf{100} \qquad \textbf{Eq. 12}$$

$$\boldsymbol{HR} = \frac{\mathbf{100}}{\mathbf{100 - CI}} \qquad \textbf{Eq. 13}$$

Some authors criticize the use of both indices in the characterization of the fluidity of the material since they affirm that, despite its empirical demonstration, it does not have a solid theoretical basis. Furthermore, they argue that both procedures are too far from the situation in AM processing and, therefore, the method is not well suited for the characterization of AM powder [246]. On the contrary, other authors support the contrary opinion, stating that they can be used to draw quantitative conclusions about fluency [245, 248, 249]. Geldart et al. find an almost perfect linear relationship between HR and the angle of repose (parameter to be discussed below) [250]. From this, it is concluded that both parameters are good indicators of the fluidity of the powder.

The angle of repose (AOR) is another generalized method for characterizing powdered materials in relation to resistance to movement between particles [251, 252]. It is especially applicable for the free flow of slightly cohesive homogeneous powders [253].

To measure the angle of repose (AOR), the powder is thrown and the angle formed between the tangent to the surface of the cone-shaped pile of powder (h) and the horizontal axis (r) is measured. (Figure 38) The lower this value, the greater the friction and the forces between the particles and, therefore, the greater the flow of the powder material [199]. In general, a value greater than 50º means that there is no free flow; between 50 and 30º corresponds to a poor flow and less than 25º, implies free flow.

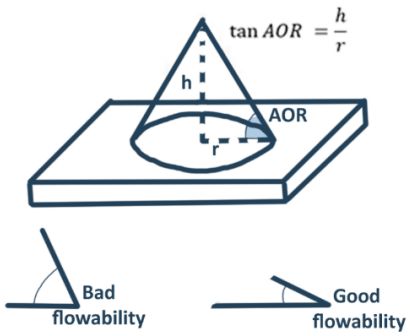

Figure 38. Angle of repose (AOR)

The results obtained depend on the equipment used, so it will be necessary to differentiate between the various test methods that make it possible to determine the AOR (nine methods according to Schwedes [252]). These methods for obtaining the angle of repose are classified into two groups: static methods and dynamic methods. Some of the different methods will be described below:

- The angle of repose spilled by free fall: the powder empties freely on a flat surface. To obtain them, static free-fall methods are used, such as a height cone, a fixed base cone, and a tilting table.
- The angle of repose spilled by hole: Dust is passed through a hole. The flow rate depends on the diameter of the hole and the size of the particles. Static methods are also used.
- The dynamic angle of repose: the powder is introduced into a rotating cylinder that has holes of different sizes.

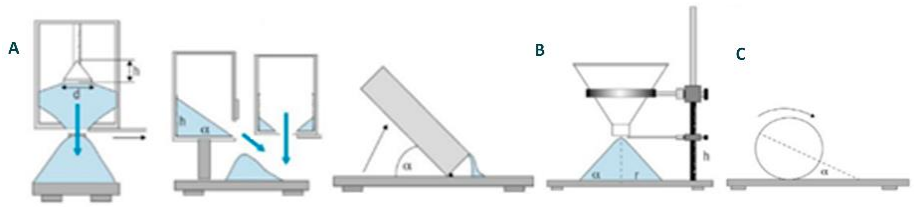

Figure 39. Different methods of obtaining the angle of repose: A and B) static methods and C) dynamic methods.

As it was discussed, AOR is closely related to HR. However, the AOR is more widely used due to its easy use. Furthermore, the use of the angle of repose is criticized by some authors, who assure that it is not a pure parameter of the measured powder. This is because its value strongly depends on the equipment used [245]. To solve this problem Geldart et al. developed their own equipment, which is commercially available.[254].

There is little information on the usability of AOR in the characterization of powders for AM. Although it is true that some authors claim that static methods are not useful to decide if a powder will be processable or not on an AM device.[255]

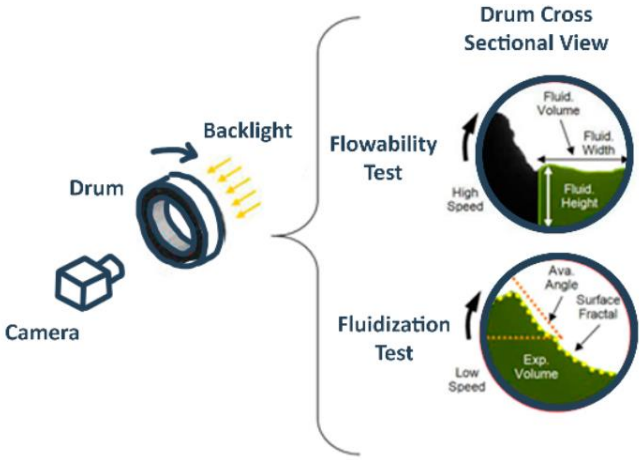

Figure 40 Diagram of the Revolution Powder Analyser indicating the analysis parameters.

Revolution Powder Analyser (RPA) is another method of characterizing powders with respect to their dynamic avalanche angle, which has gained increasing attention [246, 249, 256-261]. A rotating drum is partially filled with powder and spins automatically. A digital camera and image acquisition system collect images as the drum rotates for further analysis [262]. Using this method provides an opportunity to adjust the travel speeds of the roller to mimic actual flow characteristics of dust (Figure 41)[263]. In addition, it is equipped with a resistance and a thermocouple that allow controlling the test temperature.[257]

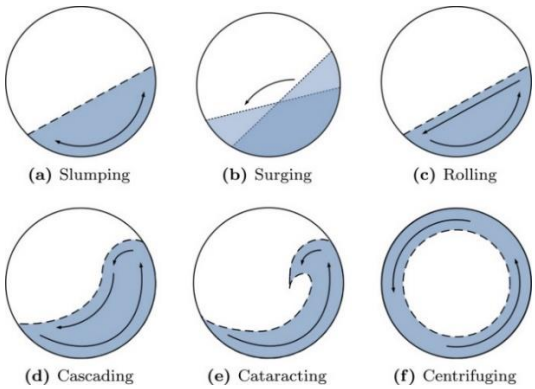

Figure 41. Six categories of granular bed motion in a rotating drum in order of increasing rotational speed, left to right and top to bottom. (a) Slumping. (b) Surging. (c) Rolling. (d) Cascading. (e) Cataracting. (f) Centrifuging.[264]

This technique allows quantifying some parameters such as (Figure 40) [261]:

- Avalanche angle. As the drum rotates, the internal friction of the powder gives it a cohesive force that makes it resemble a solid. However, at a certain angle, the weight of the powder exceeds its internal friction, causing a fall or avalanche. The maximum angle that the dust formed before the fall is called the avalanche angle.
- Avalanche energy. The energy released during the fall process. The RPA measures the changes in the gravitational potential energy of the dust by monitoring the sum of the potential energy for each pixel belonging to the sample. The potential energy is normalized in relation to the mass of the dust sample.

AOR and averaged avalanche angle are linearly related because of the similar stress state to which these techniques subject the dust [259].

Schulze criticizes dynamic avalanche measurement as this technique is based on a chaotic process and there is a lack of theory behind this [245]. In addition, the problem of particle segregation that occurs during the test is mentioned. A previous homogenization of the sample would reduce this phenomenon, the problem is that static charge would be induced in the powder sample, which influences the powder flow obtaining false results.

There is a large group of methods that are grouped under the name of shear testers [245, 252]. This group of techniques has become very popular in recent years [222, 224, 259, 265-271]. An advanced powder rheometer provides information on the energy required for a certain flow, resistance to flow based on the cohesiveness of the powder, and packaging performance.

Modular rheometers are usually used since they allow obtaining measurements adapting to the rheological requirements of the sample. For example, one way to monitor the behaviour of the metal powder flow used in AM is to use a rheometer with a dust cell (Figure 42) to measure wall friction. Wall friction measurements allow the wall friction angle to be calculated, indicating whether a powder can be homogeneously discharged from a hopper. A lower angle of wall friction indicates that dust adheres less to walls and is more easily discharged [259]. A recent comparative study of different cutting cells showed that the classification of powders with respect to their flow capacity was independent of the type of cutting cell, although some variation in numerical values was observed [272].

All the rheological parameters obtained after this test, such as the measurement stability index, the final elastic limit, the cohesion, the specific energy, the conditioned bulk density, and the flow function, correlated very well with the observed quality of the formation of the dust layer.[269]

That is why the rheology of the powders is a useful method to determine the differences in the flow properties of the powders used in AM [224, 254]. In conclusion, although further studies are needed,

powder rheology turns out to be a promising technique for characterizing AM powder with respect to flowability.

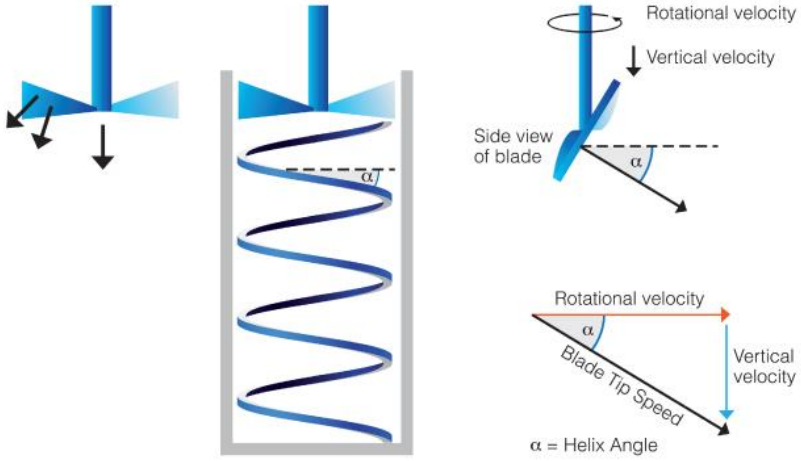

Figure 42. Schematic diagram of the functioning of rheometer with a dust cell.

As has been observed, there are different methods to quantify the flowability of the powder, and with these, different opinions about its usability. Currently, some companies or research centers are making tests using a simulator system to spread the powder from the AM machine to compare the fluidity of the different samples.[273] This is because it is believed that to test the relevant fluidity of the process, the test device should be as close as possible to the conditions of the process [245, 249, 259, 265].

In addition, new computational tools are being developed to characterize powders more thoroughly than current standards. Decost et al. developed computer vision methods to analyse the AM dust form autonomously [274, 275]. The algorithm can detect the characteristics of the dust and then create an image representation with detailed information to compare and analyse particle micrographs.

Even so, it can be concluded by saying that adequate parameters are lacking that allow a quantitative evaluation of the fluidity of the powder[276].

3.2.4. Mechanical properties

3.2.4.1. Green Strength

Green resistance is the mechanical resistance of a compact powder without sintering. This characteristic is very important in BJ processes, since it determines the ability of a green compact to maintain its size

and shape before sintering. The higher this is, the better, since it will be possible to work with the piece in green without it losing its shape, for example in the cleaning operation of the pieces after curing.

The green strength of a compacted powder is promoted by:

- Increase in the roughness of the surface of the particles, since there are more places available for mechanical interlocking;
- Increase of the dust surface. This is accomplished by increasing the irregularity and reducing the particle size;
- Decrease in the apparent density of the powder. This is a consequence of the first two factors;
- Decreased oxidation and contamination of the surface of the particles.
- Increased green density (or compaction pressure);
- Decrease in the amount of certain interfering additives. For example, the addition of small alloying elements or lubricants, avoiding mechanical interlocking.

In the case of BJ, the green strength is not defined by these parameters since the green piece maintains its shape due to the binder's curing process. Even so, it is important to take into account the above, since the remaining powder (without binder) in the bed may undergo compaction. If the green resistance of the powder is studied, the cleaning difficulty and the possibility of forming agglomerates can be predicted. These agglomerates are not desirable since the unused powder will be reused to reduce costs.

The standard green strength test is a flexural strength test using a rectangular sample of the following dimensions 12.7 x 31.7 mm and 6.35 mm thick. The sample resistance is calculated from the tension necessary to break the sample, as shown in the following equation (Eq. 14)

$$\boldsymbol{Green\ strength} = \frac{\mathbf{3} \cdot \boldsymbol{P} \cdot \boldsymbol{L}}{\mathbf{2} \cdot \boldsymbol{\omega} \cdot \boldsymbol{t}^{\mathbf{2}}}\ (\mathbf{N}/\boldsymbol{mm}^{\mathbf{2}}) \qquad \textbf{Eq. 14}$$

Where P is the breaking load expressed in Newton; L is the distance between the support bars in mm; t is the thickness and w is the width of the sample, also in mm.

Table 9 shows the relationship between green strength and compaction pressure for various types of iron powders.

Table 9. Green density and green resistance as a function of compaction pressure for various types of iron powders. [182]

Powder	Compaction pressure (N/mm^2)	Green density (g/cm^3)	Green strength (N/mm^2)
Sponge (contained 1% Zn state blended in)	415	6.2	2100
	550	6.6	3200
	690	6.8	4100
Atomized sponge (contained 0.75% Zn stearate blended in)	414	6.6	1900
	550	6.8	2700
	690	7.0	-
Reduced (contained 1% Zn stearate blended in)	415	6.5	2300
	550	6.7	3000
	690	6.9	3500
Sponge (contained 1% Zn stearate blended in)	415	6.6	2700
	550	6.7	3600
	690	6.9	3900
Electro (this one was isostatically pressed)	415	6.3	4600
	550	6.7	6200
	690	7.0	7800

3.2.5. Thermal properties

The Thermal Analysis Service encompasses all the analytical techniques that study the thermal behaviour of materials. The transformations experienced by the materials can be studied and analysed by measuring the variation of different properties of matter, in a controlled atmosphere, as a function of temperature. Properties include weight, dimension, power consumption, differential temperature, dielectric constant, and other less common attributes. [277] Below is a table with different material properties and the technique used to assess its dependence on temperature.

Table 10 Material properties and their dependence with temperature.

Property	Technique
Mass	Thermogravimetry (TGA)
Temperature	Differential Thermal Analysis (DTA)
Enthalpy	Differential Scanning Calorimetry (DSC)
Dimensions	Thermodynamic
Magnetic properties	Thermomagnetic analysis (TMA)
Electric properties	Thermoelectrometry
Particle evolution	Thermoparticles analysis (TPA)

Therefore this thermal analysis will serve to carry out decomposition and oxidation studies of the particles; determine the content of moisture, volatile matter, fixed carbon or organic matter that may be adhered

to the surface of the dust particles; study phase changes; determine the temperatures and enthalpies characteristic of the material; measure heat capacities; measure the thermal conductivity and finally, the coefficient of thermal expansion.

3.2.6. Other properties

3.2.6.1. Pyrophorocity and Toxicity

A pyrophoric substance is a substance that reacts with water, becoming spontaneously inflamed when it comes into contact with water or humid air. These materials can be safely handled in argon or nitrogen atmospheres (with some exceptions). Pyrophorocity is a potential hazard for many metals, including the most common types, as long as they are in a powder state. This is due to the large proportions of surface area between volumes, which makes the material more reactive since there is more area in contact with the air.

An empirical explosive index (EI) is used to rate the relative risk or danger of a dust, classifying the dust in the following groups: none (EI=0), weak (EI<0.1), moderate (EI€ [0.1-1.0]), strong (EI€ [1.0-10.0]) and severe (EI>10.0). The explosibility index (EI) is related to the sensitivity to ignition and the severity of the explosion. Ignition sensitivity is assumed to be a function of ignition temperature ($T_{ign.}$), minimum ignition energy ($E_{min.\ ign.}$), and minimum explosive concentration ($C_{min.}$). The severity of the explosion is assumed a function of the maximum explosion pressure ($P_{max.\ expl.}$) and the rate of pressure rise ($\Delta P_{max.}$). Ignition sensitivity, explosion severity, and explosibility index are defined as the unit for a powder that has ignition and explosion characteristics similar to those of Pittsburgh vein coal and are calculated as follows[278]:

$$\boldsymbol{Ignition\ sensitivity} = \frac{\left(\boldsymbol{T_{ign.}} \cdot \boldsymbol{E_{\min.ign.}} \cdot \boldsymbol{C_{min.}}\right)_{\boldsymbol{Pgh.\ coal\ dust}}}{\left(\boldsymbol{T_{ign.}} \cdot \boldsymbol{E_{\min.ign.}} \cdot \boldsymbol{C_{min.}}\right)_{\boldsymbol{sample\ dust}}} \qquad \textbf{Eq. 15}$$

$$\boldsymbol{Explosion\ severity} = \frac{\left(\boldsymbol{P_{max.\ expl}} \cdot \Delta\boldsymbol{P_{max.}}\right)_{\boldsymbol{sample\ dust}}}{\left(\boldsymbol{P_{max.\ expl}} \cdot \Delta\boldsymbol{P_{max.}}\right)_{\boldsymbol{Pgh.\ coal\ dust}}} \qquad \textbf{Eq. 16}$$

$$\boldsymbol{EI = ignition\ sensitivity \cdot explosion\ severity} \qquad \textbf{Eq. 17}$$

Table 11 shows the explosive index of some metallic materials depending on the size of their particles. As previously discussed, the chemical reactivity of a material increases as the ratio of surface area to volume increases. For this reason, many materials that do not normally ignite when combined with oxygen when presented in large sizes, behave differently when reduced in size, igniting. Variation in explosibility index for a given material is attributed to differences in composition, particle size, particle shape, and to the variation in reproducibility with the test equipment.

Table 11. Ignition and explosibility of metal powders[278].

Material	Size (μm) approx.	Index of explosibility
Aluminium atomized	44	>10
Al-Mg alloy	44	>10
Magnesium	74	>10
Titanium	10	>10
Iron Carbonyl	74	1.6
Boron	44	0.8
Chromium	44	0.1
Manganese	44	0.1
Molybdenum	74	<<0.1
Cobalt	44	<<0.1
Tungsten	74	<<0.1
Stainless steel	-	0

On the other hand, the toxicity of the powder is normally related to the inhalation or ingestion of the material and the resulting toxic effect on the human body. Table 12 shows data on the typical maximum allowable levels of dust in the human body.

Table 12. Typical maximum levels for occupational exposure (8h/day)[279]

Material	Concentration (μg/m^3)
Plutonium	0.0001
Beryllium	2
Nickel-carbonyl	7
Uranium	80
Chromium oxide	100
Mercury	100
Arsenic	500
Zirconium oxide	5000
Iron oxide	15000
Titanium oxide	15000
Zinc oxide	15000

The tests carried out to determine the reactivity of powders are detailed in the following standards of the *National Fire Protection Agency* (NFPA) [280]:

- NFPA 484, Chapter 4, Part 4.3 Determination of Combustibility
- NFPA 484, Chapter 4, Part 4.4 Explosiveness determination

4. Influential Factors in BJ technique.

For several years, studies related to AM (for example, processing parameters, optimization, microstructural evolution, mechanical behaviour, heat-treatment and post-processing effects on properties) have been carried out. The Figure 43 illustrates that the number of articles published reached the end of 2019 the amount of approximately 31,000 articles.

Despite the large number of AM-related studies, there is a lack of detailed information on process parameters, structure, properties, and challenges of binder injection, one of the non-fusion metal AM technologies. This is demonstrable in Figure 43, where it is shown that the papers published on this technology only represent approximately 2% of the total published in relation to AM.

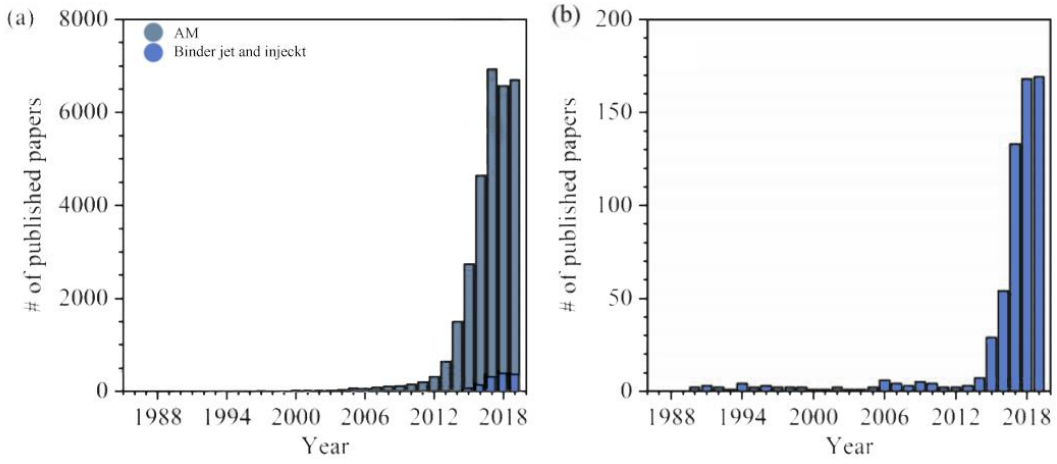

Figure 43. A comparison between numbers of (a) 3D printing and (b) Binder jet and inject papers published in peer-reviewed journals per year.

It is true that there is a basic understanding of the underlying principles that govern the printing process and affect the properties of the material before, during and after it. Many of these principles are based on established knowledge that exists in powder metallurgy (PM) and other AM processing methods that use powder (for example PBF) [214, 281-284]. However, a more exhaustive study is needed to understand the various factors that potentially influence the quality of the final part manufactured using the BJ metal technique. Some of these factors are the physical characteristics of the binder and the powder, the wettability of the powder material to the liquid binder, the properties of the powder bed, the way the powder is distributed or the way the binder is printed. [85, 173, 285-288]

Because binder injection is a very promising AM technique, this chapter will give an overview of everything currently discovered in relation to this technique. The factors or parameters to be addressed in this chapter can be classified into the following groups:

- Powder characteristics, such as powder morphology, mean size and particle size distribution, surface characteristics, powder chemistry, fluidity, packaging and wettability and their effects on the binder injection process.
- Binder (for example jetting and wetting behaviour, binder viscosity and volatility),
- Print processing parameters, such as layer thickness, binder saturation, the drying and curing time, the temperature, the orientation of the printing and the printing speed.

4.1. Optimal characteristics of the metal powder

BJ is still a relatively new technology with a lot to learn about what the requirements are for raw materials. Understanding process requirements and materials science will serve to increase performance.

The characteristics of the powder strongly influence many aspects of the BJ process operations, the properties of final parts and, consequently, the final economy of the process. That is why the need arises to study the effect of powder characteristics on the repeatability, reliability, and consistency of 3D printed samples using BJ. In addition, it will serve to accelerate the development of new materials and thus reach new markets. [132]

Recently, ASTM F3049-14 entitled "*Standard Guide for Characterizing the Properties of Metal Powders Used for Additive Manufacturing"* was introduced into the standardized powder characterization criteria for AM metal. However, additional advice is needed based on the experience of powder working processes[17]

The main characteristics of the powder typically studied in AM include:

- Shape/morphology.
- Mean size (d50) and particle size distribution (PSD),
- Flow (Hall Flow) and spreadability.
- Packing density (skeletal and/or apparent).
- Bulk and surface chemistry / composition.

Interconnecting the properties of the individual powder particle with the behaviour of bulk powder, process performance, and ultimately with the properties of the final part is a difficult task, due to the fact that some properties of dust particles can have opposite effects in the properties of the next level. It is true that studies have been carried out that determine the optimal characteristics that dust particles must

have in order to obtain final parts with the best properties and as reproducible as possible. [287, 289, 290]. Table 13 reflects this influence and indicates whether the effect is positive (+) or negative (-).

Table 13 The influence of the powder properties on different aspects of part quality based on the cited literature. "+" denotes a positive effect, "-" a negative effect and "0" for demonstrated no effect.[222]

		Part density	Surface quality	Mechanical properties	Accuracy	Internal build flaws
PSD	Narrow			**+** [291]		
	Wide	**+** [248, 291]	**+** [291]			
	Coarse		**-** [292, 293]	**-** [292] **0** [224, 294] **+** [295]	- [292]	**-** [292]
	Fine	**+** [258, 295, 296]		**-** [222]		**-** [297]
Bulk density	Low	**-** [291]	**-** [294]			**0** [222]
	High	**+** [214, 294]		**+** [294]		**+** [294]
Flowability	Low					
	High			**+** [294]		**+** [294]

4.1.1. Powder morphology

Powder morphology governs processability in BJ technology. Compared to powder metallurgy where irregularly shaped powder, obtained by water atomization, was generally used, in AM powder bed processes, particles with spherical morphology (obtained by gas atomization) are preferred. In this way, the density of the powder bed (Figure 44) increases since a lower roughness generally correlates with less friction between particles that improves fluidity.

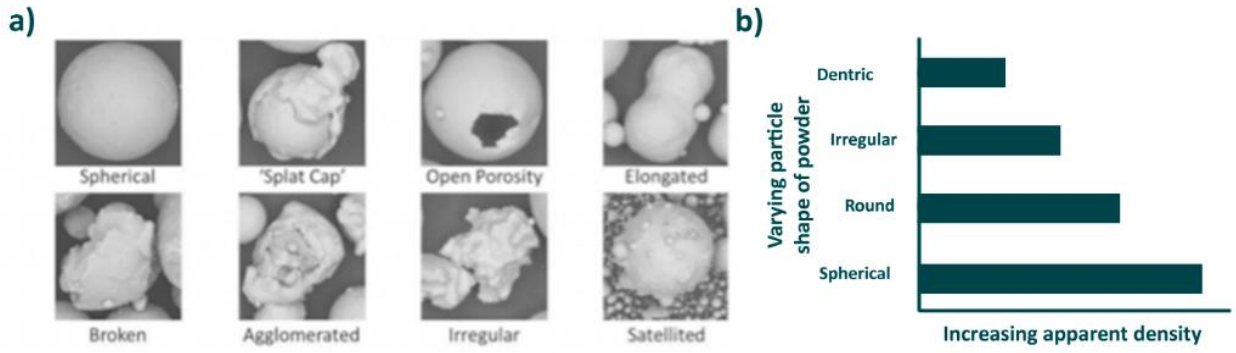

Figure 44 A) Micrographs of individual powder materials with various shape and surface features, produced using gas atomization; B)Effect of powder morphology on apparent density (this assertion is only true when held to a fixed particle size).[19]

Much of the research on the relationship between the properties of the powder and the final characteristics of the part printed by BJ have concluded that the morphology of the particles is an important factor. However, no agreement has been reached regarding its effect on the process and/or on the properties of the final part. This same argument was defended by Schulze et al., who affirms that the shape of the particle affects the flow properties, but general statements are not possible. For coarse particles, smooth spherical particles often flow better than rough, sharp, and non-spherical particles. But in the case of fine particles, which are cohesive and among which the adhesive forces play an important role, the rough particles may exhibit a more favourable flow behaviour [245].

The relationship between particle morphology and powder fluidity is confirmed by other authors, including Inaekyan et al. [298]. In their work, they compared the BJ impression of pure iron powder obtained by water atomization with another gas atomized powder and they showed that the lower the circularity and the broader the distribution of the particle size, a less fluidity and a lower packing of the powder and, therefore, a greater porosity in the pieces after sintering. On the other hand, the results of Spierings et al reached the same conclusion [246].

However, the research by Pohlman et al. revealed that PSD may be a more important factor in fluidity than particle shape [260]. Karapatis summarizes from a literature review that sphericity is favourable for good flow behaviour, optimal packing density, and performance in the layer deposition process [248].

On the other hand, Strondl et al. studied the effects of recycled powder, discovering recycled powder exhibits less fluidity compared to new powder. This event is due, as you can read in your study, to the fact that the recycled dust particles show impact marks (a more irregular morphology)[224]

In reference to some final properties of the part, such as ductility, morphology is not considered a significant factor.

To sum up, although it is clear that morphology has an impact, it will be difficult to quantify it and build an unequivocal relationship with the performance in the process and the property of the final part. Although currently there are multiphysical models that serve to study these influences in a theoretical way. [299]

4.1.2. Particle Size Mean and Distribution

PSD and mean particle size are important parameters in BJ processes, affecting flow capacity, pore size distribution and uniformity of powder bed density, thus altering the penetration of the binder drop. .

As already explained in the chapter where the properties of metallic powders were explained (page 71), both the size of the particle and the PSD are characteristics of the powder due to the production process, they are not inherent properties of the material, just as than morphology.

Normally the minimum particle size is in the range of the sub-micrometres, and its maximum value corresponds to 150 µm. These values depend on the characteristics of the BJ printer, such as its capacity or the resolution of the print head. Industries that are familiar with manufacturing parts using metal powders use fine powders with a mean size of fewer than 30 µm. Although it is true that there are currently many of these examining larger powders to meet commercial objectives [16].

Due to the experience in other manufacturing techniques that use metallic powder, there is an extensive study on the effect of these properties (size and PSD) on some specific characteristics of the process, such as the packing density of the powder bed, the fluidity and distribution of powder [258, 292, 295, 296, 300, 301]. But, conversely, there is limited study on the effect of PSD on the quality of green and/or post-processed structures manufactured by the BJ process [173, 288].

In this section, all the results of the different studies will be summarized. The consequences of using fine or coarse powder and PSD will be discussed. Although it is true that drawing conclusions to obtain the optimal configuration will be difficult, as will be seen below.

First, we will proceed to detail the influence of particle size, exposing the different results of working with large and thick particles or, on the contrary, smaller and fine particles.

On the one hand, if it works with small dust particles (less than 20 µm), there will be a greater surface area and, therefore, a higher energy state. In other words, the reaction rate will be greater in small and fine particles than in large ones. This leads to faster sintering densification and reduced process time.

Verlee et al.[302] confirmed that the small powder particles (22 µm and 31 µm) had a higher energy state because they began to densify at lower sintering temperatures compared to coarse particles. Neira Arce A. also reached this conclusion, determining that smaller particles show higher thermal conductivity [303].

Another advantage of using small size powder is its greater packing capacity. If the density of the powder bed is higher, the sintered part density will also be. At the same time, there will be a smaller linear shrinkage. Verlee et al also demonstrated that the percentage of porosity decreased significantly for fine dust particles.

A smaller powder particle size (particles smaller than 20 μm in size) also appears to be beneficial for the surface finish of manufactured parts, as well as for higher mechanical properties and densities of sintered parts. they are due to the following factors [304]

- Greater points of contact between the particles.
- Greater retention capacity of the binder due to the greater number of bonding points. That is, the smaller particles cause a slower flow of the binder between the powder bed, and therefore a greater capillary force will be required for the binder to flow and spread.

H Miyanaji et al noted that printed parts with the smallest mean particle sizes resulted in better surface finish and higher final densities after sintering because the particles are better packaged [288]and the ladder effect decreases [173, 301]. Another reason for such improvements to occur is that a small powder particle size facilitates the expansion of the droplets due to the smaller pore sizes. Admittedly, this can reduce the precision of fabricated structures as demonstrated in some studies [287, 305]. They also obtained final pieces with greater hardness using smaller dust particles.

But not everything is positive with the small particles use, it was also shown that with small particles, the vertical penetration of the binder will be less since the pores are smaller, which implies less permeability than the use of larger particles, as previously explained. Furthermore, the dimensional precision, the roughness of the surface, and the density of the green part are worsened by small particles [288]. Not forgetting that fine powders show a greater tendency to agglomeration and a lower flow capacity due to the large surface area and their nature to easily absorb moisture[304]

As a note of caution, special care should be taken when using powder smaller than 15 μm in size due to its ignition ability.

On the other hand, dust formed with larger particles has a greater flow capacity and a lower surface area. [304] From some studies, it appears that the surface roughness of the sintered parts is directly proportional to the size of the particles. Some authors attribute this to the increase in peak-to-valley ranges in dust beds formed by large particles [258, 306, 307]. This is not consistent with the trend observed in the green parts, where the large particle size seems to be beneficial for the dimensional accuracies and densities of the green parts. Therefore, while the powder with larger particles is favourable for higher

geometric precision of the green parts, they are likely to result in weaker or slower sintering kinetics and inferior qualities in the sintered parts.

Some of the conclusions drawn in relation to the effects of the PSD will be exposed making a comparison between its amplitude (wide and narrow) and its shape (unimodal and multimodal).

It is known that the wider the PSD, the more heterogeneous will be the distribution in the powder bed, having to allow more time for the fluid binder to fully penetrate. The penetration time of the binder depends on the size of the space between the particles. The greater the size of the space (macro-spaces), the curvature of the flow front decreases and, therefore, the fluid (binder) decreases its forward speed. There is a limit situation where the fluid completely stops its advance through this channel and proceeds to advance through neighbouring microholes or microchannels. This event is not desirable as the macrohole will be empty and becomes a pore of the green piece (Figure 45). [308, 309]. It is for this reason that a wider PSD decreases the densification factor during sintering, having the printed part larger pore sizes. [302]

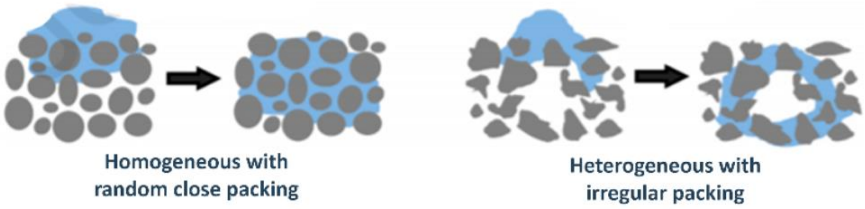

Figure 45 Illustration of fluid binder penetration within homogeneous and heterogeneous distributed powder bed.

On the other hand, wide distributions have the advantage of resulting in higher powder bed packing densities [291].

Conversely, a more evenly distributed powder bed (narrow PSD) can provide more channels for the liquid binder to penetrate. Therefore, optimizing the powder size distribution can help reduce numerous printing related problems. Furthermore, Liu et al. connects a narrower PSD with a higher tensile strength and higher hardness on the sintered parts as the densification factor on the sintered will be higher [291].

Among the few studies on the effect of the PSD shape, we find the study by Miyanaji et al.[310] In this two dust samples were compared, one with a monomodal distribution and the other bimodal. The results obtained were that the bimodal presented a higher packing density and, consequently, the sintered piece showed smaller pores. This occurs due to capillary pressure, explained above, which is higher in channels with smaller diameters [311]. In contrast, the monomodal distribution sample had a greater surface area and, therefore, a greater porosity.

Other works corroborate the relationship of the density of the packaging with the shape of the distribution. These establish that a bimodal PSD, with a mixture of 25% by volume of nanoparticles and 75% of microparticles, increases the packing capacity, increasing the green density [245, 249, 259, 312]. This phenomenon can be explained by the "roller bearing effect", where the nanopowders fill the interstitial spaces between the micropowders, effectively increasing the packing density of the raw material during mixing [249, 259, 312], and also played a decisive role in the entire sintering process improving densification but suppressing grain growth [245].

Finally comment that Spierings et al. They corroborated that the PSD must be biased in the direction of fine particles, as the finer particles fill the gaps between the coarser ones, leading to higher part densities and improved surface qualities, while the larger particles can be beneficial for higher elongations at break [258].

4.1.3. Packing Density

The packing density of the powder is a parameter that refers to the ability of the dust particles to organize themselves in the powder bed after being spread by the roller (or failing that, another type of gadget), optimizing their contact as much as possible among them. That is why the packing density determines many outcomes of the process.

The relationship between the packing density with some process parameters and with the properties of the final part is very clear. Contrary to PSD, it has the same effect on the different factors studied, which is why most of the authors tell us that a high packing density should be sought.

A higher packing density in the powder bed decreases the number of voids between particles within the bed; therefore, the porosity of the green part is also lower. As a result, the resistance of the piece in green increases[308] . In some works, it was shown that under a relative packing density of less than 90%, the voids in the part were mostly connected while, with densities of over 90%, the voids were mostly closed or the holes were not interconnected. These types of voids can theoretically improve part density while reducing shrinkage during sintering [173, 313, 314] Therefore, the powder packing density determines the pore or void volume within the powder bed that can be filled with the liquid binder, which in turn influences the mechanical properties and quality of the final part.

In summary, an important consideration is the influence on the mechanical properties of the final product. It was shown that the higher the packing density (higher packing factors), the greater the mechanical resistance [294] and the Vickers [315-317], which can be easily explained by the effect of microstructural porosity previously discussed.

The quantitative and qualitative knowledge of the packing density will serve to establish some process conditions such as the quantity of binder supplied. It is also possible to work in reverse, that is, to modify the packing density of the powder so that it adjusts to the working conditions.

Various parameters influence the behaviour of particle packing, including powder morphology, mean powder size, particle size distribution (PSD), interparticle forces, powder surface chemistry, and powder fluidity [318]. Actually, the packing density of a powder is mostly a function of its PSD, but other factors that are not intrinsic to the powder also influence, such as the selection of the distribution method (the properties of the roller/rake) or the thickness of the layer [319-322]. Next, different ways of adjusting the packing density will be explained using the most common control variables: the morphology and PSD of the particles, the thickness of the layer and the mechanism of distribution of the powder.

The intrinsic characteristics of the dust.

The effect of mean particle size was shown to have less significant effects on powder packing density[290, 323], while PSD and particle morphology are some of the most important factors[169]. In contrast, for very small particles, a very influential factor is interparticle forces, which have a negative impact on the packing density of the powder.

A wide (moderated) PSD favours higher packing densities compared to a narrow PSD [167,168]. This may be due to the effect of filling a vacuum/hole with small particles [290, 324-327]

In general, adjusting the powder packing density can be accomplished by adding fine powder particles creating a biased or multimodal PSD.

Using multimodal powder is an effective way to increase the density of the powder bed where coarse particles ensure fluidity while fine powders fill the spaces between large particles to improve the density of the powder bed [108, 306, 328].] A bimodal PSD is created by mixing two sizes of dust particles in a given ratio of volume, and making these bimodal powders produce much higher packaging factors than monodisperse raw materials [329, 330] . The bimodal approach may be more desirable to increase the behaviour of powder packaging than a broad PSD due to the fact that gap sizes are characterized by default by the largest particles in a bimodal PSD[323, 331] l compared to a random distribution of spaces in a wide PSD [19]. Since the fluidity of the powder can change due to the addition of new powder, it is required to optimize the fine to coarse powder ratio in a bimodal PSD powder. Next, according to some authors, different bimodal PSD configurations and their effect will be exposed.

Zhu et al. [332] showed that increasing the fine particles by 10% could improve the bulk density of the powder bed from approximately 77% to 88%. In contrast, McGeary [333] suggested that a mixture of coarse and fine powder with a 10: 1 ratio (coarse / fine) can lead to a maximum packing fraction of approximately 82%. Other authors also suggested a 7: 1 coarse and fine particle ratio configuration, respectively [333]. The result was a packing factor of 0.868, although the actual packing density may be much lower due to inhomogeneity and other factors[334, 335]. All of these powder packing density enhancement mechanisms based on powder morphology and PSD can currently be performed using computational simulations to optimize particle packing more efficiently and effectively. [323, 336-341]. These calculations are based on the theoretical calculation of the packing factor of a bimodal powder mixture [334] (Eq. 18):

$$f^* = f_L + (1 - f_L) \cdot f_S \qquad \textbf{Eq. 18}$$

Where: f * is the maximum packing density (theoretical), fs is the smallest fractional powder packing density and fL is the largest fractional powder packing density.

However, it was found that when using a bimodal PSD, the sintering density did not improve as the larger particles in each mixture formed a rigid structure and prevented densification [171]. Furthermore, there is a study, carried out by Zhou et al. [162], the results of which are opposite to those previously commented, since the addition of fine powder decreased the packing density of the bed. These results could be reached since the ratio between the coarse and fine particles was not adequate. As Figure X shows, the packing density (f*) as a function of the large and small particle fractions reaches a maximum value, corresponding to the maximum density (f*) for a homogeneous mixture, this value being much higher than the value obtained by the mixture density rule (Eq. 18)

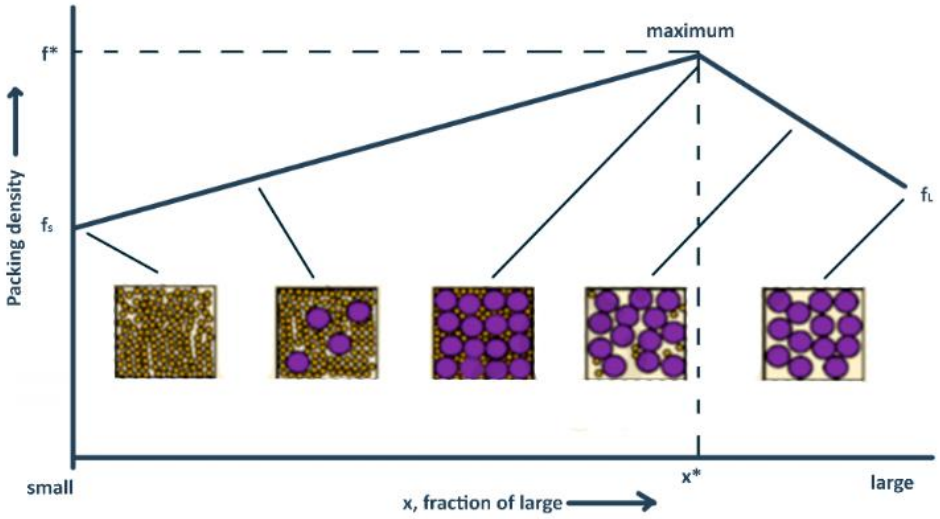

Figure 46. Influence of powder size and PSD on packing density for a bimodal mixture, showing different possible structures. [42,178].

The types of layers and the mechanism used to spread the powder.

Experimental and theoretical research carried out on optimizing the formation of dust layers in three-dimensional printing (3DP) confirms that the thinnest dust layers are suitable in many aspects, such as precision, surface quality and densification[342-347] .. However, conventional layering methods such as counter-roll (CR) layering or grout-based layering do not allow the creation of a flawless thin layer, with defects such as formation of cavities, misalignment forming a sinusoidal profile (waves and ripples) in the bed or partial displacement in some areas. For the first time, Lee [348] used a double smoothing (DS) mechanism to spread each layer. The operation of this dust dispersion mechanism is shown in Figure 47. To start, the printing platform lowers its height by a greater distance to the desired layer thickness. Once this step has been carried out, the layer is dispersed according to the CR method. Thus, a layer of provisional powder with a thickness greater than that desired is formed. The platform is then raised a distance corresponding to the excess added in the previous step. After this operation, a second smoothing CR is carried out, finally leaving a thin powder layer of thin thickness, of only about 55 µm [349]. It was shown that by CR layer thicknesses greater than 55 µm are obtained; however, the DS method could help spread the powder with a lower layer thickness of 55 µm. [349]That is why the green pieces obtained using a DS distribution method had a higher green density [193]. In addition, it was achieved that the variation of the localized density between the top and bottom was less than in CR. These experimental results are supported by studies of the theoretical foundation [321, 349, 350]. It should be mentioned that with this procedure the cavity defects were solved although the wave effect in the bed did not disappear. [W37]. It is for this reason that new powder dispersion procedures are being investigated, which allow the

defects obtained with CR and DS to be solved, but which maintains the mechanical simplicity of these two mechanisms, such as those known as Blade Vibrational spreader or Top Filling mechanism[351, 352]. The first consist in distribute the powder by means of a vibratory system (about 20 kHz) which deposits the powder evenly on the bed. The second, on the contrary, takes advantage of the effect of gravity to distribute a thin layer of dust, that is, it is like a hopper-carriage. Addressing this topic is beyond the purpose of this chapter; therefore, more details of these mechanisms will not be given.

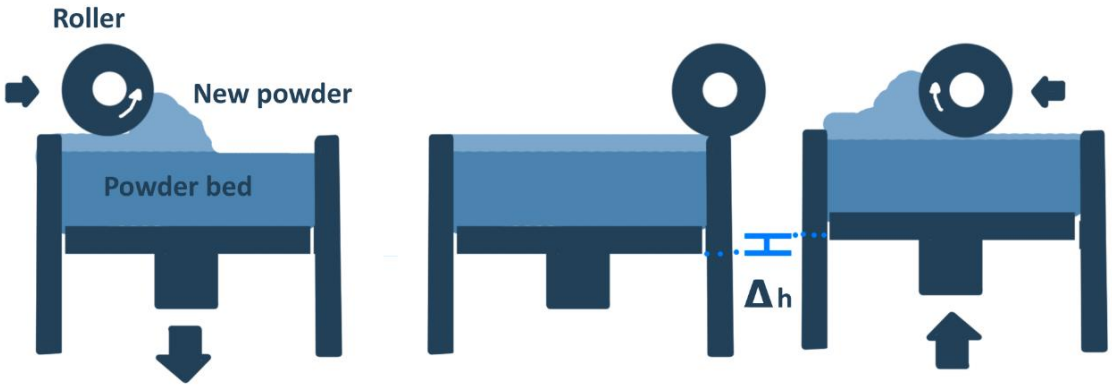

Figure 47. Schematic diagram of a double smoothing (DS) mechanism used to spread the powder.

4.1.4. Flow and Spreadability

Powder flowability is an important factor in AM technologies that use powder; in particular, flowability in BJ dictates the ability of the powder to deposit in the powder bed consistently.

In other words, a high flow capacity will imply a good distribution of the powder, being able to form on the bed a thin, homogeneous layer with a dense packing. Consequently, there will be a significant improvement in print resolution, dimensional accuracy, and density of a printed part (density in green). Conversely, poor powder fluidity will have the opposite effect, causing uneven powder dispersion and uneven powder bed surface, undesirable in BJ [353].

Therefore, in BJ we will look for the powder to have good fluidity. A higher degree of fluidity (FRI) is defined by lower basic flow energy (BFE) and lower specific energy (SE). BFE depends on many physical properties of dust particles such as their size, shape, and surface roughness. In contrast, SE is directly proportional to the cohesiveness of the powder. A low BFE and low SE powder is easy to displace because of the ease with which the particles move over each other, and this powder is more likely to have low bulk density (CBD). The CBD depends on morphology, size, and distribution of particles. A greater degree of fluidity will also be obtained when the stability index (SI) is closest to one [354].

As indicated in the previous paragraph, these terms depend on different physical and chemical parameters, including the morphology of the powder, the average size of the particles, the distribution of the size of the powder, the morphology of the surface of the powder (roughness). , the packing of the powder beds (the density of the bulk material), the composition of the powder, the cohesiveness of the particles, the temperature, and the environmental conditions [294, 355-358].

Prescott et al. defined the term "flow property" as specific characteristics of the powder particle or bulk powder that affect the flow and can be quantified. Next, the “flow properties” that have the most influence on the powder flow will be explained. [243]

The morphology of the powder is described in terms of "regularity". The more regular and/or more spherical the powder, the higher the packing density, as already mentioned in the previous section (page 96). This is due to the fact that said powder has a better flow capacity [218]. In contrast, irregularly shaped particles, such as those obtained by spraying with water, show little fluidity due to a greater adhesion between particles caused by the mechanical interlocking of angular particles [267, 359].

On the other hand, it is well known that the particle size directly influences the fluidity of the powder material. Figure 48 shows the linear dependence of the flow capacity (ffc) with the average particle size.

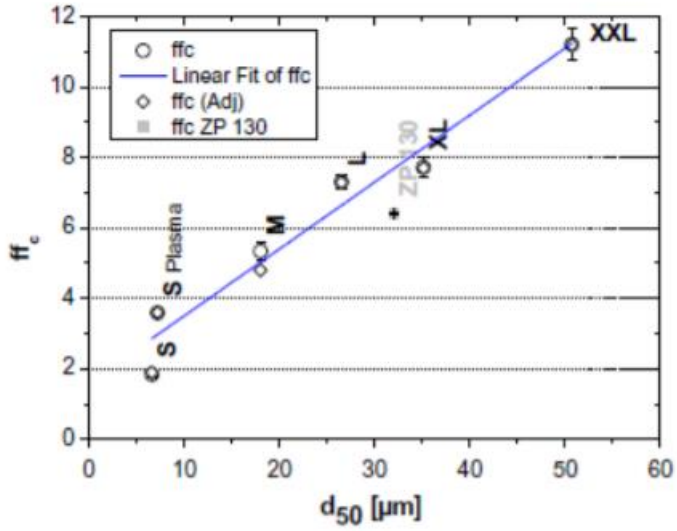

Figure 48. Dependency of flowability (ff_c) on median particle size [353, 360]

As the average powder size decreases, there is a greater tendency for dust to agglomerate, and therefore the particle flow capacity decreases. This is because the surface/volume ratio is greater and therefore the attractive forces between them are greater too. By forming the agglomerates, groups of the dust of irregular morphology, instead of filling the voids present in the bed of dust as do the disaggregated fine

particles, act as coarse irregular particles.[360]. These types of problems were corroborated by Chen et al.[361], who reported that when the particle radius is greater than 21.8 µm, the fluidity of the powder is better and therefore the quality of the powder bed as well. As the radius of the particles decreases, the impact of the Van der Waals force increases and worsens the fluidity of the powder, reducing the quality of the powder bed in the layers.

For this reason, it can be concluded by saying that fluidity generally improves with the use of coarser particles [224, 245, 248, 260, 294, 295] and with the decrease in the width of the PSD [245, 260, 362, 363].

Regarding the impact of the surface chemical properties of the particles on the behaviour of the powder flow, it should be mentioned that the greater the reactivity of the particles, the worse their fluidity. It is worth noting that agglomerates are defined as loosely bonded particles that bind together under van der Waals forces, while aggregates are considered to be made up of particles that are bonded together by solid bridges [268]. The formation of any of these configurations will be desired for the optimization of the fluidity of the powder. A factor that also influences is humidity. Specifically, fluidity decreases with increasing moisture content until saturation with liquid [218, 245, 252, 363, 364].

4.1.5. Powder segregation

In AM technologies, the powder used in each layer that forms the part must have the same properties and be distributed correctly, or what is the same, the layer must be homogeneous and identical to the rest of the layers. This guarantees the reproducibility of the pieces since if each layer were different or in the same layer there were different sections (either powder of different sizes or compositions) the printing parameters should be adjusted differently, making the process more complex since that a series of specific drivers would be needed. One way to alleviate this problem is to ensure good mixing (homogeneous mixing), even though of this, the properties of the powder together with the influences of different forces are likely to result in the segregation of the powder.

Segregation, therefore, is one of the most common problems regarding the quality of the final product when working with dust.

There are different types of segregation [365, 366]:

- Segregation by size occurs when there are significant variations in the size distribution of the particles that compose it.
- Segregation by shape, when the product presents important variations in the distribution of the shape of the particles
- Density segregation occurs in a mixture of different products. The densest component has been separated from the least dense component showing significant variations in the composition distribution.

Segregation occurs in different magnitudes, depending on both the handling technique and the physical characteristics of the powder (size, shape, and density). Material is all the more prone to segregation during handling the greater the difference between its powders.

Segregation can occur during various steps in the printing process, such as during media preparation (pre-mixing), during powder loading into the printer and dust movements within the printer, and during handling and dispensing of these in the impression bed. Among the various mechanisms that produce segregation, the most common in powder bed additive manufacturing are shown below [322, 367-370].

- Path segregation occurs when a mixture of particles is in motion, leading to the difference in body forces or gravity (which is proportional to the mass of the particle) and the drag force of the air (which is correlated with the diameter of the powder). Typically, air entrainment is the dominant force for small, light particles, while body forces are dominated for large, heavy particles. Therefore, as the powders are in motion, the particles follow various paths depending on their size and density, causing segregation.
- Sieving segregation and percolation segregation occur when the smaller particles move down between the spaces of the larger particles, leading to a higher concentration of small particles at the bottom. The difference between the two is that the sieving mechanism occurs mainly during the 3D printing process where the powders are in motion, while the percolation mechanism occurs when the powders are stored, known as sedimentation.
- Expulsion segregation is due to a density gradient, where the denser particle due to the gravity effect tends to go to the bottom during transport, in addition to pushing the less dense particles aside. This type of segregation is challenging when 3D printing mixed powder of two or more compositions to make composite parts.
- The segregation by lamination takes place because of the friction force between the particles and the roller or the instrument used for the dispersion of these. Particles that have a greater area of contact with the roller (smaller, irregular particles ...) will be exposed to greater friction, which will cause a separation between them and those that are subject to less friction.

4.1.6. Others

4.1.6.1. Chemical composition

It is obvious that the actual composition of the dust particles will influence not only the final properties of the final part but also the moisture adsorption profiles and the interaction forces between particles, as described in various previous sections.

The composition is not altered during the printing process, or should not be altered. Although it is true that there is an exception regarding one element, oxygen. The oxygen content increases over time by

58.8% of the expected level in the powder delivery condition. With increasing oxygen concentration, a degradation of the ductility and toughness of the material is observed, in addition to a slight increase in porosity [371, 372]. The correlation between oxygen content and impact resistance is known from studies carried out on different powder materials subjected to hot isostatic pressing, typical in powder metallurgy [373-376].

The formation of these oxides may possibly be related to various problems, such as the high oxygen content of the starting powder, the high oxygen content in the deposition chamber, and the non-regulated flow of shielding gas or the non-use of this, in the case of BJ technologies.

Therefore, it can be concluded that the appearance of rust during the process will complicate it. On the other hand, the formation of oxides is not only important but also the type of oxides formed and their size is very important.

4.1.6.2. Recyclability

Most of the dust is reused in subsequent construction work. This fact makes the process resource-efficient. Summarizing, the literature findings, an effect on the properties of the powder is observed but the effect on the quality of the final part is, in most cases, negligible. Research on the recyclability of dust and its effect on the BJ process has been little studied compared to other AM techniques (PBF) [377-382]. This is because, as an advantage, the BJ process works at room and atmosphere temperatures, reducing the problems related to oxidation, residual stress, elemental segregation and phase changes, which causes dust around the parts in the construction box is highly recyclable [383]. That is why most research has focused on the recyclability of dust for PBF processes, which is highly influenced by the amount of thermal exposure dust has to the construction environment[384].

Dust recycling can be done following several strategies[222] :

- Defined proportion of recycled and new powder: used and sieved powder is mixed with virgin powder after each construction in constant proportion
- Defined proportion of dust recycled from different batches: the used powder is mixed with the dust of the same age after each cycle (the cycle is defined here as the sum of the construction work after which the mass of dust is reduced from so it is not possible to build more).
- Recycled powder from the previous cycle: reintroduce the screened powder after each construction job without mixing it with other powders.
- No knowledge of powder: the used and sieved powder is added to the top of the unused virgin powder, no mixing is done.

Of the four previous strategies, the most used is the first, since it achieves lower costs in the manufacturing process but does not affect the quality of the final part. On the contrary, the last strategy is not at all desired, since the properties of the powder are completely unknown, and two powders with different properties can even be used in the printing of a piece. This would achieve a piece with different properties depending on the printing height.

4.1.6.3. Safety and reactivity

As already mentioned in different previous sections, the powder has a high surface / volume ratio. This is an advantage in different aspects of the BJ process, such as reducing sintering times. But this high reactivity requires additional attention when handling powders due to its high flammability and explosiveness. Because of this, whenever powders are used all the safety regulations and instructions must be complied. Existing documentation on dust storage safety regulations and personnel safety used for powder metallurgy processes can be reused [385]. Still, AM processes face different and novel challenges such as emptying and loading the powders into the machines, reusing the powders, and storing them.

Until now, only metal powders with very low or no reactivity index have been used. However, if you use powders with very small sizes, it would be necessary to take the appropriate measures since the area/volume ratio would increase so much that your reactivity would be dangerous. Metal powder has a high potential for danger due to high combustion temperatures and the production of energy during combustion. The reactivity, therefore, depends as much on the chemical composition as on the size of the particles and on the way they are grouped. Taking into account the following factors, the USA Office of Mines classifies powders according to their reactivity [278].

4.2. Binder

The essence of BJ manufacturing is to use a liquid binder to bond the dust particles together in the designated areas on the powder bed. Binder droplets are deposited on the bed surface through a print head. After impact, each drop travels through the powder bed due to capillary pressures and, to a lesser degree, gravitational forces. Migration of the binder in the powder bed will take place in all directions, albeit with different lateral and vertical speeds. As a consequence of this difference in propagation capacity, the binder will describe a specific profile. [386-388]

As can be seen from the description above, the binder is a critical factor in the BJ printing process. For this reason, the design or selection of the binder for BJ must be appropriate in order to satisfy the demanding demands.

Its rheological behaviour (determined by viscosity and surface tension) and its stability are adequate so that it, the binder, can perform the following functions[383]:

1. It must be able to be deposited by means of an inkjet print head, adjusting to the specific printing ranges.
2. It should not solidify (start curing) before being deposited on the bed surface, as it could clog the print head or distribution channels/lines. This is achieved by ensuring that the solvents that compose it have boiling temperatures much higher than the working temperature (ambient temperature). Otherwise, if the polymer chains or the monomers of the binder would start to crosslink, that it is known as curing.
3. The powder bed must be moistened enough for adequate diffusion to occur in the powder bed. Although it does not matter that, it flows so much that it ends up migrating or leaking much beyond the impact zone.
4. It must have sufficient bonding strength after curing to provide the green part with strong enough structural integrity. Smaller parts and larger features have lower stresses than larger parts and finer or more detailed features.
5. It must be chemically stable at a specific temperature. That is, it must hold the powder together until the temperature at which the particles begin to sinter is reached.
6. It must be able to be pyrolyzed leaving the least trace possible before the densification process of the piece in green. [53]. In metals, this is of vital importance since a significant amount of residue leads to a change in the composition of the printed material. The polymeric binders when disintegrating leave a certain amount of carbon, which, during the sintering process, can diffuse the metallic particles. If the carbon content exceeds the specifications of the alloy, the microstructure structure will undergo a significant change.

There are different types of binder depending on their composition. The most requested at BJ are water-based binders (solvent or water-based). The bond between the dust particles is formed after evaporation of the solvent [90]. Another way to classify the binders is based on the bonding mechanism used [389-392].

The profile or impression pattern that the binder will assume in the powder bed will be conditioned by different variables. These variables can be variables that affect the droplet ejection operation, variables that affect drop migration from the head to the powder bed or, once the drop has already impacted on the surface of the bed, variables that affect the migration of the binder through the bed. In this section, these variables will be studied and exposed, among which we will find the properties of the binder (morphology or rheological properties of the binder), the formation of drops, the separation between drops and the interaction between the binder and the dust.

4.2.1. Polymeric morphology and formulation

It is known that the print resolution depends mainly on the size of the binder drop, which is dictated by the binder formulation [393].

As already mentioned before, there are many types of binders [85]. However, most of them, in terms of composition, are composed of a polymer dispersed in a solvent or a low-viscosity monomer.

If a dissolved polymer is used, when applying heat, the solvent evaporates, causing the polymer chains to join together and/or join with the particles by intermolecular forces.

On the other hand, if a monomer is used, its molecules cross-link during the curing process, forming a solid framework. The metal particles are trapped or covered by said frame. The curing step prior to sintering is necessary in some binders, but in others, the simple heat applied during printing is sufficient to cure the binder.

So far, different binders have been used such as latex (colloidal dispersion of polymeric molecules) [102], polyethyleneimine [394], aqueous emulsions of aryl copolymers [395, 396] and polyvinyl alcohol (PVA) [397]. Efforts have also been made to improve the configuration of binders through different mechanisms to achieve various purposes. For example, the addition of metallic salts [398] or the suspension of metallic nanoparticles [399-401] were studied. The incorporation of nanoparticles in the binder is limited [402] due to the problems that arise such as: possible segregation of the polymer/nanoparticle mixture since the metallic nanoparticles have a significantly different density than the polymer; the clogging the nozzle hole; and finally, the production of undesirable elements resulting from the possible reaction between the nanoparticle material and the binder. Therefore, after a series of demonstrations, it can be said that metallic salts are more compatible with inkjet than nanoparticle suspensions [403, 404], and therefore more widely used.

It has also been considered to use photopolymers as binders, but they were discarded due to their high molecular weight, which prevents their total disintegration, making the sintering process difficult [405].

4.2.2. Rheology for Ink jetting

As mentioned above, the rheological properties of the binder are very important in the BJ process. Specifically, the two main characteristics are surface tension (defined by the Weber number, We) and viscosity (by the Reynolds number, Re). These two parameters can define all the behaviour of the binder during printing [406]. For example, the ability to inject a fluid through an injection nozzle is given as a function of these parameters. Specifically, it is expressed by the Ohnesorge number, which is independent of the droplet expulsion speed [402].(Eq. 19, Eq. 20 and Eq. 21)

$$Re = \frac{\rho \cdot d \cdot V}{\eta} \quad \textbf{Eq. 19}$$

$$We = \frac{\rho \cdot d \cdot V^2}{\gamma} \quad \textbf{Eq. 20}$$

$$Oh = \frac{\sqrt{We}}{Re} = \frac{\eta}{\sqrt{\gamma \cdot d \cdot \rho}} \quad \textbf{Eq. 21}$$

Where ρ is the density of the liquid (kg/m^3), V is the velocity or flow speed (m/s), d is the diameter of the drop or of the nozzle head (m), η is the dynamic viscosity of the liquid (Ns/m^2), ϒ is the surface tension (N/m).

On the other hand, we must not forget the deposition process of the binder on the powder bed. Good control of this operation will be essential to obtain a good quality piece since if the deposition of the drop is so abrupt that it splashes or deforms the bed surface, it will cause future defects in the piece as less dense parts or rough surfaces. Stow and Hadfield [407] have dedicated part of their studies to elaborate an equation that serves to determine the appropriate spatter threshold to work with a flat, homogeneous, and smooth surface. This shows the relationship of this parameter with the density of the drop, the speed of the drop and its volume, since it is a function of Re and We, as shown by the Eq. 22.

$$f(R) = \sqrt{We} \cdot \sqrt[4]{Re} \quad \textbf{Eq. 22}$$

Before going on to detail the conditions to be met in order for the binder to be appropriate for its use, we will briefly explain the droplet expulsion process and distributing them over the powder bed. BJ uses a printing system similar to printing on paper, known as "drop on demand". The nozzle expels a small drop of ink (binder) by means of a pressure explosion. There are different mechanisms of ink ejection, the most common is the use of a piezoelectric crystal that expands with electric current induction and pushes the drop through the nozzle hole. Another mechanism is through a resistor that heats the ink creating an air bubble, which pushes the fluid through the nozzle, thus creating a drop. Once the drop is created, it is expelled from the nozzle until it hits the powder bed.

Once the operation of expulsion and dispersion of the drop has been understood and taking into account the parameters described above, we proceed to detail the requirements that the binder must-have. For example, the surface tension limits the formation of the drop, which must have enough energy to be ejected, overcoming the barrier of the surface tension of the fluid. Duineveld found that Weber's minimum number must be greater than 4 to overcome this barrier [408]. On the other hand, Miyanaji et

al. [310] showed that the Weber number also has an upper limit, its maximum value being close to 50. Since if this value is exceeded, a splash will be caused when the drop is deposited on the bed.

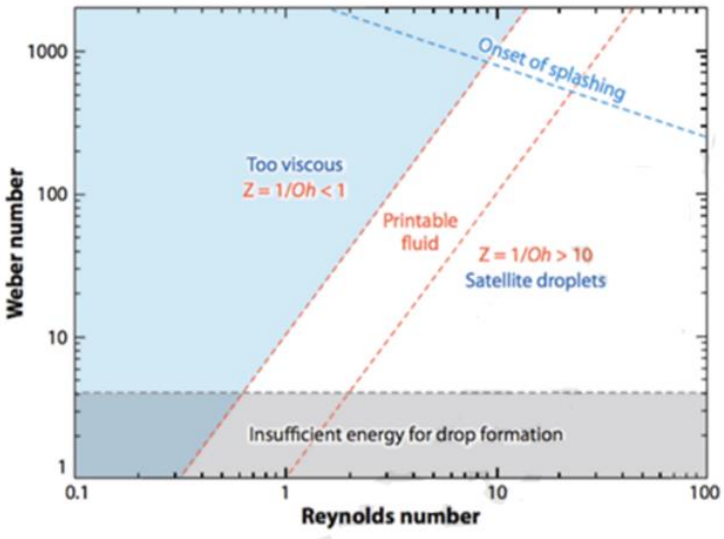

Figure 49. Jettable region for fluids based on the Weber and Reynolds numbers [402].

As the Figure 49 shows, there is also an appropriate We-Re relationship to obtain an adequate ejection or ejection of the drop. This relationship indicates that the value of the Ohnesorge (Oh) number must be between 0.1 and 1. If this number is less than 0.1, at the moment of expulsion of the drop, the effect, knows as "satellite droplets" will occur (it will not be a single drop perfectly spherical). On the other hand, if it is greater than 1, it means that the fluid is very viscous and therefore it will not be injectable. These events are shown in Figure 50 [409].

Figure 50. Images taken at the time of drop ejection showing the effect of the Ohnesorge number (Oh) [409]

4.2.3. Print head type and drop generation

This section will explain the types of print heads, which differ in the way they have to generate the drop. There are generally two large groups of print heads: drop-on-demand (DoD) print heads and continuous-

jet (CJ) print heads. Figure 51 shows a diagram of the general operation of both types. The use of one type or another will depend on the binder used.

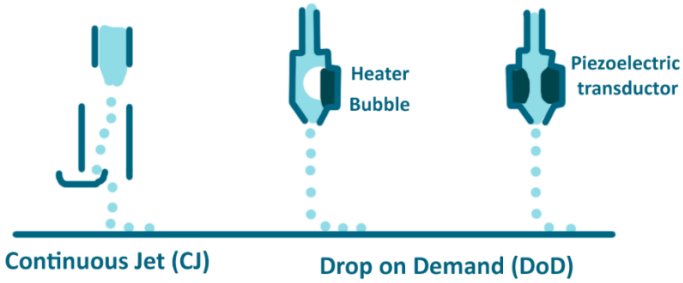

Figure 51. Schematic illustration showing the operation principles of Continuous Jet and Drop on Demand print heads [257]

The first type of head (DoD) has already been named above. This type of head produces individual drops and on-demand. Gout can be produced in different ways. For example, the piezoelectric heads produce the drop using a piezoelectric crystal that, upon an electrical impulse, expands occupying a specific volume. The advantage of these heads is that the only parameters of the binder that influence are its rheological properties. Recently, Shen et al. [410] designed a new ink deposition system that works based on the CJ print head.

Another known type of heads are thermal inkjet heads. The operation of these is based on applying heat so that rapid gasification of a certain amount of the liquid binder occurs, producing a bubble of a specific volume. This expansion inside the print head pushes the binder through the nozzle, thus expelling the drop [411, 412]. If you want to expand the information for a better understanding of this operation, you can view the explanatory video "*How HP Thermal Inkjet Printheads Work*" [W37].

On the other hand, the continuous jet (CJ) print heads produce the drops continuously and constantly. Due to this, the printing speed is higher [412]. Compared to DoD printheads, CJ printheads have higher performance due to the slower traverse speed, option of proportional deflection (no binder leakage from the print head), and more size control of overlapping primitives for a smoother part surface finish [97].

Once the existing drop expulsion systems have been explained, the effects of the jet or the drop formed in the printing process will be explained. Different physical parameters of the droplet or the jets have been studied such as fluctuations in the width of the tail, lateral deviations, expulsion speed, the formation of small nano-droplet (ink satellites) and droplet volumes [413, 414].

Parab et al. [415] observed that at the beginning of the drop ejection, it had the shape of a spherical head. As it descended, the shape it took was cylindrical but as it moved away from the head, it changed to a spherical shape with a long narrow tail. This evolution is shown in the following image.

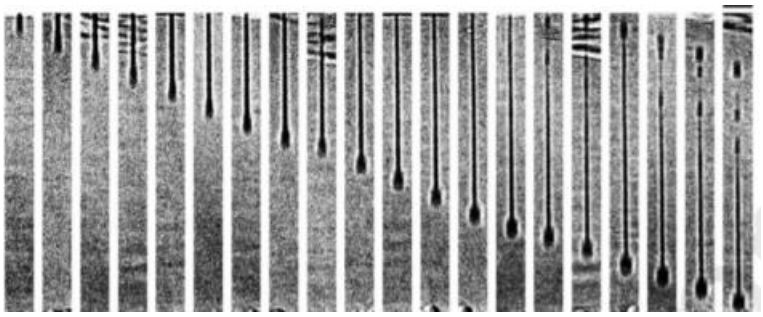

Figure 52. High-speed synchrotron x-ray imaging technique showing jetted droplet shape[415].

The study of the final tail, which later hits the bed, showed that it was unstable and moved away from the center of the nozzle [413]. These fluctuations sometimes cause the breakdown and formation of, what has been described so far, ink satellites. These satellite drops drift from the expected path, causing dimensional errors in the printed parts [416].

Another consideration should be the interaction of any element of the machine with the binder. For example, materials in contact with the binder such as the printhead chamber or all elements of the fluid lines can react (corrode, wear away) with the binder and this would not be desirable. A critical element of the printer is the nozzle since it is more prone to erode due to the passage of the binder. It can also become blocked because the solvent of the binder evaporates and the binder solidifies in the nozzle. This event occurs very commonly, due to the small size of the nozzles (below 100 µm) [85]. In addition, there is an additional obstruction due to this small size, this obstruction is caused by a shear effect when trying to pass the fluid through the nozzle. Clogging the nozzle causes one of the print lines to be missing. If it is only one of the nozzles, it will not have any effect on the final piece, but the failure of several will cause the piece to fail [417].

4.2.4. Droplet spacing and line spacing

The established profile characteristics have multiple implications for the BJ process. For example, the profile largely determines the minimum resolution of the manufacturing process and consequently influences geometric precision. The characteristic dimensions of the profile, that is, the limitations that the binder has in migrating vertically (penetration) and horizontally, influence the selection of some process parameters such as layer thickness, working temperature, or printing speed.

Among some parameters that influence the print profile or pattern is the distance between the drops. The droplets are spaced from each other; the distance in the transverse printing direction depends on the spacing of the nozzles or holes where the ink comes out (d1). On the other hand, the distance along the printhead raster direction depends on the speed at which the drops are deposited and on the spacing between the printlines (d2). (Figure 53)

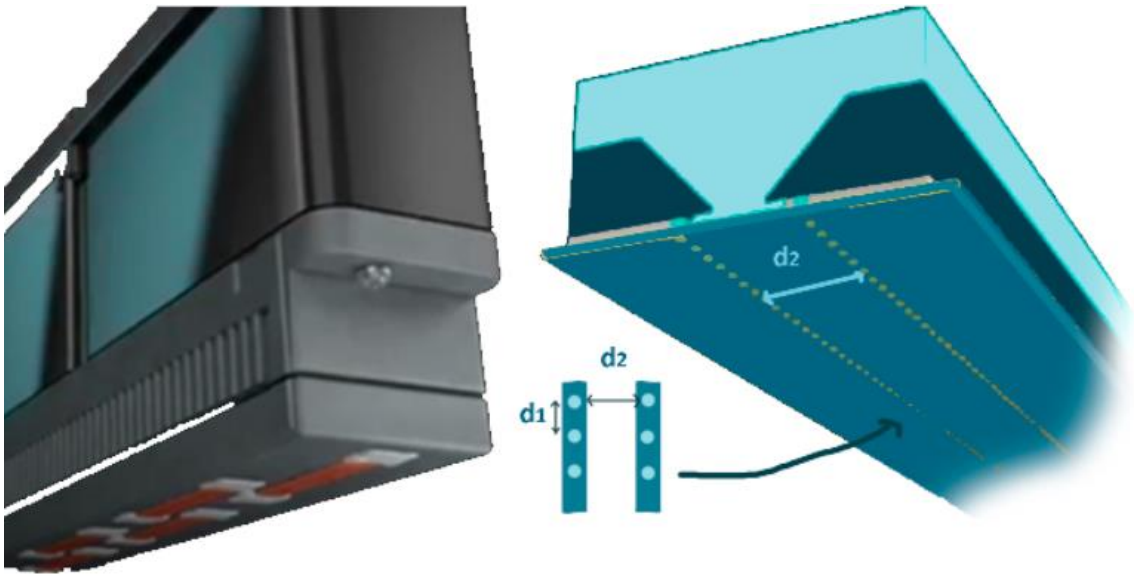

Figure 53. Diagram of a printhead, defining the distances between the heads (d1 and d2).

Next, we will detail how these two distances (d1 and d2) affect the results of BJ printing of 3D parts. Specifically, we will talk about d2 since it is the most critical distance and difficult to control [306].

On the one hand, the distance between the printing lines (d2) must be low enough so that the layers formed by the binder are cohesive, thus ensuring that the drops deposited on the bed will join without forming marginal seams between the lines [418]. However, a very small spacing has a negative effect because it increases the printing time and also increases the risk of oversaturation and/or bleeding. A study of the optimization of this parameter was carried out by Lanzetta and Sach [306], who showed that too small a spacing excessively decreases the resolution of the impression when forming large diameter lines. This oversaturation phenomenon can be alleviated by controlling the temperature after printing, since, if the viscosity of the binder can be decreased, a smooth surface with a high precision geometry will be achieved [419].

4.2.5. Interaction between binder and powder

In this section, we will study the effect that the interaction between the binder and the powder has on the printing pattern and, consequently, on the BJ process. The migration and distribution of the binder through the powder bed is very important since it will affect the microstructure and the mechanical properties of the final parts, as will be seen below.

Due to the differences in migration rates, the liquid phase under equilibrium conditions would assume a specific profile (Figure 54). Typically, the penetration depth (D) and the extension of the binder (W) can vary according to the properties of the powder (the particle size distribution, the morphology of the powder, the chemistry of the surface of the particles, the compacts of the powder bed and the wettability of the powder)[286, 420, 421], the properties of the binder (its chemistry, the physical properties of the liquid binder, including viscosity and surface tension), the interaction between the binder/powder bed and the printing parameters and conditions (working temperature or binder injection rate) [85, 383, 422-424].

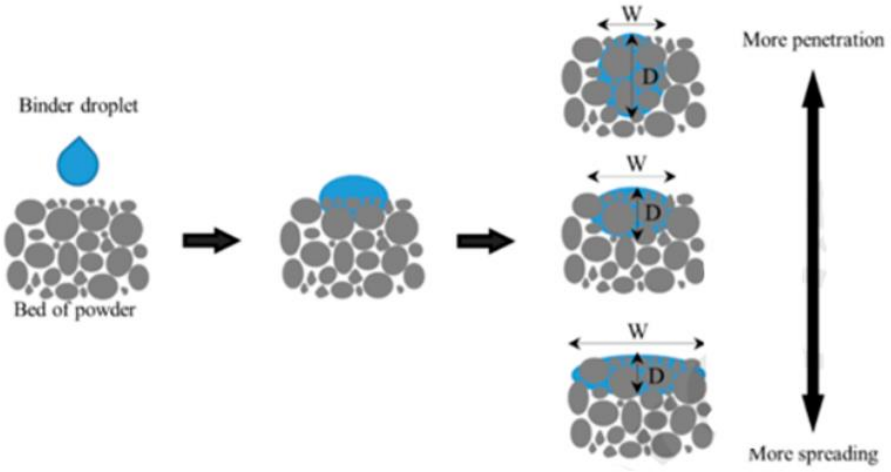

Figure 54. Diagram showing the penetration of droplets of binder into the saturated area of the powder bed.

From a physicochemical perspective, the interaction between a drop of binder and a powder material is a very complex process [425]. In addition, it is difficult to measure due to the existence of a microscopic surface area of the powder particle, which does not get wet with the binder, therefore, you may be overestimating the optimal level of binder saturation of the theoretical model. Furthermore, the depth of penetration of the actual binder may not match the drawing area of the drop of binder injected into the powder bed, leading to another possible disparity in the desired binder saturation level and print resolution [426].

The porous material interaction with the binder drops can be divided into two phases: the static and dynamic phase. While the static phase refers to the state where the penetration of the liquid droplet into the porous medium is completed, during the dynamic phase the droplet migrates to the porous material under the different conduction phases. In the BJ process, both phases are of crucial importance to control the quality of the part. The interaction of the porous droplet medium in the static phase determines the optimal saturation level required for successful printing, while the dynamic phase of interaction controls the profile of the area that is saturated by the droplet.

A model that studies the balance between the fluid and a highly porous part was developed by J. F. Bredt. In this model, the equilibrium fluid content is predicted from measurements of the capillary characteristics of the powder and the physical properties of the fluid binder. It is proposed in this model that there is a capillary pressure balance between a partially saturated region and the dry powder surrounding the feature. In this model, it is assumed that the interaction between the binder and the powder in the BJ-AM process is dominated by capillary and, to a lesser degree, gravitational forces. If you want to go deeper into this approach, you can turn to his doctoral thesis or to future bibliographic works that compile his study.[311]

The migration or infiltration dynamics of the binder, in the static phase, can be divided into four phases, as shown in Figure 55. The first two generally comply with an impact-driven propagation dynamic and the last two with capillary propagation.

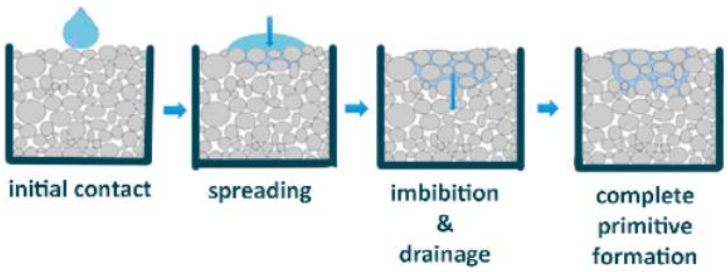

Figure 55. A scheme illustrating the interaction between the binder and the powder bed and the migration process of the binder [427].

PHASE 1 &2: initial contact & spreading

In this initial phase, a drop of binder (of few micrometres cubic of the volume) is injected through a print head onto a bed of powder. When the droplet reaches the surface of the powder bed, it has an initial impact velocity that dissipates rapidly. When the binder comes in contact with the dust particles, the kinetic energy of the droplet leads to a rapid formation of bridges and networks connecting the adjacent particles. This process can occur in the order of microseconds.

When the drop hits the bed, different granule formation mechanisms can occur (Figure 56). For example, in fine and cohesive powders, when the drop impacts, it drags loose aggregates as it penetrates the powder bed, forming spherical granules with some protuberances due to incomplete penetration of some of the aggregates. This mechanism is called "tunnel effect mechanisms". On the other hand, "crater or extension mechanisms" take place for free-flowing coarse powders, which promote high packing density. When the binder hits, at an appropriate speed, dispersion occurs as the droplet spreads across the surface of the powder to form granules that are flat disks. If, on the contrary, the speed at which the drop impacts is excessive, craters will form in the dust bed. The drop will spread through the walls of the crater, collecting in its path the particles with which it interacts. This will lead to the formation of highly spherical granules [428, 429].

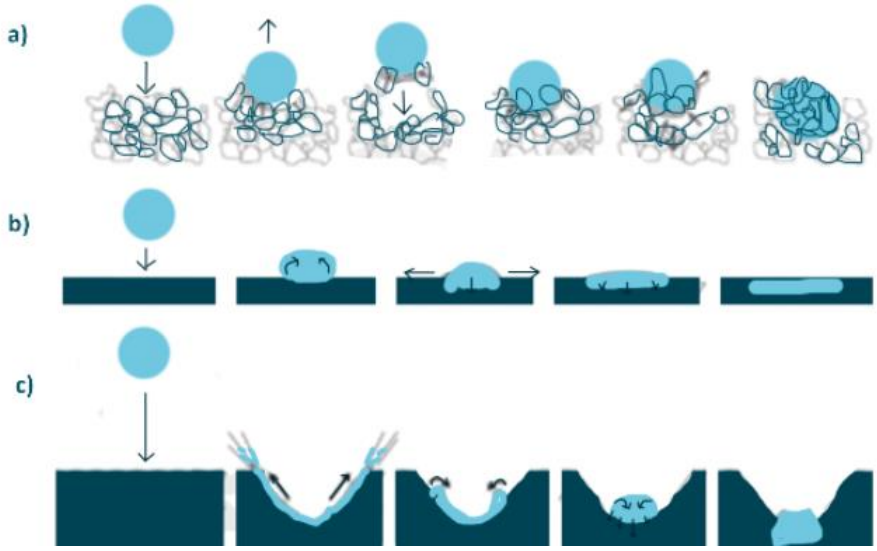

Figure 56. Schematics of the three granule formation mechanisms: (a) tunnelling, (b) spreading, and (c) crater formation [428, 429]

This phase, governed by the impact of the droplet, is affected by the volume of the droplet, the initial velocity, the inertial forces, the viscosity and the roughness of the powder bed [286, 430-432]. Next, the effect of these factors on the migration of the binder will be detailed.

In the case of the extension of the binder (W), which is mainly driven by the kinetic energy of the impact drop in this phase, the following conclusions can be reached. The greater this kinetic energy, which implies a higher speed of the drop, the greater the extension of the drop (W). On the contrary, surface roughness will influence the binder dynamics [287, 433]. The greater this roughness, the more prevented the drop will be from expanding on the surface [305, 433, 434]. The same will happen if powder with a larger average particle size is used.

On the other hand, the final depth of droplet penetration (D) exhibits the opposite trend in relation to roughness and particle size. As the lateral dispersion speed (W) decreases, vertical penetration (D) will be favoured.

PHASE 3: Imbibition & drainage

This phase consists of the advance of the binder through the powder bed. As the binder comes into contact with the powder bed, it is moistened as the binder penetrates through it. This interaction behaviour between the binder and the powder is mainly controlled by the intrinsic characteristics of both the powder bed and the liquid binder, such as the liquid viscosity, the contact angle between the material and the liquid, and the surface tension.

The dominant mechanism is the capillary force effect [286, 430, 435-437]. By contrast, gravity has a negligible effect on the binder. This is because the drop has a low volume and mass. [417]

At this stage, dust beds with larger pore sizes facilitate the penetration of the binder into the porous structure due to the improved permeability(k) [438], which can be quantified by the Kozeny equation (Eq. 23) that correlates permeability with the average diameter of the particles. [439].

$$\boldsymbol{k = \frac{\epsilon^3 \cdot D^2}{(1-\epsilon)^2}} \qquad \textbf{Eq. 23}$$

Where ϵ is the porosity of the powder bed, D is the mean diameter of the powder particles, k is the permeability of the powder bed and it is a constant.

From the following equation (Eq. 24) an estimate of the volume of the binder that has penetrated a dust bed at any given time, Vp (t) can also be known [440]:

$$\boldsymbol{V_p(t) = \frac{K}{2} \cdot \int_0^t \frac{r^2(t)}{\sqrt{t}}\, dt} \qquad \textbf{Eq. 24}$$

$$\boldsymbol{K = 8\pi \cdot k \cdot \sqrt{\frac{\gamma \cdot cos\theta}{2 \cdot \eta \cdot R_{pore}^3}}} \qquad \textbf{Eq. 25}$$

Where: r (t) is the instantaneous radius of the droplet that extends over the surface and it's a function of time; R_{pore} is the pore radius (mean pore radius obtained in BET tests); ϒ is the surface tension of the liquid; ϴ is the angle of contact of the binder in the form of a drop on the material (as shown in Figure 57) and η is the viscosity of the binder.

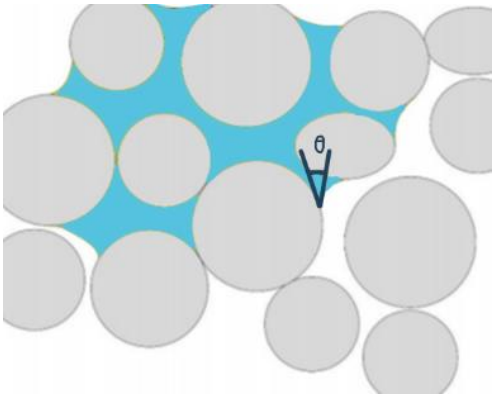

Figure 57. Local contact angle between binder and a particle in the powder bed.

The above equations corroborate the conclusions set out above, a bed formed by large particles will have a higher permeability, which leads to a fast penetration (D) and, therefore, to a smaller lateral dispersion (W). Furthermore, it was shown that the depth of interaction (D) was greater in irregularly shaped powders compared to spherical powders, which could be related to a greater mechanical locking effect between angular particles [417, 428, 429, 432, 440-443].

Therefore, as binder migration progresses, the saturated regions drain and the dry regions absorb until the driving forces of both regions become equal. This is the state where the equilibrium condition is reached in which the driving forces are equal for both imbibition and drainage.

PHASE 4: Complete primitive formation

As the equilibrium condition is reached, the printed area is saturated homogeneously. It is crucial that a sufficient amount of binder is used during printing, as the continuity of the liquid binder droplets during printing will cause the good integrity and strength of the green part.

Next, the operation of the homogeneous saturation of the binder in the corresponding area will be explained (Figure 58). Once the binder has been selectively sprayed onto the surface of the powder bed, capillary bridges are formed that join the adjacent particles. As explained above, this formation of networks is due to the binder-powder material interaction that is accelerated by the kinetic energy of the drops. The next step is the distribution of a new powder layer and injection, again, of binder on this new layer. The formation of the new capillary bridges is carried out between the adjacent particles of that same layer and with the particles of the lower layer. This is done layer by layer until obtaining a three-dimensional network that defines the geometry of the piece [444].

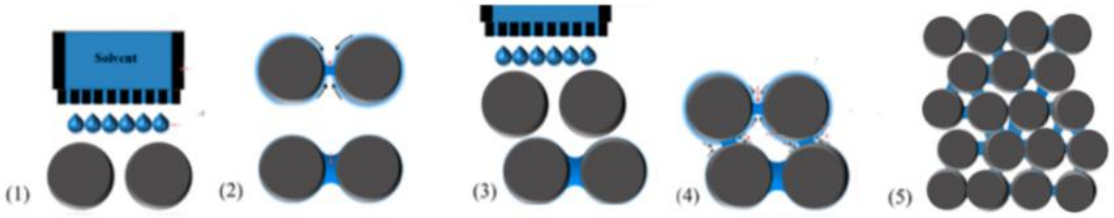

Figure 58. Small-scale explanation of the binder-powder interaction during the binder injection process.[444]

As already mentioned at the beginning of this section, the distribution/migration of the binder and its interaction with the powder bed, control the precision of the geometry, the resistance of the green part and the roughness of the final surface of the part [427], in combination with the other process control parameters. That is why the interaction between the binder and the powder is of great importance to determine the quality of the parts manufactured by the BJ process.

One of the effects of migration is on the dimensions and specifications of the part. If working with a lateral dispersion W greater than optimal, the pieces will exhibit greater inaccuracies in the lateral directions (X and Y directions). On the other hand, the precision of the samples in the z-direction decreases with increasing average particle size, or what is the same with higher penetration (D).

A troublesome effect to consider is the expulsion of dust from the surface of the powder bed due to the high speed at which the binder has impacted. This causes changes in the powder bed and can create pores in the printed parts. In addition, greater contraction occurs in the z-direction during sintering. This is not the only negative effect caused by the ejected dust, as it can cause multiple more defects. For example, if a large number of particles were ejected, there would be an empty hole that could hardly be covered or filled by the back layer. This would cause a large hole to form. This situation generally occurs with powders that are highly fluid. Another problem they could cause is if these ejected particles were randomly deposited in different positions on the bed, which would have a negative impact on the bed surface. Since this would cause a dimensional mismatch and an undesirable roughness in the final piece.

4.3. Printing parameters

The BJ process is defined by a series of parameters such as the layer thickness, the mechanism and the speed of powder distribution, the saturation level of the binder, the temperatures of each operation, the exposure times to said temperatures, the way of injecting and depositing the binder, among others. Different authors have studied the influence of these parameters on the quality and some properties of both green parts and sintered parts. [417]

A possible example of a possible configuration of the BJ parameters is presented in Table 14. These are the values used in the *M-Lab printer*, if you want more detailed information you can use the indicated bibliography [14, 55, 166]. It should be noted that this information is only indicative since the configuration of said parameters will depend on the powder used and the machine hardware.

Table 14 Printing parameters used for the M-Lab BJ-AM system [445]

	Value
Powder spreading speed (mm/s)	2
Saturation level (%)	100
Drying time (s)	80
Printing speed (mm/s)	150
Layer thickness (mm)	0.15

Shrestha and Manogharan investigated the optimization of different process parameters to obtain the best mechanical properties, finding that the most influential parameters are binder saturation (interaction of the binder with dust) and the density of the powder bed [446]. In this section, the different parameters and their effect on the final piece will be discussed.

4.3.1. Layer thickness

The layer thickness parameter is defined as the height of the powder bed along the Z-axis during printing. The values for BJ techniques usually range between 15 and 300 µm.

Normally, said value is defined by the operator/designer of the machine, and from this value, the amount of binder saturation is calculated according to equation Eq. 26. [445]

$$\boldsymbol{Saturation\ level} = \frac{\boldsymbol{V_{binder}}}{\boldsymbol{V_{air}}} \quad \textbf{Eq. 26}$$

$$\boldsymbol{V_{air}} = (\mathbf{1} - \mathbf{100} \cdot \boldsymbol{PR}) \cdot \boldsymbol{V_{envelope}} \quad \textbf{Eq. 27}$$

$$\boldsymbol{V_{envelope}} = \boldsymbol{x_{spacing}} \cdot \boldsymbol{y_{spacing}} \cdot \boldsymbol{z_{spacing}} \quad \textbf{Eq. 28}$$

Where: V_{pore} is the theoretical percentage of void space; V_{binder} is the percentage of binder used to fill the void; PR represents the packing density of the bed; $V_{envelope}$, the volume of a defined envelope; $x_{spacing}$ and $y_{spacing}$ re the distances between successive droplets in the X and Y directions respectively; and $z_{spacing}$ is the layer thickness. It should be remembered that the packing density specifies how much empty space exists in the impression material after distribution.

In addition, the layer thickness is used to process and segment the CAD model used for feature creation and therefore will influence the resolution of the green part.

The layer thickness value is defined based on the desired resolution and by the powder size, in this order of preference.

Specifically, the simple requirement that must be taken into account in relation to the size of the dust particle is that the selected layer thickness must be greater than this [225, 447]. It is true that, as already mentioned in this work, the size of the powder and the PSD are two variables that affect the ability to flow and spread of the powder and therefore will also affect the possibility of creating a specific layer thickness [295, 448, 449].

The desirable thing would be to achieve a powder layer with a uniform thickness since this will favour the printing process (diffusion of the binder) and the precision of the dimension in said processes.

As can be seen in the previous equations (Eq. 26, Eq. 27 and Eq. 28), if the thickness of the layer is modified, so will the amount of saturation of the binder and, consequently, the mechanical and dimensional characteristics of the green part.

There are multiple studies based on experiments in the literature investigating the thickness of the layer, along with other parameters related to the process, such as the saturation of the binder and the orientation of the part, the effect on the mechanical and dimension properties of the green part. [450-452] In this work, they showed how the dimensional precision varies depending on the thickness of the layer and the saturation of the binder. If you work with a thin layer of powder material, the lateral expansion (W) of the binder will be favoured since the vertical penetration (D) will be limited by the saturation of the previous layer (the one below). This excessive lateral flow of the binder leads to a dimensional mismatch and a surface roughness of the faces whose normal are in the x and y directions.

This dimensional mismatch occurs the same when too large layer is used. This is because, although the lateral expansion (W) is reduced, the fact that more binder must be injected due to the greater volume of powder per layer produces a similar effect, although it is true that the variation of the dimensions in x and y They will be less than in the previous case [451]. Furthermore, increasing the thickness of the layer can lead to a reduction in the density of the powder bed. Figure 59 illustrates the effect of layer thickness on the density of the powder bed prior to the application of the binder [446, 453, 454]. As stated, generally, a higher density of the powder bed produces a higher density of the green part where a lower shrinkage during sintering is expected for a high density of the green part [455].

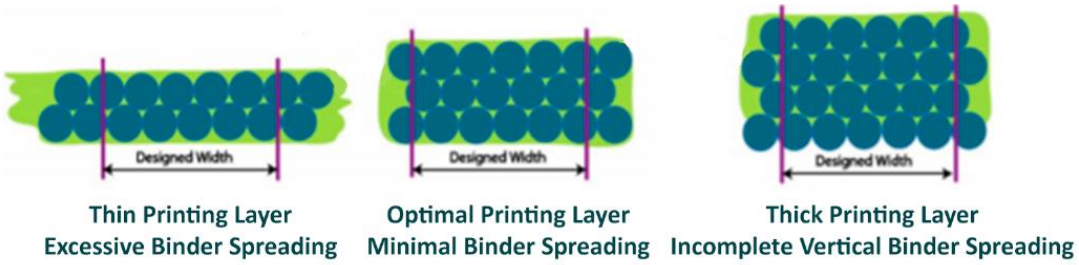

Figure 59.Effect of the layer thickness in the binder spreading process. [25]

As the Figure 59 shows, with optimum print layer thickness, vertical (D) and lateral (W) dispersion advance at the same time, producing the least possible dimensional variation and adequate resolution. [451]

The effects of print orientation and layer thickness on the physical and mechanical properties have also been studied [345]. In this investigation, it was concluded that layer thickness and print direction have a significant effect on compressive strength, as shown in the graph in Figure 60. These studies also concluded that these two parameters do not have such a significant effect on other structural properties.

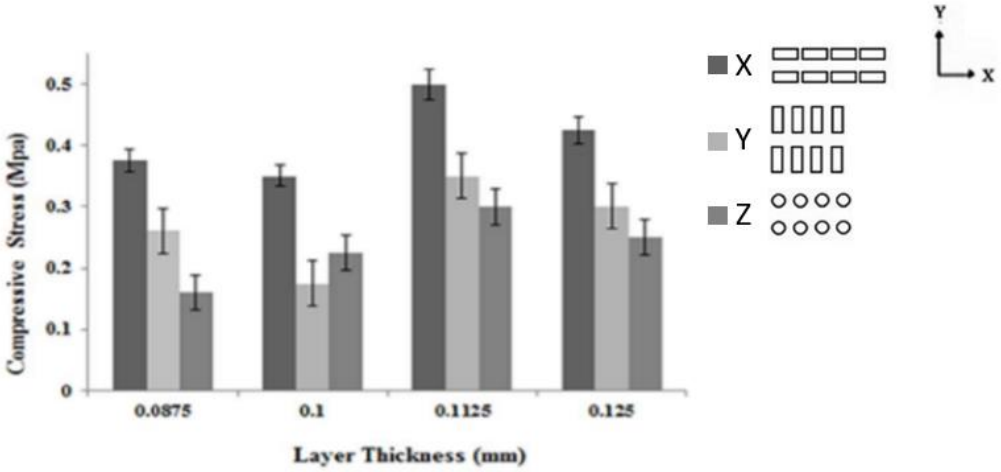

Figure 60. Comparison of compressive strength in samples with different layer thickness in various orientations (X,Y,Z) [345]

4.3.2. Powder spread and powder-spreading speed

Both rakeability and dust propagation speed must be considered to meet part requirements and cost targets. The different dust distribution mechanisms were explained in the section related to packing density and therefore it would be advisable to review it (page 96). This section will focus on speed factors.

When the term powder-spreading speed is mentioned, one is talking about a set of speeds that influence the powder distribution process. It is worth mentioning that not all machines will have to control or to define these speeds since it will depend on the mechanism used for dust distribution. For example, some machines use the roller as a dust dispensing mechanism, instead of a hopper. Generally, the most common speeds are [17, 456]:

- Coating speed (mm/s). The first powder deposition methods used a feed shaft that rose with each layer to dose the powder [457], however, the use of a hopper to feed the powder has become more common due to its advantages as regards the handling of dust. [458]. Therefore, this speed is the linear speed at which the hopper travels while the dust travels over the bed.
- Oscillator speed (rpm). It is the frequency at which the dispensing mechanism oscillates
- Roll speed (rpm). As its name indicates, it is the rotation speed of the roller.
- The propagation speed (mm/s). In many machines, the layer is spread by a rotating roller. Therefore, the propagation speed is the linear speed at which the roller moves through the bed at the same time it rotates. It is the main factor in determining the overall print speed. A value for said usual speed is between 0.1 and 16 mm/s. Although it has been shown that roll travel speeds greater than 4 mm/s can lead to a heterogeneous powder bed, which is undesirable. Another study confirmed that using speeds in that range results in higher precision [446]. However, the disadvantage of using small speeds is the increased time of the printing process.

Coordination of all speed factors is necessary to produce consistent parts while maintaining adequate productivity.

Powder flow and packing capacity have been identified as one of the most contributing factors in good powder quality [248]. Therefore, it is essential to perceive how to process dynamics influence the flow and packaging behaviour of the powder bed during BJ printing.

A proposal to quantify the layer quality was provided by Karapatis [248], who affirms that the measurement of the layer density by weighing is a good indicative parameter. On the contrary, there are other authors who deny this claim, showing that the density of powders is not a sufficient parameter to distinguish powders with respect to their rakeability and the resulting layer density [258]. Currently, there are numerical models that predict powder fluidity and packing density based on powder characteristics and BJ parameters. [459]

For example, it is known how the size and morphology of the particle influence the fluidity of the powder, and consequently the final packing density. Fine particles smaller than 5 µm do not usually exhibit good fluidity due to the Van der Walls forces that exist between them[460]. The morphology of the particles also affects the propagation of the material. Irregular particles reduce the fluidity of dust [112, 461]. The

flow characteristics affect the packing density and, consequently, the density of the final part. [97] This is why if this type of powder is used, a relatively slower propagation speed will be required [460].

Other important factors in the quality of the powder spread are related to the equipment used for the distribution of the powder and not to the properties of the powder. For example, the mechanism used for dispersion (mechanical vibration and rolling), friction conditions, the surface texture of the roll, and the geometry of the roll [462]. In addition, the propagation system can influence compaction and possible particle segregation. More importantly, the applied load can vary by an order of magnitude and therefore cause an inhomogeneity of interparticle forces in the granular packing. This event commonly happens when the roller passes through the printing area, an inhomogeneous force appearing due to the interaction between neighbouring dust particles. [459]

In order to develop reliable strategies for the production of parts with good mechanical properties and good quality (homogeneous part density, exact dimensions, and good surface finish), it is vital to work with good dust diffusion [257].

The influence of print speed (i.e., roll travel speed) on part integrity has been extensively evaluated. The best way to get a quality part is to work with the lowest possible speed. The drawback to this is that the printing time is significantly increased. However, if, on the contrary, one works with a high printing speed, the following undesired phenomena will take place: a reduction in dimensional precision [463] and a low precision in the piece since, by increasing the speed in which the binder impacts on the powder bed, fine particles are expelled from the powder producing splashes. In addition, uneven and non-uniform spreading will occur, which eventually leads to high porosity in the final product and, therefore, less mechanical resistance [29]. For this reason, the surface roughness of the powder beds is determined by the quality of the powder dispersion, among other factors [459].

In a study of Parteli and Poschel [459], a simulation was proposed where dust-roller interactions were investigated. It was demonstrated that the increase in the speed of movement of the roller led to an increase in the roughness of the surface of the bed of dust, affecting the quality of the piece. Myers et al. [393] experimentally corroborated this. In another study, the relationship between dimensional tolerance and printing direction was confirmed. Dimensional precision in the y-direction (print direction) was shown to be more dependent on print speed compared to the x-direction, following linear correlation, meaning that precision prediction is possible.

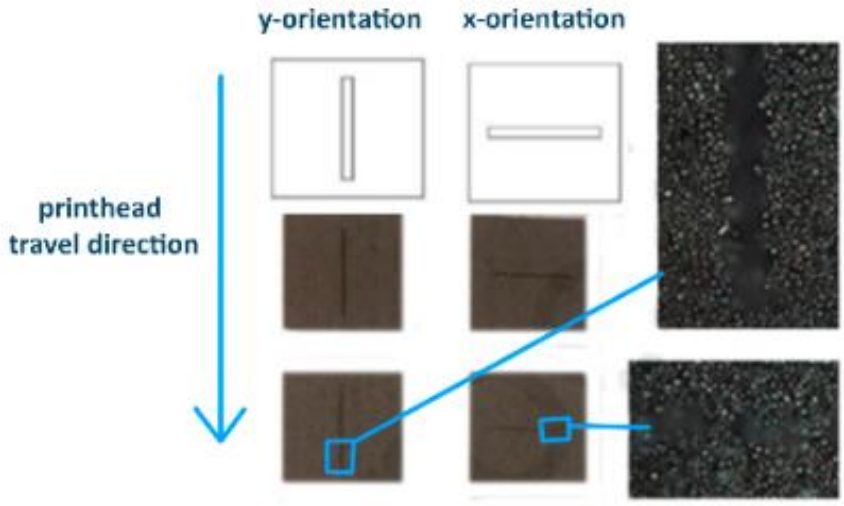

Figure 61. Effect of printing orientation on the dimensional accuracy. [287]

4.3.3. Binder saturation

The binder saturation level is defined as the ratio between the amount of liquid binder and the volume of pores in the impression material [14]. The level of saturation in the equilibrium phase is very important in the BJ-AM process and must be determined experimentally.

To estimate the theoretical binder saturation (% binder saturation), the pore volume of the powder bed is needed and can be determined from the packing density of the powder bed, as shown in equation Eq. 26 (page 119).

An optimal amount of saturation must be used in the printing process to ensure good mechanical strength, desired dimensional precision, and structural integrity. Both lower saturation and higher saturation levels are problems in the BJ process. .

Part requirements and some parameters of the production process, such as surface roughness and print speed, respectively, will determine the thickness of the layer and, together with the characteristics of the powder, the saturation of the binder will be established consecutively. For example, the study by Shrestha et al. determined that the optimal saturation level is 70% when working with a layer thickness of 100 µm, at a roller rotation speed of 6 mm / s and powder feed ratio values of 3:1 [446]. But this is not entirely true since there are many more parameters to consider such as wetting and the droplet deposition system.

Next, we will talk about the effects on binder saturation that it has: the layer thickness, the wetting, and the printing system, among other factors.

For an equal amount of binder, if the thickness of the layer is too thin, the supplied binder may be excessive and the additional binder spreads sideways. This excessive lateral flow (W) is called "bleeding." Later, in this section, this problem will be explained. Conversely, if the layer is too thick, this amount of binder may not be sufficient to cover the entire space between the particles, resulting in penetration (D) unable to bond the layers. When the layer thickness is optimized, the extension (W) / penetration (D) of the binder advances in vertical and lateral directions in which there is enough binder to fill the interstitial sites. This is why the layer thickness is a variable of the binder saturation function (Figure 62).

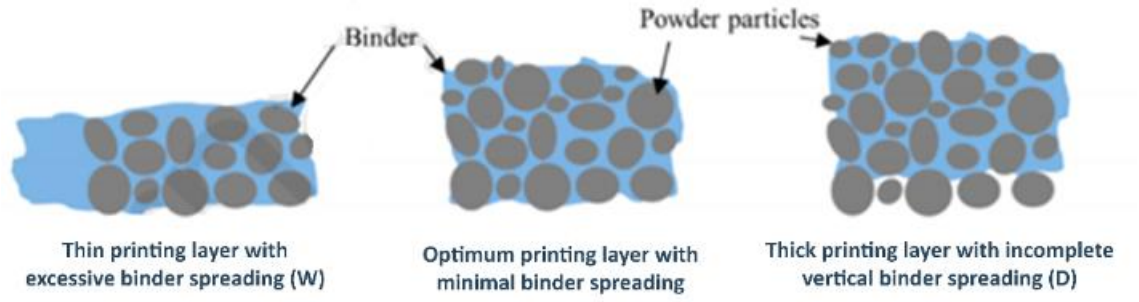

Figure 62. Different layer thicknesses and their effect on binder saturation: bleeding and lack of cohesion between layers.

Powder packing and wettability are two factors that affect binder saturation and required binder volume. Wetting, as already explained, is the ability of the binder to spread vertically and laterally through the interstices of the powder bed. Two influential properties of the material in the infiltration of the binder are [464]:

- The porosity of the powder bed, in which the greater the porosity, the interstitial voids increase, and then the infiltration decreases. Therefore, the wettability is directly influenced by the packing density of the powder bed, the higher the density, the greater the wetting capacity. [219] The explanation of this event is detailed on page 113
- The contact angle, in which the infiltration area of the liquid binder decreases as the contact angle increases.

Some authors claim that if the wettability were low, an alternative would be to add more binder [310, 465]. However, keep in mind that this could lead to an overestimation of optimal saturation levels, causing unwanted saturation in the final piece.

Another factor influencing the level of binder saturation is the system used in droplet deposition. Depending on the system used, the droplet deposition mechanisms can be: simple (little used), overlapping or overlaying, as shown in Figure 63. The latter two are the most widely used because higher binder saturation levels can be achieved and the printing process can be streamlined [125]. The overlaying mechanism is favourable when working with thick layers of powder since the area obtained is narrow and deep. On the other hand, the single drop deposition system determines a minimum resolution.

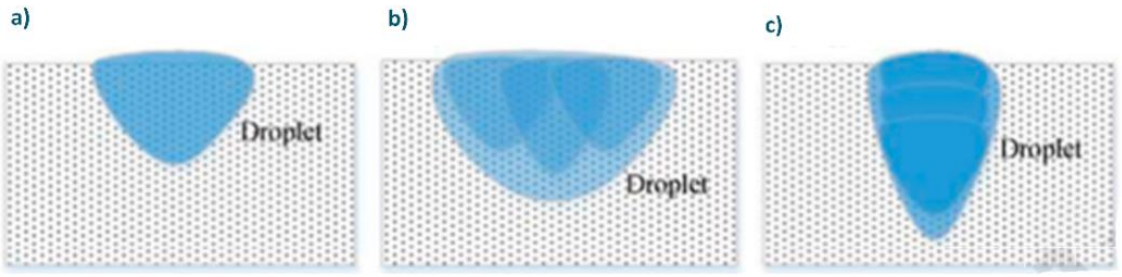

Figure 63. A comparison between droplet deposition mechanisms: a) simple, b) overlapping and c) overlaying and their effects on the saturation area [258].

The quantity has been experimentally shown to influence control of part precision, strength, and final dimensions [143, 347, 466-468]. Furthermore, adjusting the saturation level is vital not only for construction cycle time but also to minimize the cost of BJ. Therefore, it is quite beneficial to be able to predict equilibrium saturation for a bed of powder and liquid binder using a physics-based model prior to the printing process.

That is why some authors have focused their efforts on finding the optimal levels of binder saturation [285, 310, 344, 347, 465, 469, 470] and their relationship to the qualities of the green parts and the final parts, which in turn provides information on the fundamental principles of the process. [285]

It was shown that incorrect binder saturation could cause an inhomogeneous powder bed, and consequently dimensional inaccuracy and insufficient mechanical strength in printed parts [11, 471].

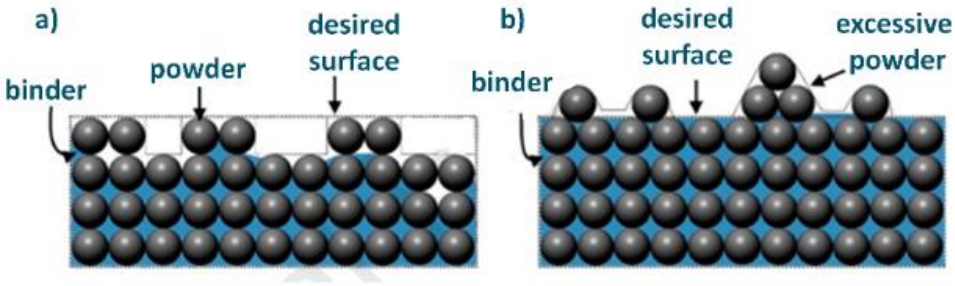

Figure 64. Some of the possible surface defects due to inadequate binder saturation level: (a) low saturation resulted in particle loss and (b) high saturation causing excessive particle stick to the surfaces and reducing dimensional accuracy [11, 472].

As shown in the image above, a binder saturation greater than equilibrium saturation will cause the binder to take up more space than it should, penetrating outside the limits designated by the part design geometry. The literature defines this fact by means of two different phenomena that are called "bleeding" and “feathering " [112, 285].

“Bleeding” is defined as the macroscopic flow of the unwanted binder that exists because the area delimited by the impression has high levels of saturation. This leads to a decrease in precision in the lower section of the part, more than the upper layers. Probably due to the gradually accumulated weights of the upper layers [285].

“Feathering” is the microscopic extension of the binder produced in the impact phase of the binder on the powder bed. Its consequences are an increase in the roughness and a widening in the x and y direction of the part due to the fact that adjacent particles adhere to said surfaces [311]. As is known, inadequate green strength leads to: distortion of dimensional accuracy, poor surface finish, and cracking or failure of end parts [347]. Therefore, excessive saturation leads to a distortion of the geometry and a decrease in the surface quality of the part due to the two aforementioned phenomena.

Other unwanted phenomena due to the high level of saturation is an excessive wetting of the powder bed, which can cause the particles to adhere to the roller and subsequently result in non-homogeneous powder beds with gaps, thus producing green parts with smaller density and lower mechanical resistance [473, 474]. Higher saturation levels also increase print time and therefore adversely affect subsequent printing.

However, another study demonstrated that increasing the saturation level of the binder resulted in greater tensile and flexural strength of the final part, although dimensional precision was sacrificed. [347]

On the other hand, if the equilibrium saturation is much higher than the saturation imposed by the machine, the printed part will not have enough mechanical resistance since there will not be enough

binder and weak bonds will be created between the dust particles and between the successive layers. This causes delamination of the layer and a high level of voids and pores that may appear after the exhaustion and sintering steps [347].

4.3.4. Drying time and heater power ratio

In addition to knowing the behaviour of the powder under mechanical stress similar to the process conditions, it is important to understand the behaviour of the powder at elevated temperature [257]. As with conventional methods, any thermal alteration can alter the microstructure of the particles and, consequently, the properties of the material.

As described in the BJ technique printing process, after deposition of the binder in the powder bed, an initial partial cure is performed, heating the entire print bed. Two variables to control for this curing operation are cure time and drying power.

Curing time depends on the saturation level of the binder, the composition and chemistry of the binder, the thickness of the layer, the wettability of the binder powder, and some characteristics of the powder bed, such as thermal conductivity, surface area, permeability, and packing density.

When the drying times are too short, the binder will not solidify and will maintain a fluid state. The effect of gravity and capillarity will cause the penetration of the binder in the vertical direction to be greater than the thickness of the layer, causing distortions in the dimensions of the part and diminishing the mechanical properties. On the contrary, a drying time that is too long can cause the nozzle to become clogged [11]. Furthermore, excessive drying causes the union between the layers to be inadequate, being a fragile union that leads to delamination of the part. The reason for this is the low amount of binder remaining in the liquid state, which is not enough to effectively form a continuous liquid phase through the interface between the previous and newly added powder layers and would cause loss of resistance between layers [310].

On the other hand, the drying power must be controlled, which is related to the temperature of the heater and, consequently, the heating rate [11, 27]. This parameter plays an important role since it controls the drying time of the liquid binder, therefore it controls the deformation, shrinkage, dimensional precision, and surface finish of the green part during the construction cycle [475]. If the power is too low, the drying will be insufficient, altering the precision and the surface finish. On the contrary, if it is very high, the drying will be so fast that it will induce uncontrolled deformations and contractions in the piece.

Generally, when the sprayed liquid binder is adequately dry, the pre-dried layers below the newly printed layer will restrict vertical penetration of the binder, and penetration of the binder occurs primarily in the

new layer in unsaturated areas between the deposited droplets. This results in improved saturation in the printed areas of the new layer and better dimensional accuracy and green strength. Therefore, optimized drying times are required for each layer for higher binder saturation. [263]

Conclusions

Metal AM is a technology with a very promising future. There are different metal 3D printing technologies, each with a number of advantages and disadvantages. One of them is the Binder Jetting. This technology has numerous advantages over other AM technologies, although it is true that each one has its own specific niche. BJ competes directly with Metal Injection Molding (MIM) processes and other powder metallurgy processes as they have some aspects of the process in common. For example, green pieces have an optimal wall thickness, just like in MIM, which will allow the binder to be removed successfully.

BJ is a technology that allows high speed along with good resolution, which translates into higher productivity. The pieces made with this technology have a microstructure and isotropic properties, as well as no residual thermal stresses. This is due to working in ambient conditions (temperature and atmosphere). Another advantage is the lower cost of the AM machine and the lower operating costs in terms of preparing part files, starting and restarting the machine, as well as minimizing waste.

Due to all the advantages it presents, this technology is expected to grow or mature at a higher speed than other AM techniques, although it is currently considered to be in an early maturity stage and there are still many interesting concepts that are unknown about the process.

This work has compiled many of the investigations carried out so far on BJ and its relationship with the properties of dust. The optimization of some printing parameters and the effect of the relationship between powder and binder are also detailed. There are other investigations focused on post-printing operations (densification or heat treatments), but this is not covered in this work.

A summary of the process factors and their correlation with the production quality of the pieces will be carried out.

Regarding the powder properties, it can be concluded that:

- The morphology determines the fluidity, the spreading capacity and the packing of the powder, being greater for the spherical particles. It is true that producing this type of particles, from gas atomization, is a more expensive process, but this cost must be assumed since if irregular powders are used, the properties of the sintered parts will not be acceptable.
- The mean size and the particle size distribution (PSD) are two very important properties of the powder, since they directly affect the fluidity and the packing density of the powder, and therefore, with the layer thickness, the powder-binder interaction, the saturation of balance of the binder, and the subsequent sintering. In BJ, it is preferred to work with powders with a larger particle size since they have a better fluidity and spreading and a lower binder saturation and their

use result in better dimensional precision and higher densities of the piece in green. Although it is true that the finest powders sinter better and with them, pieces of better resolution and better surface quality are obtained, as well as greater mechanical properties and densities of sintered parts, if the spreading was not taken into account. That is why the optimal size has not been discovered, what is clear is that particles of a size smaller than 5 um cannot be used due to security problems and also, their specific interaction force is so high that it forms agglomerates, which causes poor packaging and consequently the final piece will have poor mechanical properties. Other parameters that are affected by the size of the particles are the dispersion (W) and the penetration (D) of the binder on the powder bed. Large particles facilitate vertical permeation, while small particles facilitate lateral extension (W).

Regarding the particle size distribution, it is concluded that the powders with a bimodal distribution improve the powder packing density, the fluidity, and, therefore, the density of the sintered part and decrease the shrinkage during this sintering. Another advantage of using a bimodal mixture is that it can be sintered with a lower energy contribution compared to large single-mode powders and therefore will reduce the cost of the process. A possible future study would be to study the optimization of the proportion or distribution of particle sizes to achieve the best possible sintering density.

- Segregation is also an event that affects the dust printing capacity, as well as the flowability and packing density already mentioned above. Segregation is the separation of the different dust particles in a mixture. You should try to reduce this to the maximum in order to obtain a reproducible process and with the most homogeneous pieces possible, which do not depend on the position in the printing box.

In relation to the binder, some of the parameters that affect the quality of the piece and the process are:

- The morphology of the binder is a factor to consider since the selection of some process control parameters may vary according to said morphology. For example, for monomeric binders, the heat source, used for drying the binder, serves to drive polymerization and solidification of the binder. On the contrary, if it is a polymeric binder, the source serves to evaporate the solvent that dissolves the polymer. These two processes will require different drying times. Another important parameter is the chemical composition of the binder since, for example, the amount of added carbon can diffuse into a carbon-sensitive metal, modifying the composition of the alloy and, therefore, its microstructure. Other properties of the binder to consider are the rheological behavior and the surface tension of the binder since these will determine its injectability and dispersion through the powder bed.
- The interactions between the powder and the binder are complex and determine the optimal amount of saturation in a static state or under equilibrium conditions. On the other hand, in a dynamic state, where the binder moistens the powder bed, the interaction will determine the

precision and mechanical performance of the parts. This interaction depends on various parameters of the printing process, such as the printing speed, the speed and force of impact of the drops or the effect of capillarity, in short, on the dynamics of the flow of the binder drops.

Last but not least, some important printing process control variables are layer thickness, speed and mechanism of powder dispersion, binder saturation, and drying time or speed. Some authors point out that the saturation of the binder and the thickness of the layer are the two most critical parameters, reflecting the influence of the powder-binder interaction and the packing density on the final pieces. These print processing parameters are affected by the characteristics of the powder and the binder.

The effect of layer thickness can be explained by dividing the figure into sections, forming a stepped surface. If the thickness is very large, the surface roughness will be less and the precision too. Furthermore, many authors recommend that the layer thickness be at least three times the mean particle size.

On the other hand, an optimal amount of binder is necessary to guarantee the structural integrity, dimensional precision, and good mechanical properties of the part, in other words, for successful part manufacturing. An insufficient amount of binder results in poor bonding between layers but an excessive amount will cause over-expansion, causing an unsuitable surface finish and low dimensional precision. The selection of the saturation level so far has been an empirical process, although it is true that models based on thermodynamic principles have emerged to predict the optimum level. These models take into account the surface tension of the binder, the packing density of the powder, the surface area of the particles and the wettability of the powder material.

Although it has been said that it is not one of the critical parameters to obtain parts with good properties and finishes, the drying time during printing must be taken into account so that this process can be carried out. After depositing the binder, a heat source passes over the bed to dry the binder. The binder must be fluid enough to be able to be injected by the ink print nozzles and to be able to distribute throughout the powder bed. But if it is not dried once it has been deposited on the bed, it can lead to the powder-binder combination sticking to the roller that spreads the new powder layer, or it can cause the binder to continue distributing through the powder, obtaining low precision parts. Also, this drying time can be adjusted to reduce bleeding due to high saturation of the binder.

As it has mentioned, the development of the BJ process requires a series of considerations such as (i) formulating a powder with an optimal composition, morphology, and particle size distribution, (ii) formulating a liquid binder with properties optimal for flow and optimizing the interaction of this with the powder bed, and finally (iii) adjust the parameters of the printing process.

In general, many experimental and theoretical studies are still needed to fully understand the influences of the parameters mentioned above in the final part (their mechanical, chemical, functional, or dimensional properties). Current approximate knowledge of the necessary morphological characteristics of the powder, along with an insufficient understanding of particle chemistry and microstructure in manufacturing processes, requires a significant need towards a more complete characterization of powders prepared for BJ. The main objective of the investigation should not only be to optimize the process parameters, but also the interaction between these variables and the properties of the powder. This will result in reduced variability between constructions and parts and will make the process more controllable. Only then will BJ processes be able to rival traditional manufacturing methods and other AM technologies in terms of being recognized as a viable means of creating reproducible and reliable parts.).

Future lines of research

As already mentioned, this project corresponds to a previous study to understand and deepen the Binder Jetting metal additive manufacturing process. Therefore, this will serve to know all the details to consider in a future study. In this future study, which would have been carried out as my Master Final Project if the coronavirus pandemic had not broken out, the aim will be to characterize the samples of the metallic powder used in HP (Metal Jet 316L <22 µm) that have different behavior during printing, to understand the relationship between the properties of the powder and its printability.

Therefore, future work will focus on techniques that have the potential to characterize metallic powder in order to be able to determine the differences between dust samples that behave differently during printing. These techniques should include:

- PSD by Laser Diffraction to characterize the size of the particles and their distribution, and thus observe if there is any change between the different samples.
- SEM / EDX of embedded dust samples for detailed metallographic and elemental analysis of particles. In this elemental study, the specification or oxidation status of each element will not be known. It will also serve to perform a morphological characterization of the particles.
- XPS provides the chemical composition of the near-surface region of the samples (where EDX provides little or no information). XPS analyzes will also serve to indicate the oxidation status of each element and the study of possible chemical segregation.
- FIB / FESEM will be used to carry out a more detailed study and obtain chemical segregation in cross-sections prepared by FIB and thus seek some type of correlation with the results obtained in the XPS.
- Micro / nanomechanical characterization of the dust, implementing a "property map" to establish a relationship with possible structural or chemical variations. In other words, it is about being able to determine if there is any kind of difference between the different samples by means of a nanohardness analysis.
- TGA at low temperature (less than 300ºC) to understand changes in the oxidation behavior of fresh powder in air and possible occurrences of organic in processed powder. This technique will also serve for another future project where the intention is to study the interaction of inorganic dust with the binder (contains organic) and temperature.

The operations and fundamentals of some of these techniques are detailed in Appendix B (page 159).

Apart from this study, other possible future directions in additive binder jetting manufacturing in relation to 316 stainless steel should be considered. For example, some possible studies to be carried out may focus on informing repeatable and reproducible mechanical properties, such as hardness,

elastic limit, fatigue resistance, or creep. One could also investigate the effect of adding different additives to the 316L alloy, the effect of different printing parameters. Regarding the printing technique, an effort must also be made in the development and adoption of new alloys or materials, in order to cover new markets.

Economic Valuation of the Study

As it is a research study based on the compilation of the results of different authors, the main cost of this bibliographic work is the salary of the researchers involved. This cost will be increased by the use of certain resources such as a computer, the contract of an internet fee, or the license to access scientific articles. To these will be added the cost of electricity due to the consumption of the computer and light.

The costs of the project will be detailed below. As fixed expenses, we would find the wage of the labor, the price of the computer, the bibliographic funds service, and the internet rate. Variable costs will correspond to electricity consumption.

This project has been prepared by a student of the Master of Science and Materials Engineering at the Universitat Politècnica de Catalunya, which sets an approximate salary for student practices of 8€/h [W38]. In addition, the Master's Final Project of the study plan is equivalent to 12 ECTS credits, which corresponds to 300h [W39]. Therefore, the total cost of student work in this project amounts to 2,400€. In addition to the student's work, a tutor and a co-tutor were reviewed. Said persons must receive a salary of 24 €/h for the corresponding hours worked. The tutor has invested 25hand the co-tutor 20h.

On the other hand, in relation to the cost of acquiring bibliographic funds, we will make an estimate based on data published by the Spanish state about the expenses or investments made by the Consejo Superior de Investigaciones Científicas (CSIC) library to acquire bibliographic funds in different formats and supports. According to this source, the expenses in bibliographic funds amounted to 709,708 €/year [W40]. It is true that this expense would be distributed among all the students of the university. The university published that in this 2019-2020 academic year the UPC community consisted of 33031 grade, master, and doctorate students [W41]. Therefore, it can be said that approximately 21.50 € / year per student is being paid. As it is considered that one month has been worked (300h employed in total between 8h / day is equivalent to 37.5 days, rounding is one month), the cost of this service is equivalent to1.79 €

The internet rate currently in Spain is around 40 € per month since the average uses 100 Mbps (megabit per second) fiber optics. Finally, the price of a computer, taking into a count that a basic computer is used, is 400€. According to the Agencia Estatal de Administración Tributaria of Spain (Hacienda), the amortization of the information processing equipment is 25% per year [W42], but since it has only been used for a month, it can be said that the acquisition of a computer for this project will cost 8.33€.

Afterward, the variable cost will be detailed. Currently, the price of kWh depends on the company and the contracted rate in Spain. An estimated value can be 0.094 €/ kWh [W43]. Assuming that the basic-level computer consumes on average it consumes 220W [W44] and has been used for 300h, in total consumption it has been 66kWh. On the other hand, to calculate the consumption of a light bulb, you

must know the power of that light bulb in kW and know how long it has been used. A household LED bulb has a power of 4W and one of the traditional 80W bulbs [W45]. In this case, the average value of 42W will be considered. As it has been used for 300h in total, the consumption will be 12.6 kWh. In total the cost of electricity consumption will amount to about 7.50€ .

Adding all the previous values, the total cost of this project amounts to approximately **3**,**538** €. As previously mentioned, this cost corresponds mainly to the price of labor.

Annex A: Stainless Steel

Overview of stainless steels

Stainless steels can be defined as an alloy of iron and carbon that contains by definition a minimum of 11% chromium. Some types of stainless steel also contain other alloying elements. The main ones are nickel and molybdenum

Stain steels are one of the most used alloys of iron, there is a huge amount of applications due to a wide variety of composition in the alloy. They are characterized by their corrosion-resistant properties. The characteristics of these alloys associated with oxidation resistance are due to the spontaneous formation of an invisible and adherent chromium-rich surface oxide film. This film has the ability to self-generate and self-repair in the presence of oxygen.

In this paragraph, the different advantages and disadvantages that stainless steels generally present will be exposed. For example, low alloy steels have high resistance to corrosion under atmospheric conditions; if these are highly alloyed, corrosion resistance is obtained even in acidic media and at high temperatures. In relation to temperature, most steels resist large thermal variations, their mechanical properties almost constant. For example, some steels demonstrate exceptional hardness at cryogenic temperatures. It is worth mentioning that its mechanical resistance can be modified, some steels can be hardened by cold work, and others by heat treatments or other mechanisms as will be mentioned later. Most stainless steels can be treated with relative ease, being able to be cut, welded, forged, and machined. It is true that they can be dented or scratched and their repair, regarding aesthetics, is difficult to carry out. In short, it has many suitable properties for its employability in many industrial sectors, but it is true that its tendency to be a good thermal conductor and its considerable cost reduce its range of applications.

Chromium is an element that provides resistance to oxidation. To increase the corrosion resistance, the chromium concentration can be increased and/or other elements such as nickel or molybdenum can be added. The degree of the impenetrability of the oxide layer in certain environments depends not only on the composition of the alloy, but it is also affected by the specific medium, its temperature, and the concentration of the corrosive agent. Other elements can be added to stabilize the desired phases and obtain improved mechanical properties such as toughness. These alloying elements can, therefore, be classified according to the phase that is favoured to stabilize.

As a curiosity, here are three erroneous claims or beliefs about stainless steel. The first of them is that many consider them as a special coating applied to steel, as if it were a surface treatment, ignoring the fact that it is a solid material. It is true that common steels are usually covered or "plated" with white

metals such as chrome, nickel or zinc to modify their surface. The coatings have the disadvantage that they can be damaged, causing dire consequences on the material, such as accelerating corrosion due to the effect known as "galvanic cell formation". This does not occur in the case of stainless steels. Another belief is that stainless steels are not magnetic. This popular belief is false since stainless steels are ferromagnetic, so they do have magnetism. It is true that austenitic steels are not magnetic and there are some demagnetization treatments, hence the belief that only common steels are magnetic and therefore a way to differentiate ordinary steel from stainless steel could be through a magnet. Finally, the belief that they are stainless. Stainless steels show oxidation phenomena, the formation of the passive layer of chromium oxide. Furthermore, if they are not maintained properly or if they are exposed to unfavourable media and conditions, they can also suffer undesirable corrosion. Therefore, naming them stainless would not be entirely correct, since what happens is that they have a greater resistance to oxidation than carbon steels.

Diagram of stainless steels and their microstructures.

In this chapter, the different diagrams of the main elements of the alloys of stainless steels will be shown.

Fe-Cr diagram

Figure 65 shows the equilibrium diagram of the iron (Fe) and chromium (Cr) alloy. In this, you can see the different types of stainless steels according to the stable phase: ferritic, martensitic, austenitic, duplex and precipitated hardened.

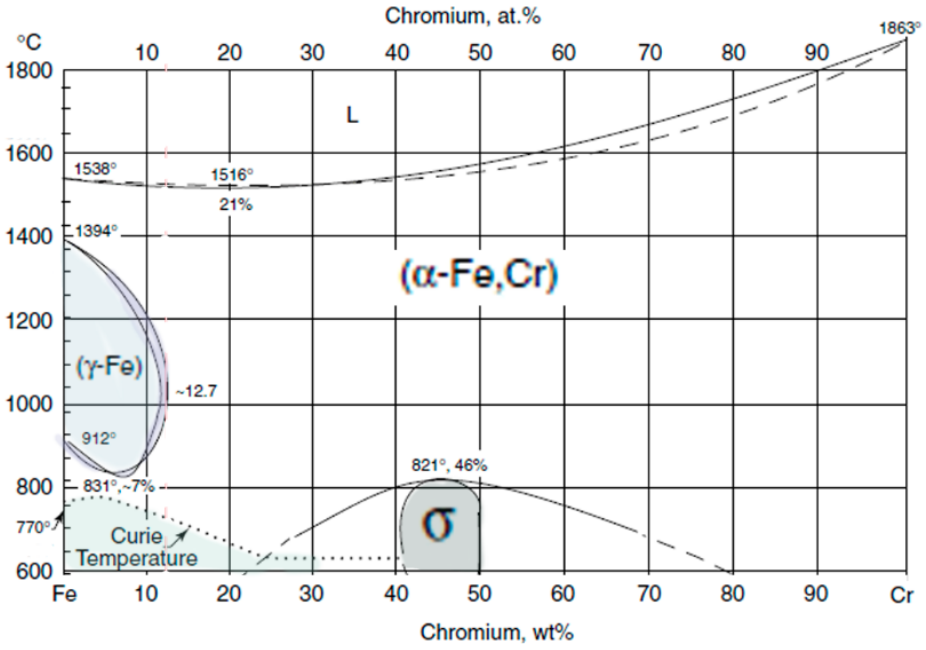

Figure 65 Fe Cr diagram [476]

As can be seen, if the alloy contains less than 12% Cr, the stable structure becomes austenite (gamma phase) upon heating. If it cools quickly, martensitic stainless steel is achieved. If, on the other hand, the alloy contains between 12 and 13% of Cr, at high temperatures biphasic structures (alpha and gamma) are formed, which when rapidly cooled, its stable structure will be formed by ferrite and martensite (ferritic-martensitic stainless steels). Alloys that contain more than 13% Cr are called ferritic stainless steels since they will maintain the ferritic structure until it reaches its melting point. It is true that there are two exceptions, the Fe-Cr alloys with chromium content between 25-42% and 48-65%, which at temperatures between 600 and 900ºC, an intermetallic phase called sigma appears that coexists with the ferrite. The sigma phase is a very hard, brittle phase and can dissolve in ferrite if heated above 900ºC.[477, 478]

Carbon influence diagram.

Carbon influences the stability of the phases. The Fe-Cr diagram is modified with the carbon concentration in the alloy. As seen in Figure 66, the gamma loop shifts to the right as it increases of % C. Therefore, it can be stated that carbon will favour the formation of the gamma phase, being a stabilizing gamma element. But this statement is not entirely correct, since amounts greater than 0.4% carbon, the gamma loop no longer expands with increasing carbon and excess carbon will form iron and chromium carbides.

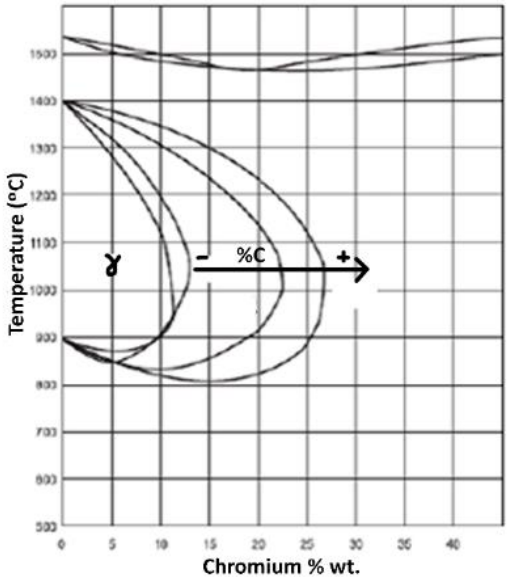

Figure 66 Influence of carbon on the Cr Fe diagram in the gamma phase.[478]

In this diagram, it can also be seen that for the Fe-Cr-C stainless steel alloys, if the Cr content is greater than 27%, ferritic phases will always be obtained, independently of the compositions of the other elements. Alternatively, it is also observed that the martensitic structure at room temperature is present if the alloy contains up to approximately 17% chromium.[478]

Fe-Cr-Ni phase diagram

Nickel expands the stability field of austenite and lowers the alpha-gamma transformation temperature. In Figure 67 the ternary diagram of Fe-Cr-Ni alloy at room temperature is shown, showing the different stable structures depending on the composition of the alloy.

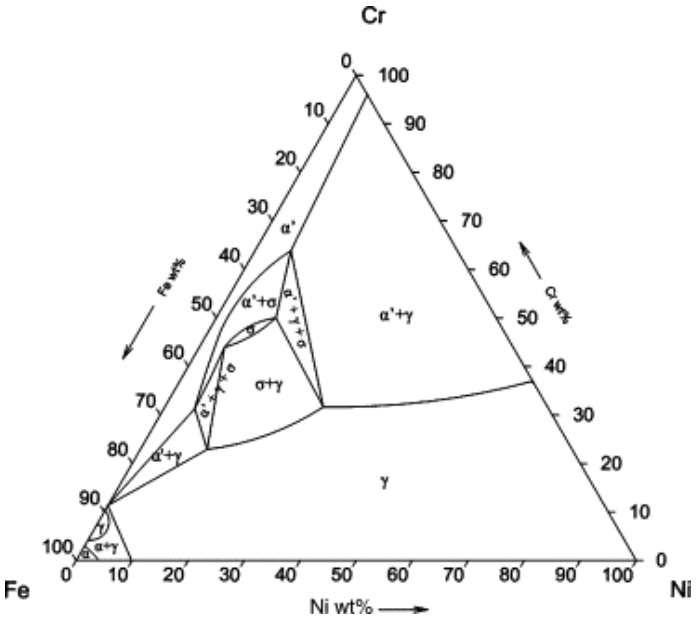

Figure 67 Fe Cr Ni diagram at room temperature [476]

The sigma phase is due to the presence of ferrite when it is kept for a long time at temperatures between 600 and 900 ºC, transforming itself into an intermetallic compound of iron and chromium. It is characterized by its loss of ductility, resilience, and high hardness. The sigma phase not only forms in steels with high chromium content but can also occur in ferritic steels with chromium contents from 14%, in austenitic and austenitic-ferritic steels. [477]

Schaeffler diagram

The Schaeffler diagram is derived from the Maurer diagram, which presents the structures that Cr-Ni steel will present according to their percentages. Anton Schaeffler improved and incorporated the influence of different alloying elements on the formation of ferrite or austenite phase. Appearing the concept of chrome and nickel equivalent. The equivalent chromium incorporates the alpha elements (elements that form and stabilize the ferrite or alpha phase) and the nickel equivalent to the gammagenes (austenite or gamma phase forming). Each element is multiplied by a correction factor that depends on its degree of influence on the formation of the corresponding phase.

$$\boldsymbol{Cr_{equivalent}} = \%\boldsymbol{Cr} + \%\boldsymbol{Mo} + \mathbf{1.5} \cdot \%\boldsymbol{Si} + \mathbf{0.5}\ \%\boldsymbol{Nb} \qquad \textbf{Eq. 29}$$

$$\boldsymbol{Ni_{equivalent}} = \%\boldsymbol{Ni} + \mathbf{30} \cdot \%\boldsymbol{C} + \mathbf{0.5} \cdot \%\boldsymbol{Mn} \qquad \textbf{Eq. 30}$$

Figure 68shows the typical phases of stainless steels when cooled at normal speeds taking into account the percentage of chromium and nickel equivalent: austenite, ferrite and martensite. [478]

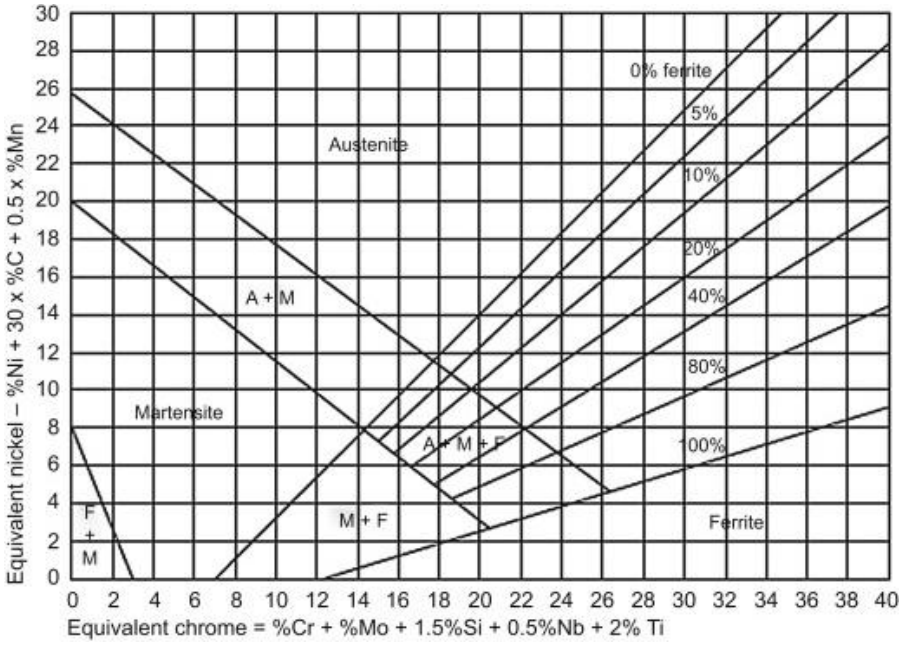

Figure 68. Schaeffler diagram[478]

Classification and the most common stainless steels.

The stain steels are classified according to metallographic phase they contain and fall into several main categories as austenitic, ferritic, martensitic, duplex steels and precipitation hardening stainless steel. It is true that some authors also speak of other grades of stainless steel such as superferritic and super austenitic stainless steel

Austenitic, ferritic, and duplex stainless steels cannot be hardened by heat treatment, and therefore, alloy and thermomechanical processing are designed to minimize the formation of phases detrimental to corrosion resistance or toughness. In austenitic stainless steels, they can also be hardened by cold deformation or by deformation-induced martensite formation. Martensitic stainless steels can be heat treated by quenching and tempering at high hardness and strength. Another way of hardening stainless steels is through the formation of precipitates (aging).

Within each of these classes of stainless steels, there are different series of steels, and within the series, there are different grades. There are many grades in addition to different denominations, each with its respective composition that gives it specific properties. Below is a summary in the Table 15 of the different types of most common stainless steels classified according to their phase. In addition, the percentages of the alloying elements will be detailed. Some types of these stainless steels will be detailed later.

As mentioned, there are many ways to name stainless steels, depending on the country and/or the institution related to their manufacture or use. The nomenclature of stainless steels follows the same standards as that of steels. Restricting only to the American system (the most used), it is relevant the influence on the designation of steels of institutions such as ASTM (*American Society for Testing and Materials*), AISI (*American Iron and Steel Institute*), ASME (*American Society of Mechanical Engineers*), SAE (*Society of Automotive Engineers*), ANSI (*American National Standards Institute*), ACI (*Alloy Casting Institute*) and AWS (*American Welding Society*). Due to the possible confusions created, the systematization has been tried to be solved by means of a unified numerical system by ASTM and SAE, under the name of UNS (*Unifred Numbering System*). It is true that it is often little known and used, due to the custom of using, normally, the nomenclature established by AISI.

What follows in this chapter is the presentation of different types of steels, along with some of their respective grades of steels.

.

Table 15. Different types of stainless steels and their composition [W46]

Stainless steel	AISI	UNS	%Cr	%Ni	%C	%Mn	%Si	%P	%S	% N	Others
AUSTENITIC	201	S20100	16.00–18.00	3.50–5.50	0.15	5.50–7.50	0.75	0.06	0.03	0.25	-
	202	S20200	17.00–19.00	4.00–6.00	0.15	7.50–10.00	0.75	0.06	0.03	0.25	-
	205	S20500	16.50–18.00	1.00–1.75	0.12–0.25	14.00–15.50	0.75	0.06	0.03	0.32–0.40	-
	254	S31254	20.00	18.00	0.02 max	-	-	-	-	0.20	6.00% Mo; 0.75% Cu;
	301	S30100	16.00–18.00	6.00–8.00	0.15	2.00	0.75	0.045	0.03	-	-
	302	S30200	17.00–19.00	8.00–10.00	0.15	2.00	0.75	0.045	0.03	0.10	-
	302B	S30215	17.00–19.00	8.00–10.00	0.15	2.00	2.00–3.00	0.045	0.03	-	-
	303	S30300	17.00–19.00	8.00–10.00	0.15	2.00	1.00	0.20	>0.15	-	0.60% Mo
	303Se	S30323	17.00–19.00	8.00–10.00	0.15	2.00	1.00	0.20	0.06	-	0.15% Se
	304	S30400	18.00–20.00	8.00–10.50	0.08	2.00	0.75	0.045	0.03	0.10	-
	304L	S30403	18.00–20.00	8.00–12.00	0.03	2.00	0.75	0.045	0.03	0.10	-
	304Cu	S30430	17.00–19.00	8.00–10.00	0.08	2.00	0.75	0.045	0.03	-	3.00-4.00% Cu
	304N	S30451	18.00–20.00	8.00–10.50	0.08	2.00	0.75	0.045	0.03	0.10–0.16	-
	305	S30500	17.00–19.00	10.50–13.00	0.12	2.00	0.75	0.045	0.03	-	-

308	S30800	19.00–21.00	10.00–12.00	0.08	2.00	1.00	0.045	0.03	-	-
309	S30900	22.00–24.00	12.00–15.00	0.2	2.00	1.00	0.045	0.03	-	-
309S	S30908	22.00–24.00	12.00–15.00	0.08	2.00	1.00	0.045	0.03	-	-
310	S31000	24.00–26.00	19.00–22.00	0.25	2.00	1.50	0.045	0.03	-	-
310S	S31008	24.00–26.00	19.00–22.00	0.08	2.00	1.50	0.045	0.03	-	-
314	S31400	23.00–26.00	19.00–22.00	0.25	2.00	1.50–3.00	0.045	0.03	-	-
316	S31600	16.00–18.00	10.00–14.00	0.08	2.00	0.75	0.045	0.03	0.10	2.00-3.00% Mo
316L	S31603	16.00–18.00	10.00–14.00	0.03	2.00	0.75	0.045	0.03	0.10	2.00-3.00% Mo
316F	S31620	16.00–18.00	10.00–14.00	0.08	2.00	1.00	0.20	>0.10	-	1.75-2.50% Mo
316N	S31651	16.00–18.00	10.00–14.00	0.08	2.00	0.75	0.045	0.03	0.10–0.16	2.00-3.00% Mo
317	S31700	18.00–20.00	11.00–15.00	0.08	2.00	0.75	0.045	0.03	<0.10	3.0–4.0% Mo
317L	S31703	18.00–20.00	11.00–15.00	0.03	2.00	0.75	0.045	0.03	<0.10	3.0–4.0% Mo
321	S32100	17.00–19.00	9.00–12.00	0.08	2.00	0.75	0.045	0.03	<0.10	%Ti= 5(C+N) min, 0.70% max
329	S32900	23.00–28.00	2.50–5.00	0.08	2.00	0.75	0.04	0.03	-	1.00–2.00% Mo
330	N08330	17.00–20.00	34.00–37.00	0.08	2.00	0.75–1.50	0.04	0.03	-	-

	347	S34700	17.00–19.00	9.00–13.00	0.08	2.00	0.75	0.045	0.03	-	Nb+Ta= 10C min, 1.00% max
	348	S34800	17.00–19.00	9.00–13.00	0.08	2.00	0.75	0.045	0.03	-	Nb+Ta=10C min, 1.00% max, but 0.10 %Ta max; 0.20% Ca
	384	S38400	15.00–17.00	17.00–19.00	0.08	2.00	1.00	0.045	0.03	-	-
	405	S40500	11.50–14.50	-	0.08	1.00	1.00	0.04	0.03	-	0.10–0.30% Al
	409	S40900	10.5–11.75	0.05	0.08	1.00	1.00	0.045	0.03	-	Ti =6(C + N)
	429	S42900	14.00–16.00	0.75	0.12	1.00	1.00	0.04	0.03	-	-
	430	S43000	16.00–18.00	0.75	0.12	1.00	1.00	0.04	0.03	-	-
	430F	S43020	16.00–18.00	-	0.12	1.25	1.00	0.06	>0.15	-	0.60% Mo
FERRITIC	430FSe	S43023	16.00–18.00	-	0.12	1.25	1.00	0.06	0.06	-	>0.15% Se
	434	S43400	16.00–18.00	-	0.12	1.00	1.00	0.04	0.03	-	0.75–1.25% Mo
	436	S43600	16.00–18.00	-	0.12	1.00	1.00	0.04	0.03	-	0.75–1.25% Mo; Nb+Ta= 5C min, 0.70% max
	442	S44200	18.00–23.00	-	0.20	1.00	1.00	0.04	0.03	-	-
	446	S44600	16.00–18.00	0.25	0.20	1.50	1.00	0.04	0.03	-	-

	403	S40300	11.50–13.00	0.60	0.15	1.00	0.50	0.04	0.03	-	-
	410	S41000	11.50–13.50	0.75	0.15	1.00	1.00	0.04	0.03	-	-
	414	S41400	11.50–13.50	1.25–2.50	0.15	1.00	1.00	0.04	0.03	-	-
	416	S41600	12.00–14.00	-	0.15	1.25	1.00	0.06	0.15 min	-	0.06% Mo
	416Se	S41623	12.00–14.00	-	0.15	1.25	1.00	0.06	0.06	-	0.15 Se min
	420	S42000	12.00–14.00	-	>0.15	1.00	1.00	0.04	0.03	-	-
MARTENSITIC	420F	S42020	12.00–14.00	-	>0.15	1.25	1.00	0.06	0.15 min	-	<0.60% Mo
	422	S42200	11.00–12.50	0.50–1.00	0.20–0.25	0.50–1.00	0.50	0.025	0.025	-	0.90–1.25 %Mo; 0.20–0.30% V; 0.90–1.25% W
	431	S41623	15.00–17.00	1.25–2.50	0.20	1.00	1.00	0.04	0.03	-	-
	440A	S44002	16.00–18.00	-	0.60–0.75	1.00	1.00	0.04	0.03	-	0.75% Mo
	440B	S44003	16.00–18.00	-	0.75–0.95	1.00	1.00	0.04	0.03	-	0.75% Mo
	440C	S44004	16.00–18.00	-	0.95–1.20	1.00	1.00	0.04	0.03	-	0.75% Mo
		S31200	24.00-26.00	5.50-6.50	0.03	2.00	1.00	0.045	0.03	0.14-0.20	2.00% Mo
DUPLEX		S31260	24.00-26.00	5.50-7.50	0.03	1.00	0.75	0.03	0.03	0.10-0.20	10.00% Wo; 3.00%Mo
		S31803	21.00-23.00	4.50-6.50	0.03	2.00	1.00	0.03	0.02	0.08-0.20	3.00% Mo

		S32001	19.50-21.50	1.00-3.00	0.03	4.00-6.00	1.00	0.03	0.03	0.05-0.17	0.60% Mo
	2205	S32205	22.00-23.00	4.50-6.50	0.03	2.00	1.00	0.03	0.02	0.14-0.20	3.50% Mo
	2304	S32304	21.50-24.50	3.00-5.50	0.03	2.50	1.00	0.03	0.03	0.05-0.20	0.60% Mo
		S32520	24.00-26.00	5.50-8.00	0.03	1.50	0.80	0.03	0.02	0.20-0.35	3.50% Mo
	255	S32550	24.00-27.00	4.50-6.50	0,04	1.50	1.00	0.04	0.03	0.10-0.25	3.50% Mo
	2507	S32750	24.00-26.00	6.00-8.00	0.03	1.20	0.80	0.035	0.02	0.24-0.32	4.00% Mo
		S32760	24.00-26.00	6.00-8.00	0.03	1.00	1.00	0.03	0.01	0.20-0.30	3.50% Mo
	329	S32900	23.00-28.00	2.50-5.00	0,06	1.00	0.75	0.04	0.03	-	
PRECIPITATION HARDENING	630	S17400	15.00-17.00	3.00-5.00	0.07	1.00	1.00	0.04	0.03	-	Cu 3-5, Ta 0.15-0.45 [13]

Martensitic stain steels

Martensitic stainless steels are essentially Fe-Cr alloys that contain between 12 and 17% Cr and between 0.15 and 1% C, enough carbon so that the martensitic structure can be produced from the heat treatments of the austenitized and the quenching.

This type of steel seeks to improve solidity and hardness, although this involves sacrificing resistance to corrosion. To improve this corrosion resistance, it must rise to almost 1% C, allowing the alloy to contain around 16% Cr to produce a martensitic structure by being able to perform austenitizing and having enough chromium to form the thin passive layer of chromium oxide.[479]

Within this type of stainless steels are the 440C alloys, which are higher hardness martensitic stainless steels, due to the martensitic matrix and the presence of primary carbides, as can be seen in the microstructure shown in Figure 69.

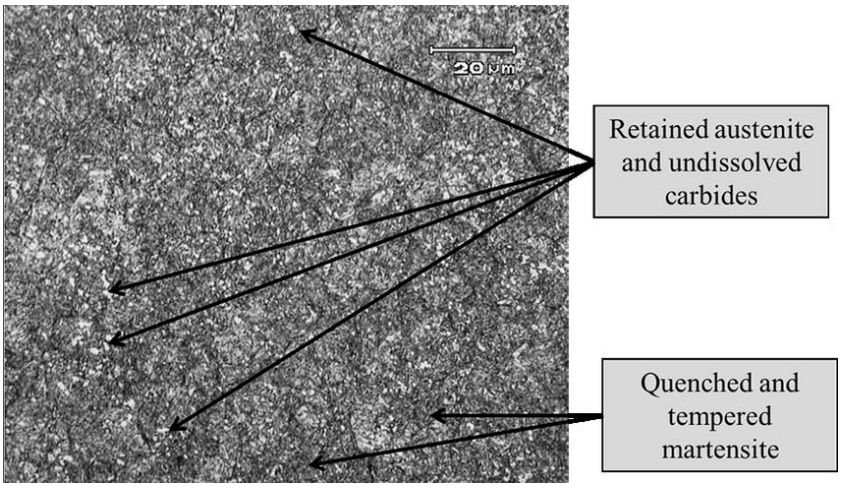

Figure 69. Martensitic stainless steel hardened by austenitized at 1010 ºC and tempered. The structure consists of primary carbides and ferrite phase retained in a martensite matrix. [W46]

Its main applications in the industry are turbine blades, valve seat linings, pump casings, valve and compressor bodies, shafts, spindles, bolts, cutlery, razor blades, and surgical instruments.

Austenitic stainless steels

This type of steels are ternary alloys of chromium nickel iron that contain between 16 and 25% of Cr and between 7 and 20% of Ni. Nickel has an FCC (face-centred cubic) structure and its presence in the alloy allows this structure to be maintained at room temperature, giving the material high moldability. These

steels also have a greater resistance to corrosion than those of the ferritic and martensitic type because the carbides are preserved in solid solution by means of rapid cooling.

If, on the other hand, said alloys cool slowly from high temperatures (600 to 870ºC), the carbides contained in the alloy precipitate in the limits of the grain, making the material susceptible to intergranular corrosion. This drawback can be avoided, in a way, by reducing the carbon content to approximately 0.03% C.

Austenitic stainless steels are best suited for use at temperatures as low as -270ºC. Due to this and their properties mentioned above, they are used in plants and equipment in the chemical and food industries. They are also often given architectural use.

AISI 316L Stainless steel

Stainless steel of grade 316L is classified as austenitic, body centred cubic (BBC). 316L has improved corrosion resistance if it is compared with others as 304L. This is because Molybdenum (Mo), which is a stabilizer of the passivating layer, has been added to the alloy.

The typical composition of the 316L stainless steel the nickel is added as an austenite stabilizer, in addition to increase the impact strength. The amount of Nickel (Ni) addition must be balanced again Chrome (Cr) and Mo content as both are ferritic stabilizer, face centred cubic (FCC).[480] The Cr and the Mo are added to increase the corrosion resistant of the stainless steel. The Cr form a passive chromium oxide layer, but is needed a minimum of about 11 wt.% Cr. [481] On the other hand, Mo also increases strength and hardness. The contribution can be seen at Mo contents as 2 wt. %. [480, 481]. Sometimes Copper (Cu) can be added to increase the corrosion resistance in acid environments, but is not as strong as Cr or Mo. [482] Other desirable characteristics may include excellent formability, high ambient temperature and cryogenic toughness, and good resistance to peeling, oxidation, and creep at elevated temperatures.[483]

Table 16. Chemical composition of AISI 316L stainless steel powder.[373]

	C	Si	Mn	Cr	Mo	Ni	Nb	Ti	Fe
Wt.%	0.02	0.50	1.80	16.70	2.00	10.00	0.02	0.05	Bal.

One common material for use in AM is stainless steel 316L due to its wide use in bio-materials, automotive parts, nuclear reactors and anywhere corrosion resistance in required. Binder jet metal parts manufactured using the 316L Stain Steel have a density close to that of metal, in other words, the porosity of the piece is negligible. This provides, sometimes, the part with mechanical properties similar to the conventionally manufactured parts. The aforementioned and the extensive existing knowledge about this

material were ones of the reasons why HP decided to use this material as the first material in metal 3d printing before moving on to other metals such as titanium or aluminium.

Although the material is widely known, the interaction of the printed part with the complex post-printing processes such as super solidus liquid phase sintering is not as well known. In this section, a description of this material will be featured below, evincing its chemical composition and other properties, focusing on the 316L powder.

The 316L stainless steel (SS316L) as an austenitic stainless steel is widely used in medicine and industry due to its good weldability and machinability and in combination with high corrosion resistance.[484]

Ferritic stainless steels

The ferritic structure of these steels is maintained at any temperature, therefore there are no transformations to other phases or the possibility of grain regeneration. Furthermore, recrystallization is possible by cold plastic deformation, previous annealing or by hot deformation.

This type of stainless steels have a composition with a maximum carbon content of 0.12% and between 11 to 30% of Cr. The chromium content has a negative influence on resilience (increasing %Cr decreases resilience). Ferritic stainless steels have a relatively low cost since they do not contain nickel. They have high resistance to corrosion and heat, but the presence of carbides reduces this resistance. New ferritic stainless steels with low levels of carbon and nitrogen have recently been developed, improving resistance to corrosion.

Its structural behaviour is governed by the guidelines of the crystalline form BCC (body-centred cubic structure). Its main application are as general construction materials.

Figure 70 shows the structure of a ferritic stainless steel consisting of an equiaxed grain ferrite matrix and dispersed carbide particles.

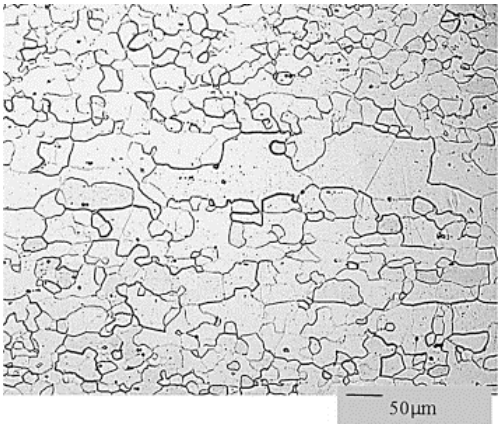

Figure 70. Microstructure of Ferrtic grain AISI409 stainless steel sheet showing fully ferritic structure.[485]

Due to their properties, we find that they are mainly used in: deep stamping of pieces; applications of resistance to cracking by corrosion of chloride stresses, in aqueous media, high-temperature oxidation and pitting corrosion; automobile exhaust pipes, radiator tanks, and sewers; decorative ornaments; parts of furnaces, nozzles and combustion chambers; and lastly hot water tanks.

Duplex steels

Duplex stainless steels, also known as austenitic-ferritic stainless steel, from the grade family with equal proportions of ferrites and austenites. These steels have a double microstructure that contributes to their high strength and high resistance to stress corrosion fracture. Another peculiar feature is that they are magnetic materials.

Due to their high chromium, nitrogen and molybdenum content, duplex steels offer good uniform and local corrosion resistance. These steels are also easy to weld. As previously mentioned, they are not hardened by heat treatment.

Duplex steels can be found in oil heat exchanger turbines, offshore platforms, gas wells, in valves used to handle seawater, or in smelter pumps. The chemical processing industry also employs them in some equipment, as do flagging and petrochemical plants. In short, they are usually used in corrosive media and at high temperatures.

Precipitation-hardened stainless steels

Their main alloying elements are iron, chromium and carbon (Fe-Cr-C), but also other alloying elements that produce the hardening by precipitation such as Molybdenum, Titanium, Nitrogen, Copper, Aluminium, Tantalum, Niobium, Boron and Vanadium.. This type of stainless steels have a chromium

percentage between 12 and 18% and nickel is between 4 and 9%. Its hardening is due to processes such as deformation hardening, aging and martensitic transformation.

The remarkable properties of these alloys are the high mechanical resistance compared to other stainless steels. It can reach a modulus of 1800MPa, much higher than that of martensitic stainless steels. It also maintains resistance to corrosion. Like duplexes, they have magnetism and good weldability.

Some of its applications are in parts that work at high temperatures such as heat exchangers and superheat tubes or steam boilers. Also aerospace and marine components, food product tanks, parts of pumps or in work tools such as saws, knives and flexible bellows type gaskets.

Stainless steel traditional manufacturing process.

The stainless steel manufacturing process begins with the selection of the raw material. The main raw material used is usually iron scrap, iron metal, ferroalloys, and other minerals. All of these must pass a rigorous control process that guarantees their quality.

Once the necessary materials have been selected, we proceed to what would be considered as the first phase, the steelworks. Here scrap metal is melted in a large capacity electric arc furnaces. These furnaces use graphite electrodes that allow high melting temperatures to be reached.

Continue refining the steel to remove impurities and reduce carbon content using a converter. The molten steel is brought to the converter using a transfer ladle. This phase begins with a blowing of oxygen and inert gas and ends with the refining of the alloy, reducing the carbon level of the broth, as mentioned. In addition, the metal present in the metal oxides is recovered and the sulphur content decreases. At this stage, the chemical composition of the alloy must also be controlled in real-time and precisely adjusted, adding the desired elements.

Subsequently, the steel broth is transferred to the pouring ladle, to later go to the trough. The trough is a large container that receives the steel from the ladle prior to its introduction into the continuous casting machine; therefore, it is a distributor where the retention of slag particles is facilitated and thus prevent it from reaching the mould. The next step is solidification through the continuous casting machine. Products obtained after solidification must be inspected to assess surface quality.

The hot rolling stage begins with the preheating of the solid steel in natural gas furnaces. The residual heat is recovered in a heat exchanger generating steam and thus reduces the carbon dioxide footprint. The first stage of rolling is carried out in a devastating reversible train in which a sheet of a specific thickness is obtained after several passes. Subsequently, jets of water are applied for chipping steel. Vertical cylinders make the edges of the sheets of good quality and thus a width within the desired range is obtained. The

winders inside the oven keep the temperature high and thus facilitate the process by preventing the material from hardening. After finishing, the steel sheet is cooled with water.

The next stage will depend on the desired thickness. If the thickness is between 2 and 10 mm, the steel sheet is passed through a winder obtaining a black coil. After this, the black coil is cold rolled. The properties of the metal must be recovered, carrying out a thermal regeneration. The annealing process consists of a heat treatment in which the austenitization temperature is exceeded and then rapidly cooled.

The thickness of the sheet can be adjusted by means of a specific reversible rolling mill, changing the cylinders at certain times in order to achieve a uniform and quality finish. Always, after each laminate, an annealing treatment must be carried out to recover the characteristic mechanical properties of stainless steels.

If you want to obtain the characteristic appearance of stainless steels, the sheet must be subjected to a pickling treatment. In addition, a matte or glossy finish can be given and, for this, the sheet will be passed through certain lines that give rise to a specific final finish. Thus, stainless steel is ready to distribute. [W47]

Annex B: Characterization techniques

Some of the most common techniques used are physical characterization including techniques for particle size analysis by laser diffraction (PSD), X-ray computed tomography (XCT) accompanied by spherical harmonic analysis (SH) for size and shape analysis, and scanning electron and light microscopy (SEM). Other techniques are sensitive to structure and chemistry, some examples are X-ray diffraction (XRD), energy-dispersive analytical X-ray analysis using X-rays generated during scanning electron microscopy(EDS-SEM), and X-ray photoelectron spectroscopy. (XPS)

In this section the applicability of these existing standardized powders measurement methods for AM powders are going to be explain.

BET technique

The gas absorption technique under isothermal conditions can be used to calculate the specific contact area of a solid in the adsorption of an inert gas at a low temperature as shown by the Brunauer-Emmett-Teller theory (BET) [486] or if the pore size is between 1.7-300 nm you can use the Barrett-Joyner-Halena model (BJH) [487]..

The BET method is based on the calculation of the number of adsorbed molecules, in this case of nitrogen, adsorbed in monolayer, that is, the number of molecules necessary to cover the wall of the solid with a single layer. When a gas comes into contact with the surface of a solid, an equilibrium between adsorbed molecules and molecules in gas phase, which depends of the gas pressure and temperature. The relationship between the adsorbed molecules and the pressure at constant temperature can be collected in an adsorption isotherm. These isotherms directly report the volume adsorbed at a certain pressure and they also allow us to calculate the surface area of the solid, the size and shape of the pore and its distribution, heats of adsorption, etc. The BET technique uses the principle of the physical adsorption of inert gas (nitrogen) to vary the relationship between the partial pressure of the gas and the vapour pressure at the temperature of the liquid gas. The technique can be performed statically or dynamically.[488]

There are also calculation procedures that allow determining the distribution of pores. The IUPAC classification for the pore size is given by macroporosity (when pore diameter is larger than 50nm), mesoporosity (between 2 and 50 nm) and microporosity (smaller than 2nm). It is known that the BET successfully accounts for pores below about 100nm, but we can obtain through mathematical analyses of BET technique such as t-plots or Dubinin-Radushkevich method the information related with smaller pores (microporosity).[489-491]

The term adsorption was introduced in 1881 to connote the condensation of gases on the free surfaces, unlike the gas absorption in which the gas molecules penetrate into the solid. Physical adsorption has been defined by the IUPAC as enrichment or emptying of one or more components in an interface.

A generalized treatment of the physical adsorption isotherm of Langmuir. The BET equation allows the calculation of the monolayer surface (Eq. 31) [492].

$$\frac{\boldsymbol{P}}{\boldsymbol{V_a(P_0 - P)}} = \frac{\mathbf{1}}{\boldsymbol{V_m \cdot C}} + \frac{\boldsymbol{C - 1}}{\boldsymbol{V_m \cdot C}} \cdot \left(\frac{\boldsymbol{P}}{\boldsymbol{P_0}}\right) \qquad \textbf{Eq. 31}$$

Where:

- V_a: amount of adsorbed gas at a pressure P
- V_m: amount of adsorbed gas when the surface is covered by a monomolecular gas layer
- C: is a constant for the gas-solid combination. It represents the relative strength of adsorption to the surface and condensation of the pore adsorbate.
- P_0: Saturation gas pressure (vapour pressure).

Experimental procedure works following the next steps: add more than 100 mg of the solid sample in a quartz recipe of 50 mL, the solid is outgassed at 100ºC overnight (approximately 20h), reaching a vacuum less than 10Pa. Then, it is weighed and analysed. The vacuum is made at room temperature and the empty space is measured in the following way: introduce helium in the manifold at 850 mmHg and it is passed to the tube and the pressure is read after its stabilization. The tube is cooled to 77K, it is stabilized and the pressure is read again. The available volume is determined by the change of pressure and temperature. The He is removed and nitrogen gas is introduced and adsorbed. Progressive nitrogen P/P_0 ratios are used to perform a multi-point BET adsorption / desorption test. The BET Surface area (S_{BET}), pore volume (V_{BET}), mean pore diameter (Φ_{BET}) and C parameter were obtained from adsorption isotherm of N_2 at 77K. [493]

Microscopy and image analysis.

Microscopy is a technique used to observe and measure the particles individually. Microscopic methods have the advantage that they not only allow the size of irregularly shaped particles to be measured, but also their shape and structure. On the other hand, the drawback is that the preparation required for the powder sample is meticulous and time consuming. This is the reason why these methods are used more in research than

There are various microscopy techniques, and their use will depend on the desired resolution. For example, the interference effects do not allow to obtain reliable results when observing particles of sizes smaller than one micrometre through an optical microscope. In contrast, scanning electron microscopy (SEM) overcomes this difficulty, being a powerful method for examining powders.

Optical microscope

Regarding the preparation of the sample to carry out a metallographic study, it is known that it can be done in a variety of ways depending on the equipment available and the material used. The general steps to be followed are outlined below.

The tablet will be prepared first. As it is a powder, a cold drawing will be carried out since we will avoid any structural modification and it will also be easier to prepare. The two main aspects that must be taken into account when selecting the resin to use are hardness and the so-called "edge effect". The hardness of the resin must be similar to the sample to be studied in order to avoid that the surface of the tablet undergoes undesired deformation after polishing. If the surface of the sample is not straight and parallel to the opposite face, when it is analysed through the microscope, it cannot be focused. On the other hand, the "edge effect" occurs when the resin and the sample do not stay completely together. This can be a problem since in this small gap, the elements used in polishing or chemical attack can reshape and cause an unwanted over-attack. If the sample is large there is no problem because only the surface would suffer this effect, but since the sample to be analysed are formed by small particles, avoiding this effect is of great importance. As mentioned, cold drawing is selected using moulds. Two types of resins can be used: methacrylate or epoxy. Methacrylate resins harden quickly (approximately 15 minutes) and there are several types, depending on the desired hardness. This type of resins is the most widely used. Epoxy resins, on the other hand, have a long hardening process (6 hours). They are transparent and are used if the edge effect needs to be minimized as much as possible. On the other hand, the type of mould also influences the edge effect. If a soft silicone mould is used, it undergoes a slight deformation during the curing of the resin and this can make the unwanted effect more pronounced. On the other hand, hard moulds like Teflon do not cause this problem. It is true that if the epoxy resins are used, only polypropylene moulds can be used since they are the only ones that will not be attacked by the epoxy resin. In the case of metallic powder, what is done is to add a small amount of powder, forming a thin layer at the bottom of the mould, and then it is completely filled with the selected resin.

After drawing, we proceed to roughing and sanding. In this process, there are different aspects to take into account such as the applied pressure, the speed of rotation, the type of sandpaper, among others. The turning speed of the sanding should be between 150 and 250 rpm. Working at higher speeds is not recommended as it would cause a scratch on the surface and then it is difficult to remove such scratches. If the metal is soft, the speeds should be as low as possible. Try to make the direction of rotation the same as that of the plate of the sample holder head. This is also done to avoid unwanted scratches. There are

different types of sandpaper and they will be used depending on the material to be sanded. Silicon Carbide sandpaper is the most widely used sandpaper, zircon sandpaper is used for grinding as it has a high sanding power, and it does not pollute as silicon sand does. Finally, diamond sandpaper is the sandpaper that achieves great flatness in the samples and removes a large amount of material in a short time. They are the most recommended in hard materials. Sanding must also take into account the applied pressure, which will depend on the grain size of the sandpaper and the material. If it is desired that the sample be not heated during sanding, water, or alcohol can be made to flow, which will act as lubricants. After each step, the surface and sandpaper must be cleaned with water.

The next step is to polish. In this operation, the turning speed will depend on the polishing material, but should never exceed 200 rpm. There are several types of fabric, depending on the polishing material and grain size. For initial polishing, monocrystalline or polycrystalline diamond cloths with a grain size between 15 and 1 micron are used. Monocrystalline diamond has the advantage of having a better value for money and is, therefore, the most widely used. Polycrystalline diamond is more efficient but its cost is higher, so it is generally used in hard materials. For final polishing, polishing oxide cloths (alumina or silicon) with a grain size of less than 1 micron are generally used. Alumina is used only when you want to do a high magnification study without scratches. Its grain size is 0.06 microns and it is widely used in the polishing of hard materials as steel particles. Final polishing with silicon or colloidal quartz is also used for high-magnification studies, but is instead used on soft materials such as aluminium, bronze, or copper. If it is titanium, a silicon gel with an acidic pH should be used, since this prevents distortion of the metallographic structure during said polishing. As can be seen, during the polishing process the cloths are changed, to obtain a smoother surface, until reaching a mirror surface. It is very important to have a great cleaning of the samples between cloth and cloth, even more than in sanding. In the case of the alumina cloth, it is vitally important to clean the cloth with water since if it is not cleaned, the cloths will crack when dried and can no longer be used.

At the end of everything, depending on the metal to be studied, a chemical attack must be carried out to reveal the phases. In addition to all of the above, there are different aspects to consider depending on the metal. [W40]

Scanning Electron Microscope (SEM)

A SEM uses a focussed beam of electrons to create a magnified image of a sample. The electron beam is scanned in a regular pattern across the surface of the sample and the electrons that come out of the sample are used to create the image, as you can see in the Figure 71.

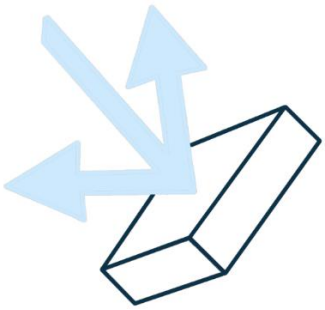

Figure 71. Electron band of SEM [W49]

Secondary electrons give information of the surface topography while backscattered electrons give images of surface composition. X-rays characteristic of the chemistry of the material are generated as a result of the interaction of the electron beam with the sample, and provide a qualitative analysis of the chemistry and, with the proper calibration of the instrument, also quantitative. (Figure 72). The interaction volume for X-ray microanalysis depends on the accelerating voltage. For steels, an accelerating voltage of 15 kV allows the analyses to have a sensitivity of a depth of approximately 1 µm. [W50]

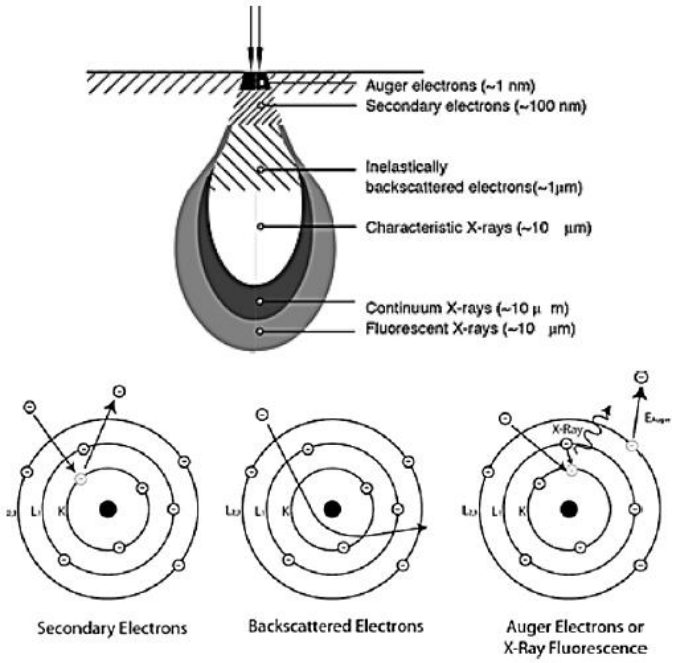

Figure 72. Volume of interaction on a compact sample and the origin of the different detectable signals and b) Different modes of emission of electrons from the incidence of an electron beam: Secondary electrons are inelastically dispersed and elastically backscattered. The Auger electrons and the X-rays are caused by the ejection of electrons from inner layers compensated by electrons from higher orbital layers, thus occupying the vacant energy level, or there is an excess of energy in the form of a characteristic X-ray or the expulsion of an electron to an outer orbital.

In an electron microscope, electromagnets are used to focus the electrons as it is shown in the Figure 73. The interaction of the electron beam with the surface of the sample affects the images that we achieve. The most significant working parameters are: the electrical voltage, the spot size, the display magnification and the working distance (WD).[494]

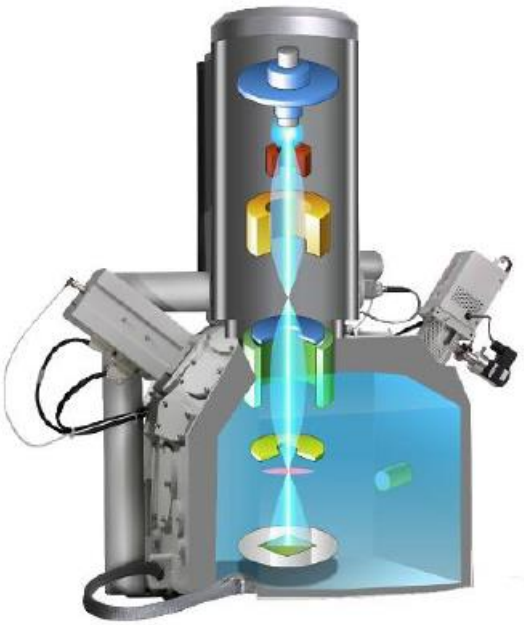

Figure 73. SEM equipment [W49]

This technique is highly versatile due to the high magnification capacity, greater than 10,000 magnifications and the ability to produce three-dimensional images. This last characteristic derives from the fact that its depth of field is one hundred times that corresponding to an optical microscope (in the range of 1 µm at 10,000 magnification and 2 mm at 10 magnification).[495]

As already mentioned, the SEM can offer different information depending on the detector used. The most commonly used detectors are detailed below:

- Secondary Electron Detector (SE) - Provides a typical black and white image of the surveyed surface topography. This is the most suitable signal for observing samples, as it has the highest resolution.
- Backward Scattered Electron Detector (BSE): also offers a surface image but with a lower resolution. Its advantage is that it is sensitive to variations in the atomic number of elements on the surface. On a smooth surface, you will see different shades of grey depending on whether there are multiple phases with different elements.

- X-ray detector (EDS): receives X-rays from each point on the surface scanned by the electron beam. Since the energy of each radiograph is characteristic of each element, it provides qualitative and quantitative analytical information on areas of the desired size on the surface. For this reason, this technique is known as EDS Microanalysis. This technique gives information about "Bulk" concentration of elements present in a sample, but very little information about the speciation or oxidation state of each element.[496, 497]
- X-ray Detector (WDS): Similar to the previous detector, but instead of receiving and processing the energy of all X-rays at the same time, it only measures the signal generated by a single element. Although this technique is slower, it makes it much more sensitive and accurate than EDS. They are complementary, since EDS offers good information on all the elements on the sample surface, and WDS can solve peaks of elements whose emission energies are very close and can detect much smaller concentrations of any element, particularly light elements.
- Electron backscatter diffraction detector (BSED): in this case, it only receives electrons diffracted by the surface of the sample that comply with Bragg's law at the point where they are generated, that is, the signal provides information about the crystal structure of the sample. If you already know the crystalline phase or phases in your sample, the system can process the received signal as Kikuchi lines and offer various crystallographic information: grain orientation, relative orientations, texture, phase identification, pressure evaluation, grain edges and size grain.

The powder sample should be prepared as follows: deposit a small amount on a sample holder, fixing it with a double-sided carbon tape. It is necessary that the tape be carbon since both it and the sample must be electrically conductive to avoid the accumulation of electrostatic charges on the surface. In order for the analysis obtained with this technique to be accurate, it is necessary to work with a smooth and flat surface and appropriate reference standards for the calibration.

The SEM is used for the study of all the morphological properties of the particles (size, shape, surface structure, coating or oxide films, inclusions, surface voids, roughness and others).

Electronic probe X-Ray Microanalysis (EPMA)

Electronic microprobe analysis (EPMA) is a modern technique, of great precision and sensitivity. EPMA is an SEM but its purpose is to perform quantitative X-ray microanalyses using dispersive wavelength (WDS) and energy dispersive (EDS) spectrometers to determine the chemical composition of a solid substance, in very small areas (on a micrometre scale). [497]

As mentioned, the SEM usually has an EDS incorporated, but there is no mistaking it for the EPMA. Compared to EDS, the sensitivity of EPMA is 100 times better, reaching concentrations as low as 10 ppm. Another advantage that it presents is the spectrum resolution is from 4 to 60 eV, which in the EDS is 150eV. In short, all these advantages and many other more characteristics such as the higher imaging speed or

the low probability of peak overlap, make the EPMA perform more direct measurements of the X-ray intensities, which translates into greater precision and accuracy.[498]

EPMA is fundamental for the development of qualitative and quantitative analysis, the principle of which is to bombard a fine electron beam directed at a specimen in order to measure wavelength and intensity of the characteristic X-rays emitted, as well as the intensities of the secondary electrons and backscattered electrons. EPMA allows simultaneous analysis of the microstructure or phase distribution together with that of the composition. [499]

In quantitative analyses, the intensities of the specimen's x-ray lines are compared to those caused by standards of known composition. The measured intensities require certain instrumental corrections, including background removal, which is primarily the source of the "continuous spectrum" (photons emitted by decelerated electrons in collisions with atoms). The composition at the analysed point is calculated based on the intensities, corrected by the "corrections matrix", which takes into account the different factors that govern the relationship between intensity and composition called "matrix effects" (atomic number (Z), absorption (A), and fluorescence (F)). This is what is commonly applied in the form of ZAF corrections [500]. Correction factors for a standard specimen of the known composition should be determined in advance through the ZAF routine. The relative intensity of the K peak is determined by making a dead time correction and a reference correction on the measured X-rays. [W51].

As previously mentioned, it resembles an SEM and is therefore made up of parts similar to those that can be observed in SEM-EDS. One of the components is an optical-electronic system (EOS), consisting of an electron gun and a series of condenser lenses and apertures. A tungsten filament is commonly used to generate the electron beam by thermos-ionic emission. The created electron beam is directed through a vacuum chamber using the lenses to be focused on the surface of the sample. Another component is the WDS spectrometer, named above. This consists of a monochromemeter and a detector. The monochromemeter is a crystal that scatters X-rays according to Bragg's law of reflection. Most electronic microprobes are equipped with several crystals of different d spacing to allow analysis of a wide range of X-ray wavelengths. The most common crystals are lithium fluoride (LIF), pentaerythritol (PET), and thallium acid phthalate (TAP). These crystals cover all the X-ray wavelengths generated by the elements from Z = 5 (Be) to Z = 92 (U). For lighter elements, a larger space is required, and therefore the use of lead sterate films or laminated materials is required. [501] Like the SEM kit, an EPAM kit has an energy dispersing spectrometer (EDS). This solid detector allows us to analyse simultaneously all the energies of the X-ray photons. This is an advantage over the WDS since it allows a much faster mapping of compositions. EDS detectors are made up of a semiconductor, usually, Silicon or Germanic, connected to a field-effect transistor (FET) that serves as a preamplifier. The absorption of the X-ray photons through the detector crystals leads to the ejection of a photoelectron that precipitates the formation of multiple

electron-hole pairs, which are then converted to a charge pulse which in turn is converted to voltage pulse that is amplified, formed and finally analysed by the associated electronics.[501, 502]

For these techniques, the sample must be conductive. One way to prepare the sample will include the powders into resin inside an aluminium tube. Once the resin has cured, a metallographic polishing will be carried out. Specimens should be finely polished or naturally have a flat surface. Then, it will be covered with a thin film of carbon, gold or aluminium by vapour deposition to guarantee electrical conductivity with the equipment sample holder. [503]

Dual Beam: Focused Ion Beam (FIB) and field emission scanning electron microscope (FESEM).

The dual beam microscope integrates the features of a field emission scanning electron microscope (FESEM) with a focused Gallium ion beam (FIB) microscope.

An FIB is comparable to a SEM, but instead of electrons, it uses a Ga^+ ion beam. Ga^+ ions are much heavier than electrons, causing stronger interaction with the sample with a lower penetration level. Because of all this, ions cause a breakdown of chemical bonds and ionization of atoms on the surface of the substrate. Since the ion beam can be focused and controlled, this effect can be used to modify the structure of the sample at the nanometre scale.

On the other hand, the FESEM can work independently, with the FIB column turned off. The FESEM is an instrument very similar to the SEM, capable of offering a wide variety of information from the surface of the sample, but with higher resolution and a much higher energy range. The operation is the same as that of a conventional SEM, an electron beam is swept over the surface of the sample. The biggest difference between FESEM and SEM is the electron source. The FESEM uses as a source of electrons a field emission gun that provides highly focused low and high energy electron beams, which greatly improves spatial resolution and allows working at very low potentials (0.02 - 5 kV). Thanks to this, the loading effect on non-conductive specimens is minimized and damage to samples sensitive to the electron beam is avoided. Another very remarkable feature of the FESEM is the use of detectors inside the lens (in lens), which work at high resolution and very low acceleration potential, so they are essential to obtain maximum performance from the equipment.

Depending on the manufacturer, the Dual Bean is made up of different components. Among the most common detectors is the secondary electron detector (SE2) that provides SEM topography images of the sample surface with a large depth of field; the backscattered electron detector (4QBSD) that is sensitive to the variation of the atomic number in the elements present in the sample; secondary electron detector in the lens, works with low energy secondary electrons and offers the highest resolution images; X-ray dispersive energy detector (EDS), which receives X-rays from each of the points on the surface over which

the electron beam passes, providing qualitative and quantitative analytical information on the surface of the sample; and a backscattered dual lens secondary electron detector (EsB) located within the electron column and independent of the secondary lens detector, offers a pure backscattered signal, with no secondary electron contamination and very low acceleration potential. The latter has two working modes:

- The secondary electron detector in the lens works with low energy secondary electrons and provides images with a higher resolution. It is very sensitive to the characteristics of the surface of the sample, which makes it very suitable for characterizing the surface of any material. It works best at low acceleration potentials (<5 kV), therefore it is highly recommended both for working with samples sensitive to the electron beam and for minimizing the loading effect on non-conductive samples.
- The backscatter (EsB) electron detector on the lens allows us to obtain a pure backscatter signal at a very low acceleration potential. It provides great Z contrast and can select electrons according to their energy, allowing us to differentiate elements that can only be distinguished by a few atoms. It can also operate at very low voltage (in the same range as the secondary detector on the lens), making it ideal for sensitive samples.

The advantage of combining electron and ion columns on the same platform is that it allows us to simultaneously obtain high-resolution SEM images and make modifications to the sample with the ion beam.

Its most common applications are related to the study of cross sections, the preparation of ultrafine samples, the three-dimensional reconstruction of the volume of a sample and lithography of electrons and ions.

Atomic Force microscopy (AFM)

The atomic force microscope (AFM) is a mechanical-optical technique capable of detecting forces of the order of the piconewtons [504, 505]. It is made up of a flexible overhang, with a sharp tip/needle at the end that serves to scan the sample. It slides on the surface of the sample exerting a low and constant force of interaction. The scanning motion is accomplished with a piezoelectric scanner, and the needle-sample interaction is monitored by reflecting a laser at the rear of the overhang. A photodiode collector detects the reflected electromagnetic wave.[506, 507] The photodiode is divided into 4 segments and the different voltages between the different segments (generally the upper 2 segments compared to the lower 2 segments) accurately determine changes in tip slope or oscillation amplitude (Figure 74).[505, 508]

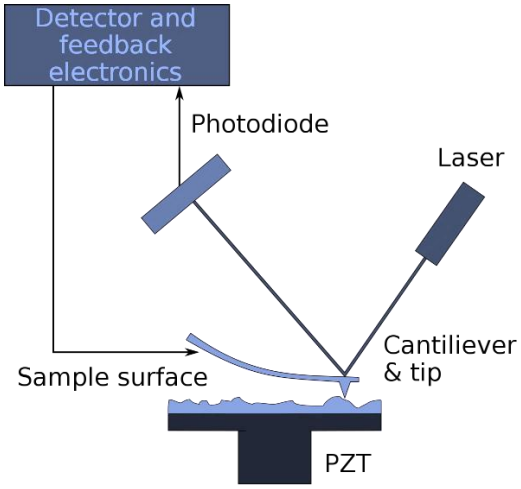

Figure 74. Atomic force microscope

Next, different ways of working that this technique presents are specified[509]:

- Contact AFM: used to measure topography. The needle is dragged on the surface of the sample.
- Tapping AFM: The operation is similar to the previous one, but in this case, an oscillating needle sweeps the surface with intermittent movements. These can damage soft samples and reduce image resolution. It is used if you want to eliminate lateral drag forces or pressures.
- Phase Image - Provides a contrast image caused by differences in sample surface adhesion and viscoelastic properties.
- Scanning tunnel microscope. It is used to carry out a topographic analysis of conductive surfaces since it uses a tunnel current, which will depend on the separation between the needle and the surface of the sample.
- Magnetic forces: measures the gradient of distribution of the magnetic force on the surface of the sample. It is done in elevation mode to follow the sample topography at a set distance.
- Lateral forces: measures the friction forces between the needle and the surface of the sample in contact mode.
- Electrochemical: measures changes in the surface and properties of conductive materials immersed in electrolytic solutions by establishing gradients or cycles of electric intensity-voltage.

Laser diffraction (LD) technique

Laser diffraction (LD) is used to measure the particle size distribution (PSD) of metal powders. A low energy laser beam passes through a suspension of particles producing a diffraction image because the laser light

is scattered at different angles, depending on the individual size of the particles.[510] Large particles scatter light at small angles relative to the laser beam, and small particles scatter light at large angles, as illustrated below (Figure 75).

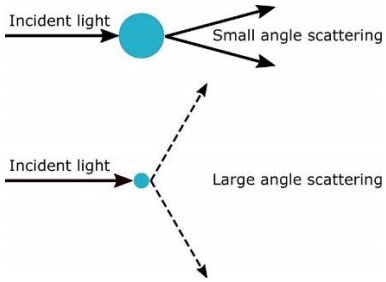

Figure 75. The different angles depending on the particle size.

The angular dependence of the intensity distribution is recorded by means of a multi-element detector, and a data processor calculates the equivalent particle size distribution from the measured signal. Particle size is recorded as a sphere diameter equivalent to volume. In other words, the spherical particle size distribution is obtained after mathematically inverting the diffracted light pattern or the total dispersion, obtaining the diameter of the spherical particles and with this the surface area (Figure 76).

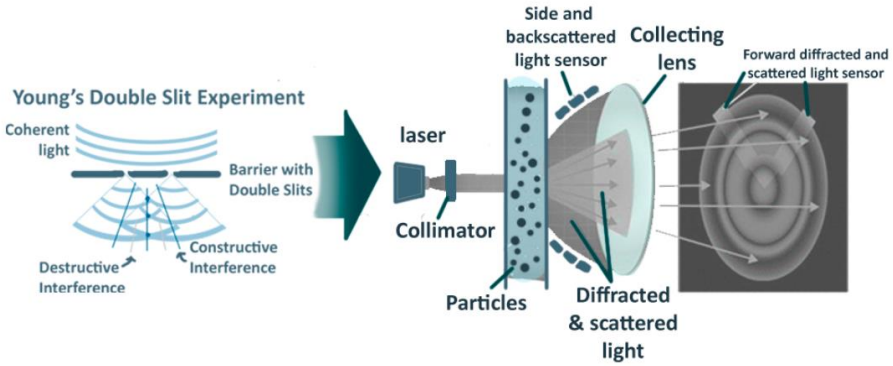

Figure 76. Basis of the operation of the Laser Diffraction technique.

In order to carry out the measurement, the particles must be dispersed either in liquid or in gaseous medium. The first technique is known as the wet method (LD-W) and a suspension is obtained. The second is called the dry method (LD-D) and it is worked with an aerosol. Depending on the type of powder material, one of the two techniques will be ideal. For metallic powders such as stainless steel, the LD-W method guarantees complete dispersion and reduces the risk of ignition. [511] Liquid dispersion of the powder is also necessary to ensure an accurate measurement since the particles must be measured individually. For this, they must be present as discrete and separate particles. It is true that the equipment

consists of a circulation unit that moves the powder in such a way that when passing through the measurement area (laser beam) it creates a laminar flow representative of the total mass, but the dispersion prevents adhesive bonding in agglomerates and therefore the results will be optimal. The liquid commonly used for this type of material is alcohol isopropanol, but it is true that any transparent liquid, with a viscosity less than 2 Pa·s and inert with metal can be used.

The main advantage of the LD method is that it is fast, and if proper dispersion is achieved, repeatable. Other advantages are: a small amount of sample is needed, the range of particle size that is detected by this technique is wide (between 0.1 and 2 µm), the waiting or preparation time between measurements is short and therefore they can be done measurements successively. The main disadvantage is that the mathematics behind the LD method assumes spherical particles.

The procedure to be followed according to the ASTM B822-10 standard consists of the following steps. After performing the blank measurement, 25 measurements of the powder sample should be made. For this, good uniform dispersion of the particles in the liquid is first achieved by vigorous mechanical mixing and / or by ultrasound. The averages obtained in each measurement must be similar to the rest of the samples for the data to be consistent. Since the measurement principle is absolute, the units of measurement do not require calibration.

The data can be analysed in two possible ways, depending on the size of the particles. One of the ways is by applying the Lorenz-Mie-Debye theory, which is an analytical solution to the Maxwell set of equations that describe electromagnetic phenomena.[512, 513]. This theory is applied to evaluate the size of the particles from the distribution of the scattered light angles, taking into account both scattering angles less than 90 ° (forward), and scattering angles greater than 90 ° (backward). In order to use the intensity distribution determined in this way to calculate the size of the particles, Mie's theory requires knowing the actual refractive index and the absorption index of the material sample. The lower limit of the particle size range to apply the Mie theory is 10 nm. If the particles are smaller, the scattering intensity stops depending on the direction, that is, the Rayleigh scattering occurs and therefore the dynamic light scattering will be used. [W52]

Conversely, if the particles are larger than 7 µm, Fraunhofer's theory should be used, which simplifies the calculation of the distribution since it describes the section of the light deflection that occurs exclusively with diffraction and also does not require that the refractive indices of the particulate material are known. The downside is that this procedure is essentially accurate for spherical particles, but is only an approximation for non-spherical particles.[510]

The results can be displayed as a frequency distribution or as a cumulative frequency distribution such as it is shown in the Figure 34.

X-Ray Computed Tomography (CT)

X-ray computed tomography (CT) is a non-destructive characterization technique based on the acquisition of X-ray radiographs of hundreds of different angles of a sample and its subsequent analysis using computational algorithms. The data obtained after scanning are thousands of cross-section images that when stacked together form a three-dimensional image of the sample. Once the images are assembled, a grayscale filter is applied to make the particles white and the background black. Specialized software is used to count and study the particles.

One way to prepare the sample for dust analysis is to embed the metal particles in epoxy cylinders about 3 mm in diameter.

The size distribution is also measured using this technique, as well as by laser diffraction, but the CT provides an independent estimate and uses different size parameters to measure the PSD. However, it uses fewer particles, so the PSD curves are generally not as smooth.[510, 514, 515]

X-Ray photoelectron spectroscopy (XPS)

High resolution XPS spectra allow the determination of the chemical species present in the samples by comparative spectrum adjustment with literature for binding energy (BE) and full width at half maximum (FWHM) for the various chemical species [516, 517], in this case pure metals and possible metallic oxides. X-ray photoelectron spectroscopy (XPS) is a surface sensitive analytical tool that provides information on the chemical state and concentration of surface elements (<10nm). X-rays are sent to the sample and ejected electrons from sample are detected. The main signal comes from the surface (a few atomic layer at surface) due to the escape depth of electrons. [218, 518, 519]

It is true that not all elements can be detected since, due to their atomic size, hydrogen and helium are not detectable. In fact, this technique has a detection limit of <0.1 atomic percent. Photoelectrons are emitted from the solid when exposed to a flow of X-ray photons of known energy, hv, where h is the Plank constant and v is the frequency of the photons. Photoelectrons come from discrete levels of electron energy associated with atoms in the analysis volume. The kinetic energy (KE) of the emitted photoelectrons, and therefore the entire photoelectron spectroscopy, is expressed by Einstein's

photoelectric law, KE = hv - BE, where BE is the energy of binding of the particular electron to the desired atom. Since hv is known, a measure of KE determines BE.

The XPS technique allows an exact and unequivocal elemental identification. The spectrum obtained is unique for each compound because the emission of the electrons occurs from the different layers, in other words, the energy separation and the relative intensities of the spectrum peaks for a given element are well known. Furthermore, ionization for the *p*, *d* or *f* layer levels leads to doublet structures in the spectrum as a result of spin-orbit interactions. Therefore, elements with higher atomic numbers have peaks that reflect the energy separations of the rotating orbit. Many of these transitions are characteristic of the element in a particular oxidation state. All these data obtained are of great interest to analyse the surface of the particles. Know if they are oxidized or if they have undergone any chemical change after being used in the AM process.[518]

One of the drawbacks of such a technique is that certain materials are sensitive to surface photoreduction and the effects of ion beam damage.[518]

The analysis is performed over a small area, - within a range of 70-100 µm2, and should be analysed in an ultra-high vacuum environment. In the case of metallic powders, it will not be necessary to neutralize the coaxial load. The powder samples were mounted on the multiple sample bar using carbon tape, it can be the one used in the SEM.

X-Ray Diffraction (XRD/XRPD)

Powder x-ray diffraction (XRD/XRPD) uses x-rays to investigate and quantify the crystalline nature of materials by measuring the diffraction of x-rays from the planes of atoms within the material (Figure 77). It is sensitive to both the type of and relative position of atoms in the material as well as the length scale over which the crystalline order persists. It can be used to measure the crystalline content of materials; identify the crystalline phases present; determine the spacing between lattice planes and the length scales over which they persist; determination of network parameters; high temperature structural studies; characterization of thin films and analysis of their crystal structure; and to study preferential ordering and epitaxial growth of crystallites. That is why it can be said that it is a qualitative and semi-quantitative technique of the crystalline forms of the materials.

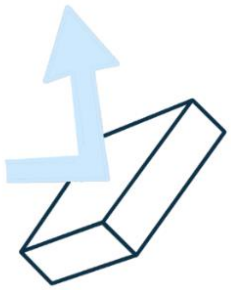

Figure 77. Electron band of XRD [W49]

The samples for analysis are typically in the form of finely divided powders, but diffraction can also be obtained from surfaces, provided they are relatively flat and not too rough. Powder XRD can also be applied to study the pseudo crystalline structure of mesoporous materials and colloidal crystals if the length scales are in the correct regime. Moreover, the materials can be of a vast array of types

In order to process the data obtained and to be able to carry out the phase identification, the diffraction database of the International Center for Data Diffraction is generally used, which catalogues the X-ray diffraction patterns of thousands of crystals. [W53]

Rietveld analysis of the diffraction data can provide quantitative estimates of the different crystal phases in terms of volumetric fraction. In the case of steel alloys, the Rietveld analysis is difficult to perform and provides semiquantitative data. [520-522] ASTM E975 standard describes a process for determining steel austenite using XRD as accurately as possible. In the case of typical Fe-Cr-Ni stainless steels, the XRD technique can be used to estimate the thickness of the protective layer, since it is easy to differentiate between crystalline forms.

A possible assembly can be the one described by *Slotwinski, J.A. et al*. They used a cavity approximately 12 mm × 20 mm and 800 µm deep and filled it with dust grains and the surface was leveled with the surface of the sample holder. The ideal is to have a fine powder, less than 5 µm in size, since a coarse particle size together with a spherical geometry results in a porous surface with a rough texture. If an attempt is made to mechanize the sample, applying pressure and heat, to obtain an ideal sample (without porosity and smooth surface) the materials to be studied will be modified, and this is not desirable. That is why the powders will be studied without any processing.[218]

The dust samples were uniformly dispersed on a ground object holder or adhered with silicone grease according to the goniometer used, if it is of vertical or horizontal displacement, respectively. The important thing is that a sufficiently high number is analysed and that the constituent grains of the alloy contains

crystals with all possible orientations to provide a significant statistic for the diffracted intensities.[523-525] The radiation used for most Fe base alloys was that of Mo with λ_{M0} = 0.7093 A corresponding to the line K_{a1} = 17.470 Kev. [526]. According to the study carried out by XX, this choice may be disadvantageous due to the poor detail of the x-ray spectrum, the angular width of which extends to 2O = 65º, with other radiation, such as Cu, covering a greater angle.

The aforementioned is based on the reduction of the intensity of the diffracted radiation due to the intense absorption of the primary radiation λ_{Cu} by the elements of the sample. The decrease in the intensity of the diffraction peaks I_o to a value I is defined by the equation Eq. 32, where x is the thickness of the material, ρ is the density of this material and μ/ρ is the mass absorption coefficient.

$$\frac{I}{I_0} = e^{\frac{\mu}{\rho}x} \qquad \textbf{Eq. 32}$$

The Table 17 shows a study carried out by JI Goldstein et al. on the effect of the absorption of primary radiation from Cu X-rays by atoms of other elements, compared to that of Mo.[526]

Table 17. Effect of absorption of the primary radiation of Cu compared to that of Mo in various elements, absorbed by the effect of blooming. (Z atomic number, A atomic weight) [526]

Absorbent element				Transmitter					
				Cu ($E_{k\alpha1}$=8048 eV)			Mo ($E_{k\alpha1}$=17479 eV)		
	Z	A	ρ [g/cm³]	μ/ρ [cm²/g]	I/I_0 [% 1μm]	I/I_0 [% 10μm]	μ/ρ [cm²/g]	I/I_0 [% 1μm]	I/I_0 [% 10μm]
C	6	12.01	2.25	4.4	99.0	90.6	0.4	99.9	99.1
Al	13	26.98	2.70	49.4	87.5	26.3	5.0	98.7	87.4
Si	14	28.09	2.70	63.7	84.2	17.9	6.5	98.3	83.9
Cr	24	52.00	7.10	250.4	16.9	0.0	29.6	81.0	12.3
Fe	25	54.94	7.40	272.4	13.3	0.0	32.7	78.5	8.9
Co	26	55.85	7.87	306.0	9.0	0.0	37.3	74.6	5.3
Ni	27	58.93	8.90	329.4	5.3	0.0	40.7	69.6	2.7
Cr	28	58.71	8.90	49.0	64.7	1.3	46.8	65.9	1.6
Cu	29	63.55	8.96	52.4	62.5	0.9	49.2	64.4	1.2
W	74	183.9	19.3	172.5	3.6	0	97.8	15.1	0

Bibliography

[W1] "3D Cad portal" [Online] Available: http://www.3dcadportal.com/errores-mas-comunes-en-archivos-stl.htm [Last Accessed: 04/03/2020]

[W2] F.COTEC, "Fabricación aditiva" Design studies 2011 [Online] Available: http:/www.informecotec.es/media/N30_Fabric_aditiva.pdf [Last Accessed: 04/03/2020]

[W3] "A Quick Guide to 3D Printing Metals" [Online] Available: https://amfg.ai/2018/04/12/metal-3d-printing/ [Last Accessed: 07/06/2020]

[W4] "AMPOWER: Management consulting for additive manufacturing" [Online] Available: https://am-power.de/ [Last Accessed: 07/06/2020]

[W5] "Guía completa: Fusión láser de lecho de polvo, te explicamos todo! 3D NATIVES" [Online] Available: https://www.3dnatives.com/es/sinterizado-directo-de-metal-por-laser-les-explicamos-todo/ [Last Accessed: 07/06/2020]

[W6] "A Complete Guide to Metal 3D Printing - Technologies that are Shaping the Future of Metal Manufacturing" [Online] Available: https://www.globenewswire.com/news-release/2020/02/21/1988469/0/en/A-Complete-Guide-to-Metal-3D-Printing-Technologies-that-are-Shaping-the-Future-of-Metal-Manufacturing.html [Last Accessed: 07/06/2020]

[W7] "Guía completa: Deposición de energía directa, te lo contamos todo! 3D NATIVES" [Online] Available: https://www.3dnatives.com/es/guia-deposicion-de-energia-directa-100920192/ [Last Accessed: 07/06/2020]

[W8] "AMFG: Metal 3D Printing: What is Direct Energy Deposition? " [Online] Available: https://amfg.ai/2018/09/27/metal-3d-printing-what-is-direct-energy-deposition/ [Last Accessed: 07/06/2020]

[W9] "AREVO" [Online] Available: https://arevo.com/ [Last Accessed: 07/06/2020]

[W10] "Metal 3d printing with Electron Beam additive manufacturing (EBAM®)" [Online] Available: https://www.sciaky.com/additive-manufacturing/electron-beam-additive-manufacturing-technology [Last Accessed: 07/06/2020]

[W11] "Tecnologías de impresión 3D (VI): Laminación de hojas" [Online] Available: http://hxx.es/2015/02/06/tecnologias-de-impresion-3d-vi-laminacion-de-hojas/ [Last Accessed: 07/06/2020]

[W12] "Fabrisonic: 'Ultrasonic additive manufacturing', 2011." [Online] Available: https://www.youtube.com/watch?v=5s0J-7W4i6s [Last Accessed: 07/06/2020]

[W13] "ExOne : 'Metal'." [Online] Available: http://www.exone.com/en/materialization/what-is-digital-part-materialization/metal [Last Accessed: 07/06/2020]

[W14] "Smith B. The ExOne Company Reports 2016 First Quarter Results" [Online] Available: . http://www.investor.exone.com/news-releases/news-release-details/exone-company-reports-2016-fourth-quarter-and-full-year-results/ [Last Accessed: 07/06/2020]

[W15] "Linnenman A. Faster Steel — And the Innovative Process That Made It Possible. ShapewaysCom 2017" [Online] Available:. https://www.shapeways.com/blog/archives/30524-faster-steel-innovative-process-made-possible.html [Last Accessed: 07/06/2020]

[W16] "ExOne Company" [Online] Available: http://www.exone.com/Systems/Production-Printers n.d. [Last Accessed: 07/06/2020]

[W17] "AMFG: All You Need to Know About Metal Binder Jetting (2019)" [Online] Available: https://amfg.ai/2019/07/03/metal-binder-jetting-all-you-need-to-know/ [Last Accessed: 07/06/2020]

[W18] "Metal 3d printing hp metal jet. Reinvent opportunities." [Online] Available: https://www8.hp.com/us/en/printers/3d-printers/products/metal-jet.html [Last Accessed: 07/06/2020]

[W19] "AMFG: Expert Interview: Oerlikon's Principal Engineer for AM, Matthew Donovan, on 3D Printing for Aerospace" [Online] Available: https://amfg.ai/2019/09/17/expert-interview-oerlikon-matthew-donovan-principal-engineer-on-3d-printing-for-aerospace/ [Last Accessed: 07/06/2020]

[W20] "New manufacturing milestone: 30,000 additive fuel nozzles" [Online] Available: https://www.ge.com/additive/stories/new-manufacturing-milestone-30000-additive-fuel-nozzles [Last Accessed: 07/06/2020]

[W21] "Printing Heads: 3D Printing Has Launched A New Era In Aircraft Design" [Online] Available: https://www.ge.com/reports/printing-heads-3d-printing-launched-new-era-aircraft-design/ [Last Accessed: 07/06/2020]

[W22] "AMFG: 3D Printing and Formula One: 5 Trends in Motorsports " [Online] Available: https://amfg.ai/2018/11/21/3d-printing-formula-one-5-trends-in-motorsports/ [Last Accessed: 07/06/2020]

[W23] "Lima Corporate's EBM: 3d printed hip plant 'could last a lifetime" [Online] Available: https://3dprintingindustry.com/news/lima-corporates-ebm-3d-printed-hip-plant-last-lifetime-130086/[Last Accessed: 07/06/2020]

[W24] "Lima Corporate Web" [Online] Available: https://www.limacorporate.com/ [Last Accessed: 07/06/2020]

[W25] "GW Plastics Bets on Metal 3D Printing for Conformal Cooling" [Online] Available: https://www.additivemanufacturing.media/blog/post/gw-plastics-bets-on-metal-3d-printing-for-conformal-cooling [Last Accessed: 07/06/2020]

[W26] "AMFG: Expert Interview: Conflux Technology's Ben Batagol on Reinventing Heat Exchange Technology with 3D Printing" [Online] Available: https://amfg.ai/2019/06/12/expert-interview-ben-batagol-conflux-technology/ [Last Accessed: 07/06/2020]

[W27] "Analysis of *2020 Additive Manufacturing Market Outlook and Summary of Opportunities* report"[Online] Available: https://www.3dprintingmedia.network/the-additive-manufacturing-market-2019/ [Last Accessed: 08/06/2020]

[W28] "Additive Manufacturing Industry Grows To Almost $12 Billion In 2019" [Online] Available: https://www.forbes.com/sites/tjmccue/2020/05/08/additive-manufacturing-industry-grows-to-almost-12-billion-in-2019/#33bca2c65678 [Last Accessed: 08/06/2020]

[W29] "Informe Wohlers 2020" [Online] Available: http://wohlersassociates.com/2020report.htm [Last Accessed: 08/06/2020]

[W30] "Wohlers Report 2018, the rise of 3D Printing and where the Industry is Headed" Available: https://amfg.ai/2018/05/18/2018-wohlers-report-terry-wohlers-interview-3-printing/ [Last Accessed: 04/12/2020]

[W31] "AMFG: Metal 3D Printing: A Definitive Guide (2019) " [Online] Available: https://amfg.ai/2019/06/26/metal-3d-printing-a-definitive-guide/#The_Machines [Last Accessed: 07/06/2020]

[W32] "The Additive Manufacturing Industry Landscape 2020 (Uptdate)" [Online] Available: https://amfg.ai/2020/05/26/the-additive-manufacturing-industry-landscape-2020-231-companies-driving-digital-manufacturing/?cn-reloaded=1 [Last Accessed: 08/06/2020]

[W33] "What is the outlook for 3D printer sales in 2020?" [Online] Available: https://www.3dnatives.com/en/3d-printer-sales-2020-study-210420204/ [Last Accessed: 08/06/2020]

[W34] "Metal 3D printers in 2020: a comprehensive guide" [Online] Available: https://www.aniwaa.com/buyers-guide/3d-printers/best-metal-3d-printer/ [Last Accessed: 07/06/2020]

[W35] "AMPOWER AM report" [Online] Available: https://additive-manufacturing-report.com/ [Last Accessed: 08/06/2020]

[W36] "Senvol database" [Online] Available: http://senvol.com/database/ [Last Accessed: 08/06/2020]

[W37] "How HP Thermal Inkjet Printheads Work HP Inkjet HP" [Online] Available: https://www.youtube.com/watch?v=g0sJR9S-jtg [Last Accessed: 07/06/2020]

[W38] "Practiques estudiants UPC" [Online] Available https://eebe.upc.edu/ca/estudis/practiques-academiques-externes [Last Accessed: 17/06/2020]

[W39] "Màster universitari en Ciència i Enginyeria de Materials (en extinció)" [Online] Available https://eebe.upc.edu/ca/estudis/estudis-de-master/master-en-ciencia-i-enginyeria-de-materials-en-extincio/pla-destudis [Last Accessed: 17/06/2020]

[W40] "Presupuestos Biblioteca CSIC" [Online] Available http://biblioteca.cchs.csic.es/docs/proyecto_biblioteca/T4PresupuestodelaBiblioteca.pdf [Last Accessed: 17/06/2020]

[W41] "Número de estudiantes y personal en el curso 2019-2020 en la UPC" [Online] Available https://www.upc.edu/es/la-upc/la-institucion/hechos-y-cifras [Last Accessed: 17/06/2020]

[W42] "Tablas de amortización de según la Agencia Tributaria Española" [Online] Available https://www.agenciatributaria.es/AEAT.internet/Inicio/_Segmentos_/Empresas_y_profesionales/Empresas/Impuesto_sobre_Sociedades/Periodos_impositivos_a_partir_de_1_1_2015/Base_imponible/Amortizacion/Tabla_de_coeficientes_de_amortizacion_lineal_.shtml [Last Accessed: 17/06/2020]

[W43] "Tarifa de consume de electricidad en España" [Online] Available [Last Accessed: https://tarifaluzhora.es/ 17/06/2020]

[W44] "Consumo energético de un PC" [Online] Available [Last Accessed: https://hardzone.es/2015/03/31/cuanto-cuesta-la-electricidad-que-consume-tu-pc/ 17/06/2020]

[W45] "Consumo energético de una bombilla " [Online] Available https://certific.es/calcular-consumo-bombilla.html#:~:text=Consumo%20energ%C3%ADa%20bombilla%20%3D%20(60%20%2F,x%2024%20horas%20%3D%201.44%20kWh [Last Accessed: 17/06/2020]

[W46] "ACERO INOXIDABLE" [Online] Available: http://blog.utp.edu.co/metalografia/7-aceros-inoxidables/ [Last Accessed: 07/06/2020]

[W47] "Cómo se fabrica el acero inoxidable. PORTALINOX" [Online] Available: https://portalinox.es/como-se-fabrica-acero-inoxidable/ [Last Accessed: 07/06/2020]

[W48] "NEURTEX INSTRUMENTS: Preparaciones metalográficas. Recomendaciones generals y particulares para: Hierro, Hierro Fundido, Aluminio, Bronce, Acero Inoxidable, Fibra de Carbono, Magnesio, Inconel y Titanio" [Online] Available: https://www.interempresas.net/FeriaVirtual/Catalogos_y_documentos/9373/AMPreparacionesMetalograficas.pdf [Last Accessed: 07/06/2020]

[W49] "MYSCOPE. Train for advanced research" [Online] Available: https://myscope.training/index.html [Last Accessed: 07/06/2020]

[W50] "La microscopía electrónica de barrido SEM" [Online]. Available: https://www.patologiasconstruccion.net/2012/12/la-microscopia-electronica-de-barrido-sem-iconcepto-y-usos/ [Last Accessed: 07/06/2020]

[W51] "Microscopio electrónico de barido (SEM)" [Online] Available: https://www2.uned.es/cristamine/mineral/metodos/sem.htm [Last Accessed: 07/06/2020]

[W52] "LA TEORÍA DE MIE" [Online] Available: https://www.fritsch.es/medicion-de-particulas/conocimientos-de-fritsch/la-teoria-de-mie/ [Last Accessed: 07/06/2020]

[W53] "International Centre for Diffraction Data" [Online] Available: http://www.icdd.com [Last Accessed: 07/06/2020]

1. Commerce, U.S.D.o., *The emerging digital economy*. 1998: US Department of Commerce.

2. TAPSCOTT, D., *Digital Economy: Promise and Peril in the Age of Networked Intelligence McGraw Hill.* Inc, New York, 1996.

3. Teece, D.J., *Profiting from innovation in the digital economy: Enabling technologies, standards, and licensing models in the wireless world.* Research Policy, 2018. **47**(8): p. 1367-1387.

4. Buisán, M. and F. Valdés, *La industria conectada 4.0.* La Economía Digital en España, ICE, 2017. **898**: p. 89-99.

5. Geissbauer, R., J. Vedso, and S. Schrauf, *Industry 4.0: Building the digital enterprise.* Retrieved from PwC Website: https://www. pwc. com/gx/en/industries/industries-4.0/landing-page/industry-4.0-building-your-digital-enterprise-april-2016. pdf, 2016.

6. Frazier, W.E., *Metal additive manufacturing: a review.* Journal of Materials Engineering and Performance, 2014. **23**(6): p. 1917-1928.

7. Ngo, T.D., et al., *Additive manufacturing (3D printing): A review of materials, methods, applications and challenges.* Composites Part B: Engineering, 2018. **143**: p. 172-196.

8. Hull, C.W., *Method for production of three-dimensional objects by stereolithography*, 1990, Google Patents.

9. Wohlers, T. and T. Gornet, *History of additive manufacturing.* Wohlers report, 2014. **24**(2014): p. 118.

10. Bourell, D., et al., *Materials for additive manufacturing.* CIRP Annals, 2017. **66**(2): p. 659-681.

11. Chen, H. and Y.F. Zhao, *Process parameters optimization for improving surface quality and manufacturing accuracy of binder jetting additive manufacturing process.* Rapid Prototyping Journal, 2016.

12. Conner, B.P., et al., *Making sense of 3-D printing: Creating a map of additive manufacturing products and services.* Additive Manufacturing, 2014. **1**: p. 64-76.

13. DebRoy, T., et al., *Additive manufacturing of metallic components–process, structure and properties.* Progress in Materials Science, 2018. **92**: p. 112-224.

14. Gao, W., et al., *The status, challenges, and future of additive manufacturing in engineering.* Computer-Aided Design, 2015. **69**: p. 65-89.

15. Ghaffar, S.H., J. Corker, and M. Fan, *Additive manufacturing technology and its implementation in construction as an eco-innovative solution.* Automation in Construction, 2018. **93**: p. 1-11.

16. Gokuldoss, P.K., S. Kolla, and J. Eckert, *Additive manufacturing processes: Selective laser melting, electron beam melting and binder jetting—Selection guidelines.* Materials, 2017. **10**(6): p. 672.

17. Mostafaei, A., et al., *Powder bed binder jet printed alloy 625: Densification, microstructure and mechanical properties.* Materials & Design, 2016. **108**: p. 126-135.

18. Seifi, M., et al., *Overview of materials qualification needs for metal additive manufacturing.* Jom, 2016. **68**(3): p. 747-764.

19. Tan, J.H., W.L.E. Wong, and K.W. Dalgarno, *An overview of powder granulometry on feedstock and part performance in the selective laser melting process.* Additive Manufacturing, 2017. **18**: p. 228-255.

20. Mirzababaei, S. and S. Pasebani, *A Review on Binder Jet Additive Manufacturing of 316L Stainless Steel.* Journal of Manufacturing and Materials Processing, 2019. **3**(3): p. 82.

21. Herzog, D., et al., *Additive manufacturing of metals.* Acta Materialia, 2016. **117**: p. 371-392.

22. Alcisto, J., et al., *Tensile properties and microstructures of laser-formed Ti-6Al-4V.* Journal of materials engineering and performance, 2011. **20**(2): p. 203-212.

23. Do, T., P. Kwon, and C.S. Shin, *Process development toward full-density stainless steel parts with binder jetting printing.* International Journal of Machine Tools and Manufacture, 2017. **121**: p. 50-60.

24. Guo, N. and M.C. Leu, *Additive manufacturing: technology, applications and research needs.* Frontiers of Mechanical Engineering, 2013. **8**(3): p. 215-243.

25. Kruth, J.-P., M.-C. Leu, and T. Nakagawa, *Progress in additive manufacturing and rapid prototyping.* CIRP Annals-Manufacturing Technology, 1998. **47**(2): p. 525-540.

26. Mueller, B., *Additive manufacturing technologies–Rapid prototyping to direct digital manufacturing.* Assembly Automation, 2012.

27. Meteyer, S., et al., *Energy and material flow analysis of binder-jetting additive manufacturing processes. Procedia CIRP 15: 19–25*, 2014.

28. De Schutter, G., et al., *Vision of 3D printing with concrete—technical, economic and environmental potentials.* Cement and Concrete Research, 2018. **112**: p. 25-36.

29. Cerdas, F., et al., *Life cycle assessment of 3D printed products in a distributed manufacturing system.* Journal of Industrial Ecology, 2017. **21**(S1): p. S80-S93.

30. Yeh, C.-C. and Y.-F. Chen, *Critical success factors for adoption of 3D printing.* Technological Forecasting and Social Change, 2018. **132**: p. 209-216.

31. Murr, L.E., et al., *Fabrication of metal and alloy components by additive manufacturing: examples of 3D materials science.* Journal of Materials Research and technology, 2012. **1**(1): p. 42-54.

32. Ford, S. and M. Despeisse, *Additive manufacturing and sustainability: an exploratory study of the advantages and challenges.* Journal of Cleaner Production, 2016. **137**: p. 1573-1587.

33. Gebler, M., A.J.S. Uiterkamp, and C. Visser, *A global sustainability perspective on 3D printing technologies.* Energy Policy, 2014. **74**: p. 158-167.

34. Campbell, T., et al., *Could 3D printing change the world.* Technologies, Potential, and Implications of Additive Manufacturing, Atlantic Council, Washington, DC, 2011. **3**.

35. Core, B., *3D printing metals 2018-2028: technology and market analysis.* IDTechEx, available at: www. idtechex. com/research/reports/3d-printing-metals-2018-2028-000547. asp, 2017.

36. Duda, T. and L.V. Raghavan, *3D metal printing technology.* IFAC-PapersOnLine, 2016. **49**(29): p. 103-110.

37. Das, S., D.L. Bourell, and S. Babu, *Metallic materials for 3D printing.* MRS Bulletin, 2016. **41**(10): p. 729-741.

38. Lee, J.-Y., J. An, and C.K. Chua, *Fundamentals and applications of 3D printing for novel materials.* Applied Materials Today, 2017. **7**: p. 120-133.

39. Wehrs, J., *Financing for growth in additive manufacturing*, 2018, Massachusetts Institute of Technology.

40. Buswell, R.A., et al., *3D printing using concrete extrusion: A roadmap for research.* Cement and Concrete Research, 2018. **112**: p. 37-49.

41. Sames, W.J., et al., *The metallurgy and processing science of metal additive manufacturing.* International Materials Reviews, 2016. **61**(5): p. 315-360.

42. Pal, S., et al., *The effect of post-processing and machining process parameters on properties of stainless steel PH1 product produced by direct metal laser sintering.* Procedia Engineering, 2016. **149**: p. 359-365.

43. Yan, C., Y. Shi, and L. Hao, *Investigation into the differences in the selective laser sintering between amorphous and semi-crystalline polymers.* International polymer processing, 2011. **26**(4): p. 416-423.

44. Standard, A., *Standard terminology for additive manufacturing technologies.* ASTM International F2792-12a, 2012.

45. Gordon, R., *Trends in commercial 3D printing and additive manufacturing.* 3D Printing and Additive Manufacturing, 2015. **2**(2): p. 89-90.

46. Murr, L.E., et al., *Metal fabrication by additive manufacturing using laser and electron beam melting technologies.* Journal of Materials Science & Technology, 2012. **28**(1): p. 1-14.

47. Vaupotič, B., M. Brezočnik, and J. Balič, *Use of PolyJet technology in manufacture of new product.* Journal of Achievements in Materials and Manufacturing Engineering, 2006. **18**(1-2): p. 319-322.

48. AlMangour, B. and J.-M. Yang, *Understanding the deformation behavior of 17-4 precipitate hardenable stainless steel produced by direct metal laser sintering using micropillar compression*

and TEM. The International Journal of Advanced Manufacturing Technology, 2017. **90**(1-4): p. 119-126.

49. Xie, F., et al., *Structural and mechanical characteristics of porous 316L stainless steel fabricated by indirect selective laser sintering.* Journal of Materials Processing Technology, 2013. **213**(6): p. 838-843.

50. Ibrahim, K.A., B. Wu, and N.P. Brandon, *Electrical conductivity and porosity in stainless steel 316L scaffolds for electrochemical devices fabricated using selective laser sintering.* Materials & Design, 2016. **106**: p. 51-59.

51. Mahamood, R., et al., *Revolutionary Additive Manufacturing: An Overview.* Lasers in Engineering (Old City Publishing), 2014. **27**.

52. Udroiu, R., *POWDER BED ADDITIVE MANUFACTURING SYSTEMS AND ITS APPLICATIONS.* Academic journal of manufacturing engineering, 2012. **10**(4).

53. Kirka, M.M., et al., *Solidification and solid-state transformation sciences in metals additive manufacturing.* Scripta Materialia, 2017. **135**: p. 130-134.

54. Cordero, Z.C., et al., *Powder bed charging during electron-beam additive manufacturing.* Acta Materialia, 2017. **124**: p. 437-445.

55. Bose, A., *Non-Melting-Based Metal Additive Manufacturing Technologies.* Powder Metallurgy, 2019. **2**: p. 29.

56. Körner, C., *Additive manufacturing of metallic components by selective electron beam melting—a review.* International Materials Reviews, 2016. **61**(5): p. 361-377.

57. Adeyemi, A., E.T. Akinlabi, and R.M. Mahamood, *Powder bed based laser additive manufacturing process of stainless steel: A review.* Materials Today: Proceedings, 2018. **5**(9): p. 18510-18517.

58. Ren, L., et al., *Process parameter optimization of extrusion-based 3D metal printing utilizing PW–LDPE–SA binder system.* Materials, 2017. **10**(3): p. 305.

59. Akinlabi, E.T., R.M. Mahamood, and S.A. Akinlabi, *Advanced Manufacturing Techniques Using Laser Material Processing*. 2016: IGI Global.

60. Mahamood, R. and E. Akinlabi, *Laser Power and Powder flow rate influence on the metallurgy and microhardness of Laser metal Deposited Titanium alloy.* Materials Today: Proceedings, 2017. **4**(2): p. 3678-3684.

61. Mahamood, R. and E. Akinlabi, *Effect of processing parameter on wear resistance property of laser material deposited titanium-alloy composite.* Journal of Optoelectronics and Advanced Materials, 2015. **17**(September-October 2015): p. 1348-1360.

62. Mahamood, R.M. and E.T. Akinlabi, *Processing parameters optimization for material deposition efficiency in laser metal deposited titanium alloy.* Lasers in Manufacturing and Materials Processing, 2016. **3**(1): p. 9-21.

63. Mahamood, R.M. and E.T. Akinlabi, *Effect of laser power and powder flow rate on the wear resistance behaviour of laser metal deposited TiC/Ti6Al4 V composites.* Materials Today: Proceedings, 2015. **2**(4-5): p. 2679-2686.

64. Mahamood, R. and E.T. Akinlabi, *Laser metal deposition of functionally graded Ti6Al4V/TiC.* Materials & Design, 2015. **84**: p. 402-410.

65. Mahamood, R.M., E.T. Akinlabi, and S. Akinlabi, *Laser power and scanning speed influence on the mechanical property of laser metal deposited titanium-alloy.* Lasers in Manufacturing and Materials Processing, 2015. **2**(1): p. 43-55.

66. Yi, S., et al., *Study of the key technologies of LOM for functional metal parts.* Journal of materials processing technology, 2004. **150**(1-2): p. 175-181.

67. Himmer, T., et al., *Recent developments in metal laminated tooling by multiple laser processing.* Rapid prototyping journal, 2003.

68. Xu, B., et al., *Research on micro-electric resistance slip welding of copper electrode during the fabrication of 3D metal micro-mold.* Journal of Materials Processing Technology, 2013. **213**(12): p. 2174-2183.

69. White, D.R., *ULTRASONIC CONSOLIDATION OF ALUMINUM TOOLING.* Advanced materials & processes, 2003. **161**(1): p. 64-65.

70. Schick, D., et al., *Microstructural Characterization of Bonding Interfaces in Aluminum 3003 Blocks Fabricated by Ultrasonic Additive Manufacturing-Methods were examined to link microstructure and linear weld density to the mechanical properties of ultrasonic additive manufacturing.* Welding Journal, 2010. **89**(5): p. 105S.

71. Dehoff, R. and S. Babu, *Characterization of interfacial microstructures in 3003 aluminum alloy blocks fabricated by ultrasonic additive manufacturing.* Acta Materialia, 2010. **58**(13): p. 4305-4315.

72. Fujii, H.T., M. Sriraman, and S. Babu, *Quantitative evaluation of bulk and interface microstructures in Al-3003 alloy builds made by very high power ultrasonic additive manufacturing.* Metallurgical and Materials Transactions A, 2011. **42**(13): p. 4045-4055.

73. Friel, R.J. and R.A. Harris, *Ultrasonic additive manufacturing–a hybrid production process for novel functional products.* Procedia CIRP, 2013. **6**: p. 35-40.

74. Huang, C.-H., S.R. Schmid, and J.E. Wang, *Thermal effects on polymer laminated steel formability in ironing.* J. Manuf. Sci. Eng., 2001. **123**(2): p. 225-230.

75. Hehr, A. and M.J. Dapino, *Interfacial shear strength estimates of NiTi–Al matrix composites fabricated via ultrasonic additive manufacturing.* Composites Part B: Engineering, 2015. **77**: p. 199-208.

76. Sriraman, M., et al., *Thermal transients during processing of materials by very high power ultrasonic additive manufacturing.* Journal of Materials Processing Technology, 2011. **211**(10): p. 1650-1657.

77. Mueller, B. and D. Kochan, *Laminated object manufacturing for rapid tooling and patternmaking in foundry industry.* Computers in Industry, 1999. **39**(1): p. 47-53.

78. Bryden, B., et al., *Laminated steel tooling in the aerospace industry.* Materials & Design, 2000. **21**(4): p. 403-408.

79. Bryden, B., D. Wimpenny, and I. Pashby, *Manufacturing production tooling using metal laminations.* Rapid Prototyping Journal, 2001.

80. Panda, S.K., et al., *Optimization of fused deposition modelling (FDM) process parameters using bacterial foraging technique.* Intelligent information management, 2009. **1**(02): p. 89.

81. Greulich, M., M. Greul, and T. Pintat, *Fast, functional prototypes via multiphase jet solidification.* Rapid Prototyping Journal, 1995.

82. Giberti, H., M. Strano, and M. Annoni. *An innovative machine for Fused Deposition Modeling of metals and advanced ceramics*. in *MATEC web of conferences*. 2016. EDP Sciences.

83. Cooper, R.G., *Winning at new products: accelerating the process from idea to launch.* 2001.

84. Wong, K.V. and A. Hernandez, *A review of additive manufacturing, ISRN Mech.* Eng, 2012. **1012**: p. 2012.

85. Utela, B., et al., *A review of process development steps for new material systems in three dimensional printing (3DP).* Journal of Manufacturing Processes, 2008. **10**(2): p. 96-104.

86. Shivpuri, R., et al., *Evaluation of 3D printing for dies in low volume forging of 7075 aluminum helicopter parts.* Rapid Prototyping Journal, 2005.

87. Utela, B., R.L. Anderson, and H. Kuhn. *Advanced ceramic materials and processes for three-dimensional printing (3DP)*. in *Solid Freeform Fabr. Symp. Proc*. 2006.

88. Hwa, L.C., et al., *Recent advances in 3D printing of porous ceramics: A review.* Current Opinion in Solid State and Materials Science, 2017. **21**(6): p. 323-347.

89. Wang, X., et al., *3D printing of polymer matrix composites: A review and prospective.* Composites Part B: Engineering, 2017. **110**: p. 442-458.

90. Bose, S., et al., *Additive manufacturing of biomaterials.* Progress in materials science, 2018. **93**: p. 45-111.

91. Harun, W., et al., *A review of powder additive manufacturing processes for metallic biomaterials.* Powder Technology, 2018. **327**: p. 128-151.

92. Ho, C.M.B., S.H. Ng, and Y.-J. Yoon, *A review on 3D printed bioimplants.* International Journal of Precision Engineering and Manufacturing, 2015. **16**(5): p. 1035-1046.

93. Liu, W., et al., *Application and performance of 3D printing in nanobiomaterials.* Journal of Nanomaterials, 2013. **2013**.

94. Elahinia, M., et al., *Fabrication of NiTi through additive manufacturing: A review.* Progress in Materials Science, 2016. **83**: p. 630-663.

95. Bhushan, B. and M. Caspers, *An overview of additive manufacturing (3D printing) for microfabrication.* Microsystem Technologies, 2017. **23**(4): p. 1117-1124.

96. Sachs, E., et al., *Three-dimensional printing: the physics and implications of additive manufacturing.* CIRP annals, 1993. **42**(1): p. 257-260.

97. Sachs, E.M., et al., *Three-dimensional printing techniques*, 1993, Google Patents.

98. Gibson, I., D.W. Rosen, and B. Stucker, *Additive manufacturing technologies*. Vol. 17. 2014: Springer.

99. Michaels, S., E.M. Sachs, and M.J. Cima. *Metal parts generation by three dimensional printing*. in *1992 International Solid Freeform Fabrication Symposium*. 1992.

100. Campbell, I., et al., *Wohlers report 2018: 3D printing and additive manufacturing state of the industry: annual worldwide progress report*. 2018: Wohlers Associates.

101. Mostafaei, A., et al., *Microstructural evolution and magnetic properties of binder jet additive manufactured Ni-Mn-Ga magnetic shape memory alloy foam.* Acta Materialia, 2017. **131**: p. 482-490.

102. Allen, S.M. and E.M. Sachs, *Three-dimensional printing of metal parts for tooling and other applications.* Metals and Materials, 2000. **6**(6): p. 589-594.

103. Paranthaman, M.P., et al., *Binder jetting: A novel NdFeB bonded magnet fabrication process.* Jom, 2016. **68**(7): p. 1978-1982.

104. Mostafaei, A., et al., *Effect of solutionizing and aging on the microstructure and mechanical properties of powder bed binder jet printed nickel-based superalloy 625.* Materials & Design, 2016. **111**: p. 482-491.

105. Nandwana, P., et al., *Powder bed binder jet 3D printing of Inconel 718: Densification, microstructural evolution and challenges ☆.* Current Opinion in Solid State and Materials Science, 2017. **21**(4): p. 207-218.

106. Enneti, R.K., et al., *Sintering of WC-12% Co processed by binder jet 3D printing (BJ3DP) technology.* International Journal of Refractory Metals and Hard Materials, 2018. **71**: p. 28-35.

107. Garzón, E.O., J.L. Alves, and R.J. Neto, *Post-process influence of infiltration on binder jetting technology*, in *Materials design and applications*. 2017, Springer. p. 233-255.

108. Levy, A., et al., *Additive manufacturing of complex-shaped graded TiC/steel composites.* Materials & Design, 2017. **118**: p. 198-203.

109. Zak Fang, Z., *Sintering of advanced materials: fundamental and processes*, 2010, Cambridge, UK: Woodhead Publishing Limited.

110. German, R.M., P. Suri, and S.J. Park, *liquid phase sintering.* Journal of materials science, 2009. **44**(1): p. 1-39.

111. Kingery, W., *Densification during sintering in the presence of a liquid phase. I. Theory.* Journal of Applied Physics, 1959. **30**(3): p. 301-306.

112. Miyanaji, H., et al., *Process development of porcelain ceramic material with binder jetting process for dental applications.* Jom, 2016. **68**(3): p. 831-841.

113. Yap, Y.L., et al., *Material jetting additive manufacturing: An experimental study using designed metrological benchmarks.* Precision engineering, 2017. **50**: p. 275-285.

114. Varotsis, B., *How to design parts for Binder Jetting 3D printing.* 3D Hubs, 2018.

115. Kumbhar, N. and A. Mulay, *Post processing methods used to improve surface finish of products which are manufactured by additive manufacturing technologies: A review.* Journal of The Institution of Engineers (India): Series C, 2018. **99**(4): p. 481-487.

116. Castro, M., et al., *Behaviour of infiltrating materials on Calcium Sulphate hemihydrate parts made by 3D printing.* Procedia Manufacturing, 2017. **13**: p. 848-855.

117. Elliot, A. and L.J. Love, *Operator burden in metal additive manufacturing.* Solid Freeform Fabrication, 2016: p. 1890-1899.

118. Mostafaei, A., et al. *Binder jet printing of partial denture metal framework from metal powder*. in *Materials Science and Technology Conference and Exhibition*. 2017.

119. Edgar, J. and S. Tint, *Additive manufacturing technologies: 3D printing, rapid prototyping, and direct digital manufacturing.* Johnson Matthey Technology Review, 2015. **59**(3): p. 193-198.

120. Gatsos, T., et al., *Review on Computational Modeling of Process–Microstructure–Property Relationships in Metal Additive Manufacturing.* JOM, 2020. **72**(1): p. 403-419.

121. Zhang, F., et al., *3D printing technologies for electrochemical energy storage.* Nano Energy, 2017. **40**: p. 418-431.

122. Azhari, A., et al., *Binder-jet powder-bed additive manufacturing (3D printing) of thick graphene-based electrodes.* Carbon, 2017. **119**: p. 257-266.

123. Miyanaji, H., J.M. Akbar, and L. Yang, *Fabrication and characterization of Graphite/Nylon 12 composite via binder Jetting additive manufacturing process.* Solid Freeform Fabrication, Austin, Texas, USA, 2017.

124. Gaytan, S.M., et al. *Analysis of ferroelectric ceramic fabricated by binder jetting technology*. in *Proceedings of Solid Freeform Fabrication Symposium*. 2013.

125. Gaytan, S., et al., *Fabrication of barium titanate by binder jetting additive manufacturing technology.* Ceramics International, 2015. **41**(5): p. 6610-6619.

126. Holland, S., T. Foster, and C. Tuck, *Creation of Food Structures Through Binder Jetting*, in *Fundamentals of 3D Food Printing and Applications*. 2019, Elsevier. p. 257-288.

127. Holland, S., et al., *Design and characterisation of food grade powders and inks for microstructure control using 3D printing.* Journal of food Engineering, 2018. **220**: p. 12-19.

128. Holland, S., C. Tuck, and T. Foster, *Selective recrystallization of cellulose composite powders and microstructure creation through 3D binder jetting.* Carbohydrate polymers, 2018. **200**: p. 229-238.

129. Manogharan, G., M. Kioko, and C. Linkous, *Binder jetting: a novel solid oxide fuel-cell fabrication process and evaluation.* Jom, 2015. **67**(3): p. 660-667.

130. Chhabra, M. and R. Singh, *Obtaining desired surface roughness of castings produced using ZCast direct metal casting process through Taguchi's experimental approach.* Rapid Prototyping Journal, 2012.

131. Deng, C., et al., *Effects of hollow structures in sand mold manufactured using 3D printing technology.* Journal of Materials Processing Technology, 2018. **255**: p. 516-523.

132. Hodder, K.J. and R.J. Chalaturnyk, *Bridging additive manufacturing and sand casting: Utilizing foundry sand.* Additive Manufacturing, 2019. **28**: p. 649-660.

133. Kim, D.-H., et al., *Mechanical Analysis of Ceramic/Polymer Composite with Mesh-Type Lightweight Design Using Binder-Jet 3D Printing.* Materials, 2018. **11**(10): p. 1941.

134. Kong, L., et al., *Microstructure characteristics and fractal analysis of 3D-printed sandstone using micro-CT and SEM-EDS.* Journal of Petroleum Science and Engineering, 2019. **175**: p. 1039-1048.

135. Maravola, M., et al., *Epoxy infiltrated 3D printed ceramics for composite tooling applications.* Additive Manufacturing, 2019. **25**: p. 59-63.

136. Mitra, S., et al., *Study of the evolution of transport properties induced by additive processing sand mold using X-ray computed tomography.* Journal of Materials Processing Technology, 2020. **277**: p. 116495.

137. Rojas-Nastrucci, E.A., et al., *Ka-band characterization of binder jetting for 3-D printing of metallic rectangular waveguide circuits and antennas.* IEEE Transactions on Microwave Theory and Techniques, 2017. **65**(9): p. 3099-3108.

138. Shangguan, H., et al., *3D-printed rib-enforced shell sand mold for aluminum castings.* The International Journal of Advanced Manufacturing Technology, 2018. **96**(5-8): p. 2175-2182.

139. Snelling, D.A., C.B. Williams, and A.P. Druschitz, *Mechanical and Material Properties of Castings produced via 3d printed molds.* Additive Manufacturing, 2019. **27**: p. 199-207.

140. Vangapally, S., et al., *Effect of lattice design and process parameters on dimensional and mechanical properties of binder Jet Additively manufactured stainless steel 316 for bone scaffolds.* Procedia Manufacturing, 2017. **10**: p. 750-759.

141. Huang, G.-L., S.-G. Zhou, and T. Yuan, *Development of a wideband and high-efficiency waveguide-based compact antenna radiator with binder-jetting technique.* IEEE Transactions on Components, Packaging and Manufacturing Technology, 2017. **7**(2): p. 254-260.

142. Rojas-Nastrucci, E.A., et al. *Metallic 3D printed Ka-band pyramidal horn using binder jetting*. in *2016 IEEE MTT-S Latin America Microwave Conference (LAMC)*. 2016. IEEE.

143. Feng, P., et al., *Mechanical properties of structures 3D printed with cementitious powders.* Construction and Building Materials, 2015. **93**: p. 486-497.

144. Ingaglio, J., et al., *Material characteristics of binder jet 3D printed hydrated CSA cement with the addition of fine aggregates.* Construction and Building Materials, 2019. **206**: p. 494-503.

145. Lowke, D., et al., *Particle-bed 3D printing in concrete construction–Possibilities and challenges.* Cement and Concrete Research, 2018. **112**: p. 50-65.

146. Nematollahi, B., M. Xia, and J. Sanjayan, *Enhancing Strength of Powder-Based 3D Printed Geopolymers for Digital Construction Applications*, in *Rheology and Processing of Construction Materials*. 2019, Springer. p. 417-425.

147. Xia, M., B. Nematollahi, and J. Sanjayan, *Post-processing Techniques to Enhance Strength of Portland Cement Mortar Digitally Fabricated Using Powder-Based 3D Printing Process*, in *Rheology and Processing of Construction Materials*. 2019, Springer. p. 457-464.

148. Xia, M. and J. Sanjayan, *Method of formulating geopolymer for 3D printing for construction applications.* Materials & Design, 2016. **110**: p. 382-390.

149. Zeidler, H., et al., *3D printing of biodegradable parts using renewable biobased materials.* Procedia Manufacturing, 2018. **21**: p. 117-124.

150. Brunello, G., et al., *Powder-based 3D printing for bone tissue engineering.* Biotechnology advances, 2016. **34**(5): p. 740-753.

151. Du, W., et al. *Binder jetting additive manufacturing of ceramics: a literature review*. in *ASME 2017 International Mechanical Engineering Congress and Exposition*. 2017. American Society of Mechanical Engineers Digital Collection.

152. Mancuso, E., et al., *Three-dimensional printing of porous load-bearing bioceramic scaffolds.* Proceedings of the Institution of Mechanical Engineers, Part H: Journal of Engineering in Medicine, 2017. **231**(6): p. 575-585.

153. Shakor, P., et al., *Modified 3D printed powder to cement-based material and mechanical properties of cement scaffold used in 3D printing.* Construction and Building Materials, 2017. **138**: p. 398-409.

154. Shirazi, S.F.S., et al., *A review on powder-based additive manufacturing for tissue engineering: selective laser sintering and inkjet 3D printing.* Science and technology of advanced materials, 2015. **16**(3): p. 033502.

155. Lam, C.X.F., et al., *Scaffold development using 3D printing with a starch-based polymer.* Materials Science and Engineering: C, 2002. **20**(1-2): p. 49-56.

156. Liravi, F. and E. Toyserkani, *A hybrid additive manufacturing method for the fabrication of silicone bio-structures: 3D printing optimization and surface characterization.* Materials & Design, 2018. **138**: p. 46-61.

157. Liravi, F. and M. Vlasea, *Data related to the experimental design for powder bed binder jetting additive manufacturing of silicone.* Data in brief, 2018. **18**: p. 1477.

158. Liravi, F. and M. Vlasea, *Powder bed binder jetting additive manufacturing of silicone structures.* Additive Manufacturing, 2018. **21**: p. 112-124.

159. Rabinskiy, L., et al. *Fabrication of porous silicon nitride ceramics using binder jetting technology*. in *IOP Conference Series: Materials Science and Engineering*. 2016. IOP Publishing.

160. Suwanprateeb, J. and R. Chumnanklang, *Three-dimensional printing of porous polyethylene structure using water-based binders.* Journal of Biomedical Materials Research Part B: Applied Biomaterials: An Official Journal of The Society for Biomaterials, The Japanese Society for Biomaterials, and The Australian Society for Biomaterials and the Korean Society for Biomaterials, 2006. **78**(1): p. 138-145.

161. Kladeftira, M., et al., *Printing Whisper Dishes. Large-scale binder jetting for outdoor installations.* 2018.

162. Squelch, A., *3D printing rocks for geo-educational, technical, and hobbyist pursuits.* Geosphere, 2018. **14**(1): p. 360-366.

163. Vogler, D., et al., *A comparison of tensile failure in 3D-printed and natural sandstone.* Engineering Geology, 2017. **226**: p. 221-235.

164. Akmal, J.S., et al., *Implementation of industrial additive manufacturing: Intelligent implants and drug delivery systems.* Journal of functional biomaterials, 2018. **9**(3): p. 41.

165. Díaz-Moreno, C.A., et al., *Binder jetting additive manufacturing of aluminum nitride components.* Ceramics International, 2019. **45**(11): p. 13620-13627.

166. Infanger, S., et al., *Powder bed 3D-printing of highly loaded drug delivery devices with hydroxypropyl cellulose as solid binder.* International journal of pharmaceutics, 2019. **555**: p. 198-206.

167. Lichtenberger, J.P., et al., *Using 3D printing (additive manufacturing) to produce low-cost simulation models for medical training.* Military medicine, 2018. **183**(suppl_1): p. 73-77.

168. Naitoh, M., et al., *Dimensional accuracy of a binder jet model produced from computerized tomography data for dental implants.* Journal of oral implantology, 2006. **32**(6): p. 273-276.

169. Rahman, Z., et al., *Printing of personalized medication using binder jetting 3D printer*, in *Precision Medicine for Investigators, Practitioners and Providers*. 2020, Elsevier. p. 473-481.

170. Wilts, E.M., et al., *Comparison of Linear and 4-Arm Star Poly (vinyl pyrrolidone) for Aqueous Binder Jetting Additive Manufacturing of Personalized Dosage Tablets.* ACS applied materials & interfaces, 2019. **11**(27): p. 23938-23947.

171. Wu, B.M., et al., *Solid free-form fabrication of drug delivery devices.* Journal of Controlled Release, 1996. **40**(1-2): p. 77-87.

172. Ziaee, M., E.M. Tridas, and N.B. Crane, *Binder-jet printing of fine stainless steel powder with varied final density.* Jom, 2017. **69**(3): p. 592-596.

173. Bai, Y., G. Wagner, and C.B. Williams, *Effect of particle size distribution on powder packing and sintering in binder jetting additive manufacturing of metals.* Journal of Manufacturing Science and Engineering, 2017. **139**(8).

174. Gibson, I., D. Rosen, and B. Stucker, *Binder jetting*, in *Additive manufacturing technologies*. 2015, Springer. p. 205-218.

175. Van Noort, R., *The future of dental devices is digital.* Dental materials, 2012. **28**(1): p. 3-12.

176. Dawood, A., et al., *3D printing in dentistry.* British dental journal, 2015. **219**(11): p. 521.

177. Shopova, D., et al., *Study of dental specialists awareness of additive manufacturing in dental practice.* 2019.

178. Javaid, M. and A. Haleem, *Current status and challenges of Additive manufacturing in orthopaedics: an overview.* Journal of clinical orthopaedics and trauma, 2019. **10**(2): p. 380-386.

179. Holmes, M., *Additive manufacturing continues composites market growth.* Reinforced Plastics, 2019. **63**(6): p. 296-301.

180. Alhnan, M.A., et al., *Emergence of 3D printed dosage forms: opportunities and challenges.* Pharmaceutical research, 2016. **33**(8): p. 1817-1832.

181. Campbell, I., et al., *Wohlers Report 2017 3D Printing and Additive Manufacturing State of the Industry: Annual Worldwide Progress Report*. 2017: Wohlers Associates.

182. Upadhyaya, G.S., *Powder metallurgy technology*. 1997: Cambridge Int Science Publishing.

183. Antony, L.V. and R.G. Reddy, *Processes for production of high-purity metal powders.* Jom, 2003. **55**(3): p. 14-18.

184. Lawley, A., *Preparation of metal powders.* Annual Review of Materials Science, 1978. **8**(1): p. 49-71.

185. Tenhover, M.A., R.S. Henderson, and J.R. Fox, *Amorphous metal alloy powders and synthesis of same by solid state chemical reduction reactions*, 1985, Google Patents.

186. Sherrington, P. and R. Oliver, *Spray Drying, from Granulation, a Monograph in Powder Science and Technology.* Heyden, New York, 1981: p. 122-139.

187. Lagutkin, S., et al., *Atomization process for metal powder.* Materials Science and Engineering: A, 2004. **383**(1): p. 1-6.

188. Ashgriz, N., *Handbook of atomization and sprays: theory and applications*. 2011: Springer Science & Business Media.

189. Contreras, J.M., A. Jiménez-Morales, and J.M. Torralba, *Improvement of rheological properties of Inconel 718 MIM feedstock using tailored particle size distributions.* Powder Metallurgy, 2008. **51**(2): p. 103-106.

190. Nobrega, B.N., J. Ristow, Waldyr, and R. Machado, *MIM processing and plasma sintering of nickel base superalloys for aerospace and automotive applications.* Powder Metallurgy, 2008. **51**(2): p. 107-110.

191. Anderson, I.E., D. Byrd, and J. Meyer, *Highly tuned gas atomization for controlled preparation of coarse powder.* Materialwissenschaft und Werkstofftechnik, 2010. **41**(7): p. 504-512.

192. Dawes, J., R. Bowerman, and R. Trepleton, *Introduction to the additive manufacturing powder metallurgy supply chain.* Johnson Matthey Technology Review, 2015. **59**(3): p. 243-256.

193. Feng, Y. and T. Qiu, *Preparation, characterization and microwave absorbing properties of FeNi alloy prepared by gas atomization method.* Journal of alloys and compounds, 2012. **513**: p. 455-459.

194. Kuhn, H., *Powder metallurgy processing: the techniques and analyses*. 2012: Elsevier.

195. Nasr, G.G., A.J. Yule, and L. Bendig, *Industrial sprays and atomization: design, analysis and applications*. 2013: Springer Science & Business Media.

196. Sam, F.F., *Powder metallurgy of titanium alloys*, in *Advances in Powder Metallurgy*. 2013, Elsevier. p. 202-240.

197. Zhang, D., *Processing of advanced materials using high-energy mechanical milling.* Progress in Materials Science, 2004. **49**(3-4): p. 537-560.

198. Kassym, K. and A. Perveen, *Atomization processes of metal powders for 3D printing.* Materials Today: Proceedings, 2020.

199. Backmark, U., N. Backstrom, and L. Arnberg, *Production of Metal Powder by Ultrasonic Gas Atomization.(Retroactive Coverage).* Powder Metallurgy International, 1986. **18**(6): p. 422-424.

200. Angelo, P. and R. Subramanian, *Powder metallurgy: science, technology and applications*. 2008: PHI Learning Pvt. Ltd.

201. Brewin, P., P. Walker, and P. Nurthen, *Production of high alloy powders by water atomization.* Powder metallurgy, 1986. **29**(4): p. 281-285.

202. Yenwiset, S. and T. Yenwiset, *Design and construction of water atomizer for making metal powder.* Journal of Metals, Materials and Minerals, 2011. **21**(1): p. 75-81.

203. Seki, Y., et al., *Effect of atomization variables on powder characteristics in the high-pressured water atomization process.* Metal Powder Report, 1990. **45**(1): p. 38-40.

204. Hamill, J., C. Schade, and N. Myers, *Water atomized fine powder technology.* Gas, 2001. **80**: p. 90.

205. Roberts, P. *Commercial Atomization by the Rotating Electrode Process*. in *Symposium on Advances in Atomizing Processes, International Powder Metallurgy Confierence, Toronto, Canada*. 1984.

206. Xin, X., et al., *In vitro biocompatibility of Co–Cr alloy fabricated by selective laser melting or traditional casting techniques.* Materials Letters, 2012. **88**: p. 101-103.

207. Zeoli, N., H. Tabbara, and S. Gu, *CFD modeling of primary breakup during metal powder atomization.* Chemical engineering science, 2011. **66**(24): p. 6498-6504.

208. Smirnov, M., M. Kaplan, and M. Sevostyanov. *Receiving finely divided metal powder by inert gas atomization*. in *IOP Conference Series: Materials Science and Engineering*. 2018. IOP Publishing.

209. Zhang, L., et al., *Manufacture by selective laser melting and mechanical behavior of a biomedical Ti–24Nb–4Zr–8Sn alloy.* Scripta Materialia, 2011. **65**(1): p. 21-24.

210. Canakci, A. and T. Varol, *A novel method for the production of metal powders without conventional atomization process.* Journal of Cleaner Production, 2015. **99**: p. 312-319.

211. Buchbinder, D., et al., *High power selective laser melting (HP SLM) of aluminum parts.* Physics Procedia, 2011. **12**: p. 271-278.

212. Ahsan, M.N., et al., *A comparative study of laser direct metal deposition characteristics using gas and plasma-atomized Ti–6Al–4V powders.* Materials Science and Engineering: A, 2011. **528**(25-26): p. 7648-7657.

213. Heidloff, A., et al., *Advanced gas atomization processing for Ti and Ti alloy powder manufacturing.* Jom, 2010. **62**(5): p. 35-41.

214. Li, R., et al., *Densification behavior of gas and water atomized 316L stainless steel powder during selective laser melting.* Applied surface science, 2010. **256**(13): p. 4350-4356.

215. Schade, C.T., T.F. Murphy, and C. Walton. *Development of atomized powders for additive manufacturing*. in *Powder Metallurgy Word Congress, Accessed on 2nd July*. 2014.

216. Lawley, A., *Atomization of specialty alloy powders.* JOM, 1981. **33**(1): p. 13-18.

217. Öztürk, S. and F. Arslan, *Production of rapidly solidified metal powders by water cooled rotating disc atomisation.* Powder metallurgy, 2001. **44**(2): p. 171-176.

218. Slotwinski, J.A., et al., *Characterization of metal powders used for additive manufacturing.* Journal of research of the National Institute of Standards and Technology, 2014. **119**: p. 460.

219. Mani, M., et al., *Measurement science needs for real-time control of additive manufacturing powder bed fusion processes.* 2015.

220. Monzón, M., et al., *Standardization in additive manufacturing: activities carried out by international organizations and projects.* The international journal of advanced manufacturing technology, 2015. **76**(5-8): p. 1111-1121.

221. Slotwinski, J. and S. Moylan. *Metals-based additive manufacturing: metrology needs and standardization efforts*. in *2014 ASPE Spring Topical Meeting: Dimensional Accuracy and Surface Finish in Additive Manufacturing, Berkeley, CA, Apr*. 2014.

222. Vock, S., et al., *Powders for powder bed fusion: a review.* Progress in Additive Manufacturing, 2019: p. 1-15.

223. Mikli, V., et al., *Characterization of powder particle morphology.* Proceedings of the Estonian Academy of Sciences: Engineering(Estonia), 2001. **7**(1): p. 22-34.

224. Strondl, A., et al., *Characterization and control of powder properties for additive manufacturing.* Jom, 2015. **67**(3): p. 549-554.

225. Sutton, A.T., et al., *Powders for additive manufacturing processes: Characterization techniques and effects on part properties.* Solid Freeform Fabrication, 2016. **1**: p. 1004-1030.

226. Bückle, H., *Progress in micro-indentation hardness testing.* Metallurgical reviews, 1959. **4**(1): p. 49-100.

227. Davis, J.R. and S. Semiatin, *American Society for Metals-ASM Metals Handbook.* Vol. 14_ Forming and Forging-ASM International, 1989.

228. Davis, J.R., *ASM specialty handbook: tool materials*. 1995: ASM international.

229. Rawle, A., *Basic of principles of particle-size analysis.* Surface coatings international. Part A, Coatings journal, 2003. **86**(2): p. 58-65.

230. Börjesson, E., et al., *Entrapment of air during imbibition of agglomerated powder beds.* Journal of Food Engineering, 2017. **201**: p. 26-35.

231. Zou, R., M. Gan, and A. Yu, *Prediction of the porosity of multi-component mixtures of cohesive and non-cohesive particles.* Chemical engineering science, 2011. **66**(20): p. 4711-4721.

232. German, R.M., *Powder metallurgy science.* Metal Powder Industries Federation, 105 College Rd. E, Princeton, N. J. 08540, U. S. A, 1984. 279, 1984.

233. HIRSCHHORN, J., *Powder compaction.* HIRSCHHORN, JS Introduction to Powder Metallurgy. New York, American Powder Metallurgy Institute, 1969: p. 96-152.

234. Valdek, M., et al., *Characterization of Powder Particle Morphology.* Proc. Estonian Acad. Sci. Eng, 2001. **7**(1): p. 22-34.

235. Mostafaei, A., et al., *Comparison of characterization methods for differently atomized nickel-based alloy 625 powders.* Powder Technology, 2018. **333**: p. 180-192.

236. Heim, K., et al., *High resolution pore size analysis in metallic powders by X-ray tomography.* Case Studies in Nondestructive Testing and Evaluation, 2016. **6**: p. 45-52.

237. Webb, P.A., *Volume and density determinations for particle technologists.* Micromeritics Instrument Corp, 2001. **2**(16): p. 01.

238. Standard, B., *British Standard.* BS 7533-1 Guide for the Structural Design of Heavy Duty Pavements Constructed of Clay or Concrete Pavers, 2001.

239. Viana, M., et al., *About pycnometric density measurements.* Talanta, 2002. **57**(3): p. 583-593.

240. Mellin, P., et al., *Evaluating flowability of additive manufacturing powders, using the Gustavsson flow meter.* Metal powder report, 2017. **72**(5): p. 322-326.

241. Peterson, J. and W. Small, *Evaluation of metal powders using Arnold density meter and Hall flowmeter.* Powder metallurgy, 1994. **37**(1): p. 37-41.

242. Trasorras, J., R. Parameswaran, and A. Cocks, *Mechanical behavior of metal powders and powder compaction modeling.* ASM handbook, 1998. **7**: p. 326-342.

243. Prescott, J.K. and R.A. Barnum, *On powder flowability.* Pharmaceutical technology, 2000. **24**(10): p. 60-85.

244. Sun, Y., et al., *Manipulation and characterization of a novel titanium powder precursor for additive manufacturing applications.* Jom, 2015. **67**(3): p. 564-572.

245. Schulze, D., *Powders and bulk solids.* Behaviour, Characterization, Storage and Flow. Springer, 2008. **22**.

246. Spierings, A.B., et al., *Powder flowability characterisation methodology for powder-bed-based metal additive manufacturing.* Progress in Additive Manufacturing, 2016. **1**(1-2): p. 9-20.

247. Shah, R.B., M.A. Tawakkul, and M.A. Khan, *Comparative evaluation of flow for pharmaceutical powders and granules.* Aaps Pharmscitech, 2008. **9**(1): p. 250-258.

248. Karapatis, P., *A sub-process approach of selective laser sintering*, 2002, EPFL.

249. Schmid, M., et al. *Flowability of powders for selective laser sintering (SLS) investigated by round robin test*. in *High Value Manufacturing: Advanced Research in Virtual and Rapid Prototyping: Proceedings of the 6th International Conference on Advanced Research in Virtual and Rapid Prototyping*. 2013.

250. Geldart, D., et al., *Characterization of powder flowability using measurement of angle of repose.* China Particuology, 2006. **4**(03n04): p. 104-107.

251. McGlinchey, D., *Characterisation of bulk solids.* 2005.

252. Schwedes, J., *Review on testers for measuring flow properties of bulk solids.* Granular matter, 2003. **5**(1): p. 1-43.

253. McGlinchey, D., *Bulk solids handling: equipment selection and operation*. 2009: John Wiley & Sons.

254. Geldart, D., E. Abdullah, and A. Verlinden, *Characterisation of dry powders.* Powder technology, 2009. **190**(1-2): p. 70-74.

255. Nguyen, Q.B., et al., *Characteristics of inconel powders for powder-bed additive manufacturing.* Engineering, 2017. **3**(5): p. 695-700.

256. Amado, A., et al., *Advances in SLS powder characterization.* Group, 2011. **7**(10): p. 12.

257. Amado, A., M. Schmid, and K. Wegener, *Flowability of SLS powders at elevated temperature*, 2014, ETH Zurich.

258. Bourell, D., et al., *Influence of the particle size distribution on surface quality and mechanical properties in AM steel parts.* Rapid Prototyping Journal, 2011.

259. Krantz, M., H. Zhang, and J. Zhu, *Characterization of powder flow: Static and dynamic testing.* Powder Technology, 2009. **194**(3): p. 239-245.

260. Pohlman, N.A., J.A. Roberts, and M.J. Gonser, *Characterization of titanium powder: Microscopic views and macroscopic flow.* Powder technology, 2012. **228**: p. 141-148.

261. Soh, J.L., C.V. Liew, and P.W. Heng, *New indices to characterize powder flow based on their avalanching behavior.* Pharmaceutical development and technology, 2006. **11**(1): p. 93-102.

262. Clayton, J., *Optimising metal powders for additive manufacturing.* Metal Powder Report, 2014. **69**(5): p. 14-17.

263. Aragón, J., et al. *Design and manufacture of a mechanical system for teaching the diffraction phenomenon*. in *Journal of Physics: Conference Series*. 2019. IOP Publishing.

264. Morrison, A., et al., *The shape and behaviour of a granular bed in a rotating drum using Eulerian flow fields obtained from PEPT.* Chemical Engineering Science, 2016. **152**: p. 186-198.

265. Clayton, J., *Characterizing powders to optimise additive manufacturing.* Online verfügbar unter: http://www. tctmagazine. com/3D-printing-news/characterising-powders-to-optimise-additive-manufacturing/_, 2014.

266. Clayton, J., D. Millington-Smith, and B. Armstrong, *The application of powder rheology in additive manufacturing.* Jom, 2015. **67**(3): p. 544-548.

267. Freeman, R., *Measuring the flow properties of consolidated, conditioned and aerated powders—a comparative study using a powder rheometer and a rotational shear cell.* Powder Technology, 2007. **174**(1-2): p. 25-33.

268. Hare, C., et al., *Analysis of the dynamics of the FT4 powder rheometer.* Powder Technology, 2015. **285**: p. 123-127.

269. Lyckfeldt, O. *Powder rheology of steel powders for additive manufacturing*. in *International Powder Metallurgy Congress and Exhibition, Euro PM 2013*. 2013. European Powder Metallurgy Association (EPMA).

270. Strondl, A., A. Angré, and D. Chasoglou. *Characterisation of steel powders-Correlation between particle characteristics and bulk powder properties*. in *International Powder Metallurgy Congress and Exhibition, Euro PM 2013, 15 September 2013 through 18 September 2013, 110976*. 2013. European Powder Metallurgy Association (EPMA).

271. Yan, Z., et al., *Investigating mixing and segregation using discrete element modelling (DEM) in the Freeman FT4 rheometer.* International journal of pharmaceutics, 2016. **513**(1-2): p. 38-48.

272. Koynov, S., B. Glasser, and F. Muzzio, *Comparison of three rotational shear cell testers: Powder flowability and bulk density.* Powder Technology, 2015. **283**: p. 103-112.

273. ISO, *Surface active agents–powders and granules–measurement of the angle of repose*, 1977, International Organization for Standardization Genève.

274. DeCost, B.L. and E.A. Holm, *Characterizing powder materials using keypoint-based computer vision methods.* Computational Materials Science, 2017. **126**: p. 438-445.

275. DeCost, B.L., et al., *Computer vision and machine learning for autonomous characterization of am powder feedstocks.* Jom, 2017. **69**(3): p. 456-465.

276. Van den Eynde, M., L. Verbelen, and P. Van Puyvelde, *Assessing polymer powder flow for the application of laser sintering.* Powder Technology, 2015. **286**: p. 151-155.

277. Chaira, D., *Development of nano-structured duplex and ferritic stainless steels by pulverisette planetary milling followed by pressureless sintering.* Materials Characterization, 2015. **99**: p. 220-229.

278. Jacobson, M., A.R. Cooper, and J. Nagy, *Explosibility of metal powders*. Vol. 6516. 1964: US Department of the Interior, Bureau of Mines.

279. Clark, F.H., *Advanced techniques in powder metallurgy*. 1963: Rowman and Littlefield.

280. Association, N.F.P., *NFPA 61: Standard for the Prevention of Fires and Dust Explosions in Agricultural and Food Processing Facilities*. 2002.

281. Gülsoy, H., S. Özbek, and T. Baykara, *Microstructural and mechanical properties of injection moulded gas and water atomised 17-4 PH stainless steel powder.* Powder metallurgy, 2007. **50**(2): p. 120-126.

282. Rombouts, M., et al., *Laser metal deposition of Inconel 625: microstructure and mechanical properties.* Journal of Laser Applications, 2012. **24**(5): p. 052007.

283. Suri, P., R.P. Koseski, and R.M. German, *Microstructural evolution of injection molded gas-and water-atomized 316L stainless steel powder during sintering.* Materials Science and Engineering: A, 2005. **402**(1-2): p. 341-348.

284. Zhang, L., et al., *A comparative investigation on MIM418 superalloy fabricated using gas-and water-atomized powders.* Powder technology, 2015. **286**: p. 798-806.

285. Miyanaji, H., et al., *Optimal process parameters for 3D printing of porcelain structures.* Procedia Manufacturing, 2016. **5**: p. 870-887.

286. Derby, B., *Inkjet printing of functional and structural materials: fluid property requirements, feature stability, and resolution.* Annual Review of Materials Research, 2010. **40**: p. 395-414.

287. Holman, R.K., et al., *Spreading and infiltration of inkjet-printed polymer solution droplets on a porous substrate.* Journal of colloid and interface science, 2002. **249**(2): p. 432-440.

288. Miyanaji, H., N. Momenzadeh, and L. Yang, *Effect of powder characteristics on parts fabricated via binder jetting process.* Rapid Prototyping Journal, 2019.

289. Zheng, J., W.B. Carlson, and J.S. Reed, *The packing density of binary powder mixtures.* Journal of the European Ceramic Society, 1995. **15**(5): p. 479-483.

290. Sohn, H.Y. and C. Moreland, *The effect of particle size distribution on packing density.* The Canadian Journal of Chemical Engineering, 1968. **46**(3): p. 162-167.

291. Liu, B., et al., *Investigation the effect of particle size distribution on processing parameters optimisation in selective laser melting process.* Additive manufacturing research group, Loughborough University, 2011: p. 227-238.

292. Abd-Elghany, K. and D. Bourell, *Property evaluation of 304L stainless steel fabricated by selective laser melting.* Rapid Prototyping Journal, 2012.

293. Lutter-Günther, M., et al. *Einfluss der Korngrößenverteilung auf Fließfähigkeit und Bauteilqualität beim Laserstrahlschmelzen. Influence of particle size distribution on powder flowability and part properties in laser beam melting*. in *Proceedings of the 14th rapid technical conference. Carl Hanser, München*. 2017.

294. Ziegelmeier, S., et al., *An experimental study into the effects of bulk and flow behaviour of laser sintering polymer powders on resulting part properties.* Journal of Materials Processing Technology, 2015. **215**: p. 239-250.

295. Spierings, A.B. and G. Levy. *Comparison of density of stainless steel 316L parts produced with selective laser melting using different powder grades*. in *Proceedings of the Annual International Solid Freeform Fabrication Symposium*. 2009. Austin, TX.

296. Badrossamay, M., et al., *Improving productivity rate in SLM of commercial steel powders.* Technical Paper-Society of Manufacturing Engineers, 2009: p. 1-13.

297. Kappes, B., et al. *Machine learning to optimize additive manufacturing parameters for laser powder bed fusion of Inconel 718*. in *Proceedings of the 9th International Symposium on Superalloy 718 & Derivatives: Energy, Aerospace, and Industrial Applications*. 2018. Springer.

298. Inaekyan, K., et al. *Binder-jetting additive manufacturing with water atomized iron powders*. in *Proceedings of the AMPM 2016 Conference on Additive Manufacturing, Held with MPIF/APMI International Conference on Powder Metallurgy & Particulate Materials, Boston, MA, USA*. 2016.

299. Leitz, K.-H., et al., *Fundamental analysis of the influence of powder characteristics in Selective Laser Melting of molybdenum based on a multi-physical simulation model.* International Journal of Refractory Metals and Hard Materials, 2018. **72**: p. 1-8.

300. Sutton, A.T., et al., *Powder characterisation techniques and effects of powder characteristics on part properties in powder-bed fusion processes.* Virtual and physical prototyping, 2017. **12**(1): p. 3-29.

301. Townsend, A., et al., *Surface texture metrology for metal additive manufacturing: a review.* Precision Engineering, 2016. **46**: p. 34-47.

302. Verlee, B., T. Dormal, and J. Lecomte-Beckers, *Density and porosity control of sintered 316L stainless steel parts produced by additive manufacturing.* Powder Metallurgy, 2012. **55**(4): p. 260-267.

303. Neira-Arce, A., *Thermal Modeling and Simulation of Electron Beam Melting for Rapid Prototyping on Ti6Al4V Alloys.* 2012.

304. Lu, K., M. Hiser, and W. Wu, *Effect of particle size on three dimensional printed mesh structures.* Powder Technology, 2009. **192**(2): p. 178-183.

305. Clarke, A., et al., *Spreading and imbibition of liquid droplets on porous surfaces.* Langmuir, 2002. **18**(8): p. 2980-2984.

306. Lanzetta, M. and E. Sachs, *Improved surface finish in 3D printing using bimodal powder distribution.* Rapid Prototyping Journal, 2003.

307. Spierings, A.B., M. Schneider, and R. Eggenberger, *Comparison of density measurement techniques for additive manufactured metallic parts.* Rapid Prototyping Journal, 2011.

308. Zhou, Z., et al., *Printability of calcium phosphate: calcium sulfate powders for the application of tissue engineered bone scaffolds using the 3D printing technique.* Materials Science and Engineering: C, 2014. **38**: p. 1-10.

309. Hapgood, K.P., et al., *Drop penetration into porous powder beds.* Journal of Colloid and Interface Science, 2002. **253**(2): p. 353-366.

310. Miyanaji, H., S. Zhang, and L. Yang, *A new physics-based model for equilibrium saturation determination in binder jetting additive manufacturing process.* International Journal of Machine Tools and Manufacture, 2018. **124**: p. 1-11.

311. Bredt, J.F., *Binder stability and powder/binder interaction in three-dimensional printing.* 1997.

312. Hildebrandt, C., et al., *Evaluation and prediction of powder flowability in pharmaceutical tableting.* Pharmaceutical development and technology, 2019. **24**(1): p. 35-47.

313. Elliott, A., et al., *Infiltration of nanoparticles into porous binder jet printed parts.* American Journal of Engineering and Applied Sciences, 2016. **9**(1).

314. Bai, J., et al. *Porosity evolution in additively manufactured aluminium alloy during high temperature exposure*. in *IOP Conference Series: Materials Science and Engineering*. 2017. IOP Publishing.

315. Ahmad, K.R., et al., *The influence of alumina particle size on sintered density and hardness of discontinuous reinforced aluminum metal matrix composite.* Jurnal Teknologi, 2005. **42**(1): p. 49-57.

316. Lu, G., G.M. Lu, and Z. Xiao, *Mechanical properties of porous materials.* Journal of Porous Materials, 1999. **6**(4): p. 359-368.

317. Tao, Q., et al., *Enhanced Vickers hardness by quasi-3D boron network in MoB 2.* RSC advances, 2013. **3**(40): p. 18317-18322.

318. German, R., *Pore size and shape*, in *Particle Packing Characteristics*. 1989, Metal Powder Industries Federation Princeton, NJ. p. 298-300.

319. Brouwers, H., *Particle-size distribution and packing fraction of geometric random packings.* Physical review E, 2006. **74**(3): p. 031309.

320. Desmond, K.W. and E.R. Weeks, *Influence of particle size distribution on random close packing of spheres.* Physical Review E, 2014. **90**(2): p. 022204.

321. Haeri, S., *Optimisation of blade type spreaders for powder bed preparation in Additive Manufacturing using DEM simulations.* Powder Technology, 2017. **321**: p. 94-104.

322. Haeri, S., et al., *Discrete element simulation and experimental study of powder spreading process in additive manufacturing.* Powder Technology, 2017. **306**: p. 45-54.

323. Benson, J.M. and E. Snyders, *The need for powder characterisation in the additive manufacturing industry and the establishment of a national facility.* South African Journal of Industrial Engineering, 2015. **26**(2): p. 104-114.

324. Hudson, T. and P. Harrowell, *Dense packings of hard spheres of different sizes based on filling interstices in uniform three-dimensional tilings.* The Journal of Physical Chemistry B, 2008. **112**(27): p. 8139-8143.

325. Kummerfeld, J.K., T.S. Hudson, and P. Harrowell, *The densest packing of AB binary hard-sphere homogeneous compounds across all size ratios.* The Journal of Physical Chemistry B, 2008. **112**(35): p. 10773-10776.

326. Schaertl, W. and H. Sillescu, *Brownian dynamics of polydisperse colloidal hard spheres: Equilibrium structures and random close packings.* Journal of Statistical Physics, 1994. **77**(5-6): p. 1007-1025.

327. Visscher, W.M. and M. Bolsterli, *Random packing of equal and unequal spheres in two and three dimensions.* Nature, 1972. **239**(5374): p. 504-507.

328. Bai, Y., G. Wagner, and C.B. Williams. *Effect of bimodal powder mixture on powder packing density and sintered density in binder jetting of metals*. in *2015 Annual International Solid Freeform Fabrication Symposium*. 2015.

329. Rahaman, M.N., *Ceramic Processing and Sintering Second edition.* MATERIALS ENGINEERING-NEW YORK-, 2003. **23**.

330. Spath, S., P. Drescher, and H. Seitz, *Impact of particle size of ceramic granule blends on mechanical strength and porosity of 3D printed scaffolds.* Materials, 2015. **8**(8): p. 4720-4732.

331. Mao, T., D.C. Kuhn, and H. Tran, *Spread and rebound of liquid droplets upon impact on flat surfaces.* AIChE Journal, 1997. **43**(9): p. 2169-2179.

332. Zhu, H., J. Fuh, and L. Lu, *The influence of powder apparent density on the density in direct laser-sintered metallic parts.* International Journal of Machine Tools and Manufacture, 2007. **47**(2): p. 294-298.

333. McGeary, R., *Mechanical packing of spherical particles.* Journal of the American ceramic Society, 1961. **44**(10): p. 513-522.

334. German, R.M., *Prediction of sintered density for bimodal powder mixtures.* Metallurgical Transactions A, 1992. **23**(5): p. 1455-1465.

335. Karapatis, N., et al. *Optimization of powder layer density in selective laser sintering*. in *1999 International Solid Freeform Fabrication Symposium*. 1999.

336. Byholm, T., M. Toivakka, and J. Westerholm, *Effective packing of 3-dimensional voxel-based arbitrarily shaped particles.* Powder Technology, 2009. **196**(2): p. 139-146.

337. Chen, H., et al., *Powder-spreading mechanisms in powder-bed-based additive manufacturing: Experiments and computational modeling.* Acta Materialia, 2019. **179**: p. 158-171.

338. Dong, K., C. Wang, and A. Yu, *A novel method based on orientation discretization for discrete element modeling of non-spherical particles.* Chemical Engineering Science, 2015. **126**: p. 500-516.

339. Höhner, D., S. Wirtz, and V. Scherer, *A study on the influence of particle shape on the mechanical interactions of granular media in a hopper using the discrete element method.* Powder technology, 2015. **278**: p. 286-305.

340. Jia, X., et al., *Validation of a digital packing algorithm in predicting powder packing densities.* Powder Technology, 2007. **174**(1-2): p. 10-13.

341. Lu, G., J. Third, and C. Müller, *Discrete element models for non-spherical particle systems: From theoretical developments to applications.* Chemical Engineering Science, 2015. **127**: p. 425-465.

342. Basalah, A., S. Esmaeili, and E. Toyserkani, *On the influence of sintering protocols and layer thickness on the physical and mechanical properties of additive manufactured titanium porous bio-structures.* Journal of Materials Processing Technology, 2016. **238**: p. 341-351.

343. Doyle, M., et al., *Effect of layer thickness and orientation on mechanical behavior of binder jet stainless steel 420+ bronze parts.* Procedia Manufacturing, 2015. **1**: p. 251-262.

344. Enneti, R.K. and K.C. Prough, *Effect of binder saturation and powder layer thickness on the green strength of the binder jet 3D printing (BJ3DP) WC-12% Co powders.* International Journal of Refractory Metals and Hard Materials, 2019. **84**: p. 104991.

345. Farzadi, A., et al., *Effect of layer thickness and printing orientation on mechanical properties and dimensional accuracy of 3D printed porous samples for bone tissue engineering.* PloS one, 2014. **9**(9).

346. Sheydaeian, E., et al., *On the effect of throughout layer thickness variation on properties of additively manufactured cellular titanium structures.* Additive Manufacturing, 2017. **18**: p. 40-47.

347. Vaezi, M. and C.K. Chua, *Effects of layer thickness and binder saturation level parameters on 3D printing process.* The International Journal of Advanced Manufacturing Technology, 2011. **53**(1-4): p. 275-284.

348. Lee, S.-J.J., *Powder layer generation for three dimensional printing*, 1992, Massachusetts Institute of Technology.

349. Cao, S., et al., *Experimental and theoretical investigation on ultra-thin powder layering in three dimensional printing (3DP) by a novel double-smoothing mechanism.* Journal of Materials Processing Technology, 2015. **220**: p. 231-242.

350. Nan, W. and M. Ghadiri, *Numerical simulation of powder flow during spreading in additive manufacturing.* Powder technology, 2019. **342**: p. 801-807.

351. Chen, H., et al., *Packing quality of powder layer during counter-rolling-type powder spreading process in additive manufacturing.* International Journal of Machine Tools and Manufacture, 2020: p. 103553.

352. Fouda, Y.M. and A.E. Bayly, *A DEM study of powder spreading in additive layer manufacturing.* Granular Matter, 2020. **22**(1): p. 10.

353. Butscher, A., et al., *Printability of calcium phosphate powders for three-dimensional printing of tissue engineering scaffolds.* Acta biomaterialia, 2012. **8**(1): p. 373-385.

354. Mussatto, A., et al., *Evaluation via powder metallurgy of nano-reinforced iron powders developed for selective laser melting applications.* Materials & Design, 2019. **182**: p. 108046.

355. Du, W., et al. *Binder Jetting Additive Manufacturing of Ceramics: Comparison of Flowability and Sinterability Between Raw and Granulated Powders*. in *ASME 2019 14th International Manufacturing Science and Engineering Conference*. 2019. American Society of Mechanical Engineers Digital Collection.

356. Smith, L. and P. Midha, *Computer simulation of morphology and packing behaviour of irregular particles, for predicting apparent powder densities.* Computational materials science, 1997. **7**(4): p. 377-383.

357. Spath, S. and H. Seitz, *Influence of grain size and grain-size distribution on workability of granules with 3D printing.* The International Journal of Advanced Manufacturing Technology, 2014. **70**(1-4): p. 135-144.

358. Thomas, Y., et al., *Effect of Atmospheric humidity and temperature on the flowability of lubricated powder metallurgy mixes.* Advances in Powder Metallurgy & Particulate Materials-2009, 2009. **1**(3-Compaction and Forming Processes).

359. Chan, L.C. and N.W. Page, *Particle fractal and load effects on internal friction in powders.* Powder Technology, 1997. **90**(3): p. 259-266.

360. Teunou, E., J. Fitzpatrick, and E. Synnott, *Characterisation of food powder flowability.* Journal of Food Engineering, 1999. **39**(1): p. 31-37.

361. Chen, H., et al., *Flow behavior of powder particles in layering process of selective laser melting: Numerical modeling and experimental verification based on discrete element method.* International Journal of Machine Tools and Manufacture, 2017. **123**: p. 146-159.

362. Kurz, H. and G. Münz, *The influence of particle size distribution on the flow properties of limestone powders.* Powder Technology, 1975. **11**(1): p. 37-40.

363. Tang, H., et al., *Effect of powder reuse times on additive manufacturing of Ti-6Al-4V by selective electron beam melting.* Jom, 2015. **67**(3): p. 555-563.

364. Lu, S.L., et al., *Microstructure and mechanical properties of long Ti-6Al-4V rods additively manufactured by selective electron beam melting out of a deep powder bed and the effect of subsequent hot isostatic pressing.* Metallurgical and Materials Transactions A, 2015. **46**(9): p. 3824-3834.

365. Perry, J.H., *Manual del ingeniero químico*, 1966.

366. Arriola, L.T. and A.L. Roa, *Transporte y almacenamiento de materias primas en la industria básica*. 1970: Ed. Blume.

367. Klisiewicz, P., J.A. Roberts, and N.A. Pohlman, *Segregation of titanium powder with polydisperse size distribution: Spectral and correlation analyses.* Powder Technology, 2015. **272**: p. 204-210.

368. Mosby, J., S.R. de Silva, and G.G. Enstad, *Segregation of particulate materials–mechanisms and testers.* KONA Powder and Particle Journal, 1996. **14**: p. 31-43.

369. Tang, P. and V. Puri, *Methods for minimizing segregation: a review.* Particulate Science and Technology, 2004. **22**(4): p. 321-337.

370. Williams, J.C., *The segregation of particulate materials. A review.* Powder technology, 1976. **15**(2): p. 245-251.

371. Hebert, R.J., *metallurgical aspects of powder bed metal additive manufacturing.* Journal of Materials Science, 2016. **51**(3): p. 1165-1175.

372. Pidge, P.A. and H. Kumar, *Additive manufacturing: A review on 3 D printing of metals and study of residual stress, buckling load capacity of strut members.* Materials Today: Proceedings, 2020. **21**: p. 1689-1694.

373. Saboori, A., et al., *Critical Features in the Microstructural Analysis of AISI 316L Produced By Metal Additive Manufacturing.* Metallography, Microstructure, and Analysis, 2020. **9**(1): p. 92-96.

374. Bautista, A., et al., *Oxidation behavior at 900° C of austenitic, ferritic, and duplex stainless steels manufactured by powder metallurgy.* Oxidation of Metals, 2003. **59**(3-4): p. 373-393.

375. Anderson, I.E. and J.C. Foley, *Determining the role of surfaces and interfaces in the powder metallurgy processing of aluminum alloy powders.* Surface and Interface Analysis: An International Journal devoted to the development and application of techniques for the analysis of surfaces, interfaces and thin films, 2001. **31**(7): p. 599-608.

376. Zheng, L., et al., *Investigations on the growing, cracking and spalling of oxides scales of powder metallurgy Rene95 nickel-based superalloy.* Applied surface science, 2011. **257**(23): p. 9762-9767.

377. Ardila, L., et al., *Effect of IN718 recycled powder reuse on properties of parts manufactured by means of Selective Laser Melting.* Physics Procedia, 2014. **56**: p. 99-107.

378. Jacob, G., et al., *Effects of powder recycling on stainless steel powder and built material properties in metal powder bed fusion processes*. 2017: US Department of Commerce, National Institute of Standards and Technology.

379. Maamoun, A.H., et al., *Thermal post-processing of AlSi10Mg parts produced by Selective Laser Melting using recycled powder.* Additive Manufacturing, 2018. **21**: p. 234-247.

380. Niñerola, V.P.R., *Powder recyclability in electron beam melting for aeronautical use.* Aircraft Engineering and Aerospace Technology: An International Journal, 2015. **87**(2): p. 147-155.

381. O'Leary, R., et al., *An investigation into the recycling of Ti-6Al-4V powder used within SLM to improve sustainability.* InImpact: The Journal of Innovation Impact, 2016. **8**(2): p. 377.

382. Popov Jr, V.V., et al., *The effect of powder recycling on the mechanical properties and microstructure of electron beam melted Ti-6Al-4 V specimens.* Additive Manufacturing, 2018. **22**: p. 834-843.

383. Mostafaei, A., et al., *Binder jet 3D printing–process parameters, materials, properties, and challenges.* Progress in Materials Science, 2020: p. 100684.

384. Santecchia, E., S. Spigarelli, and M. Cabibbo, *Material Reuse in Laser Powder Bed Fusion: Side Effects of the Laser—Metal Powder Interaction.* Metals, 2020. **10**(3): p. 341.

385. Savolainen, J. and M. Collan, *Additive manufacturing technology and business model change–a review of literature.* Additive Manufacturing, 2020: p. 101070.

386. Denesuk, M., et al., *Capillary penetration of liquid droplets into porous materials.* Journal of colloid and interface science, 1993. **158**(1): p. 114-120.

387. Denesuk, M., et al., *Dynamics of incomplete wetting on porous materials.* Journal of Colloid and interface science, 1994. **168**(1): p. 142-151.

388. Washburn, E.W., *The dynamics of capillary flow.* Physical review, 1921. **17**(3): p. 273.

389. Bredt, J.F., T.C. Anderson, and D.B. Russell, *Three dimensional printing material system and method*, 2003, Google Patents.

390. Bredt, J.F., S. Clark, and G. Gilchrist, *Three dimensional printing material system and method*, 2006, Google Patents.

391. Khoshnevis, B., *Selective inhibition of bonding of power particles for layered fabrication of 3-D objects*, 2003, Google Patents.

392. Sachs, E.M., et al., *Jetting layers of powder and the formation of fine powder beds thereby*, 2003, Google Patents.

393. Myers, K., et al., *The Effect of Print Speed on Surface Roughness and Density Uniformity of Parts Produced Using Binder Jet 3D Printing.*

394. Kernan, B.D., et al., *Three-dimensional printing of tungsten carbide–10 wt% cobalt using a cobalt oxide precursor.* International Journal of Refractory Metals and Hard Materials, 2007. **25**(1): p. 82-94.

395. Cima, M., et al. *Structural ceramic components by 3D printing*. in *1995 International Solid Freeform Fabrication Symposium*. 1995.

396. Sachs, E., et al. *Progress on tooling by 3D printing; conformal cooling, dimensional control, surface finish and hardness*. in *1997 International Solid Freeform Fabrication Symposium*. 1997.

397. LEWIS, R.M., *Powder binder interactions in 3D inkjet printing.* 2014.

398. Sachs, E., M. Cima, and J. Cornie, *Three-dimensional printing: rapid tooling and prototypes directly from a CAD model.* CIRP annals, 1990. **39**(1): p. 201-204.

399. Bai, J.G., K.D. Creehan, and H.A. Kuhn, *Inkjet printable nanosilver suspensions for enhanced sintering quality in rapid manufacturing.* Nanotechnology, 2007. **18**(18): p. 185701.

400. Wohlers, T.T. and T. Caffrey, *Wohlers report 2014: 3D printing and additive manufacturing state of the industry annual worldwide progress report*. 2014: Wohlers Associates Fort Collins, CO.

401. Zhao, H., et al., *Fabricating an effective calcium zirconate layer over the calcia grains via binder-jet 3D-printing for improving the properties of calcia ceramic cores.* Additive Manufacturing, 2020. **32**: p. 101025.

402. Derby, B. and N. Reis, *Inkjet printing of highly loaded particulate suspensions.* MRS bulletin, 2003. **28**(11): p. 815-818.

403. Bai, Y. and C.B. Williams, *Binder jetting additive manufacturing with a particle-free metal ink as a binder precursor.* Materials & Design, 2018. **147**: p. 146-156.

404. Sachs, E.M., et al., *Metal and ceramic containing parts produced from powder using binders derived from salt*, 2003, Google Patents.

405. McCarthy, D. and C. Williams. *Creating complex hollow metal geometries using additive manufacturing and electroforming*. in *International Solid Freeform Fabrication Symposium*. 2012.

406. Dini, F., et al., *A review of binder jet process parameters; powder, binder, printing and sintering condition.* Metal Powder Report, 2019.

407. Song, J. and H. Nur, *Defects and prevention in ceramic components fabricated by inkjet printing.* Journal of materials processing technology, 2004. **155**: p. 1286-1292.

408. Duineveld, P.C., et al. *Ink-jet printing of polymer light-emitting devices*. in *Organic Light-Emitting Materials and Devices V*. 2002. International Society for Optics and Photonics.

409. Noguera, R., M. Lejeune, and T. Chartier, *3D fine scale ceramic components formed by ink-jet prototyping process.* Journal of the European Ceramic Society, 2005. **25**(12): p. 2055-2059.

410. Shen, X. and H.E. Naguib, *A robust ink deposition system for binder jetting and material jetting.* Additive Manufacturing, 2019. **29**: p. 100820.

411. Kwon, K.-S. and W. Kim, *A waveform design method for high-speed inkjet printing based on self-sensing measurement.* Sensors and Actuators A: Physical, 2007. **140**(1): p. 75-83.

412. Pond, S.F., *Inkjet technology and product development strategies.* 2000.

413. Hutchings, I., G. Martin, and S. Hoath, *High speed imaging and analysis of jet and drop formation.* Journal of Imaging Science and Technology, 2007. **51**(5): p. 438-444.

414. Martin, G.D., S.D. Hoath, and I.M. Hutchings. *Inkjet printing-the physics of manipulating liquid jets and drops*. in *Journal of Physics: Conference Series*. 2008. IOP Publishing.

415. Parab, N.D., et al., *Real time observation of binder jetting printing process using high-speed X-ray imaging.* Scientific reports, 2019. **9**(1): p. 1-10.

416. Kurz, A., J. Bauer, and M. Wagner, *Piezo-Plunger Jetting Technology: An Experimental Study on Jetting Characteristics of Filled Epoxy Polymers.* Fluids, 2019. **4**(1): p. 23.

417. Miyanaji, H., et al., *Process development for green part printing using binder jetting additive manufacturing.* Frontiers of Mechanical Engineering, 2018. **13**(4): p. 504-512.

418. Basaran, O.A., *Small-scale free surface flows with breakup: Drop formation and emerging applications.* AIChE Journal, 2002. **48**(9): p. 1842-1848.

419. Baker, P.R., *Three dimensional printing with fine metal powders*, 1997, Massachusetts Institute of Technology.

420. Holman, R.K., et al., *Surface adsorption effects in the inkjet printing of an aqueous polymer solution on a porous oxide ceramic substrate.* Journal of colloid and interface science, 2002. **247**(2): p. 266-274.

421. Moon, J., et al., *Ink-jet printing of binders for ceramic components.* Journal of the American Ceramic Society, 2002. **85**(4): p. 755-762.

422. Clarke, P., et al., *Sea level finger printing as a direct test for the source of global meltwater pulse 1a.* Science, 2002. **295**: p. 2438-2441.

423. Lim, N., et al., *Screen printed resonant tags for electronic article surveillance tags.* IEEE Transactions on Advanced Packaging, 2009. **32**(1): p. 72-76.

424. Picha, K., C. Spackman, and J. Samuel, *Droplet spreading characteristics observed during 3D printing of aligned fiber-reinforced soft composites.* Additive Manufacturing, 2016. **12**: p. 121-131.

425. Gambaryan-Roisman, T., *Liquids on porous layers: wetting, imbibition and transport processes.* Current opinion in colloid & interface science, 2014. **19**(4): p. 320-335.

426. Oostveen, M.L., G.M. Meesters, and J.R. van Ommen, *Quantification of powder wetting by drop penetration time.* Powder Technology, 2015. **274**: p. 62-66.

427. Bai, Y., et al., *Characterizing Binder–Powder Interaction in Binder Jetting Additive Manufacturing Via Sessile Drop Goniometry.* Journal of Manufacturing Science and Engineering, 2019. **141**(1).

428. Emady, H.N., D. Kayrak-Talay, and J.D. Litster, *Modeling the granule formation mechanism from single drop impact on a powder bed.* Journal of colloid and interface science, 2013. **393**: p. 369-376.

429. Emady, H.N., et al., *Granule formation mechanisms and morphology from single drop impact on powder beds.* Powder technology, 2011. **212**(1): p. 69-79.

430. Jung, S. and I.M. Hutchings, *The impact and spreading of a small liquid drop on a non-porous substrate over an extended time scale.* Soft Matter, 2012. **8**(9): p. 2686-2696.

431. Lee, J., et al., *Universal rescaling of drop impact on smooth and rough surfaces.* Journal of Fluid Mechanics, 2016. **786**.

432. Agland, S. and S.M. Iveson, *The impact of liquid drops on powder bed surfaces.* Chemeca 99: Chemical Engineering: Solutions in a Changing Environment, 1999: p. 218.

433. Benkreira, H., *The effect of substrate roughness on air entrainment in dip coating.* Chemical Engineering Science, 2004. **59**(13): p. 2745-2751.

434. Range, K. and F. Feuillebois, *Influence of surface roughness on liquid drop impact.* Journal of colloid and interface science, 1998. **203**(1): p. 16-30.

435. Jung, S., S.D. Hoath, and I.M. Hutchings, *The role of viscoelasticity in drop impact and spreading for inkjet printing of polymer solution on a wettable surface.* Microfluidics and nanofluidics, 2013. **14**(1-2): p. 163-169.

436. Lee, H., *Drop formation in a liquid jet.* IBM Journal of Research and Development, 1974. **18**(4): p. 364-369.

437. Tan, H., T. Tran, and C. Chua, *A review of printed passive electronic components through fully additive manufacturing methods.* Virtual and Physical Prototyping, 2016. **11**(4): p. 271-288.

438. Alleborn, N. and H. Raszillier, *Spreading and sorption of a droplet on a porous substrate.* Chemical Engineering Science, 2004. **59**(10): p. 2071-2088.

439. Costa, H.L. and I.M. Hutchings. *Ink-jet printing for patterning engineering surfaces*. in *NIP & digital fabrication conference*. 2008. Society for Imaging Science and Technology.

440. Denesuk, M., *Modelling of dynamic wetting phenomena.* 1990.

441. Forny, L., A. Marabi, and S. Palzer, *Wetting, disintegration and dissolution of agglomerated water soluble powders.* Powder Technology, 2011. **206**(1-2): p. 72-78.

442. Mundozah, A.L., et al., *Hydrophobic/hydrophilic static powder beds: Competing horizontal spreading and vertical imbibition mechanisms of a single droplet.* Powder technology, 2018. **330**: p. 275-283.

443. Weber, S., et al., *Agglomerate stability in fluidized beds of glass beads and silica sand.* Powder technology, 2006. **165**(3): p. 115-127.

444. Salehi, M., et al., *A paradigm shift towards compositionally zero-sum binderless 3D printing of magnesium alloys via capillary-mediated bridging.* Acta Materialia, 2019. **165**: p. 294-306.

445. Miyanaji, H., *Binder jetting additive manufacturing process fundamentals and the resultant influences on part quality.* 2018.

446. Shrestha, S. and G. Manogharan, *Optimization of binder jetting using Taguchi method.* Jom, 2017. **69**(3): p. 491-497.

447. Simchi, A., *The role of particle size on the laser sintering of iron powder.* Metallurgical and Materials Transactions B, 2004. **35**(5): p. 937-948.

448. Cooke, A. and J. Slotwinski, *Properties of metal powders for additive manufacturing: a review of the state of the art of metal powder property testing*. 2012: US Department of Commerce, National Institute of Standards and Technology.

449. Hoffmann, A. and H. Finkers, *A relation for the void fraction of randomly packed particle beds.* Powder Technology, 1995. **82**(2): p. 197-203.

450. Fremond, M., *Shape memory alloy*, in *Shape memory alloys*. 1996, Springer. p. 1-68.

451. Lu, K. and W.T. Reynolds, *3DP process for fine mesh structure printing.* Powder technology, 2008. **187**(1): p. 11-18.

452. Miyazaki, S., *Development and characterization of shape memory alloys*, in *Shape memory alloys*. 1996, Springer. p. 69-147.

453. Mostafaei, A., et al., *Microstructural evolution and mechanical properties of differently heat-treated binder jet printed samples from gas-and water-atomized alloy 625 powders.* Acta Materialia, 2017. **124**: p. 280-289.

454. Zhang, W., et al., *Three-dimensional printing of complex-shaped alumina/glass composites.* Advanced Engineering Materials, 2009. **11**(12): p. 1039-1043.

455. Elliott, A.M., et al., *A method for measuring powder bed density in binder jet additive manufacturing process and the powder feedstock characteristics influencing the powder bed density*, 2016, Oak Ridge National Lab.(ORNL), Oak Ridge, TN (United States). High ….

456. Jimenez, E.M., et al., *Parametric analysis to quantify process input influence on the printed densities of binder jetted alumina ceramics.* Additive Manufacturing, 2019. **30**: p. 100864.

457. Heywood, B., *Design and manufacture of a powder deposition system for a powder bed on a three dimensional printer.* Bachelor of Science, Mechanical Engineering, MIT, US, 1993.

458. Pruitt, B.L., *The design of an automated powder deposition system for a three-dimensional printing machine*, 1991, Massachusetts Institute of Technology.

459. Parteli, E.J. and T. Pöschel, *Particle-based simulation of powder application in additive manufacturing.* Powder Technology, 2016. **288**: p. 96-102.

460. Ramakrishnan, N., et al., *Studies on preparation of ceramic inks and simulation of drop formation and spread in direct ceramic inkjet printing.* Journal of Materials Processing Technology, 2005. **169**(3): p. 372-381.

461. Yang, L., et al. *Development of a 3D printing method for production of dental application*. in *Proceedings of the 24th International Solid Freeform Fabrication Symposium. Austin, TX, USA*. 2013.

462. Shanjani, Y., E. Toyserkani, and C. Wei. *Modeling and Characterization of Biomaterials Spreading Properties in Powder-Based Rapid Prototyping Techniques*. in *ASME 2007 International Mechanical Engineering Congress and Exposition*. 2007. American Society of Mechanical Engineers Digital Collection.

463. Miyanaji, H., N. Momenzadeh, and L. Yang, *Effect of printing speed on quality of printed parts in Binder Jetting Process.* Additive Manufacturing, 2018. **20**: p. 1-10.

464. Wang, Y., et al., *Simulation and experimental study of binder droplet infiltration in 3DP technology.* Modern Physics Letters B, 2018. **32**(23): p. 1850272.

465. Miyanaji, H. and L. Yang. *Equilibrium saturation in binder jetting additive manufacturing processes: theoretical model vs. experimental observations*. in *International Solid Freeform Fabrication Symposium*. 2016.

466. Asadi-Eydivand, M., et al., *Effect of technical parameters on porous structure and strength of 3D printed calcium sulfate prototypes.* Robotics and Computer-Integrated Manufacturing, 2016. **37**: p. 57-67.

467. Suwanprateeb, J., et al., *Influence of printing parameters on the transformation efficiency of 3D-printed plaster of paris to hydroxyapatite and its properties.* Rapid Prototyping Journal, 2012.

468. Szucs, T.D. and D. Brabazon. *Effect of saturation and post processing on 3D printed calcium phosphate scaffolds*. in *Key Engineering Materials*. 2009. Trans Tech Publ.

469. Caputo, M., et al., *Electron microscopy investigation of binder saturation and microstructural defects in functional parts made by additive manufacturing.* Microscopy and Microanalysis, 2016. **22**(S3): p. 1770-1771.

470. Castilho, M., et al., *The role of shell/core saturation level on the accuracy and mechanical characteristics of porous calcium phosphate models produced by 3Dprinting.* Rapid Prototyping Journal, 2015.

471. Schmutzler, C., T.H. Stiehl, and M.F. Zaeh, *Empirical process model for shrinkage-induced warpage in 3D printing.* Rapid Prototyping Journal, 2019.

472. Fayazfar, H., et al., *A critical review of powder-based additive manufacturing of ferrous alloys: Process parameters, microstructure and mechanical properties.* Materials & Design, 2018. **144**: p. 98-128.

473. Kafara, M., et al., *Influence of binder quantity on dimensional accuracy and resilience in 3D-printing.* Procedia Manufacturing, 2018. **21**: p. 638-646.

474. Patirupanusara, P., et al., *Effect of binder content on the material properties of polymethyl methacrylate fabricated by three dimensional printing technique.* journal of materials processing technology, 2008. **207**(1-3): p. 40-45.

475. Zhou, Y., et al., *The verification of the mechanical properties of binder jetting manufactured parts by instrumented indentation testing.* Procedia Manufacturing, 2015. **1**: p. 327-342.

476. Zabala, A.I., *Aceros Inoxidables y Aceros resistentes al calor.* Editorial Limusa, 1981.

477. Villavicencio Cevallos, J.C., *Relación, Microestructura/Propiedad en la Soldadura Gtaw entre Aceros Inoxidables y Aceros al Carbono*, 2010.

478. Ibarra Echeverría, M., E. Núñez Solís, and J. Huerta Ibáñez, *Manual de Aceros inoxidables.* INDURA SA, Cerritos, Chile, 2010.

479. Venables, J., *The martensite transformation in stainless steel.* The Philosophical Magazine: A Journal of Theoretical Experimental and Applied Physics, 1962. **7**(73): p. 35-44.

480. Revie, R.W., *Uhlig's corrosion handbook*. Vol. 51. 2011: John Wiley & Sons.

481. Cheng, Y., J. Bullerwell, and F. Steward, *Electrochemical investigation of the corrosion behavior of chromium-modified carbon steels in water.* Electrochimica Acta, 2003. **48**(11): p. 1521-1530.

482. Okada, H., et al., *Copper in iron and steel*, 1982, John Wiley and Sons, New York.

483. Krauss, G., *Steels: processing, structure, and performance*. 2015: Asm International.

484. Chen, W., et al., *Effect of powder feedstock on microstructure and mechanical properties of the 316L stainless steel fabricated by selective laser melting.* Metals, 2018. **8**(9): p. 729.

485. Banerjee, M., *Comprehensive Materials Finishing, Vol. 2 Surface and Heat Treatment Processes; Hashmi, S., Ed*, 2017, Elsevier: New York, NY, USA.

486. Brunauer, S., P.H. Emmett, and E. Teller, *Adsorption of gases in multimolecular layers.* Journal of the American chemical society, 1938. **60**(2): p. 309-319.

487. Barrett, E.P., L.G. Joyner, and P.P. Halenda, *The determination of pore volume and area distributions in porous substances. I. Computations from nitrogen isotherms.* Journal of the American Chemical society, 1951. **73**(1): p. 373-380.

488. Tóth, J., *Thermodynamical correctness of gas/solid adsorption isotherm equations.* Journal of colloid and interface science, 1994. **163**(2): p. 299-302.

489. Schroeder-Pedersen, A., J. Kjøller, and B. Larsen, *A comparison of calculated geometric surface area and measured BET surface area for a metal powder.* Journal of testing and evaluation, 1997. **25**(4): p. 365-369.

490. Misra, D.N., *Adsorption on heterogeneous surfaces: A dubinin-radushkevich equation.* Surface Science, 1969. **18**(2): p. 367-372.

491. Remy, M. and G. Poncelet, *A new approach to the determination of the external surface and micropore volume of zeolites from the nitrogen adsorption isotherm at 77 K.* The Journal of Physical Chemistry, 1995. **99**(2): p. 773-779.

492. Rudziński, W., J. Jagiełło, and Y. Grillet, *Physical adsorption of gases on heterogeneous solid surfaces: evaluation of the adsorption energy distribution from adsorption isotherms and heats of adsorption.* Journal of Colloid and Interface Science, 1982. **87**(2): p. 478-491.

493. Zielinski, J.M. and L. Kettle, *Physical characterization: surface area and porosity.* London: Intertek, 2013.

494. i Iñíguez, R.B., *El Microscopi electrònic de" scanning".* Treballs de la Societat Catalana de Biologia, 1971: p. 38-45.

495. Lozano, V., M.J. Yáñez, and A. Morales, *Principios y práctica de la microscopía electrónica.* Mexico: Consejo Nacional de Investigaciones Científicas y Técnicas (CONICET), 2014.

496. Goldstein, J., et al., *Scanning Electron Microscopy and X-Rays Microanalysis: A text for biologists, Materials scientist and geologist*, 2012, New York: Phlenum press.

497. Seoane, J.R. and X. Llovet Ximenes, *Handbook of instrumental techniques for materials, chemical and biosciences research.* 2012.

498. Laigo, J., et al., *SEM, EDS, EPMA-WDS and EBSD characterization of carbides in HP type heat resistant alloys.* Materials characterization, 2008. **59**(11): p. 1580-1586.

499. Ro, C.-U., et al., *Chemical speciation of individual atmospheric particles using low-Z electron probe X-ray microanalysis:: characterizing "Asian Dust" deposited with rainwater in Seoul, Korea.* Atmospheric Environment, 2001. **35**(29): p. 4995-5005.

500. Bence, A.E. and A.L. Albee, *Empirical correction factors for the electron microanalysis of silicates and oxides.* The Journal of Geology, 1968. **76**(4): p. 382-403.

501. Alarcón, G.M.O.M.C. and G.M.C.A.R. Reyes, *EPMA: ELECTRONIC MICROSOUNDS; PRINCIPLES OF OPERATION EPMA: MICROSONDA ELECTRÓNICA; PRINCIPIOS DE FUNCIONAMIENTO.*

502. Kniseley, R. and F. Laabs, *Applications of cathodoluminescence in electron microprobe analysis: in Anderson CA, ed., Microprobe Analysis*, 1973, Wiley.

503. Kerrick, D.M., L.B. Eminhizer, and J.F. Villaume, *The role of carbon film thickness in electron microprobe analysis.* American Mineralogist: Journal of Earth and Planetary Materials, 1973. **58**(9-10): p. 920-925.

504. Oncins, G. and J. Díaz, *La microscopia de fuerzas atómicas.*

505. Oncins Marco, G. and J. Díaz Marcos, *Atomic force microscopy: probing the nanoworld.* Capítol del llibre: Handbook of instrumental techniques for materials, chemical and biosciences research, Centres Científics i Tecnològics. Universitat de Barcelona, Barcelona, 2012. Part I. Materials technologies (MT), MT. 7, 10 p., 2012.

506. Binnig, G., et al., *Atomic resolution with atomic force microscope.* EPL (Europhysics Letters), 1987. **3**(12): p. 1281.

507. Tranchida, D., et al., *Scanning near-field ellipsometry microscopy: imaging nanomaterials with resolution below the diffraction limit.* Nanoscale, 2011. **3**(1): p. 233-239.

508. Roa, J., F. Dias, and M. Segarra, *Magnetical Response and Mechanical Properties of High Temperature Superconductors, YBaCu3O7-X Materials.* Superconductors–Properties, Technology, and Applications, InTech Ed., Croatia, 2012: p. 181-218.

509. Binnig, G., C.F. Quate, and C. Gerber, *Atomic force microscope.* Physical review letters, 1986. **56**(9): p. 930.

510. Hackley, V.A., et al., *Particle size analysis by laser diffraction spectrometry: application to cementitious powders*. 2004: US Department of Commerce, National Institute of Standards and Technology.

511. Bowen, P., *Particle size distribution measurement from millimeters to nanometers and from rods to platelets.* Journal of Dispersion Science and Technology, 2002. **23**(5): p. 631-662.

512. Sugimoto, K. and S. Matsuda, *Analysis of Passive Films on Austeno-Ferritic Stainless Steel by Microscopic Ellipsometry.* Journal of The Electrochemical Society, 1983. **130**(12): p. 2323.

513. Eshel, G., et al., *Critical evaluation of the use of laser diffraction for particle-size distribution analysis.* Soil Science Society of America Journal, 2004. **68**(3): p. 736-743.

514. Garboczi, E.J., *Three-dimensional mathematical analysis of particle shape using X-ray tomography and spherical harmonics: Application to aggregates used in concrete.* Cement and concrete research, 2002. **32**(10): p. 1621-1638.

515. Erdogan, S., et al., *Three-dimensional shape analysis of coarse aggregates: New techniques for and preliminary results on several different coarse aggregates and reference rocks.* Cement and Concrete Research, 2006. **36**(9): p. 1619-1627.

516. Powell, C., *Elemental binding energies for X-ray photoelectron spectroscopy.* Applied Surface Science, 1995. **89**(2): p. 141-149.

517. Moulder, J.F., *Handbook of X-ray photoelectron spectroscopy.* Physical electronics, 1995: p. 230-232.

518. Edited by Brundle, C.R., C.A. Evans, and S. Wilson, *Encyclopedia of materials characterization: surfaces, interfaces, thin films*. 1992: Butterworth-Heinemann.

519. Vickerman, J.C. and I.S. Gilmore, *Surface analysis: the principal techniques*. 2011: John Wiley & Sons.

520. McCusker, L., et al., *Rietveld refinement guidelines.* Journal of Applied Crystallography, 1999. **32**(1): p. 36-50.

521. Rietveld, H., *A profile refinement method for nuclear and magnetic structures.* Journal of applied Crystallography, 1969. **2**(2): p. 65-71.

522. Rietveld, H., *Line profiles of neutron powder-diffraction peaks for structure refinement.* Acta Crystallographica, 1967. **22**(1): p. 151-152.

523. Wang, X., M. Lei, and J. Zhang, *Surface modification of 316L stainless steel with high-intensity pulsed ion beams.* Surface and Coatings Technology, 2007. **201**(12): p. 5884-5890.

524. Vives, S., E. Gaffet, and C. Meunier, *X-ray diffraction line profile analysis of iron ball milled powders.* Materials Science and Engineering: A, 2004. **366**(2): p. 229-238.

525. Goehner, R.P. and M.C. Nichols, *X-ray powder Diffraction.* ASM Handbook., 1986. **10**: p. 333-343.

526. Goldstein, J.I., et al., *Scanning electron microscopy and X-ray microanalysis*. 2017: Springer.